

**Titre:** Correlation between vibration excitation forces and the dynamic characteristics of two-phase flow in a rotated triangular tube bundle  
Title:

**Auteur:** Changqing Zhang  
Author:

**Date:** 2007

**Type:** Mémoire ou thèse / Dissertation or Thesis

**Référence:** Zhang, C. (2007). Correlation between vibration excitation forces and the dynamic characteristics of two-phase flow in a rotated triangular tube bundle [Ph.D. thesis, École Polytechnique de Montréal]. PolyPublie.  
Citation: <https://publications.polymtl.ca/8005/>

 **Document en libre accès dans PolyPublie**  
Open Access document in PolyPublie

**URL de PolyPublie:** <https://publications.polymtl.ca/8005/>  
PolyPublie URL:

**Directeurs de recherche:** Michel J. Pettigrew, & Njuki W. Mureithi  
Advisors:

**Programme:** Unspecified  
Program:

UNIVERSITÉ DE MONTRÉAL

CORRELATION BETWEEN VIBRATION EXCITATION FORCES AND THE  
DYNAMIC CHARACTERISTICS OF TWO-PHASE FLOW IN A ROTATED  
TRIANGULAR TUBE BUNDLE

CHANGQING ZHANG  
DÉPARTEMENT DE GÉNIE MÉCANIQUE  
ÉCOLE POLYTECHNIQUE DE MONTRÉAL

THÈSE PRÉSENTÉ EN VUE DE L'OBTENTION  
DU DIPLÔME DE PHILOSOPHIAE DOCTOR  
(GÉNIE MÉCANIQUE)  
NOVEMBRE 2007



Library and  
Archives Canada

Bibliothèque et  
Archives Canada

Published Heritage  
Branch

Direction du  
Patrimoine de l'édition

395 Wellington Street  
Ottawa ON K1A 0N4  
Canada

395, rue Wellington  
Ottawa ON K1A 0N4  
Canada

*Your file* *Votre référence*

*ISBN: 978-0-494-37138-1*

*Our file* *Notre référence*

*ISBN: 978-0-494-37138-1*

#### NOTICE:

The author has granted a non-exclusive license allowing Library and Archives Canada to reproduce, publish, archive, preserve, conserve, communicate to the public by telecommunication or on the Internet, loan, distribute and sell theses worldwide, for commercial or non-commercial purposes, in microform, paper, electronic and/or any other formats.

The author retains copyright ownership and moral rights in this thesis. Neither the thesis nor substantial extracts from it may be printed or otherwise reproduced without the author's permission.

#### AVIS:

L'auteur a accordé une licence non exclusive permettant à la Bibliothèque et Archives Canada de reproduire, publier, archiver, sauvegarder, conserver, transmettre au public par télécommunication ou par l'Internet, prêter, distribuer et vendre des thèses partout dans le monde, à des fins commerciales ou autres, sur support microforme, papier, électronique et/ou autres formats.

L'auteur conserve la propriété du droit d'auteur et des droits moraux qui protègent cette thèse. Ni la thèse ni des extraits substantiels de celle-ci ne doivent être imprimés ou autrement reproduits sans son autorisation.

---

In compliance with the Canadian Privacy Act some supporting forms may have been removed from this thesis.

Conformément à la loi canadienne sur la protection de la vie privée, quelques formulaires secondaires ont été enlevés de cette thèse.

While these forms may be included in the document page count, their removal does not represent any loss of content from the thesis.

Bien que ces formulaires aient inclus dans la pagination, il n'y aura aucun contenu manquant.

  
**Canada**

UNIVERSITÉ DE MONTRÉAL

ÉCOLE POLYTECHNIQUE DE MONTRÉAL

Cette thèse intitulée:

CORRELATION BETWEEN VIBRATION EXCITATION FORCES AND THE  
DYNAMIC CHARACTERISTICS OF TWO-PHASE FLOW IN A ROTATED  
TRIANGULAR TUBE BUNDLE

présenté par: ZHANG, Changqing

en vue de l'obtention du diplôme de: Philosophiae Doctor

a été dûment acceptée par le jury d'examen constitué de:

M. PELLETIER, Dominique, Ph.D., président

M. PETTIGREW, Michel J., Post grad. dipl., membre et directeur de recherche

M. MUREITHI, Njuki W., Ph.D., membre et codirecteur de recherche

M. TEYSSEDOU, Alberto., Ph.D., membre

M. WEAVER, David S., Ph.D., membre

## ACKNOWLEDGMENTS

Firstly, the author is profoundly grateful to his supervisor, Professor Michel J. Pettigrew and co-supervisor Professor Njuki W. Mureithi, for their scholarly guidance, enthusiastic dedication and financial support throughout the doctoral work. The author will be forever indebted to their diligent efforts for the publications and dissertation.

The author would like to acknowledge the technical support provided by Mr. Thierry Lafrance for the test section modification and loop operation, Mr. Bénédicte Besner for the development of the fiber-optic probes and the data acquisition system, and Mr. Nour Aimène for the instrumentation of strain gages throughout the project.

The author expresses his gratitude to Professor Emmanuel de Langre and Professor Alberto Teysedou for the valuable discussions and constructive suggestion on the modeling work.

Thanks are due to former student Dragos Pamfil for the test section design and the initial development of the fiber-optic probes.

Thanks are again due to Mr. Bénédicte Besner for his help in translation process of “Résumé” and “Condensé en français”.

Finally, the author conveys his deepest sense of gratitude to his wife, Wenping Wang, and their lovely son, Zhiyuan Zhang, for their inspiration and encouragement through the doctoral study.

## RÉSUMÉ

L'endommagement des tubes se produit dans beaucoup d'échangeurs de chaleur avant qu'ils aient atteint leur vie normale. L'usure des tubes est souvent le résultat à long terme d'usure par frottement causé par la vibration de faible amplitude due aux forces d'excitation aléatoires dans un écoulement diphasique. Dans cette étude, les caractéristiques d'un écoulement diphasique transverse dans un faisceau de tubes, qui contribuent aux forces fluides, sont examinés, et les forces d'excitation vibratoire sont mesurées.

Un programme expérimental a été entrepris avec des faisceaux de tubes de configuration triangulaire-tourné soumis à un écoulement air-eau pour simuler des mélanges diphasiques. Les faisceaux, qui ont eu un rapport pas sur diamètre de 1.5, ont été construits avec des cylindres de diamètre relativement grand (38 mm). Ceci a permis l'obtention de mesures des écoulements diphasiques beaucoup plus détaillées dans l'espace entre les cylindres (19 mm). Des sondes à fibre optique ont été développées pour mesurer le taux de vide. Des mesures locales de vitesses d'écoulement et de diamètres de bulles ou encore des longueurs caractéristiques des bulles du mélange diphasiques ont été obtenus en employant des doubles sondes. Les forces de traîné et de portance ont été mesurées avec des cylindres équipés de jauges de contrainte et soumis à un éventail de taux de vide ainsi qu'à plusieurs vitesses d'écoulement.

Les distributions de taux de vide, vitesse des bulles ainsi que leurs diamètres dans les faisceaux de tubes triangulaires tournés ont été obtenues. Des forces quasi-périodiques inattendues mais significatives dans les directions de traîné et de portance ont été mesurées. Ces forces sont généralement plus grandes dans la direction de la traîné. Cependant, la fréquence des forces d'excitation est relativement basse (c.-à-d., 3-6 Hz) et ne dépendent pas directement de la vitesse d'écoulement. D'un autre côté, on a observé une fréquence d'excitation beaucoup plus élevée (jusqu'à 16 Hz) dans la

direction de la portance à des vitesses plus élevées. La fréquence semble directement reliée à la vitesse d'écoulement dans la direction de la portance. Les recherches ont prouvé que les forces quasi-périodiques de traîné et de portance sont générées par des mécanismes différents qui n'ont pas été observés jusqu'ici. Les forces quasi-périodiques de traîné semblent reliées aux fluctuations du flux de moment de force dans le chemin principal de l'écoulement entre les cylindres. Les forces quasi-périodiques de portance, d'autre part, sont la plupart du temps corrélées avec des oscillations dans le sillage des cylindres. Les forces quasi-périodiques de portance sont liées aux mesures du taux de vide local dans le secteur instable de sillage entre les cylindres amont et aval. Les forces de résistance quasi-périodiques de traîné sont bien corrélées avec des mesures similaires dans le chemin principal de l'écoulement entre les cylindres.

Des modèles semi-analytiques ont été développés pour comprendre la nature des forces d'excitation vibratoire et pour corréler ces forces avec les caractéristiques dynamiques de l'écoulement diphasique dans un faisceau de tubes triangulaire tourné. La relation entre les forces de portance et de traîné et les caractéristiques dynamiques de l'écoulement diphasique sont établies par les équations de mécanique des fluides sur les moments de forces. Un modèle a été développé pour corréler la fluctuation du taux de vide dans le chemin principal de l'écoulement et les forces de traîné dynamiques. Un deuxième modèle a été développé pour corréler les oscillations dans le sillage des cylindres et des forces dynamiques de portance. Bien que préliminaire, chaque modèle peut prévoir les forces correspondantes relativement bien.

## ABSTRACT

Tube failures are occurring in many heat exchangers before they have reached their design life. These tube failures are often the results of long-term fretting-wear caused by low-amplitude vibration due to random excitation forces in two-phase flow. In this study, the characteristics of two-phase cross flow in tube bundles that contribute to fluid forces are examined and vibration excitation forces are measured.

An experimental program was undertaken with rotated triangular tube arrays subjected to air-water flow to simulate two-phase mixtures. The arrays, which had a pitch-to-diameter ratio of 1.5, were made of relatively large diameter cylinders (38 mm). This resulted in larger gaps (19 mm) between cylinders to allow for detailed two-phase flow measurements. Fiber-optic probes were developed to measure local void fraction. Local flow velocities and bubble diameters or characteristic lengths of the two-phase mixture are obtained by using double probes. Both the dynamic lift and drag forces were measured with strain gage instrumented cylinders subjected to a wide range of void fractions and flow rates.

The distributions of void fraction, bubble velocity and bubble diameters in rotated-triangular tube bundles were obtained. Somewhat unexpected but significant quasi-periodic forces in both the drag and lift directions were measured. These forces are generally larger in the drag direction. However, the excitation force frequency is relatively low (i.e., 3-6 Hz) and not directly dependent on flow velocity in the drag direction. On the other hand much higher frequency (up to 16 Hz) was observed in the lift direction at the higher flow velocities. The frequency appears directly related to flow velocity in the lift direction. The investigation showed that the quasi-periodic drag and lift forces are generated by different mechanisms that have not been observed so far. The quasi-periodic drag forces appear related to the momentum flux fluctuations in the main flow path between the cylinders. The quasi-periodic lift forces, on the other hand,



are mostly correlated to oscillations in the wake of the cylinders. The quasi-periodic lift forces are related to local void fraction measurements in the unsteady wake area between upstream and downstream cylinders. The quasi-periodic drag forces correlate well with similar measurements in the main flow stream between cylinders.

Semi-analytical models were developed to understand the nature of the vibration excitation forces and to correlate those forces to the dynamic characteristics of the two-phase flow in a rotated triangular tube bundle. The relationships between the lift or drag forces and the dynamic characteristics of two-phase flow are established through fluid mechanics momentum equations. A model was developed to correlate the void fraction fluctuation in the main flow path and the dynamic drag forces. A second model was developed for correlating the oscillation in the wake of the cylinders and the dynamic lift forces. Although still preliminary, each model can predict the corresponding forces relatively well.

## CONDENSÉ EN FRANÇAIS

### Introduction

Beaucoup d'échangeurs de chaleur sont soumis à des écoulements diphasiques transverses. Les forces d'excitation induites par ces écoulements causent des vibrations, qui peuvent aboutir à l'usure des tubes à long terme, ou encore de la fatigue. Les détails de l'écoulement et des mesures de force d'excitation vibratoire dans les faisceaux de tubes soumis aux écoulements diphasiques transverses sont requis pour comprendre les mécanismes d'excitation vibratoire.

Avant 1980, très peu de travaux ont été effectués pour étudier les vibrations dans un faisceau de tubes soumis à des écoulements diphasiques transverses. Pettigrew et Gorman (1973) étaient les premiers à conduire des expériences de vibration sur des faisceaux de tubes soumis aux écoulements diphasiques transverses air-eau. Depuis, quelques études ont été conduites dans ce secteur, par exemple, Heilker et Vincent (1981) en écoulement transverse air-eau, Axisa et al. (1984) en air-eau, et aussi en écoulement transverse eau-vapeur, Pettigrew et al. (1989a, 1989b) et Taylor et al. (1989) en écoulement transverse air-eau. Une excellente revue effectuée par Pettigrew et Taylor (1994) donne une vue d'ensemble des vibrations induites par les écoulements diphasiques dans les composants de centrales nucléaires.

Depuis 1994, plusieurs chercheurs ont contribué à l'obtention de résultats significatifs, en particulier, Feenstra et al. (1995, 2002) en Fréon 11 diphasique, Mann et Marjinger (1995) en Fréon 12 diphasique, Lian et al. (1997) en air-eau, de Langre et Villard (1998) en air-eau et en eau-vapeur, Nakamura et al. (1995, 2002), Mureithi et al. (2002) et Hirota et al. (2002) en eau-vapeur, tous en écoulement transverse. En plus, des études complètes sur les vibrations des faisceaux de tubes en mélange air-eau et avec Fréon 22 en écoulements diphasiques transverses ont été conduites aux laboratoires de Chalk

River par Taylor et al. (1996, 2001) et Pettigrew et al. (2001, 2002). Dans ces études, presque tous les aspects concernant les vibrations induites par les écoulements diphasiques ont été étudiés, tels que les instabilités fluide-élastique, l'excitation aléatoire par turbulence, la masse hydrodynamique, l'amortissement diphasique, l'effet des régimes d'écoulements, de la configuration des faisceaux de tubes (incluant différents diamètres de tubes et de rapport pas sur diamètre) et des différentes propriétés d'écoulements diphasiques, sur les mécanismes d'excitation de vibration. Bien que certains travaux expérimentaux et théoriques sur les vibrations en écoulement diphasique aient été effectués, comparativement, le travail sur l'excitation aléatoire en turbulence, particulièrement sur les mécanismes fondamentaux d'excitation de la turbulence en écoulement diphasique traverse, est insuffisant.

Des mesures détaillées des écoulements diphasiques et des forces d'excitation vibratoire sont requises pour comprendre les mécanismes fondamentaux d'excitations aléatoires. En plus, nos résultats préliminaires (Pettigrew et al. 2005) montrent que des forces quasi-périodiques inattendues mais significatives ont été mesurées en portance et en trainé. Cependant d'autres études sur l'amplitude et l'origine de ces forces sont nécessaires. On propose des mesures détaillées des écoulements diphasiques et des forces d'excitation vibratoire à l'intérieur du faisceau de tubes dans cette étude. Cette information sera utilisée pour comprendre les mécanismes périodiques et aléatoires d'excitation de vibration dans les écoulements diphasiques transverses.

L'objectif général de ce travail est de comprendre les mécanismes fondamentaux d'excitation de vibration dans des faisceaux de tubes soumis à des écoulements diphasiques transverses. Plus spécifiquement, l'intention est de conduire des mesures détaillées des caractéristiques des écoulements diphasiques ainsi que des forces d'excitation. On utilisera cette information pour corréler les forces quasi-périodiques et aléatoires d'excitation par turbulence avec les caractéristiques dynamiques de l'écoulement diphasique. Les objectifs spécifiques de cette étude sont: 1) Mesurer les

caractéristiques détaillées des écoulements diphasiques telles que le taux de vide, la vitesse des bulles et la taille des bulles entre les tubes à des positions différentes dans la section d'essai; 2) Déterminer expérimentalement les forces d'excitation qui sont associés aux tubes d'échangeur de chaleur soumis à des écoulements diphasiques transverses. La série d'essais englobera un éventail de conditions d'écoulement avec une rangée de cylindres triangulaire-tournés; 3) Corréler les forces quasi-périodiques et aléatoires d'excitation par turbulence avec les caractéristiques dynamiques de l'écoulement diphasique; et 4) Comprendre la nature des forces périodiques et aléatoires d'excitation par turbulence.

### **Considérations expérimentales**

L'analyse des vibrations induites en écoulement diphasique exige des paramètres appropriés pour exprimer les données expérimentales. Les mélanges diphasiques sont rarement homogènes ou uniformes tout au long de la section. Par exemple, il peut y avoir plus de liquide près des murs de la conduite et la vitesse moyenne d'écoulement de la phase gazeuse peut être légèrement plus élevée que celle de la phase liquide causant un glissement entre les phases (Pettigrew et Taylor 1994). Pour simplifier, un modèle diphasique homogène sans glissement entre les deux phases est employé dans cette thèse.

Un programme expérimental a été entrepris avec des rangées de tubes triangulaires tournés soumis à un écoulement air-eau pour simuler des mélanges diphasiques. Les rangées, qui ont un rapport de pas sur diamètre de 1.5, sont conçues avec des cylindres de diamètres relativement grands (38 mm). Ce qui cause un grand espace (19 mm) entre les cylindres pour faciliter des mesures diphasiques détaillées d'écoulement.

Deux genres d'expériences ont été effectués, la première était de mesurer les caractéristiques dynamiques de l'écoulement diphasique tel que le taux de vide, la

vitesse des bulles ainsi que leurs tailles. L'autre était de mesurer les forces d'excitation des vibrations générées dans le faisceau de tubes soumis à des écoulements diphasiques transverses.

Des sondes de fibre optique ont été développées pour mesurer les caractéristiques dynamiques de l'écoulement diphasique. Les forces de trainé et de portance ont été mesurées avec des tubes équipés de jauges de déformation. Une tentative a été faite pour utiliser cette information pour comprendre les mécanismes d'excitation de vibration dans les écoulements diphasiques transverses.

La boucle comprend une pompe à débit variable allant jusqu'à 25 l/s, un débitmètre magnétique, un réservoir de 2500 l, un circuit d'alimentation d'air comprimé de l'ordre de 250 l/s. L'air comprimé a été injecté au-dessous d'un mélangeur conçu pour homogénéiser et distribuer le mélange diphasique uniformément au-dessous de la section d'essai. Le débit d'air a été mesuré avec des plaques à orifice reliées à un capteur de pression différentiel et à un système électronique d'affichage. La boucle a opéré à température ambiante et la pression dans la section d'essai était légèrement au-dessus de l'atmosphère. Une courte description de chaque composant est donnée comme suit:

Les tubes de 38 mm de diamètre ont été arrangés dans cinq configurations différentes:

- 1) Un tube simple avec des demi-tubes sur le mur latéral dans la section d'essai étroite;
- 2) Un tube simple sans les demi-tubes sur le mur latéral dans la section d'essai étroite;
- 3) Deux tubes avec trois différents pas le long de l'écoulement dans la section d'essai étroite (sans les demi-tubes sur le mur latéral);
- 4) Faisceaux de tubes triangulaires tournés de 6 rangées avec  $P/D=1.5$  dans la section d'essai étroite; et
- 5) Faisceaux de tubes triangulaires tournés de 7 rangées avec  $P/D=1.5$  dans la section d'essai plus large.

Les tubes sont en acrylique transparent, de 191 mm de longueur et ont une épaisseur de paroi de 1.70 mm. Tous les tubes sont vides. Les fréquences naturelles (tubes en porte-à-

faux) sont de 70 Hz dans l'eau et de 70 à 150 Hz dans les mélanges air-eau. Deux paires de jauges de déformation diamétralement opposées ont été installées à l'intérieur de chaque tube à 90 degrés l'une de l'autre pour mesurer les forces dans le sens de l'écoulement (portance) et perpendiculairement à l'écoulement (trainé). Les paires de jauges de déformation ont été reliées à un pont de Wheatstone dans la configuration de demi-pont. La fréquence naturelle des cylindres en porte-à-faux étant beaucoup plus haute (c.-à-d., >150Hz) que les fréquences des forces d'excitation, le cylindre en porte-à-faux fonctionne essentiellement comme capteur dynamique de force. Avant que le cylindre instrumenté ait été inséré dans la section des essais, la relation force statique-déformation a été déterminée par l'intermédiaire d'un minutieux calibrage.

Les signaux des jauges de contrainte ont été enregistrés et analysés sur un analyseur de spectre en temps réel à 16 canaux (OROS 38) couplés à un ordinateur portatif. Un taux d'échantillonnage de 2 KHz a été sélectionné. Pour chaque essai, un temps suffisant a été accordé pour avoir un spectre en fréquence stable (habituellement 5 minutes). Le logiciel NVGates couplé au système dynamique d'analyse spectrale OROS a été employé pour effectuer les corrélations et les analyses spectrales des forces d'excitation de vibration.

La fibre multi-mode utilisée dans cette étude, a été fabriquée par Ceram Optecs. Le diamètre du cœur, de la gaine et du revêtement, est de 100, 140 et 170  $\mu\text{m}$  respectivement. Une double sonde en fibre optique comporte deux fibres optiques insérées dans un tube d'acier inoxydable. Les bouts des sondes sont distancés axialement d'environ 150  $\mu\text{m}$ . Chaque sonde a un bout conique fait par une attaque chimique avec de l'acide fluorhydrique.

Pour chaque mesure, les données des sondes ont été enregistrées pendant une période de 20 secondes avec un échantillonnage de 2 MHz. Un logiciel d'analyse de donnée a été développé pour obtenir le temps  $T_i$  auquel la particule gazeuse, d'indice  $i$ , touche la

sonde, et la durée de ce contact,  $\tau_i$ . Le taux de vide peut être obtenu en calculant le rapport entre la durée totale de contact, mesurée à partir d'une des deux sondes, et le temps total de l'essai,  $T$ . La vitesse des bulles de la phase gazeuse peut être estimée à partir du temps transitoire entre les deux bouts de la sonde, qui sont à une distance connue (environ 150  $\mu\text{m}$ ). La taille des bulles,  $d$ , peut être déduite à partir du produit de la vitesse des bulles et de la durée du contact.

Pour les mesures simultanées des écoulements et des forces, le taux de vide et les signaux de force ont été analysés sur un analyseur de spectre en temps réel (OR38) avec 16 canaux couplés à un ordinateur portable.

## Résultats

Les résultats expérimentaux et analytiques sont présentés sous forme de cinq communications techniques, qui constituent les chapitres 3 à 7 de cette thèse. Dans le chapitre 3, des mesures diphasiques détaillées de l'écoulement pour des taux de vide homogènes de 50 et 80%, à une vitesse d'écoulement inter-cylindrique de 5 m/s, ont été faites. Les mesures de force pour des taux de vide homogènes de 50 et de 80% et pour une gamme de vitesse d'écoulement de 1 m/s à 15 m/s ont été également prises. Les résultats des mesures d'écoulement indiquent que le mélange diphasique tend à s'écouler entre les cylindres et que dans cette région, la vitesse d'écoulement est assez uniforme. En fait, le parcours de l'écoulement ressemble à celui observé pour une série de coudes de 60° en deux dimensions. Ainsi, il n'est pas surprenant que la distribution du taux de vide ne soit pas uniforme. Le plus bas taux de vide correspond à l'extrados et le plus haut taux de vide à l'intrados à la sortie des coudes comme prévu pour un écoulement diphasique. La distribution du taux de vide doit complètement s'inverser d'un côté à l'autre à l'intérieur de la moitié de la distance inter-cylindre. Cela implique un mélange considérable à chaque intervalle de moitié de distance inter-tube. Donc, il n'est pas surprenant que le mélange diphasique soit assez homogène et que la différence de

vitesse entre les phases soit petite. Des mesures de force ont été prises avec un cylindre instrumenté situé dans la quatrième position de l'extrémité en amont de la section d'essai. Les résultats des mesures de forces indiquent la présence des forces quasi-périodiques inattendues dans la direction de la portance et dans la direction de l'écoulement (trainé). Ces forces sont significativement plus grandes dans la direction de la trainé. Ceci était inattendu et différent de l'excitation aléatoire turbulente typique.

Des mesures plus détaillées et plus complètes des forces sont discutées au chapitre 4. La corrélation des forces d'excitation vibratoire le long du cylindre et l'effet des positions des cylindres sur les forces d'excitation ont été examinés. Les résultats des mesures de force indiquent que des forces quasi-périodiques inattendues mais significatives ont été mesurées dans la direction de la portance et de la trainé. Ces forces sont sensiblement plus grandes dans la direction de la trainé. Cependant, la fréquence de ces force d'excitation est relativement basse (c.-à-d., 3-6 Hz) et elle n'est pas directement dépendante de la vitesse d'écoulement dans la direction de la trainé. D'un autre coté, on a observé des fréquences beaucoup plus élevées (jusqu'à 16 Hz) dans la direction de la portance à des vitesses plus élevées d'écoulements. La fréquence semble directement reliée à la vitesse d'écoulement dans la direction de la portance. Les forces périodiques semblent bien corrélées le long du cylindre. Les forces de trainé sont mieux corrélées que les forces de portance. Les forces périodiques dépendent également de la position du cylindre dans le faisceau. Étonnamment, les spectres des forces pour le cylindre isolé et les cylindres en amont sont tout à fait semblables. Dans la direction de la portance les spectres du cylindre isolé sont en grande partie sur une large bande aléatoire en apparence et légèrement plus petite que les forces d'excitation en portance pour les cylindres en amont.

Le chapitre 5 vise à présenter la compréhension de la nature de ces forces quasi-périodiques inattendues de portance et de trainé. Des mesures simultanées de l'écoulement et des forces ont été faites. Les recherches ont prouvé que les forces quasi-



périodiques de portance et de trainé sont produites par des mécanismes différents qui n'ont pas été observés précédemment. Les forces quasi-périodiques de trainé semblent reliées aux fluctuations du flux de moment de force dans le chemin principal de l'écoulement entre les cylindres. Les forces quasi-périodiques de portance, d'autre part, sont la plupart du temps corrélées avec des oscillations dans le sillage des cylindres. Les forces quasi-périodiques de portance sont liées aux mesures du taux de vide local dans le secteur instable de sillage entre les cylindres en amont et en aval. Les forces de quasi-périodiques de trainé sont bien corrélées avec des mesures similaires dans le chemin principal de l'écoulement entre les cylindres.

Des études supplémentaires des forces quasi-périodiques d'excitation de vibration dans les faisceaux de tubes triangulaires tournés soumis à des écoulements diphasiques sont discutées dans le chapitre 6. Ces recherches ont fourni plus d'évidence que les forces quasi-périodiques de portance sont réellement dues aux oscillations du sillage entre les cylindres en amont et en aval. On a démontré que les forces quasi-périodiques de portance et de trainé ne devraient pas augmenter avec la position du cylindre dans une rangée de cylindres de configuration triangulaire-tourné. On a également montré que ces forces de portance et de trainé quasi-périodiques sont essentiellement semblables à celles observées dans la section d'essai étroite et existent également dans la section d'essai plus large.

L'objectif du chapitre 7 est de développer des modèles semi-analytiques pour corréler les forces d'excitation vibratoire aux caractéristiques dynamiques de l'écoulement diphasique dans un faisceau de tubes triangulaire tourné et de comprendre la nature des forces d'excitation vibratoire. Les rapports entre les forces de trainé ou de portance et les caractéristiques dynamiques des écoulements diphasiques sont établis par des équations de moments de force de la mécanique des fluides. Un modèle a été développé pour corréler la fluctuation du taux de vide dans le chemin principal et les forces de trainé dynamiques. Un deuxième modèle a été développé pour corréler les oscillations du

sillage entre les cylindres et les forces dynamiques de portance. Chaque modèle peut prévoir relativement bien les forces correspondantes.

### **Contributions et recommandations principales**

A partir de cette étude, plusieurs contributions au développement de normes de conception et à la compréhension des mécanismes fondamentaux d'excitation vibratoire peuvent être notées. La première contribution est le grand corps de données empiriques produites en laboratoire. Ces données couvrent un éventail de taux de vide et de débits. Ces données devraient être utiles à d'autres chercheurs et aux concepteurs d'échangeur de chaleur.

Une deuxième contribution majeure est la constatation que le mécanisme quasi-périodique d'excitation régit la vibration induite par écoulement diphasique dans des faisceaux de tubes. Deux mécanismes quasi-périodiques d'excitation différents non observés avant, ont été trouvés. Ces mécanismes ont été découverts par des mesures détaillées des écoulements diphasiques et des forces d'excitation. Les forces de trainé quasi-périodiques semblent reliées aux fluctuations des moments de force dans le chemin principal d'écoulement entre les cylindres. Ces fluctuations de moment de force sont provoquées par des fluctuations du taux de vide dans le chemin principal d'écoulement entre les cylindres. Les forces quasi-périodiques de portance, d'autre part, sont la plupart du temps corrélées aux oscillations dans le sillage des cylindres. Les forces quasi-périodiques de portance sont très différentes des forces de vortex dans les écoulements monophasiques. Peu de données sur les forces d'excitation vibratoire peuvent être trouvées dans la littérature. C'est principalement parce que la plupart des chercheurs jusqu'ici se sont concentrés sur l'instabilité fluide-élastique. Une source de données qui a été découverte est celle de Taylor 1994. Elle a trouvé des crêtes de forces quasi-périodiques semblables en portance et en trainé dans les spectres de force. Malheureusement, pas plus d'attention n'a été prêtée à ce sujet car elle était principalement intéressée par l'excitation aléatoire.

Une troisième contribution significative est le développement de deux modèles semi-analytiques. Les rapports entre les forces de trainé et de portance et les caractéristiques dynamiques de l'écoulement diphasique sont établis par les équations de mécanique des fluides. Un modèle a été développé pour corrélérer les fluctuations de taux de vide dans le chemin principal de l'écoulement et les forces de trainé dynamiques. Il peut également être employé pour estimer les forces périodiques dues aux écoulements diphasiques dans des coudes de système de tuyauterie. Un deuxième modèle a été développé pour corrélérer les oscillations dans le sillage des cylindres et les forces dynamiques de portance. Bien que des développements ultérieurs soient nécessaires, ces modèles préliminaires sont encourageants puisque des prévisions plausibles ont été obtenues.

Une quatrième contribution est l'élaboration d'une méthode simple et innovatrice pour mesurer la corrélation. Deux demi-cylindres instrumentés ont été conçus pour mesurer la corrélation sur la longueur du cylindre. Les corrélations sur la longueur du cylindre des forces dues au vortex alterné en écoulement d'eau et des forces quasi-périodiques de portance et/ou trainé en air-eau ont été mesurées. Cette méthode s'est avérée être efficace pour évaluer la corrélation dans cette étude.

Une cinquième contribution est la mesure du taux de vide, de la vitesse des bulles et des profils de la taille de bulle dans le faisceau de tubes pour plusieurs écoulements typiques. Les résultats des mesures d'écoulement indiquent que l'écoulement tend à aller entre les cylindres et que dans le chemin principal, la vitesse d'écoulement est assez uniforme. En fait, le chemin d'écoulement ressemble à une série de coudes bidimensionnels de  $60^\circ$ . Ainsi, il n'est pas surprenant que la distribution du taux de vide ne soit pas uniforme. Le plus bas taux de vide correspond à l'extrados et le plus haut taux de vide à l'intrados à la sortie des coudes comme il était prévu dans les coudes pour un écoulement diphasique. La distribution du taux de vide est complètement renversée d'un côté à l'autre à partir de la moitié de la distance inter-cylindrique. Elle implique que l'écoulement diphasique soit bien mélangé dans un faisceau de tubes triangulaire tourné.

Elle implique également que le régime diphasique d'écoulement dans les faisceaux de tubes tournés puisse être tout à fait différent que celui dans un tuyau ascendant.

Cette étude a probablement comme conséquence plus de questions que de réponses. La connaissance nécessaire pour poser des questions appropriées peut être une contribution significative aux travaux futurs.

Les recommandations pour les travaux futurs dans ce secteur incluent ce qui suit: 1) Des cartes de régime d'écoulement pour l'écoulement diphasique transverse dans des faisceaux de tubes sont nécessaires. Ceci exigera des développements de techniques sophistiquées de visualisation d'écoulement pour déterminer le modèle local d'écoulement. Par exemple, de nouvelles méthodes comme le système PIV pour mesurer les écoulements, devraient être considérées; 2) Des essais pour la même configuration de faisceau de tubes mais pour de plus petits diamètres de tubes sont nécessaires pour déterminer si ces mécanismes quasi-périodiques d'excitation vibratoire sont significatifs dans des géométries beaucoup plus réalistes; 3) Des essais avec d'autres fluides diphasiques sont exigés pour déterminer si ces mécanismes quasi-périodiques d'excitation vibratoire dans un écoulement air-eau existent également dans des écoulements eau-vapeur; et 4) Les deux modèles semi-analytiques doivent être raffinés.

## TABLE OF CONTENTS

Acknowledgements.....	iv
Résumé.....	v
Abstract.....	vii
Condensé en français.....	ix
Table of contents.....	xx
List of tables.....	xxv
List of figures.....	xxvi
List of symbols.....	xxxiii
CHAPTER 1: INTRODUCTION.....	1
1.1 Motivation.....	1
1.2 Review of the literature.....	5
1.2.1 Two-phase cross flow in tube bundles.....	5
1.2.2 Turbulence-induced excitation in tube bundles due to two-phase cross flow.....	8
1.3 Objectives.....	12
1.4 Thesis outlines.....	13
CHAPTER 2: EXPERIMENTAL CONSIDERATIONS.....	14
2.1 Two-phase flow.....	14
2.1.1 Flow parameter definitions.....	14
2.1.2 Upward two-phase flow inside vertical tubes.....	15
2.1.3 Two-phase cross flow in tube bundles.....	17
2.1.4 Air-water and steam-water.....	20
2.2 Experiments.....	21
2.2.1 Experimental approach.....	21
2.2.2 Air-water loop.....	21

2.2.3 Tube geometries.....	24
2.2.4 Instrumentation.....	25
2.2.5 Fiber-optic probe tests.....	26
2.2.6 Test conditions.....	29
2.2.7 Experimental results.....	29
2.3 List of publications.....	30

CHAPTER 3: DETAILED FLOW AND FORCE MEASUREMENTS IN	
A ROTATED TRIANGULAR TUBE BUNDLE SUBJECTED TO	
TWO-PHASE CROSS FLOW.....	31
3.1 Abstract.....	32
3.2 Introduction.....	32
3.3 Experimental considerations.....	33
3.3.1 Test loop.....	33
3.3.2 Test section.....	34
3.3.3 Fiber-optic probes for two-phase flow measurements.....	35
3.3.4 Instrumentation.....	38
3.4 Results.....	38
3.4.1 Flow measurements.....	38
3.4.2 Dynamic lift and drag force measurements .....	43
3.5 Discussion.....	45
3.6 Conclusions.....	46
3.7 References.....	46

CHAPTER 4: VIBRATION EXCITATION FORCE MEASUREMENTS IN	
A ROTATED TRIANGULAR TUBE BUNDLE SUBJECTED TO	
TWO-PHASE CROSS FLOW.....	48
4.1 Abstract.....	49
4.2 Introduction.....	49

4.3 Experimental considerations.....	50
4.3.1 Test loop.....	50
4.3.2 Test section.....	52
4.3.3 Instrumentation.....	52
4.4 Results.....	53
4.4.1 Vibration excitation forces in the interior position of the bundle.....	53
4.4.2 Correlation of vibration excitation forces along the cylinder in the interior position of the bundle.....	56
4.4.3 Effect of cylinder positions on excitation forces.....	58
4.5 Discussion.....	61
4.6 Conclusions.....	62
4.7 Acknowledgments.....	62
4.8 Nomenclature.....	63
4.9 References.....	63

**CHAPTER 5: CORRELATION BETWEEN VIBRATION EXCITATION FORCES  
AND THE DYNAMIC CHARACTERISTICS OF  
TWO-PHASE CROSS FLOW IN**

<b>A ROTATED TRIANGULAR TUBE BUNDLE.....</b>	<b>65</b>
5.1 Abstract.....	66
5.2 Introduction.....	66
5.3 Nomenclature.....	68
5.4 Experimental consideration.....	68
5.4.1 Test section.....	68
5.4.2 Fiber-optic probes for two-phase flow measurements.....	70
5.4.3 Instrumentation.....	70
5.5 Experimental results and discussion.....	71
5.5.1 Dynamic lift and drag force measurements.....	71
5.5.2 Dynamic characteristics of two-phase flow .....	73

5.5.3 Correlation between void fraction fluctuations and dynamic lift and drag forces.....	81
5.6 Future work.....	82
5.7 Conclusion.....	84
5.8 Acknowledgments.....	84
5.9 References.....	84

## CHAPTER 6: FURTHER STUDY OF QUASI-PERIODIC VIBRATION

### EXCITATION FORCES IN ROTATED TRIANGULAR TUBE

#### BUNDLES SUBJECTED TO TWO-PHASE CROSS FLOW..... 86

6.1 Abstract.....	87
6.2 Introduction.....	87
6.3 Experimental considerations.....	90
6.3.1 Test sections.....	90
6.3.2 Instrumentation.....	91
6.4 Results and discussion.....	92
6.4.1 Comparison between periodic vortex shedding forces in water and quasi-periodic lift forces in air/water flow.....	92
6.4.2 Effect of cylinder position on the quasi-periodic drag and lift forces.....	95
6.4.3 Quasi-periodic drag and lift forces in the wider test section.....	97
6.5 Conclusion.....	102
6.6 Acknowledgments.....	103
6.7 References.....	103

## CHAPTER 7: DEVELOPMENT OF MODELS CORRELATING VIBRATION

### EXCITATION FORCES TO DYNAMIC CHARACTERISTICS OF

#### TWO-PHASE FLOW IN A TUBE BUNDLE..... 106

7.1 Abstract.....	107
-------------------	-----



7.2 Introduction.....	107
7.3 Experiment.....	109
7.3.1 Experimental set-up.....	109
7.3.2 Experimental results.....	112
7.4 Correlation between vibration excitation forces and the dynamic characteristics of two-phase flow.....	117
7.4.1 Model to correlate void fraction fluctuations in the main flow path and the dynamic drag forces.....	117
7.4.2 Model to correlate oscillations in the wake of the cylinders and the dynamic lift forces.....	124
7.5 Conclusion.....	127
7.6 Acknowledgments.....	128
7.7 References.....	128
 CHAPTER 8: DISCUSSIONS AND CONCLUSIONS .....	 130
8.1 Review of objectives.....	130
8.2 Further discussion.....	131
8.2.1 Periodic vortex shedding.....	132
8.2.2 Periodicity excited by shear layers.....	133
8.3 Main contributions.....	135
8.4 Recommendations for future work.....	137
 REFERENCES.....	 138
 APPENDIX.....	 147

## LIST OF TABLES

<b>Table 1.1</b>	Vibration excitation mechanisms in cross flow (Pettigrew et al. 1998).....	4
<b>Table 3.1</b>	Comparison between input and measured air flow rate.....	42
<b>Table 5.1</b>	Coherence between void fraction fluctuations and the dynamic lift and drag forces at the quasi-periodic frequency for 80% void fraction at 5 m/s pitch flow velocity.....	83
<b>Table 5.2</b>	Coherence between void fraction fluctuations and the dynamic lift and drag forces at the quasi-periodic frequency for 80% void fraction at 10 m/s pitch flow velocity.....	83
<b>Table 7.1</b>	Comparison between measured and estimated r.m.s. drag forces (N/m) within 0 to 20 Hz.....	123
<b>Table 7.2</b>	Comparison between measured and estimated r.m.s. drag forces (N/m) within 0 to 10 Hz.....	123
<b>Table 7.3</b>	Comparison between measured and estimated r.m.s. lift forces (N/m) at the dominant frequency.....	127

## LIST OF FIGURES

<b>Fig. 1.1</b>	Important FIV areas within a nuclear steam generator (This example is from a poster of a 600 MWe CANDU Advanced Series steam generator manufactured by Babcock and Wilcox International, Taylor, 1994).....	3
<b>Fig. 2.1</b>	Flow regimes in upward two-phase flow in vertical tubes: (a) Bubble flow, (b) Slug flow, (c) Churn flow, (d) Wispy-annular flow, and (e) Annular flow (Collier and Thome, 1996) .....	16
<b>Fig. 2.2</b>	McQuillan and Whalley flow pattern map for upward two-phase flow inside a vertical tube (McQuillan and Whalley, 1985) showing our flow condition data.....	17
<b>Fig. 2.3</b>	Grant map for two-phase cross flow in cylinder arrays (Pettigrew and Taylor 1994) showing our flow condition data.....	18
<b>Fig. 2.4</b>	Flow pattern map for two-phase cross cylinder arrays (Ulbrich and Mewes, 1994) showing our flow condition data.....	19
<b>Fig. 2.5</b>	Flow regime map for a normal square tube bundle and comparison with the map proposed by Ulbrich and Mewes (1994), taken from Noghrehkar et al. (1999).....	20
<b>Fig. 2.6</b>	Test loop.....	22
<b>Fig. 2.7</b>	Test sections: (a) Narrow test section and (b) Wider test section.....	24
<b>Fig. 2.8</b>	Sketch of strain gauge instrumented tube.....	25
<b>Fig. 2.9</b>	Principle of fiber-optic probe measurements: (a) Reflection and refraction (transmission) in a medium, (b) Total reflection in air, and (c) Refraction in water.....	27
<b>Fig. 2.10</b>	Double fiber-optic probe.....	28
<b>Fig. 2.11</b>	Sketch of electric circuit for fiber-optic probe measurement system.....	28
<b>Fig. 3.1</b>	Test loop.....	34

<b>Fig. 3.2</b>	Test section.....	35
<b>Fig. 3.3</b>	Double fiber-optic probe.....	36
<b>Fig. 3.4</b>	Void fraction measurement.....	37
<b>Fig. 3.5</b>	Bubble velocity and bubble size measurements.....	37
<b>Fig. 3.6</b>	Typical results of flow measurements: (a) Void fraction; (b) Bubble velocity; and (c) Bubble size.....	39
<b>Fig. 3.7</b>	Summary of results of flow measurements: void fraction (%) for $U_p=5\text{m/s}$ at (a) $\alpha=50\%$ , (b) $\alpha=80\%$ ; bubble velocity (m/s) for $U_p=5\text{m/s}$ at (c) $\alpha=50\%$ , (d) $\alpha=80\%$ .....	41
<b>Fig. 3.7</b>	<b>continued</b> Summary of results of flow measurements: Bubble size (mm) for $U_p=5\text{m/s}$ at (e) $\alpha=50\%$ , (f) $\alpha=80\%$ .....	42
<b>Fig. 3.8</b>	Typical dynamic force spectra.....	44
<b>Fig. 3.9</b>	Relationship between periodic force frequency and pitch velocity: (a) $\alpha=50\%$ and (b) $\alpha=80\%$ .....	44
<b>Fig. 3.10</b>	Relationship between r.m.s. periodic force and pitch velocity: (a) $\alpha=50\%$ and (b) $\alpha=80\%$ .....	45
<b>Fig. 4.1</b>	Test loop.....	51
<b>Fig. 4.2</b>	Test section.....	51
<b>Fig. 4.3</b>	Typical dynamic force spectra for the interior cylinder at 80% void fraction: (a) Lift force spectra and (b) Drag force spectra.....	54
<b>Fig. 4.4</b>	Relationship between periodic force frequency and pitch velocity.....	55
<b>Fig. 4.5</b>	Relationship between r.m.s. periodic force and pitch velocity.....	55
<b>Fig. 4.6</b>	Typical dynamic force spectra for the left interior half-length cylinder at 80% void fraction: (a) Lift force spectra and (b) Drag force spectra.....	55
<b>Fig. 4.7</b>	Typical dynamic force spectra for the right interior half-length cylinder at 80% void fraction: (a) Lift force spectra and (b) Drag force spectra.....	56
<b>Fig. 4.8</b>	Comparison of force spectra for 80% void fraction at 5 m/s pitch flow velocity: (a) Lift force spectra and (b) Drag force spectra.....	57

<b>Fig. 4.9</b>	Comparison of force spectra for 80% void fraction at 10 m/s pitch flow velocity: (a) Lift force spectra and (b) Drag force spectra.....	57
<b>Fig. 4.10</b>	Coherences of the two half-length cylinders for 80% void fraction: (a) at 5 m/s pitch flow velocity and (b) at 10 m/s pitch flow velocity.....	58
<b>Fig. 4.11</b>	Typical dynamic force spectra for the upstream cylinder at 80% void fraction: (a) Lift force spectra and (b) Drag force spectra.....	59
<b>Fig. 4.12</b>	Typical dynamic force spectra for the downstream cylinder at 80% void fraction: (a) Lift force spectra and (b) Drag force spectra.....	59
<b>Fig. 4.13</b>	Comparison of lift spectra along the flow path for 80% void fraction: (a) at 5 m/s pitch velocity and (b) at 10 m/s pitch velocity.....	60
<b>Fig. 4.14</b>	Comparison of drag spectra along the flow path for 80% void fraction: (a) at 5 m/s pitch velocity and (b) at 10 m/s pitch velocity.....	60
<b>Fig. 4.15</b>	Typical dynamic force spectra for the single cylinder at 80% void fraction: (a) Lift force spectra and (b) Drag force spectra.....	61
<b>Fig. 4.16</b>	The relationship between Lockhart-Martinelli parameter and Strouhal number (from Ref [14]).....	62
<b>Fig. 5.1</b>	Test section.....	69
<b>Fig. 5.2</b>	Idealized two-phase flow signal from fiber-optic probes.....	69
<b>Fig. 5.3</b>	Probe positions for flow measurements.....	71
<b>Fig. 5.4</b>	Typical dynamic force spectra for 80% void fraction at 5 m/s pitch flow velocity: (a) Lift force spectra and (b) Drag force spectra.....	72
<b>Fig. 5.5</b>	Typical dynamic force spectra for 80% void fraction at 10 m/s pitch flow velocity: (a) Lift force spectra and (b) Drag force spectra.....	73
<b>Fig. 5.6</b>	Power spectra of the local void fraction fluctuation at four different positions on the right side of the main flow path for 80% void fraction at 5 m/s pitch flow velocity: (a) L60° position, (b) L90° position, (c) U60° position, and (d) U90° position.....	74
<b>Fig. 5.7</b>	Power spectra of the local void fraction fluctuation at four different positions on the right side of the main flow path for 80% void fraction at 10	

- m/s pitch flow velocity: (a) L60° position, (b) L90° position, (c) U60° position, and (d) U90° position.....75
- Fig. 5.8** Power spectra of the local void fraction fluctuation at four different positions on the left side of the main flow path for 80% void fraction at 5 m/s pitch flow velocity: (a) L60° position, (b) L90° position, (c) U60° position, and (d) U90° position.....76
- Fig. 5.9** Power spectra of the local void fraction fluctuation at four different positions on the left side of the main flow path for 80% void fraction at 10 m/s pitch flow velocity: (a) L60° position, (b) L90° position, (c) U60° position, and (d) U90° position.....77
- Fig. 5.10** Power spectra of the local void fraction fluctuation at four different positions along the center line of the main flow path for 80% void fraction at 5 m/s pitch flow velocity: (a) L60° position, (b) L90° position, (c) U60° position, and (d) U90° position.....78
- Fig. 5.11** Power spectra of the local void fraction fluctuation at four different positions along the center line of the main flow path for 80% void fraction at 10 m/s pitch flow velocity: (a) L60° position, (b) L90° position, (c) U60° position, and (d) U90° position.....79
- Fig. 5.12** Power spectra of the local void fraction fluctuation at points L<sub>0</sub> and L<sub>1</sub> of U90° position: (a), (b) for 80% void fraction at 5 m/s pitch flow velocity, and (c), (d) for 80% void fraction at 10 m/s pitch flow velocity, respectively.....80
- Fig. 5.13** Two-phase flow structure in a rotated triangular tube bundle: (a) simplified figure (FP: flow path, SZ: “stagnation” zone), (b) flow picture (1: low void fraction mixture belonging to the stagnation zone, 2: oscillating high void fraction mixture in stagnation zone, 3: flow path, 4: rigid tubes).....81
- Fig. 5.14** Coherences between the local void fraction fluctuation and the dynamic lift and drag forces for 80% void fraction: (a), (b) void fraction fluctuation at L60°-C and drag force, and (c), (d) void fraction fluctuation at U90°-L and

	lift force, at 5 m/s and 10 m/s pitch flow velocity, respectively.....	82
<b>Fig. 6.1</b>	Test sections: (a) Narrow test section and (b) Wider test section.....	91
<b>Fig. 6.2</b>	Typical dynamic lift force spectra for water flow at 1 m/s pitch flow velocity: (a) single cylinder, (b), (c) and (d) two cylinders at different pitches (4.5D, 3D and 1.5D, respectively).....	93
<b>Fig. 6.3</b>	Typical dynamic lift force spectra for 80% void fraction at 5 m/s pitch flow velocity: (a) single cylinder, (b), (c) and (d) two cylinders at different pitches (4.5D, 3D and 1.5D, respectively).....	94
<b>Fig. 6.4</b>	Typical dynamic lift and drag force spectra for 80% void fraction at 5 m/s pitch flow velocity: (a) Lift force spectra and (b) Drag force spectra.....	95
<b>Fig. 6.5</b>	Typical dynamic lift and drag force spectra for 80% void fraction at 10 m/s pitch flow velocity: (a) Lift force spectra and (b) Drag force spectra.....	96
<b>Fig. 6.6</b>	Correlation of the lift and drag forces between different cylinder positions for 80% void fraction at 5 m/s pitch flow velocity: (a) Lift and (b) Drag...	97
<b>Fig. 6.7</b>	Correlation of the lift and drag forces between different cylinder positions for 80% void fraction at 10 m/s pitch flow velocity: (a) Lift and (b) Drag.....	97
<b>Fig. 6.8</b>	Comparison of the dynamic lift and drag forces between the wider test section and the narrow test section for 80% void fraction at 5 m/s pitch flow velocity: (a), (b) and (c) for lift forces, and (d), (e) and (f) for drag forces.....	99
<b>Fig. 6.9</b>	Comparison of the dynamic lift and drag forces between the wider test section and the narrow test section for 80% void fraction at 10 m/s pitch flow velocity: (a), (b), and (c) for lift forces, and (e), (f), and (g) for drag forces.....	100
<b>Fig. 6.9</b>	<b>continued</b> (d) for the lift force and (h) for the drag force.....	101
<b>Fig. 6.10</b>	Correlation of the lift and drag forces between different cylinder positions for 80% void fraction at 5 m/s pitch flow velocity: (a) Lift and (b) Drag.....	101

<b>Fig. 6.11</b>	Correlation of the lift and drag forces between different cylinder positions for 80% void fraction at 10 m/s pitch flow velocity: (a) Lift and (b) Drag.....	101
<b>Fig. 7.1</b>	Test section.....	110
<b>Fig. 7.2</b>	Idealized two-phase flow signal from fiber-optic probes.....	110
<b>Fig. 7.3</b>	The main flow path and probe positions for flow measurements.....	111
<b>Fig. 7.4</b>	Typical dynamic force spectra for 80% void fraction at 5 m/s pitch flow velocity: (a) Drag force spectra and (b) Lift force spectra.....	113
<b>Fig. 7.5</b>	Power spectra of the local void fraction fluctuation at four different positions on the right side of the main flow path for 80% void fraction at 5 m/s pitch flow velocity: (a) L60°-R position, (b) L90°-R position, (c) U60°-R position, and (d) U90°-R position.....	113
<b>Fig. 7.6</b>	Power spectra of the local void fraction fluctuation at four different positions on the left side of the main flow path for 80% void fraction at 5 m/s pitch flow velocity: (a) L60°-L position, (b) L90°-L position, (c) U60°-L position, and (d) U90°-L position.....	114
<b>Fig. 7.7</b>	Power spectra of the local void fraction fluctuation at four different positions along the center line of the main flow path for 80% void fraction at 5 m/s pitch flow velocity: (a) L60°-C position, (b) L90°-C position, (c) U60°-C position, and (d) U90°-C position.....	115
<b>Fig. 7.8</b>	Power spectra of the local void fraction fluctuation at points L <sub>0</sub> and L <sub>1</sub> of U90° position for 80% void fraction at 5 m/s pitch flow velocity.....	115
<b>Fig. 7.9</b>	Two-phase flow structure in a rotated triangular tube bundle: (a) simplified figure (FP: flow path, SZ: “stagnation” zone), (b) flow picture (1: low void fraction mixture belonging to the stagnation zone, 2: oscillating high void fraction mixture in stagnation zone, 3: flow path, 4: rigid tubes).....	116
<b>Fig. 7.10</b>	Sketch of 60° elbow for modeling drag forces.....	118
<b>Fig. 7.11</b>	Coherences between the local void fraction fluctuation at L60°-C and the dynamic drag force for 80% void fraction at 5 m/s pitch flow velocity....	124



<b>Fig. 7.12</b>	Sketch of 60° elbow for modeling lift forces.....	125
<b>Fig. 8.1</b>	Pressure spectra for a range of flow velocities for two tandem cylinders (D=12.7 mm, L/D=3, Mohany and Ziada, 2005).....	134
<b>Fig. 8.2</b>	Comparison of the Strouhal numbers of vortex shedding and at the onset of resonance for both the pre-coincidence range and the post coincidence range, ■, for pre-coincidence; ▲, for post-coincidence; ○, for vortex shedding (Mohany and Ziada, 2005), and Strouhal number for 80% homogeneous void fraction two-phase flow in this study. All values of Strouhal number are based on center-to-center distance $L$ .....	134

## LIST OF SYMBOLS

$A$	flow area [m <sup>2</sup> ]
$D$	tube diameter [m]
$d$	bubble size [m]
$d_e$	equivalent or hydraulic diameter (used twice the minimum gap) [m]
$e$	width of the wake [m]
$\bar{e}$	unit vector
$f$	frequency [Hz]
$f_s$	sampling rate of the probe signal [Hz]
$f_s$	Strouhal frequency [Hz]
$F_x(t)$	estimated dynamic lift force along the cylinder length [N/m]
$F_y(t)$	estimated dynamic drag force along the cylinder length [N/m]
$F_{Elbow,Y}^{rms}(t)$	r.m.s. drag excitation force of 60° elbow [N/m]
$F_Y^{rms}(t)$	r.m.s. drag excitation force along the cylinder length [N/m]
$g$	acceleration of gravity [m/s <sup>2</sup> ]
$L$	center to center distance between cylinders [m]
$L$	tube length [m]
$\dot{m}$	mass flux [kg/(m <sup>2</sup> s)]
$P$	tube pitch [m]
$P_t$	gauge pressure within test section [psi]
$Q$	volumetric flow rate [l/s]
$S$	sampling point of the probe signal
$S$	Strouhal number
$S_{F_{Elbow,Y}}(f)$	PSD of drag excitation force of 60° elbow [(N/m) <sup>2</sup> s]
$S_Y(f)$	PSD of drag excitation force per unit length [(N/m) <sup>2</sup> s]
$U$	flow velocity (m/s)
$X$	Martinelli parameter

$R$	radius of the center line of the main flow path [m]
$R_l$	mean radius of the wake in the main flow path [m]
$t$	time [s]
$T$	period of time [s]
$u(t)$	wake transverse oscillation velocity [m/s]
$V$	control volume of 60° elbow [m <sup>3</sup> ]
$V$	bubble velocity [m/s <sup>2</sup> ]
$x(t)$	wake transverse oscillation displacement [m]

### Greek

$\alpha$	homogeneous void fraction
$\alpha(t)$	instantaneous local void fraction
$\delta$	time lag between the inlet and outlet of 60° elbow [s]
$\mu$	dynamic fluid viscosity [Ns/m <sup>2</sup> ]
$\rho$	fluid density [kg/m <sup>3</sup> ]
$\rho$	homogeneous two-phase flow density [kg/m <sup>3</sup> ]
$\theta$	angular position along 60° elbow [rad]
$\tau$	gas phase contact time (with probe) [s]
$\tau$	time lag between the inlet and any position ( $\theta$ ) along 60° elbow [s]
$\omega$	angular frequency [rad/s]
$\Delta h_{tips}$	distance between two probe tips [m]
$\Delta T_i$	time difference of the $i^{th}$ gaseous particle touching two probes [s]

### Subscripts

$a$	air
$F$	force
$g$	gap
$g, G$	gas

<i>l, L</i>	liquid
<i>m</i>	flow meter
<i>p</i>	pitch
<i>pg</i>	pitch and gas
<i>s</i>	sampling
<i>S</i>	Strouhal
<i>S</i>	surface
<i>t</i>	test section
<i>V</i>	volume
<i>w</i>	water
<i>x, X</i>	horizontal direction
<i>y, Y</i>	vertical direction
$\infty$	free stream

### **Abbreviation**

FIV	flow-induced vibration
FP	flow path
PDF	probability density function
PSD	power spectral density
r.m.s.	root mean square
SZ	stagnation zone
STP	standard pressure
@ STP	at standard pressure

## CHAPTER 1

### INTRODUCTION

#### 1.1 Motivation

Flow-induced vibration (FIV) is becoming an important problem in power and process plant equipment. This is because high strength and lightweight materials, and advanced methods of analysis are used by design engineers to optimize costs and increase efficiency. This leads to greater structural flexibility, which often results in fluid-structure interaction problems. Thus, the study on flow-induced vibration became an important area of research. The nuclear industry has paid particular attention to this field, because nuclear component failures caused by FIV could force entire plant to shutdown for costly repairs and to suffer loss of production. Actually, the nuclear industry has played a leader role in flow-induced vibration research related to power plants and process equipment. Meanwhile, FIV research is also underway in other disciplines, such as the aircraft industry and civil engineering, where either aircraft wings might suffer from bending-torsion flutter, or civil engineering structures might suffer from fluidelastic instability.

Since 1980, a series of symposia on flow-induced vibration in heat exchangers or in reactor system components have been sponsored by the ASME (American Society of Mechanical Engineering). Many dedicated researchers from all over the world have contributed to the state of art in this field. So far, knowledge in the area of flow-induced vibrations has gradually accumulated and several relevant books (Blevins, 1990; Paidoussis, 1998; Au-Yang, 2001), which are very helpful to the researchers and practicing engineers in this field, have been published.

Several distinguished researchers (Pettigrew and Taylor, 1994; Pettigrew et al., 1998; Weaver et al., 2000) in flow-induced vibration have provided excellent reviews related to power and process plant components. These reviews not only outlined the state of the art in this field, but pointed out open questions and future work. Our attention will be focused on vibration problems in nuclear steam generator. A cut-out view of a CANDU 600 MW steam generator is given in Fig. 1.1. Several flow situations are possible in these recirculating-type steam generators. There are three cross flow areas which are labelled in Fig. 1.1. On the shell side, the tubes are subjected to water cross flow in the recirculated water entrance region near the tubesheet (label 1) and in the internal preheater region (label 2). Within the tube bundle, the shell-side flow is mostly axial. It is water at the bottom and gradually becomes water-steam two-phase as boiling occurs. As mentioned by Pettigrew et al. (1998), two-phase cross flow is predominant in the U-bend region (label 3) where the steam quality reaches 15-25% or even higher in some design. This corresponds to over 80% void fraction.

Generally four mechanisms are responsible for the excitation of tube arrays in cross flow (Pettigrew et al., 1998). These mechanisms are random turbulence buffeting, vortex shedding or Strouhal periodicity, fluidelastic instability and acoustic resonance. Table 1.1 summarizes these vibration mechanisms for a single cylinder and tube bundles in liquid, gas and two-phase flow, respectively. Of these four mechanisms, both fluidelastic instability and vortex shedding can cause large-amplitude vibration in a tube bundle and may quickly lead to catastrophic tube failures. Extensive research and advances in the areas of fluidelastic instability and vortex shedding within the last two or three decades made it possible for designers to predict and therefore eliminate the possibility of disastrous tube failures. However, unlike vortex-induced vibration, fluidelastic instability or acoustic resonance, turbulence-induced vibration is inherent to fluid flow and cannot be avoided in practice. Random excitation forces cause relatively small-amplitude vibrations that will not lead to short-term failure. These vibrations can

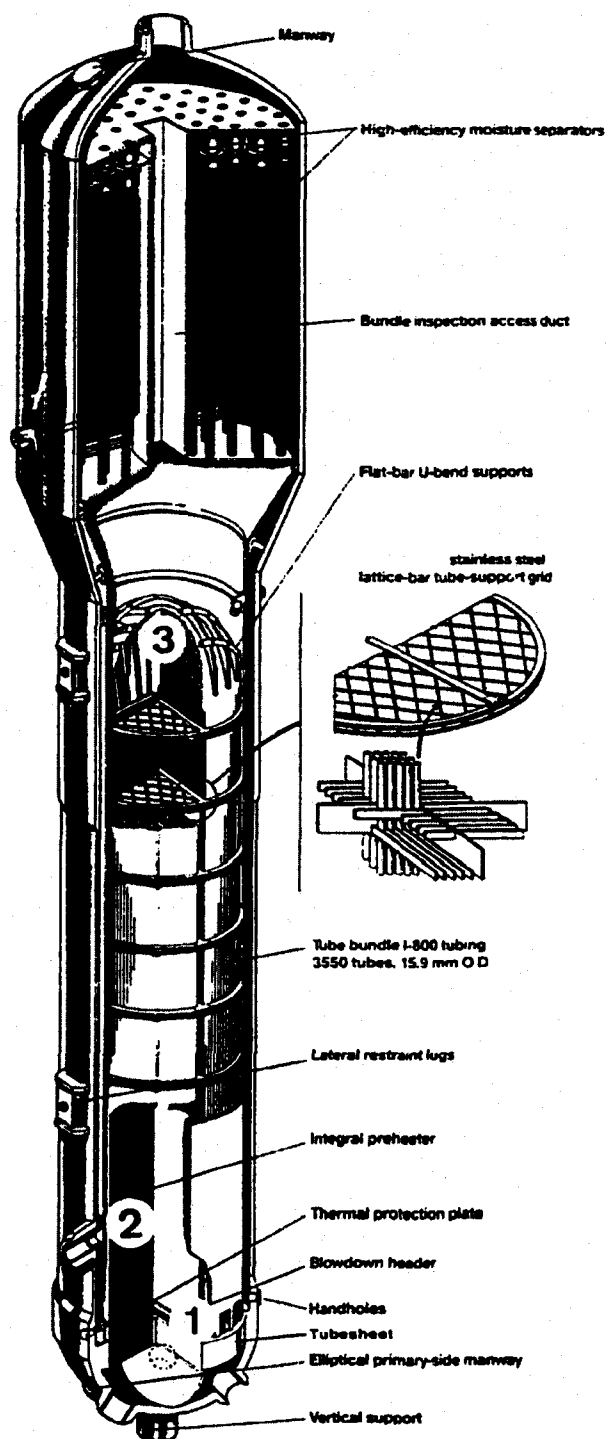


**Fig. 1.1** Important FIV areas within a nuclear steam generator  
 (This example is from a poster of a 600 MWe CANDU Advanced Series steam generator manufactured by Babcock and Wilcox International, Taylor, 1994)

lead to long-term fretting-wear, which results from progressive damage due to continuous rubbing of a tube against its supports. With the aging of nuclear reactors, the importance of random vibrations on the maximum safe operating lifetime of each component needs to be assessed. As well, the new design for more reliable and long lasting steam generators requires an accurate design guideline dealing with the random excitation. The study of random turbulence excitation becomes more urgent and necessary.

This study was originally oriented to the study of random excitation mechanisms in tube arrays subjected to two-phase air-water flow. To this end, the flow distribution within tube arrays and the resulting excitation forces are investigated. Experimental data generated from this study are expected to provide a good understanding of the underlying vibration mechanism. They are also expected to provide a database for the design of nuclear steam generator.

**Table1.1** Vibration excitation mechanisms in cross flow (Pettigrew et al., 1998)

Flow situation	Fluidelastic instability	Periodic shedding	Turbulence excitation	Acoustic resonance
<u>Single cylinder</u>				
Liquid	—	***	**	*
Gas	—	**	*	*
Two-phase flow	—	*	**	—
<u>Tube bundle</u>				
Liquid	***	**	**	*
Gas	***	*	*	***
Two-phase flow	***	*	**	—

\*\*\*Most important, \*\*Should be considered, \*Less likely, and —Does not apply



## 1.2 Review of the literature

Before further investigation on vibration excitation mechanisms in tube bundles due to two-phase cross flow is undertaken, it is appropriate to review the state of the art on two-phase cross flow in tube bundles and two-phase flow-induced vibration in tube bundles.

### 1.2.1 Two-phase cross flow in tube bundles

The nature of two-phase flow regimes inside tube bundles is an important consideration in predicting two-phase flow-induced vibration phenomena (Pettigrew and Taylor, 1994). Although many previous studies have addressed two-phase flow regimes inside tubes, much fewer experimental studies have dealt with flow regimes for upward two-phase flow across horizontal tube bundles. This is due to the fact that the measurements required for flow regime identification inside the tube bundle are more complicated, and therefore the experiments have mostly been restricted to visual observations of two-phase flow regimes from the outside of the tube bundle. Recently, several studies have shown that the flow regime in tube bundles can be identified by measuring the probability density function (PDF) with optical or resistivity void probes (Lian et al., 1997; Noghrehkar et al., 1999). It is expected that bubbly regime has a single low-frequency peak, annular-dispersed flow has a single high-frequency peak, and intermittent flow has either a broad-band PDF or it shows both peaks. Generally speaking, the visual observation technique for flow regime identification is limited to determine the flow regime near the shell. Void probe measurements show significantly different amplitudes of void fluctuations at different positions within a tube bundle. This implies that different flow regimes exist near the test section wall than inside the tube bundle.

Grant and Murray (1972) were the first to study two-phase flow regimes in tube bundles. They used a normal triangular tube bundle of  $P/D=1.25$ , with thirty nine 19

mm diameter tubes. Their experiments were carried out in vertical air-water cross flow, and the two-phase flow regimes were determined by visual observations through transparent tube end plates. They identified bubbly, intermittent and dispersed (spray) flow regimes and proposed a flow regime map based on dimensionless superficial gas and liquid velocities. Their flow regime map revised in terms of a Martinelli parameter,  $X$ , and a dimensionless gas velocity,  $U_g$ , may be found in Chapter 2.

Taylor et al. (1989) conducted two-phase cross flow studies related to turbulence-induced excitation, and reported some results on flow regime in tube bundles. They observed that two dominant flow regimes existed in the four tube bundle configurations (normal and rotated square, normal and rotated triangular) they tested. They found that continuous flow prevailed below 80-90% homogeneous void fraction, and intermittent flow occurred above 80-90% homogeneous void fraction. They described that intermittent flow was characterized by periodic flooding (mostly liquid) following by bursts of mostly gas flow. It was believed that continuous flow was mostly bubbly at lower void fractions and mostly froth at higher void fractions. They proposed the concept that bundle-scale flow regime and localized tube-scale (or inter-tube) flow regime are responsible for tube vibrations.

Dowlati et al. (1992) noted that some two-phase flow regimes, as determined by visual observation from outside the bundle, occurred under significantly different conditions from those observed in a circular tube. In particular, bubbly flow appeared to persist up to a much higher void fraction of about 60% compared to about 30% in tubes. They thought that visual observations of two-phase flow from outside the tube bundle may only determine the nature of flow near the wall, and that the actual flow regime inside the bundle may not be the same as that observed from outside.

Ulbrich and Mewes (1994) studied vertical two-phase air-water cross flow in a normal square tube bundle of  $P/D=1.5$ . Their test section included 10 rows of five 20 mm

diameter tubes, 200 mm in length, in each row. Flow regimes were determined by visual observation using still and video photography techniques, respectively. Time traces of pressure drop measured between the second and ninth row were also used to aid in their flow regime identification. This flow regime map is presented in Chapter 2.

Noghrehkar et al. (1999) conducted experiments on normal triangular and normal square tube bundles of  $P/D=1.47$ , which contained 26 and 24 rows of five 12.7 mm diameter tubes in each row, respectively. A resistivity void probe was used to measure the local void fraction and the probability density function (PDF) of local void fraction fluctuations. The measurements were used in an objective statistical method to determine the two-phase flow regime. They found that the intermittent flow regime persists up to much higher liquid flow rates compared to that in the flow regime map proposed by Ulbrich and Mewes (1994). They believed that this was due to the difference in the flow regime identification methods used. For the normal triangular tube bundle, it was found that the results were similar except that bubbly-intermittent flow regime transition occurred at higher gas flow rates compared to the normal square tube bundle. More efficient break-up of large gas slugs in rotated tube bundles was probably responsible for that. Their flow regime map may be found in Chapter 2.

Additionally, Azzopardi and Baker (2003) compiled the data from several studies on the periodic structure associated to different two-flow patterns. The accumulated database, containing more than 1250 points, showed similar trends in the characteristic frequency associated with two-phase flow. Their analysis shows that flow patterns in both vertical and horizontal pipes are characterized by periodic structures. Data were correlated as Strouhal number against the Lockhart-Martinelli parameter with some degree of success.

So far the study of the effect of two-phase periodic structures on vibration in tube bundles has not been reported.

### 1.2.2 Turbulence-induced excitation in tube bundles due to two-phase cross flow

Prior to 1980, very little work had been done to study flow-induced vibration of tube bundles subjected to two-phase cross flow. Pettigrew and Gorman (1973) were the first to conduct vibration experiments on tube bundles subjected to air-water two-phase cross flow. Their research remained the only source of two-phase vibration data until the 1980s (Taylor et al., 1996). Since then a few studies were conducted in this area, for examples, Heilker and Vincent (1981) in air-water cross flow, Axisa et al. (1984) in both air-water and steam-water cross flow, Pettigrew et al. (1989a, b) and Taylor et al. (1989) in air-water cross flow. An excellent review by Pettigrew and Taylor (1994) provided a complete overview of two-phase flow-induced vibration in nuclear power plant components.

Since 1994, several researchers have contributed relevant results, particularly, Feenstra et al. (1995, 2002) in Freon 11 two-phase flow, Mann and Marjinger (1995) in Freon 12 two-phase flow, Lian et al. (1997) in air-water cross flow, de Langre and Villard (1998) in air-water and steam-water cross flow, Nakamura et al. (1995, 2002), Mureithi et al. (2002) and Hirota et al. (2002) in steam-water cross flow. As well, comprehensive studies on vibration of tube bundles subjected to both air-water and Freon 22 two-phase cross flow were conducted at the Chalk River Laboratories by Taylor et al. (1996, 2001) and Pettigrew et al. (2001, 2002). In the above studies, almost all the aspects relevant to two-phase cross flow-induced vibrations, such as fluidelastic instability, random turbulence excitation, hydrodynamic mass, two-phase damping, effects of flow regime, of bundle configurations (including different tube diameters and pitch ratios), of different two-phase flow properties, on vibration excitation mechanisms, were investigated. Although some experimental and theoretical work on two-phase flow-induced vibration has been done, comparatively, the work on random turbulence excitation, especially on the fundamental excitation mechanism of turbulence in two-phase cross flow, is insufficient. A review of the scarce information on random

turbulence excitation in tube bundles subjected to two-phase cross flow is given as follows.

### **Experimental approaches to determine random excitation forces**

Generally, there are two experimental approaches to determine the magnitude of the power spectral density function (PSD) of random excitation due to two-phase cross flow (Taylor, 1994; Taylor and Pettigrew, 2000). The first is to measure directly the excitation forces with force transducers. The second is to deduce the excitation forces from the tube vibration response. With this method, usually strain gauges are used to measure tube response from which the excitation forces are deduced using random vibration theory. However, random theory involves some assumptions. For the experimental database (de Langre and Villard, 1998) available today, the second method was used more extensively. This is probably due to the fact that the experimental set-ups were primarily intended to study fluidelastic instability. However, the tube response measurements could be used to study random excitation at the flow rates below the onset of fluidelastic instability.

### **Two aspects of the study of random turbulence excitation**

Essentially, the study of random turbulence excitation is two-fold. First, there is the practical aspect which is to recommend useful design guidelines as discussed in Axisa et al. (1990), Taylor et al. (1996), and de Langre and Villard (1998). A second aspect is the fundamental understanding of turbulence excitation mechanisms (Taylor et al., 1994; Nakamura et al., 1995). Some researchers have addressed both aspects (Taylor et al., 1996; Pettigrew et al., 2001, 2002).

### **Effects of flow regimes (including void fraction and mass flux), of bundle configurations (including different pitch ratios), of different two-phase flow mixtures, on random excitation mechanism**

Pettigrew et al. (2001) conducted experiments on tube bundles of different geometries in air-water flow, such as normal and rotated triangular, as well as normal and rotated

square configurations of P/D of 1.2 to 1.5 over a range of mass flux and void fraction. They found that random turbulence is not much affected by pitch-to-diameter ratio (P/D) or by neighboring tube vibration, and that the vibration response is roughly proportional to the mass flux. They also found that the effect of tube bundle configuration is small. Pettigrew et al. (2002) found that random turbulence is much lower in Freon-134a than in air-water flow. It was also found that the effect of void fraction and mass flux is relatively small above 50% void fraction and is very different than air-water flow. They examined the effect of flow regime and found that the air-water flow tests fell in bubbly and plug flow regime while the Freon tests were in the bubbly to churn flow regime. They concluded that churn flow probably reduces the effect of changing void fraction and mass flux. Similar observations were reported by Pettigrew et al. (1995) for Freon-22 and Taylor et al. (1996) for air-water flow. Nakamura et al. (1995) conducted experiments on turbulent buffeting forces for both air-water and steam-water two-phase flows. It was found that the excitation forces in steam-water flow in slug and froth flow regimes are similar to those in air-water flow and that these excitation forces are primarily caused by impacting of the intermittently riding water slugs.

#### **Practical design guideline for random turbulence excitation**

Taylor et al. (1996) got data from two experimental programs to determine the characteristics of the random excitation forces due to air-water cross flow in tube bundles. Their tests were carried out on cantilevered, clamped-pinned, and clamped-clamped tubes in normal square, rotated and normal-triangular configurations. The experimental studies collected random excitation data using one of the two methods mentioned above. Power spectra were analyzed to determine the effect of parameters such as tube diameter, frequency, flow rate, void fraction, and flow regime on the random excitation forces. Normalized expressions for the excitation force power spectra were found to be flow-regime dependent. The proposed formulations could be used to produce preliminary two-phase flow design guidelines for random excitation of heat exchanger tubes.

de Langre and Villard (1998) investigated the random buffeting excitation forces exerted on tubes in tube bundles due to two-phase cross flow. The spectral magnitude of random forces was examined by using most of the available experimental data on direct or indirect force measurements in this area. Different fluid mixtures, such as steam-water, air-water and various types of Freon, as well as different thermo-hydraulic or geometrical situations were taken into account. A formulation was developed to analyse and scale two-phase flow data, in a manner similar in principle to that used successfully in the modelling of buffeting in single-phase flow. Dynamic pressure, viscosity and surface tension were not found to be relevant parameters, but gravity forces could be used to define appropriate dimensionless spectra for all cases. The proposed scaling parameters as well as the effects of flow regimes and fluid mixtures were discussed. An upper bound on the magnitude of random excitation forces, which could be used as a practical design guideline, was proposed.

#### **The study of fundamental turbulence excitation mechanisms**

Nakamura et al. (1995) conducted experiments on turbulent buffeting forces for both air-water flow and steam-water two-phase flows. The mechanism producing these forces, and a method for evaluating the tube response caused by two-phase flow, were presented. This work is probably one of the limited studies on the investigation of fundamental excitation mechanisms for turbulent buffeting in two-phase cross flow. They found that the peak value of the excitation force is relatively independent of gas flow velocity. It was concluded that the main source of buffeting forces in slug or froth two-phase flow is due to the impact forces caused by the intermittently rising water slugs. An empirical treatment was introduced to deal with excitation forces. The slug speed, the fluid forces acting on the tube, and the period of occurrence of the rising water slug were estimated. The accuracy of this prediction method was estimated by comparing the theoretical response with the measured one.

Taylor (1994) indicated that broad frequency peaks are found in the two-phase flow power spectra at higher void fractions and these frequency peaks often dominate the power spectra and significantly affect the r.m.s. excitation forces. It was found, after detailed investigation that these broad frequency peaks were not related to acoustic pressure pulses. It was concluded that these broad frequency peaks due to the presence of bubble-like structures in the two-phase mixture. It was pointed out that the bubble size and pitch velocity can be related to the frequency at which bubbles are passing a tube. Limited bubble size measurements were taken. However, more attention was paid to formulate dimensionless power spectra for collapsing the data for the purpose of a design guideline. The mechanism for these broad frequency peaks was not explored in details. It may be useful to mention that the broad frequency peaks observed by Taylor (1994) were based on dimensionless force spectra similar to those for collapsing single-phase flow data. Further analysis of the force spectra directly obtained from force measurements revealed quasi-periodic forces or narrow frequency peaks. Pettigrew et al. (2005) also found that unexpected but significant quasi-periodic forces exist in both the drag and lift direction. Further investigations on these forces are needed.

### **1.3 Objectives**

It may be inferred from the above review that the understanding of random vibration excitation mechanisms in tube bundles subjected to two-phase cross flow are not fully reached. Detailed measurements of two-phase flow and excitation forces are required to understand the underlying random excitation mechanisms. Additionally our preliminary results (Pettigrew et al., 2005) show that unexpected but significant quasi-periodic forces were measured in both the drag and lift direction. Further investigations in the magnitudes and origin of these forces are needed. Detailed two-phase flow and force measurements within the tube bundle are proposed in this study. Then, this information will be used to understand periodic and random vibration excitation mechanisms in two-phase cross flow.



The general objective of this work is to understand the underlying vibration excitation mechanisms in tube bundles subjected to two-phase cross flow. More specifically, the intention is to conduct detailed measurements of two-phase flow characteristics and excitation forces, and then use this information to correlate quasi-periodic and random turbulence excitation forces with the dynamic characteristics of two-phase flow. Specific objectives of this study are:

- 1) To measure the detailed characteristics of two-phase flow such as void fraction, bubble velocity and bubble size between the tubes at different position in the test section;
- 2) To determine experimentally the excitation forces associated with heat exchanger tubes subjected to two-phase cross flow. The test matrix will encompass a wide range of flow conditions with a rotated-triangular array of cylinders;
- 3) To correlate quasi-periodic and random turbulence excitation forces with the dynamic characteristics of two-phase flow; and
- 4) To understand the nature of periodic and random turbulence excitation forces.

#### **1.4 Thesis outline**

This thesis consists of eight chapters including this chapter. The second chapter is dedicated to the description of the experimental methods and two-phase flow. The third to seventh chapter addresses the above objectives in the form of papers having their own abstract, introduction, method, results, discussion, and list of references. Further discussions, full conclusions and recommendations will be given in Chapter 8. Finally, appendix is given at the end of the thesis, which contains the tables and figures of results, as well as some additional experimental details.

## CHAPTER 2

### EXPERIMENTAL CONSIDERATIONS

The experimental portion of this study was carried out by the author in the laboratory of the BWC/AECL/NSERC Chair of Fluid-Structure Interaction, École Polytechnique de Montréal. This chapter describes the nature of two-phase-flow, the experimental apparatus and the method.

#### 2.1 Two-phase flow

As mentioned in Section 1.2.1, the nature of two-phase flow regimes inside tube bundles is an important consideration in understanding two-phase flow-induced vibration phenomena (Pettigrew and Taylor, 1994). The state of the art on two-phase flow regime in tube bundles was reviewed in Section 1.2.1. In this section, flow parameter definitions are first introduced. Then, a more detailed introduction on two-phase flow is presented. It includes upward two-phase flow inside vertical tubes and vertical two-phase cross flow in tube bundles.

##### 2.1.1 Flow parameter definitions

The analysis of two-phase flow-induced vibration requires suitable parameters to express the experimental data. Two-phase flow mixtures are rarely homogeneous or uniform across a flow channel. For example, there may be more liquid near the channel walls and the average flow velocity of the gas phase may be somewhat higher than that of the liquid phase causing slip between the phases (Pettigrew and Taylor, 1994). For the sake of simplicity, a homogeneous two-phase model without slip between the two phases is used in this thesis. According to this model, the homogeneous void fraction is given by

$$\alpha = \frac{Q_a}{Q_a + Q_w} \quad (2-1)$$

where  $Q_a$  and  $Q_w$  are the volume flow rates of air and water, respectively.

Using this homogeneous void fraction, the homogeneous density,  $\rho$ , freestream velocity,  $U_\infty$ , and freestream mass flux,  $\dot{m}_\infty$ , are defined as follows:

$$\rho = \alpha\rho_a + (1 - \alpha)\rho_w \quad (2-2)$$

$$U_\infty = \frac{(\rho_a Q_a + \rho_w Q_w)}{\rho A_\infty} = \frac{Q_a + Q_w}{A_\infty} \quad (2-3)$$

$$\dot{m}_\infty = \rho U_\infty \quad (2-4)$$

where  $A_\infty$  is the freestream cross-sectional area (see Section 2.2.2). Regardless of tube bundle configuration or orientation, the reference gap velocity (also called the pitch velocity) is defined as

$$U_p = U_\infty \left( \frac{P}{P - D} \right) \quad (2-5)$$

where  $P$  is the pitch or distance between tube centres and  $D$  is the tube diameter.

Similarly, the pitch mass flux,  $\dot{m}_p$ , and the tube bundle flow area,  $A_p$ , are defined as

$$\dot{m}_p = \dot{m}_\infty \frac{P}{P - D} = \rho U_p \quad (2-6)$$

$$A_p = A_\infty \frac{(P - D)}{P} \quad (2-7)$$

### 2.1.2 Upward two-phase flow inside vertical tubes

Several studies on two-phase flow patterns or regimes in upward flow inside vertical tubes have been conducted (Taitel et al., 1980; McQuillan and Whalley, 1985). Some

general conclusions have already been reached. The flow patterns most commonly recognized in upward air-water flow in a vertical tube are shown in Fig. 2.1. Four main flow patterns, namely, bubble flow, slug flow, churn flow and annular flow (including wispy annular flow) may be distinguished. The patterns found in air-water flow are also expected to be found in steam-water flow. When two-phase flow occurs in tubes, it is often important to be able to predict which flow pattern is likely to occur for a given combination of phase properties and flow rates and for any given tube diameter. Flow pattern predictions are usually obtained from flow pattern maps. There are two types of flow maps. One is based on experiment, and the other is deduced from theory. Most of the experimental work has been done in small diameter tubes containing low pressure air-water flow and high pressure steam-water flow. One example of a flow map from such data is given in Fig.2.2 (McQuillan and Whalley, 1985). The abscissa and ordinate axes of the flow map define the gas and liquid-phase superficial velocity, respectively. This map can be used in determining the flow regimes found in upward two-phase flow. Our flow condition data are also shown in Fig.2.2.

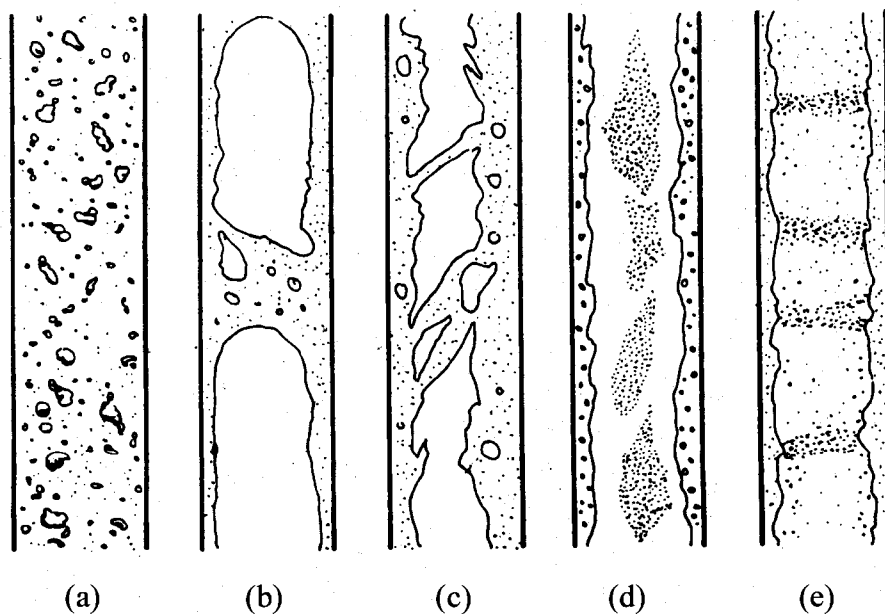


**Fig. 2.1** Flow regimes in upward two-phase flow in vertical tubes: (a) Bubble flow, (b) Slug flow, (c) Churn flow, (d) Wispy-annular flow, and (e) Annular flow (Collier and Thome, 1996)

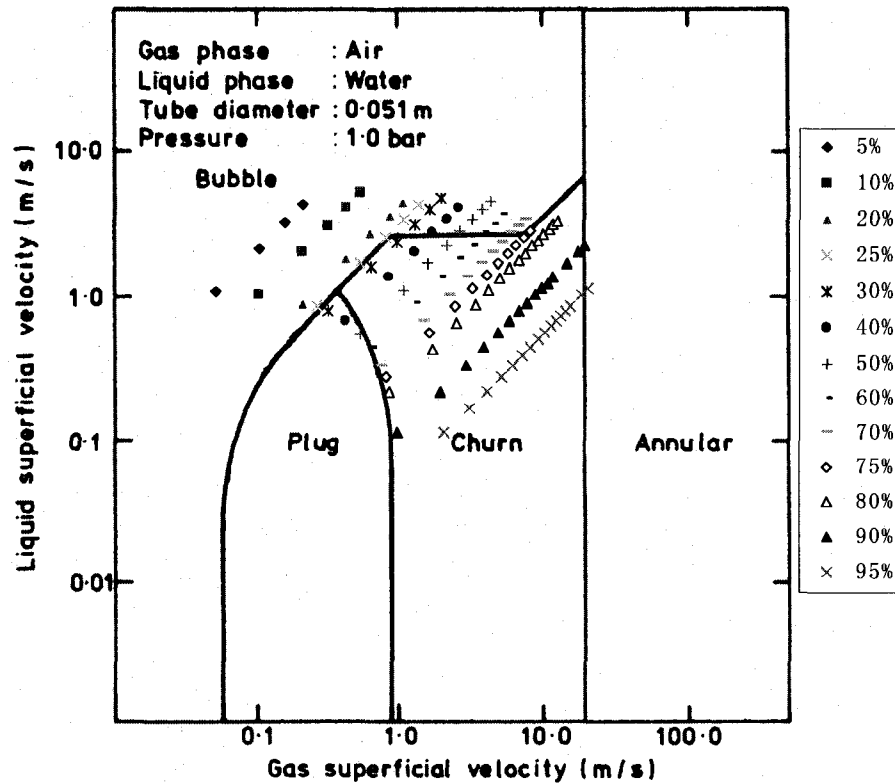


Fig. 2.2 McQuillan and Whalley flow pattern map for upward two-phase flow inside a vertical tube (McQuillan and Whalley, 1985) showing our flow condition data

### 2.1.3 Two-phase cross flow in tube bundles

The flow regimes in a tube bundle will be different than those in upward flow inside vertical tubes due to the presence of a tube bundle in an open channel. As discussed in Section 1.2.1, very few researchers have examined flow regimes in vertical cross flow over tube bundles. Grant and Murray (1972) were the first to study two-phase flow regime in a tube bundle. They identified bubbly, intermittent and dispersed (spray) flow regimes and proposed a flow regime map based on dimensionless superficial gas and liquid velocities. A revised Grant's map is as shown in Fig. 2.3. The abscissa is the Martinelli parameter,  $X$ , which, in this case, is defined assuming turbulent homogenous flow and assuming that the total mass flux,  $\dot{m}$ , is equal to  $(\dot{m}_g + \dot{m}_l)$ . This Martinelli parameter can be calculated using the following equation:

$$X = \left( \frac{1-\alpha}{\alpha} \right)^{0.9} \left( \frac{\rho_l}{\rho_g} \right)^{0.4} \left( \frac{\mu_l}{\mu_g} \right)^{0.1} \quad (2-8)$$

where  $\mu_l$  and  $\mu_g$  are the dynamic viscosity of water and gas, respectively. The ordinate is the dimensionless gas velocity,  $U_g$ , defined as follows:

$$U_g = \frac{\dot{m}_{pg}}{\left[ d_e g \rho_g (\rho_l - \rho_g) \right]^{0.5}} \quad (2-9)$$

where  $d_e \cong 2(P-D)$ , is the equivalent (or hydraulic) diameter,  $\dot{m}_{pg}$  is pitch mass flux of gas, and  $g$  is the acceleration due to gravity.

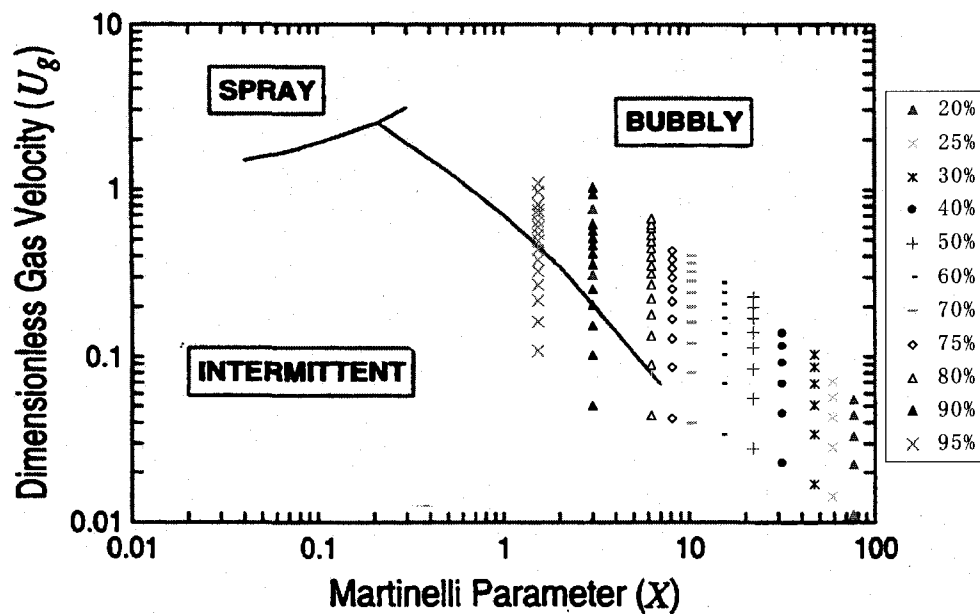
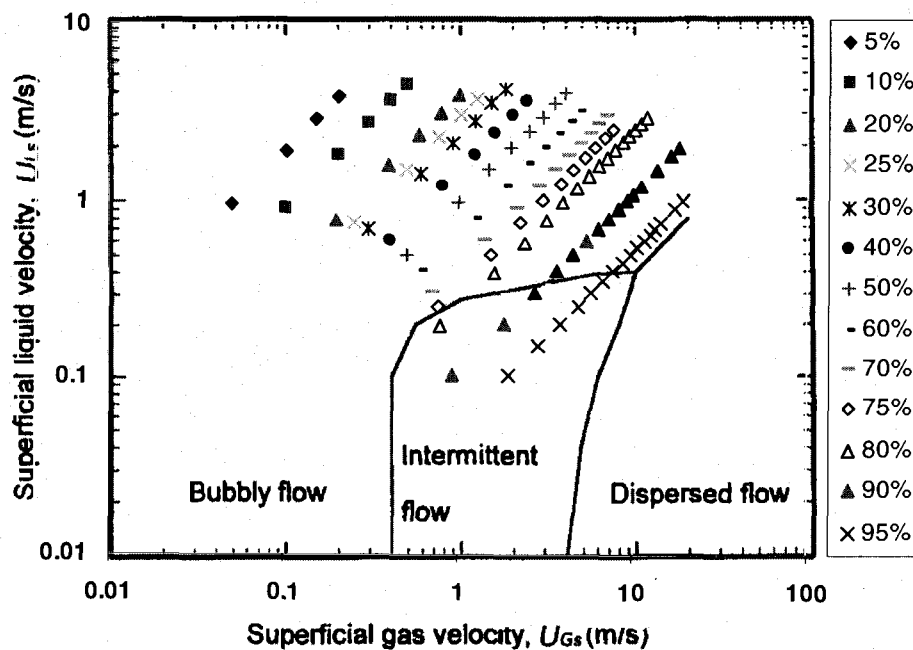


Fig. 2.3 Grant map for two-phase cross flow in cylinder arrays (Pettigrew and Taylor, 1994) showing our flow condition data

In Grant's map, bubble flow and dispersed (spray) flow probably are better be described as "continuous flow", while intermittent flow is characterized by periodic flooding (mostly liquid) followed by bursts of mostly gas flow (Taylor et al., 1989). Our flow condition data are also shown in Fig.2.3.

Ulbrich and Mewes (1994) performed a comprehensive analysis of available flow regime data resulting in flow regime boundaries that cover a much larger range of flow rates. They found that their new transition lines had an 86 percent agreement with available data. Their flow map is shown in Fig. 2.4. Our flow condition data are also shown in Fig.2.4. If this map is compared with Grant's map by using our flow condition data, it seems that they fit quite well, especially the transition between intermittent flow to continuous flow.



**Fig. 2.4** Flow pattern map for two-phase cross cylinder arrays (Ulbrich and Mewes, 1994) showing our flow condition data

Almost every study of flow regimes in tube bundles has concluded that three distinct flow regimes, namely, bubble flow, intermittent flow and dispersed flow exist. More recently, Noghrehkar et al. (1999) developed a flow regime map by measuring the probability density function (PDF) of the gas component of the flow. Their flow map is shown in Fig. 2.5 (Noghrehkar et al., 1999). Our flow condition data are not shown in Fig.2.5. Datum points in Fig.2.5 are from Noghrehkar et al. (1999).

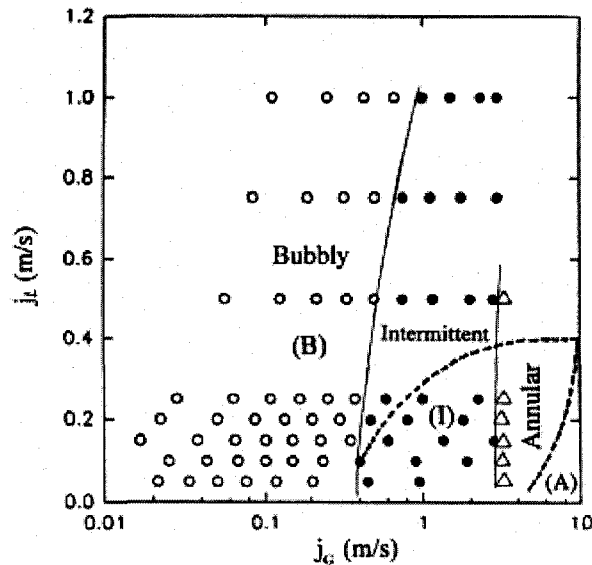


**Fig. 2.5** Flow regime map for a normal square tube bundle and comparison with the map proposed by Ulbrich and Mewes (1994), taken from Noghrehkar et al. (1999)

#### 2.1.4 Air-water and steam-water

The two-phase mixtures used in this study is air-water flow, which is the most economic and safe, and therefore most commonly used by researchers in this area. In reality steam generators operate in steam-water two-phase flow. However, steam-water experiments are relatively more costly and difficult due to the higher temperatures and pressures. Some two-phase flow mixtures, like various types of Freon, which are quite close to steam-water in property ratios between the two phases, are also used as working fluids. In all cases, one question is left which is how to find suitable methods for scaling the two-phase flow-induced vibration data.

Axisa et al. (1984) showed that the test using air-water flow instead of steam-water flow is valid for fluidelastic instability over the range of flow regimes they have encountered. Damping appears to be somewhat smaller in steam-water than in air-water mixtures, at least for higher void fractions. This was attributed to differences in surface tension, viscosity, density ratio between phases and flow regime characteristics of the flow. For turbulence-induced excitation, Taylor et al. (1989) believed that air-water mixtures



provide a conservative approximation to the random excitation forces that a steam-water mixture would produce, since the properties of steam and water are more closely matched.

## **2.2 Experiments**

### 2.2.1 Experimental approach

An experimental program was undertaken with rotated triangular tube arrays subjected to air-water flow to simulate two-phase mixtures. The arrays, which had a pitch-to-diameter ratio of 1.5, were made of relatively large diameter cylinders (38 mm). This resulted in larger gaps (19 mm) between cylinders to allow for detailed two-phase flow measurements.

Two kinds of experiments were carried out, one was to measure the dynamic characteristics of two-phase flow such as void fraction, bubble velocity and bubble size. The other was to measure the vibration excitation forces generated within the tube bundle subjected to two-phase cross flow.

Fiber-optic probes were developed to measure the dynamic characteristics of two-phase flow. Both the dynamic lift and drag forces were measured with strain gauge instrumented cylinders. An attempt was made to use this information to understand vibration excitation mechanisms in two-phase cross flow.

### 2.2.2 Air-water loop

The loop comprised a 25 l/s variable speed pump, a magnetic flow meter, a 2500 l tank, a 250 l/s compressed air supply system and connecting piping as shown in Fig. 2.6. The compressed air was injected below a suitably designed mixer to homogenize and

distribute the two-phase mixture uniformly below the test-section. The air flow was measured with orifice plates connected to a differential pressure transducer and electronic readout system. The loop was operated at room temperature and the pressure in the test section was slightly above atmospheric. A short description of each component is given as follows.

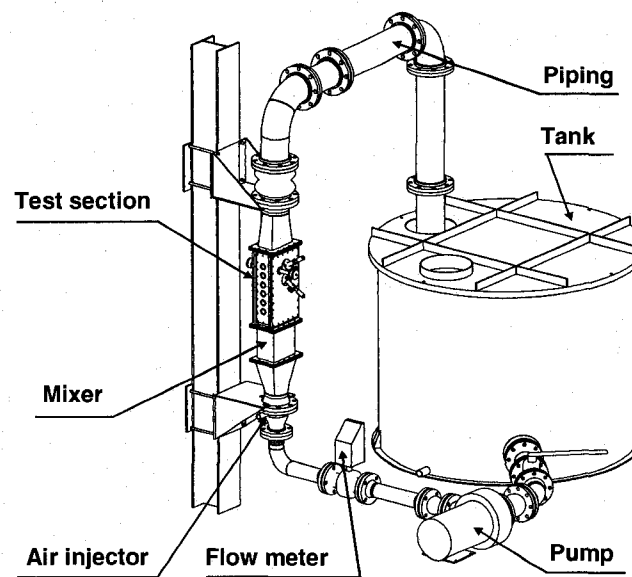


**Fig. 2.6** Test loop

### **Water pump**

A Goulds Model SSH 23SH2K5E0 electric variable speed pump is used to circulate water inside the loop. It can provide a maximum gauge pressure of 103 kPa (15 psig). Combined with the two-phase flow loop, the maximum flow rate is approximately 30 l/s.

### **Water flowmeter**

A Danfoss type Mag 5000 magnetic flowmeter located at a reasonable distance from the exit of the pump was used to measure the water flow rate. The precision of the reading is a half percent of the measured value.

**Air injector**

The air injector is located in the downstream of the water flowmeter. The compressed air comes from the service air supply at 689 kPa gauge press (100 psig). The flow rate is controlled by a manual valve located near the air-water loop. The maximum capacity available is around 500 SCFM (236 l/s at standard atmospheric conditions, i.e. 101.3 kPa and 21 °C).

**Orifice plate (not shown)**

Two Rosemont Type 1195 orifice plates installed in the compressed air supply system are used to measure the air flow. The bore size of the first orifice plate is 13 mm in diameter. It is used for air flows between 10 and 50 SCFM (4.7 and 23.6 l/s at STP). The second plate has a 30 mm bore diameter for air flows between 50 and 500 SCFM (23.6 and 236 l/s at STP). The possible measurement error of the two plates is one and half percent of the nominal value.

**Test sections**

Two different test sections were used in this study. They were 495 mm high vertical rectangular boxes with horizontal cross sections of 99×191 mm and 199×191 mm, respectively, as shown in Fig. 2.7. They were placed vertically at a distance of about 1.5 m above the laboratory floor. The narrow test section consists of a column of six 38 mm diameter cylinders flanked on either side by half cylinders to simulate essentially the flow path in a large array of cylinders in a rotated triangular configuration. The wider test section is similar but includes three columns of cylinders instead of one. The tube free-end wall and the two side walls, as well as the tubes are all made from transparent acrylic, which allowed for flow visualization.

**Mixer**

A static mixer, which consists of parallel corrugated steel sheets (1/32 inch or 0.8 mm thick) assembled in a crisscross pattern at 45 degrees to the flow direction, is used to homogenize the two-phase mixture upstream of the test section.

### Water tank

At the downstream end, a 2500 liter tank collects the two-phase mixture. Water is stored to be recirculated in the loop while the air escapes through a port located on the top of the tank.

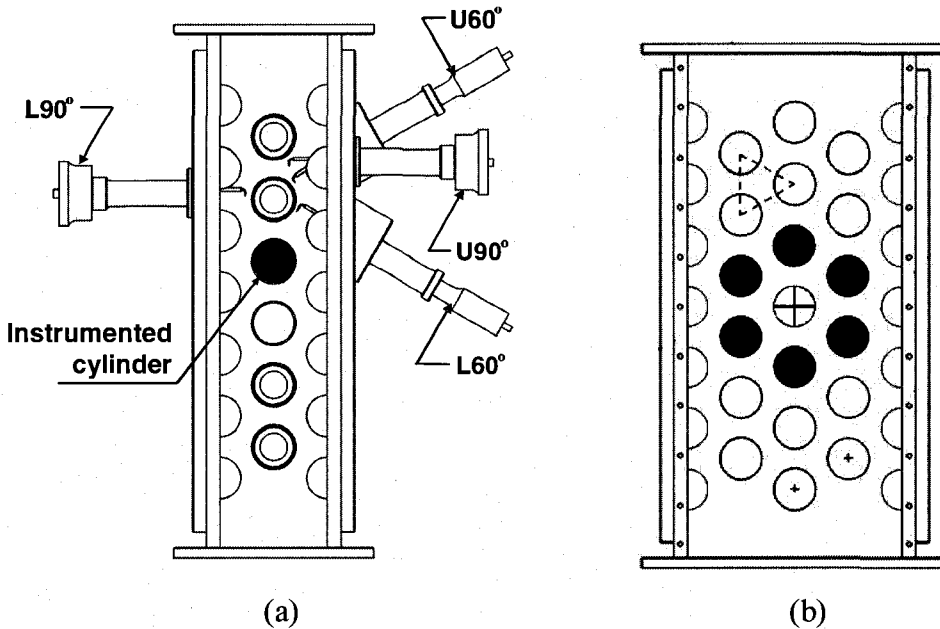


Fig. 2.7 Test sections: (a) Narrow test section and (b) Wider test section

### 2.2.3 Tube geometries

The 38 mm diameter tubes were arranged in five different configurations.

- 1) A single tube with half-tubes at the side walls in the narrow test section;
- 2) A single tube without half-tubes at the side walls in the narrow test section;
- 3) Two tubes with three different pitch along the flow in the narrow test section (without half-tubes at the side walls);
- 4) Rotated triangular tube bundles of 6 rows with  $P/D=1.5$  in the narrow test section;
- 5) Rotated triangular tube bundles of 7 rows with  $P/D=1.5$  in the wider test section.

The tube material was transparent acrylic. The tubes are 191 mm in length and have a wall thickness of 1.70 mm. All the tubes were empty. The natural frequencies (cantilevered tube) are 70 Hz in water and 70 to 150 Hz in air-water mixtures.

#### 2.2.4 Instrumentation

The vibration excitation forces were measured with Vishay CEA-06-125UN-350 strain gauges, which were glued with epoxy to the inner diameter of the tube and located as close as possible to the fixed end. Two pairs of diametrically opposite strain gauge were installed in each tube at 90 degrees from one to another to measure the forces in flow direction (drag) and in the direction normal to the flow (lift). The strain gauge instrumented tube is shown in Fig. 2.8. The strain gauge pairs were connected to a Wheatstone bridge in half-bridge configuration. The natural frequency of the cantilever cylinders was much higher (i.e., >150Hz) than the excitation force frequencies such that the cantilever cylinder functioned essentially as a dynamic force transducer. Before the instrumented cylinder was inserted into the test section, the static strain-force relation was determined via a careful calibration. Detailed calibration data may be seen in appendix.

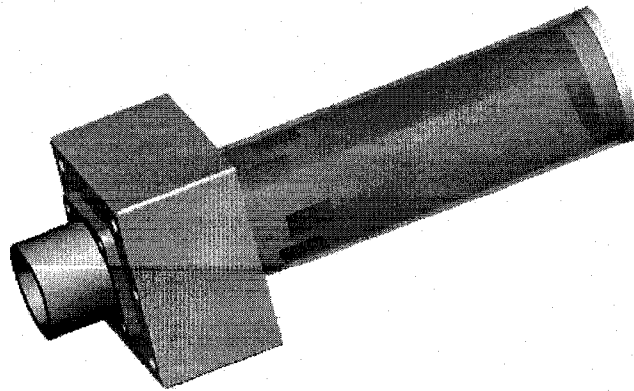


**Fig. 2.8** Sketch of strain gauge instrumented tube

The signals from strain gauges were routinely recorded and analyzed on an OROS 38 8-32 channel real-time multi-analyzer/recorder coupled to a microcomputer. A sampling rate of 2 kHz was chosen. For each test run, sufficient time was allowed for a steady state to be attained (usually 5 minutes). The NV Gate software coupled with the OROS dynamic analysis system was used to carry out correlation and spectral analyses of the vibration excitation forces.

#### 2.2.5 Fiber-optic probe tests

##### **Principle of fiber-optic probe measurements**

Fiber-optic probes were used to measure two-phase flow characteristics, such as void fraction, bubble velocity and bubble size. Bubble passage frequency could also be deduced from the analysis of the probe signal in the frequency domain. Other non-intrusive methods such as the absorption of X and  $\gamma$ -rays as well as Laser-Doppler techniques are often used to measure void fraction but they have limitations that made them unsuitable for this application. The X and  $\gamma$ -ray absorption technique yields only a chord-averaged value of the void fraction and require complicated data analysis, while the Laser-Doppler technique can not measure high void fractions (Taylor, 1994). Therefore, it is appreciate to use fiber-optic probe techniques for measuring local void characteristics over a large range of void fractions.

Fiber-optic probe techniques for measuring void fraction are generally based on the Snell-Descartes refraction law and take advantage of the fact that the indices of refraction of liquid and gas phases are quite different. As liquid-gas interfaces pass by the tip of the fiber-optic probe, the system changes from a refraction state to a total reflection state. Fiber-optic probe acts as a phase sensor based on this. Phase detection occurs at the surface of the probe tip. Let us take two-phase air-water flow as an example. The refractive indices of air, water and glass fiber, are 1.0, 1.33 and 1.46, respectively. The surface of the probe tip will reflect incoming light internally if air

surrounds it due to higher refractive index of air than that of glass fiber, and will refract light if water surrounds it due to the similar refractive indices of the water and the glass fiber. A receptor is designed to accept the reflected light and to transform this optical signal into an electrical signal. Thus, the probe produces a signal which clearly discriminates gas from liquid as they appear at the probe tip. This signal can be processed into 0-1 ideal signal, where 1 means air phase and 0 means water phase. Fig. 2.9 shows the principle of fiber-optic probe measurements.

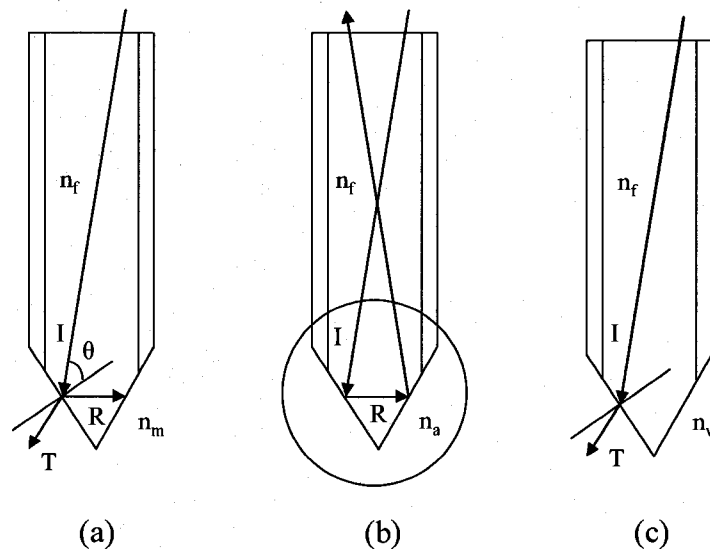


**Fig. 2.9** Principle of fiber-optic probe measurements: (a) Reflection and refraction (transmission) in a medium, (b) Total reflection in air, and (c) Refraction in water

### Fiber-optic probe measurement system

The multimode fiber used in this study, was made by Ceram Optecs. The diameters of core, cladding and coating, are 100, 140 and 170  $\mu\text{m}$ , respectively. Fig. 2.10 shows a double fiber-optic probe, which comprises two fiber-optic probes inserted in one stainless tube. The probe tips are 150  $\mu\text{m}$  apart axially. Each probe has a conical tip made by chemical etching with hydrofluoric acid.

The sketch of the electric circuit for the fiber-optic probe measurement system is shown in Fig. 2.11. It consists of one laser source with 30 mW power and  $832 \pm 15 \mu\text{m}$

wavelength, two photo-detectors with  $4 \mu\text{A}/\mu\text{W}$  sensitivity, two charge amplifiers, two couplers and one scope. The output signal was recorded with a NI PCI-6110 data acquisition card with high sampling rate. Fiber-optic probe data were analyzed in 20-s samples at a frequency of  $2 \times 10^6$  Hz, with a custom-built LabView<sup>TM</sup> program that provided bubble (void) periods and void fractions.

### Determination of the two-phase flow characteristics

Refer to Chapter 3.

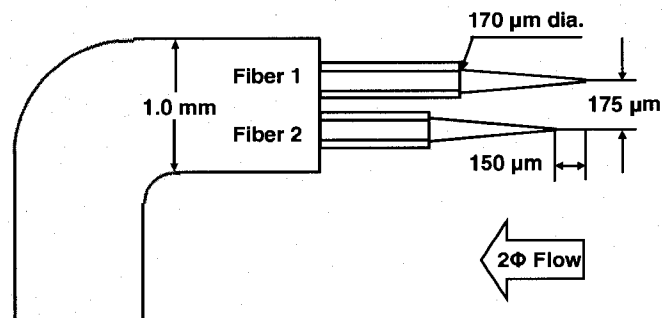


Fig. 2.10 Double fiber-optic probe

### Optical System

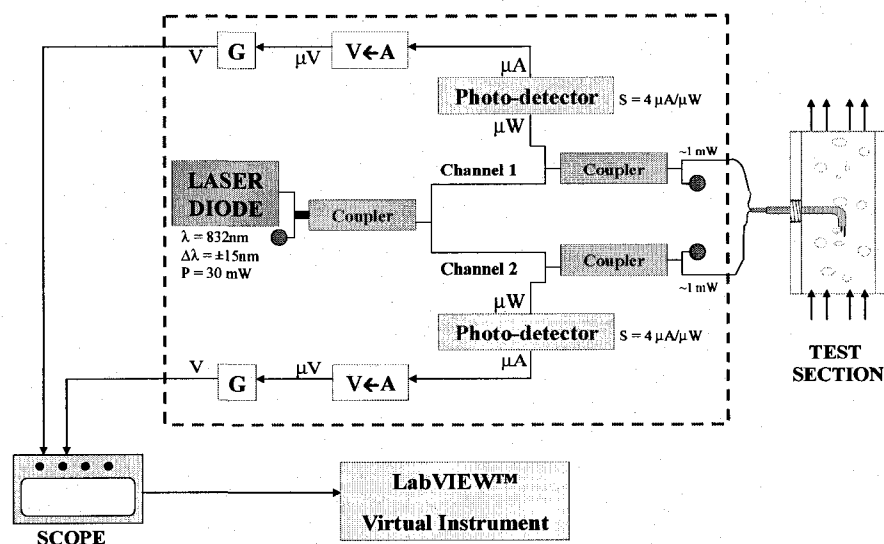


Fig. 2.11 Sketch of electric circuit for fiber-optic probe measurement system



### 2.2.6 Test conditions

#### **Flow measurements**

At the beginning some flow measurements were conducted in the narrow test section. Typical test cases at 50% and 80% homogeneous void fraction at 5 m/s pitch flow velocity were carried out.

#### **Force measurements**

Force measurements were taken over a homogeneous void fraction range from 5% to 95% and a pitch flow velocity range from 1 m/s to 20 m/s in the narrow test section. Later similar tests were carried out for 80% and 90% homogeneous void fractions and a pitch flow velocity range from 1 m/s to 10 m/s in the wider test section. The later tests aim at verifying the existence of quasi-periodic drag and lift forces in a more realistic larger tube array.

#### **Simultaneous flow and force measurements**

Two-phase flow, and dynamic lift and drag force measurements were performed simultaneously. Four flow conditions were investigated in detail, i.e., 80% and 90% homogeneous void fractions at a nominal pitch flow velocity of 5 m/s and 10 m/s. These measurements were taken to understand the nature of the observed drag and lift quasi-periodic forces.

Detailed flow conditions are given in the appendix A1.

### 2.2.7 Experimental results

Experimental and analytical results are presented in the form of the following technical papers. Additionally, the appendix contains the tables and figures outlining the results, as well as some additional experimental details.

### 2.3 List of publications

The following papers have been submitted for publications during the course of this PhD program, three of which have been published, and one of which has been accepted.

- 1). M. J. Pettigrew, **C. Zhang**, N. W. Mureithi and D. Pamfil, Detailed flow and force measurements in a rotated triangular tube bundle subjected to two-phase cross flow, *Journal of Fluids and Structures* 2005; 20 (4): 567-575.
- 2). **C. Zhang**, M. J. Pettigrew, and N. W. Mureithi, Vibration excitation force measurements in a rotated triangular tube bundle subjected to two-phase cross flow, *ASME Journal of Pressure Vessel Technology* 2007; 129 (1): 21-27.
- 3). **C. Zhang**, M. J. Pettigrew, and N. W. Mureithi, Correlation between vibration excitation forces and the dynamic characteristics of two-phase cross flow in a rotated triangular tube bundle, *ASME Journal of Pressure Vessel Technology* 2008; 130 (1).
- 4). **C. Zhang**, M. J. Pettigrew, and N. W. Mureithi, Further study of quasi-periodic vibration excitation forces in rotated triangular tube bundles subjected to two-phase cross-flow, *ASME Journal of Pressure Vessel Technology* (Accepted for publication September 2007).
- 5). **C. Zhang**, M. J. Pettigrew, and N. W. Mureithi, Development of models correlating vibration excitation forces to dynamic characteristics of two-phase flow in a tube bundle, *International Journal of Multiphase Flow* (Submitted October 2007).

Additionally, one relevant paper has been published.

- 6). N. W. Mureithi, **C. Zhang**, M. Ruël, and M. J. Pettigrew, Fluidelastic instability tests on an array of tubes preferentially flexible in the flow direction, *Journal of Fluids and Structures* 2005; 21(1), 75-87.

## CHAPTER 3

# DETAILED FLOW AND FORCE MEASUREMENTS IN A ROTATED TRIANGULAR TUBE BUNDLE SUBJECTED TO TWO-PHASE CROSS FLOW

M. J. Pettigrew\*, C. Zhang, N. W. Mureithi and D. Pamfil

BWC/AECL/NSERC Chair of Fluid-Structure Interaction, Department of Mechanical  
Engineering, École Polytechnique, Montréal, QC, Canada H3T 1J4

Published in *Journal of Fluids and Structures* 2005; 20 (4): 567-575

### **3.1 Abstract**

Two-phase cross-flow exists in many shell-and-tube heat exchangers. A detailed knowledge of the characteristics of two-phase cross flow in tube bundles is required to understand and formulate flow-induced vibration parameters such as damping, fluidelastic instability, and random excitation due to turbulence. An experimental program was undertaken with a rotated-triangular array of cylinders subjected to air/water flow to simulate two-phase mixtures. The array is made of relatively large diameter cylinders (38 mm) to allow for detailed two-phase flow measurements between cylinders. Fiber-optic probes were developed to measure local void fraction. Local flow velocities and bubble diameters or characteristic lengths of the two-phase mixture are obtained by using double probes. Both the dynamic lift and drag forces were measured with a strain gage instrumented cylinder.

### **3.2 Introduction**

Two-phase cross-flow exists in many shell-and-tube heat exchangers, for instance, in the U-tube region of nuclear steam generators. A detailed knowledge of the characteristics of two-phase cross flow in tube bundles is required to understand and formulate flow-induced vibration parameters such as damping, hydrodynamic mass, fluidelastic instability, and random excitation due to turbulence. The information is also required to validate tube-scale thermal-hydraulic analyses and to understand local crud deposition mechanisms.

Prior to 1980, very little work had been done to study flow-induced vibration of tube bundles subjected to two-phase cross flow. Since then a few studies were conducted in this area. This work was reviewed by Pettigrew and Taylor (1994). Since 1994, several researchers have contributed relevant results, in particular, Feenstra et al. (1995, 2002) in Freon 11 two-phase flow, Mann and Mayinger (1995) in Freon 12 two-phase flow,

and Nakamura et al. (2002), Mureithi et al. (2002) and Hirota et al. (2002) in steam-water cross-flow. Also, comprehensive studies on vibration of tube bundles subjected to both air-water and Freon 22 two-phase cross-flow were conducted at the Chalk River Laboratories (Pettigrew et al., 2001 and 2002). To our knowledge, no detailed measurements of two-phase flow in tube arrays have ever been done.

An experimental program was undertaken with a rotated-triangular array of cylinders subjected to air/water flow to simulate two-phase mixtures. The array, which has a pitch-to-diameter ratio of 1.5, is made of relatively large diameter cylinders (38 mm). This results in larger gaps (19 mm) between cylinders to allow for detailed two-phase flow measurements.

Fiber-optic probes were developed to measure local void fraction. Local flow velocities and bubble diameters or characteristic lengths of the two-phase mixture are also obtained by using double probes. Both the dynamic lift and drag forces were measured with a strain gauge instrumented cylinder. The results of these detailed two-phase flow and force measurements are presented in this paper. An attempt is made to use this information to understand vibration excitation mechanisms in two-phase cross flow.

### **3.3 Experimental considerations**

#### **3.3.1 Test loop**

The experiments were done in an air-water loop to simulate two-phase flows. The loop comprised a 25 l/s variable speed pump, a magnetic flow meter, a 2500 l tank, a 250 l/s compressed air supply system and connecting piping as shown in Fig. 3.1.

The compressed air was injected below a suitably designed mixer to homogenize and distribute the two-phase mixture uniformly below the test-section. The air flow was

measured with orifice plates connected to a differential pressure transducer and electronic readout system. The loop was operated at room temperature and the pressure in the test-section was slightly above atmospheric.

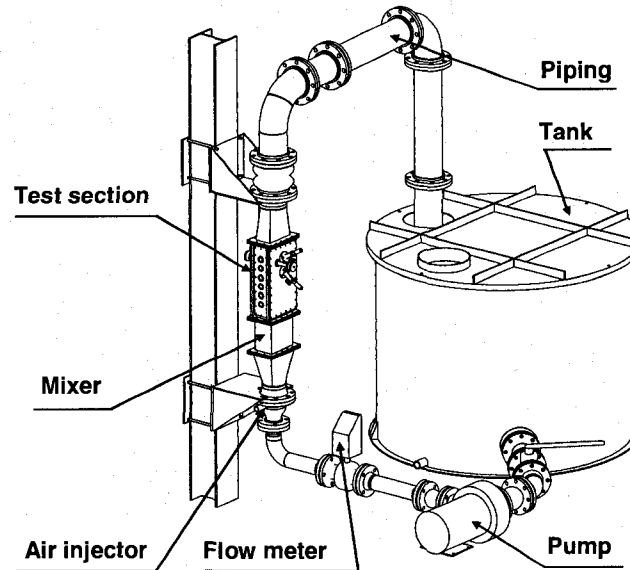


**Fig. 3.1** Test loop

### 3.3.2 Test section

The test section, which has an essentially rectangular cross section ( $99 \times 191$  mm), is shown in Fig. 3.2. It consists of a column of six 38 mm diameter cylinders flanked on either side by half cylinders to simulate essentially the flow path in a large array of cylinders in a rotated triangular configuration.

The pitch-to-diameter ratio,  $P/D$ , was 1.5 resulting in an inter-cylinder gap of 19 mm which allowed sufficient space for detailed flow measurements. The test-section length-to-gap width ratio is ten, thus, adequate to maintain essentially two-dimensional flow. The measurements were taken every millimeter with fiber-optic probes assembled within a traversing mechanism. The tip of the probes could be positioned accurately with a micrometer head.

The probe assemblies were installed at four principal positions in the array as shown in Fig. 3.2. These positions are henceforth called lower and upper 60° for the narrow gaps between cylinders and lower and upper 90° for the larger flow areas between upstream and downstream cylinders. One cylinder was instrumented with strain gauges to measure the dynamic drag and lift forces due to the two-phase flow.

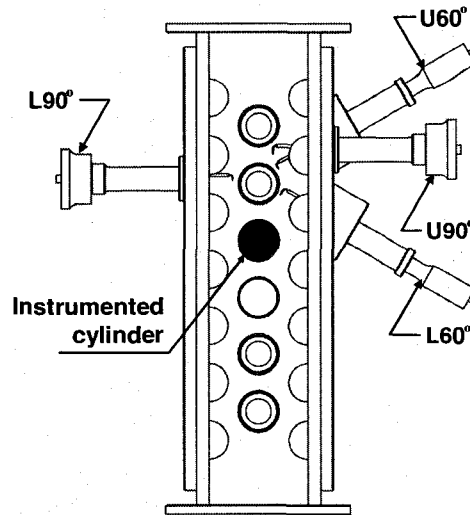


Fig. 3.2 Test section

### 3.3.3 Fiber-optic probes for two-phase flow measurements

Fig. 3.3 shows a double fiber-optic probe, which comprises two fiber-optic probes inserted in one stainless tube. Each probe has a conical tip and is made of an optical fiber of 170  $\mu\text{m}$  diameter. It acts as a phase sensor based on the different level of light reflection between air and water. Two flow conditions were investigated in detail, i.e. 50 and 80% homogeneous void fraction at a nominal pitch flow velocity,  $U_p$ , of 5 m/s.

For each measurement, the probe data were recorded for a period of 20 seconds at a  $2 \times 10^6$  Hz sampling rate. A data analysis software was developed to obtain the time,  $T_i$ , at which the  $i^{\text{th}}$  gaseous particle touches the probe, and the duration of this contact,  $\tau_i$ , as schematically illustrated in Fig. 3.4. The void fraction can be obtained from either probe

from the ratio of integrated gas phase contact times,  $\tau_i$ , over the total test time,  $T$ . It can be expressed as

$$\alpha(x, T) = \frac{1}{T} \sum_i \tau_i. \quad (3.1)$$

The bubble or gas phase velocity can be estimated from the transit time between the two tips, which are a known distance apart (around 150  $\mu\text{m}$ ), as shown in Fig. 3.5. It can be expressed as

$$V_i(x, t) = \frac{\Delta h_{\text{ups}}}{\Delta T_i}, \quad (3.2)$$

where,

$$\Delta T_i = \frac{1}{f_s} (S_{2i} - S_{1i}). \quad (3.3)$$

where  $f_s$  is the sampling rate for the signal, and  $S_{1i}$ ,  $S_{2i}$  are the sampling points when the  $i$ th bubble contacts the first probe and second probe respectively.

The bubble size,  $d$ , can be deduced from the product of bubble velocity and contact duration. This is expressed as

$$d_{1i} = V(x, t)\tau_{1i} \text{ and } d_{2i} = V(x, t)\tau_{2i} \quad (3.4)$$

for probe 1 and 2, respectively.

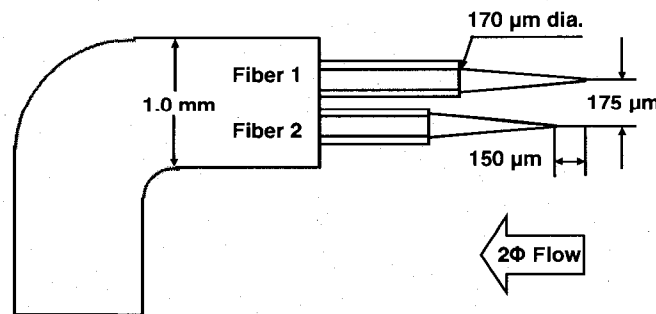


**Fig. 3.3** Double fiber-optic probe



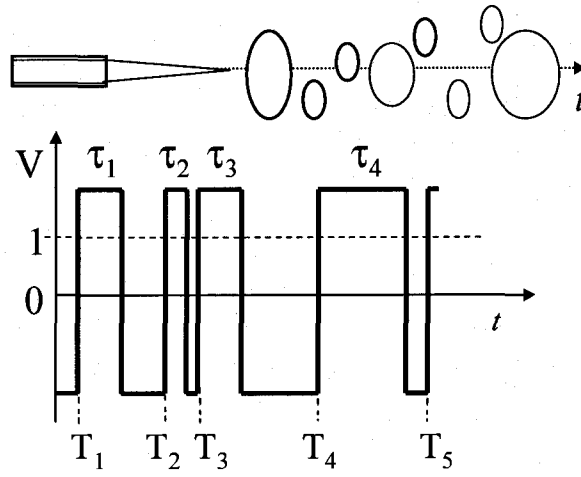


Fig. 3.4 Void fraction measurement

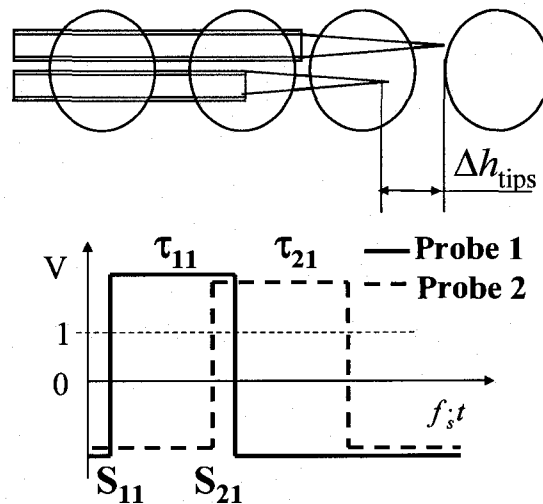


Fig. 3.5 Bubble velocity and bubble size measurements

In this study, the bubble velocity is the average value of the velocities of analyzed bubbles. Analyzed bubbles are the bubbles that satisfy two criteria. One is that the calculated velocity has to be within a velocity range between 1 and 10 m/s (for the  $U_p=5\text{m/s}$  case). The other is that the relative error of bubble sizes between the first probe and second probe,  $(d_{1i}-d_{2i})/d_{1i}$ , be less than 5%. The bubble size is the average of  $V\tau_{1i}$  from the first probe.

### 3.3.4 Instrumentation

Both the dynamic lift and drag forces were measured with a strain gage instrumented cylinder in the fourth position from the upstream end of the test-section (Fig. 3.2). The instrumented cylinder was cantilevered and surrounded by rigid tubes. Two pairs of diametrically opposite strain gages were installed in the cylinder at 90 deg from each other to measure the forces in the flow direction (drag) and in the direction normal to the flow (lift). The strain gages were connected to strain indicators. Before the instrumented cylinder was inserted into the test section, the static strain-force relation was determined via a careful calibration. The signals were routinely analyzed on an OR38 8-32 channel real time multi-analyzer/recorder coupled to a laptop computer.

## **3.4 Results**

### 3.4.1 Flow measurements

Typical detailed measurements along the lower 60° line across the narrowest gap between cylinders are shown in Fig. 3.6. Due to assembly problems, the probe tips were not exactly on the 60° and 90° lines. In fact the tips were roughly 2 mm downstream of the lines. Although this will be corrected in future tests, we do not believe this slight misalignment affected much the results. The measurements were taken every millimeter across the 19 mm gap. The measurements were remarkably stable as may be seen by the lack of scatter in the data. The measurements of void fraction, bubble velocity (gas phase velocity) and bubble size (characteristic lengths of the two-phase mixture) are shown in Figs 3.6(a), (b) and (c) respectively. These measurements correspond to homogeneous flow conditions of 80% void fraction and gap flow velocity of 4.33 m/s (pitch velocity of 5 m/s). The average measured gap bubble velocity and void fraction are respectively, 4.55 m/s and 73 %. This indicates nearly homogeneous two-phase flow conditions. The slip between the gas and liquid phase is small. The bubble sizes range from 0.5 to 5 mm.

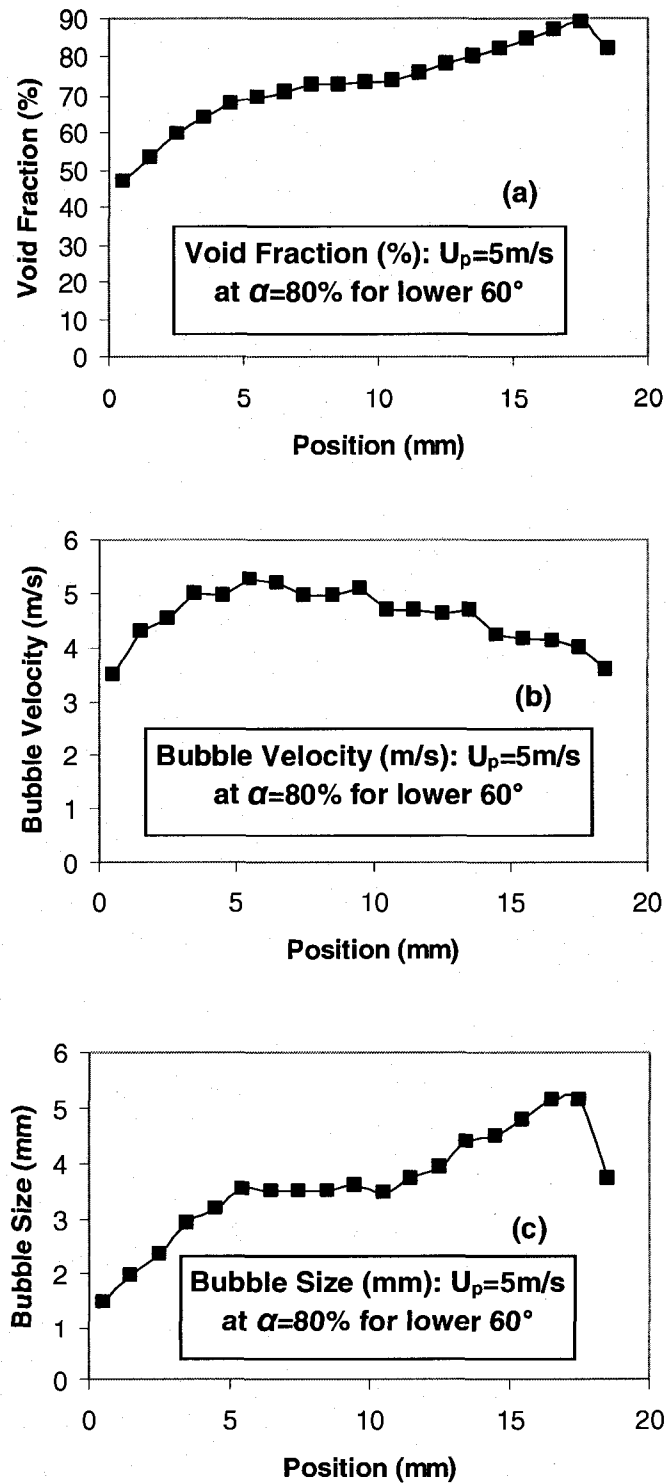
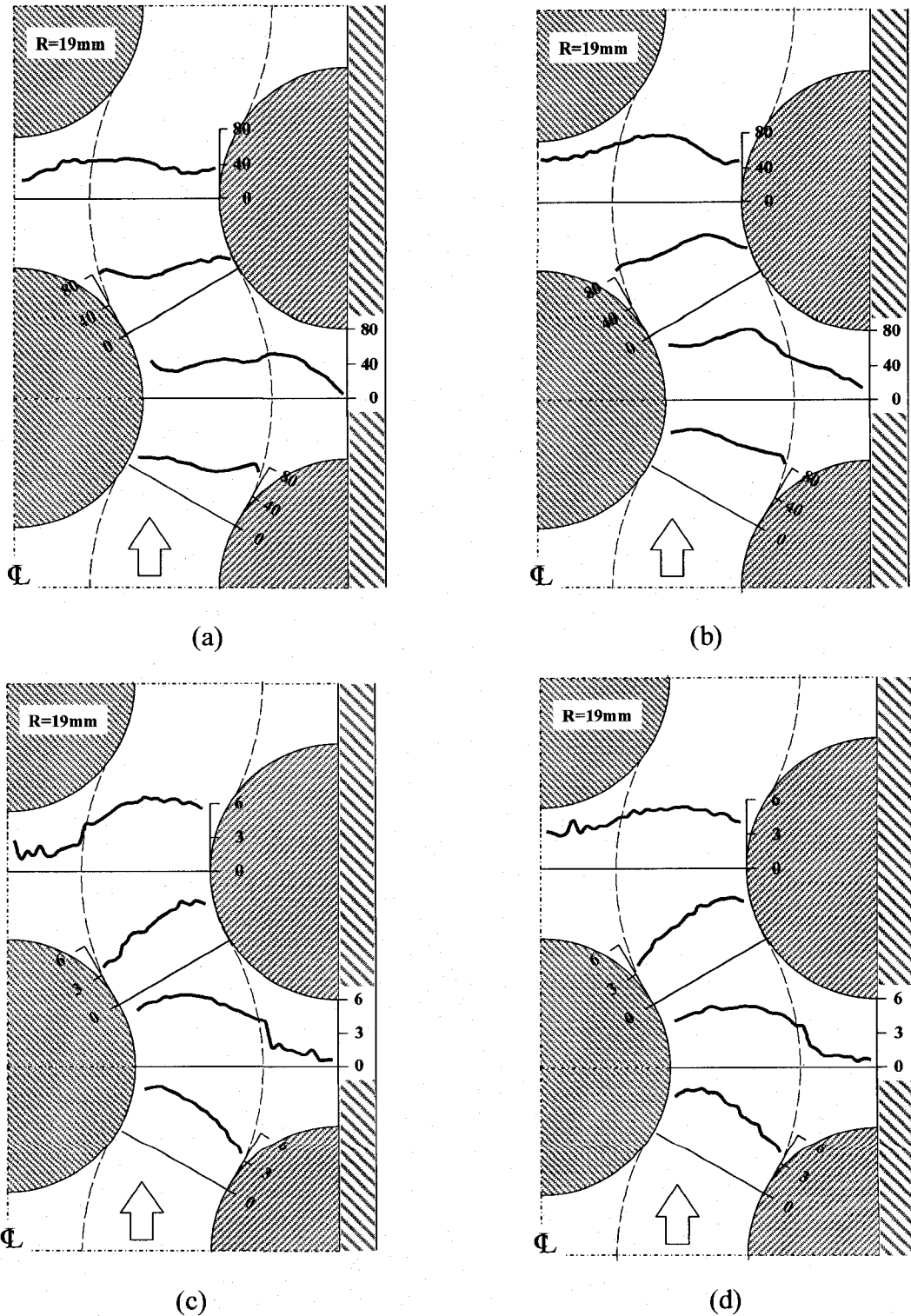


Fig. 3.6 Typical results of flow measurements: (a) Void fraction; (b) Bubble velocity; and (c) Bubble size

The results for all the flow measurements are summarized in Fig. 3.7. It shows that the flow velocity is relatively uniform across the lower and upper  $60^\circ$  gaps between cylinders. The flow velocity distribution in the lower and upper  $90^\circ$  space between cylinders is much less uniform. There is also a region of low flow velocity immediately upstream and downstream of the cylinders. It also shows an abrupt increase in velocity at a position corresponding to a transition between a more stagnant region between tubes and the main stream of the flow. It appears from both these measurements and visual observation that the flow streams through the available flow path between cylinders. This flow path is outlined with dash lines in Fig. 3.7. The region of low flow and the transition are more pronounced in between the half-tubes near the wall of the test-section than in the centre of the test-section. This is not surprising, since the wake between cylinders in the centre of the test-section is quite unsteady due to the absence of a solid boundary.

The void fraction distribution in the narrow  $60^\circ$  gaps is nearly uniform for the 80% void fraction tests whereas it is much less uniform for the 50% tests (Fig. 3.7(b) versus Fig. 3.7(a)). Interestingly, the void fraction distribution for the lower  $60^\circ$  gap is the mirror image of that for the upper  $60^\circ$  gap. This is expected because of symmetry. The void fraction is generally lower in the more stagnant regions between cylinders.

The bubble size distribution in the narrow  $60^\circ$  gaps is very similar to the void fraction distributions in the same locations (Fig. 3.7(e) versus Fig. 3.7(a) and Fig. 3.7(f) versus Fig. 3.7(b)). This is reasonable because the bubble size should be consistent with the void fraction. The bubble size distribution in the lower and upper  $90^\circ$  space is essentially similar to the void fraction distributions in the same location except in the centre of the test section for the upper  $90^\circ$  measurement (Fig.3.7(e) versus Fig. 3.7(a) and Fig. 3.7(f) versus Fig. 3.7(b)). This requires further investigation.



**Fig. 3.7** Summary of results of flow measurements: void fraction (%) for  $U_p=5\text{m/s}$  at (a)  $\alpha=50\%$ , (b)  $\alpha=80\%$ ; bubble velocity (m/s) for  $U_p=5\text{m/s}$  at (c)  $\alpha=50\%$ , (d)  $\alpha=80\%$

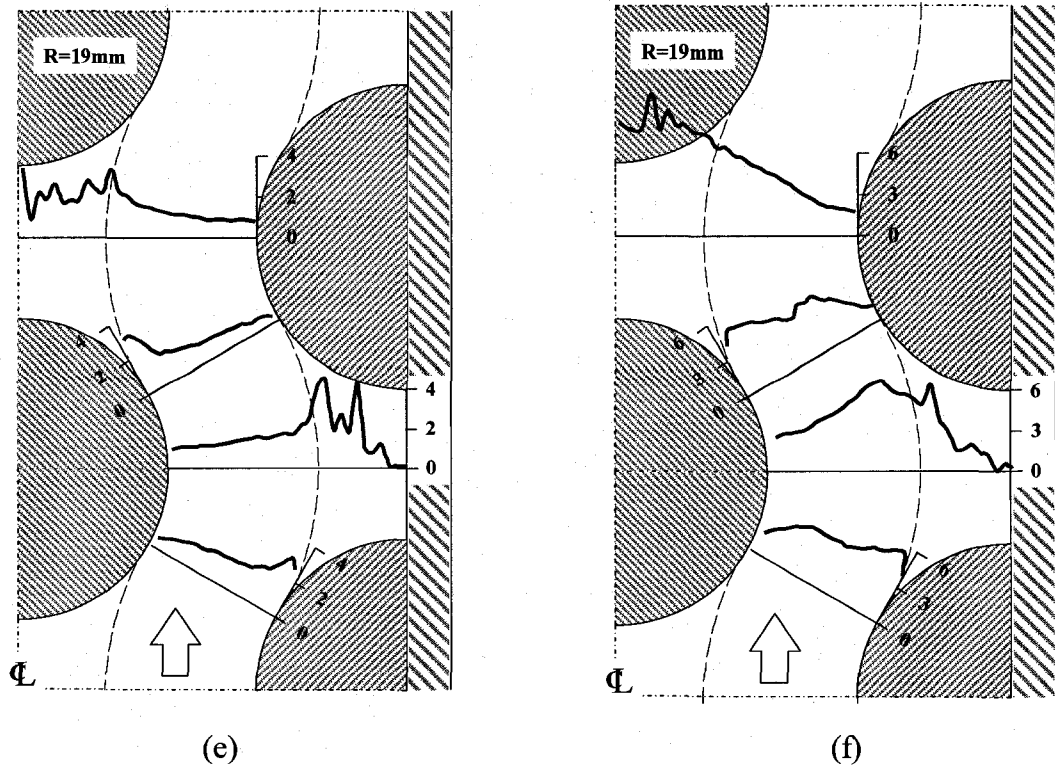


**Fig. 3.7 continued** Summary of results of flow measurements: Bubble size (mm) for  $U_p=5\text{m/s}$  at (e)  $\alpha=50\%$ , (f)  $\alpha=80\%$

The bubble flow velocities and the corresponding measured void fraction in the lower and upper  $60^\circ$  gaps were integrated to obtain the total volumetric gas flow. The values are compared to the measured volumetric air flow at the inlet of the test-section in Table 3.1. The values are similar, thereby giving some degree of confidence in the measurement method.

**Table 3.1** Comparison between input and measured air flow rate

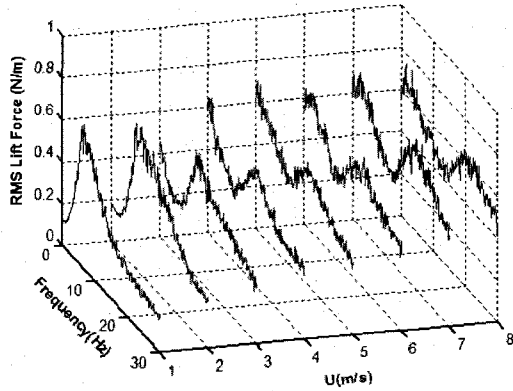
Probe	$\alpha=50\%$		$\alpha=80\%$	
	Input (l/s)	Measured (l/s)	Input (l/s)	Measured (l/s)
Upper $60^\circ$	15.7	14.64	25	23.67
Lower $60^\circ$	15.7	15.61	25	23.97

### 3.4.2 Dynamic lift and drag force measurements

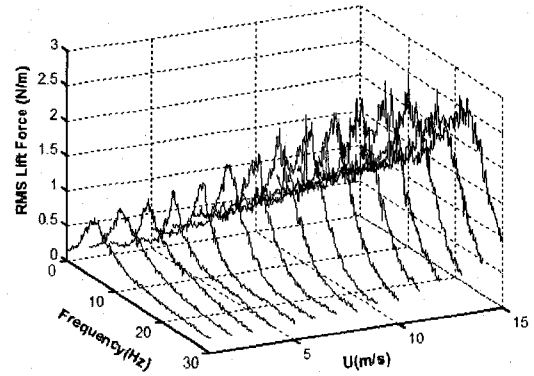
Force measurements were taken with an instrumented cylinder located in the fourth cylinder position from the upstream end of the test-section. Typical lift and drag force spectra are shown in Fig. 3.8. The spectra reveal narrow band or quasi-periodic forces. This is somewhat unexpected and unlike typical random turbulence excitation. For the case of 80% void fraction, in the lift direction the periodic force frequency increases from about 5.75 to 21.75 Hz for a corresponding increase in flow velocity of 1 to 15 m/s (Fig. 3.9(b)). This yields Strouhal numbers from 0.22 to 0.06. Although periodic wake shedding was not expected at such high void fraction, the wake between cylinders was observed visually to be quite unsteady.

Periodicity was also observed in the drag direction as shown in Figs 3.8(c) and (d). Surprisingly, for the case of 80% void fraction, the frequency of the periodic drag forces decreases slightly from 6.6 to 3.0 Hz at 6 m/s flow velocity and then increases slightly from 3.0 to 6.6 Hz for an increase in flow velocity from 6 to 15 m/s. The resulting drag forces increase with flow velocity from 1 to 8 m/s and then decrease slightly above 8 m/s flow velocity. They reach a maximum of roughly 6 N/m r.m.s. at 8 m/s flow velocity which is not insignificant. This behavior is still in search of an explanation. It is probably related to two-phase flow patterns. Some very sharp peaks at low frequency (around 2 Hz) also appeared at high mass fluxes as shown in Figs 3.8(c) and (d). They are probably due to low frequency loop oscillations.

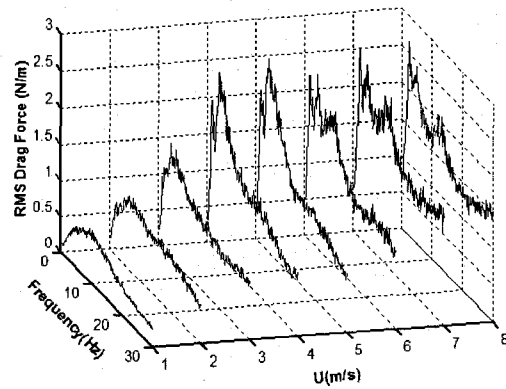
The same results presented in terms of the relation between frequency and pitch velocity, and the relation between r.m.s. periodic force and pitch velocity may be found in Figs 3.9 and 3.10.



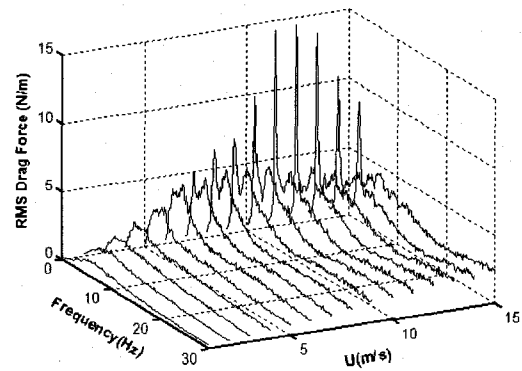
(a) Lift force spectra for  $\alpha=50\%$



(b) Lift force spectra for  $\alpha=80\%$

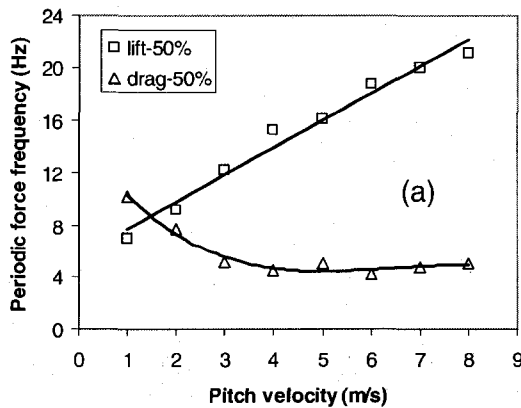


(c) Drag force spectra for  $\alpha=50\%$

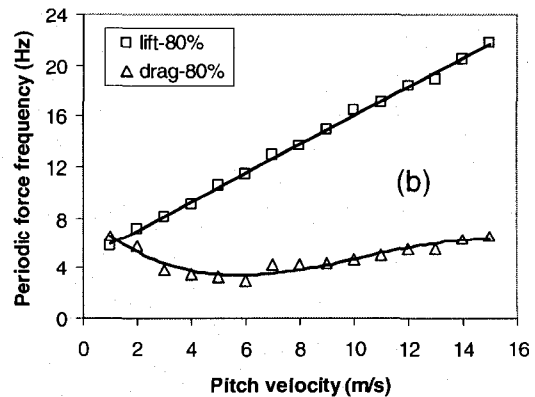


(d) Drag force spectra for  $\alpha=80\%$

**Fig. 3.8** Typical dynamic force spectra



(a)



(b)

**Fig. 3.9** Relationship between periodic force frequency and pitch velocity:  
(a)  $\alpha=50\%$  and (b)  $\alpha=80\%$



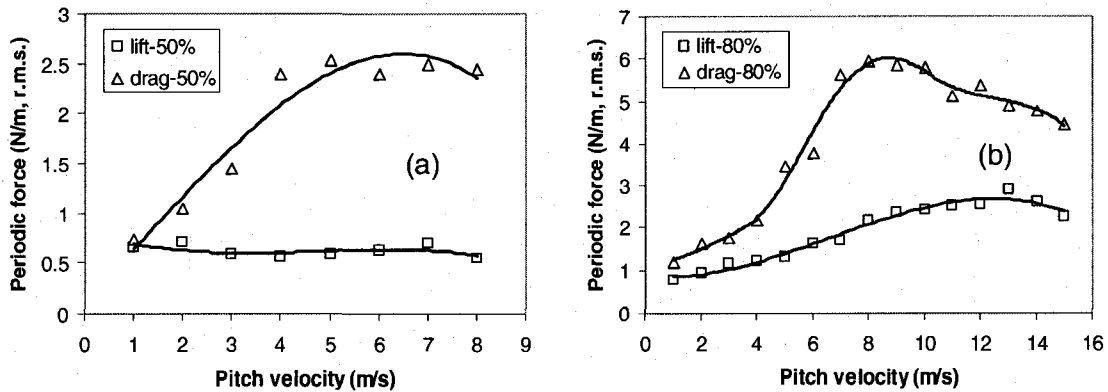


**Fig. 3.10** Relationship between r.m.s. periodic force and pitch velocity:  
(a)  $\alpha=50\%$  and (b)  $\alpha=80\%$

### 3.5 Discussion

The results of flow measurement indicate that the flow tends to stream between the cylinders and that within that stream the flow velocity is fairly uniform. In fact, the flow path resembles a series of two-dimensional  $60^\circ$  elbows. Thus, it is not surprising that the void fraction distribution is not uniform. The lowest void fraction corresponds to the extrados and the highest void fraction to the intrados at the exit of the elbows (Figs 3.7(a) and (b)) as would be expected of two-phase flow in elbows. The void fraction distribution has to completely reverse from one side to the other within half a cylinder pitch. That implies considerable mixing at each half-pitch interval. Thus, it is not surprising that the two-phase mixture is fairly homogeneous and the slip between phases is small.

The results of force measurement indicate that unexpected quasi-periodic forces were measured in both the drag and lift direction. These forces are significantly larger in the drag direction.

### 3.6 Conclusions

Detailed flow and force measurements were taken in a rotated triangular array of cylinders subjected to two-phase cross-flow. The results show that the two-phase flow tends to stream between the cylinders and that within that stream the flow velocity is fairly uniform. The two-phase flow within the stream is fairly homogeneous and the slip between phases appears to be relatively small. Unexpected quasi-periodic forces were measured in both the drag and lift direction.

### 3.7 References

- Feenstra, P.A., Judd, R.L. and Weaver, D.S., 1995. Fluidelastic instability of a tube array subjected to two-phase R 11 cross flow. *Journal of Fluids and Structures* 9, 747-771.
- Feenstra, P.A., Weaver, D.S. and Judd, R.L., 2002. Modelling two-phase flow-excited damping and fluidelastic instability in tube arrays. *Journal of Fluids and Structures* 16, 811-840.
- Hirota, K., Nakamura, T., Kasahara, J., Mureithi, N.W., Kusakabe, T. and Takamatsu, H., 2002. Dynamics of an in-line tube array subjected to steam-water cross-Flow. Part III: fluidelastic instability tests and comparison with theory. *Journal of Fluids and Structures* 16, 153-173.
- Mann, W. and Mayinger, F., 1995. Flow-induced vibration of tube bundles subjected to single- and two-phase cross-flow. *Proceedings of the 2nd International Conference on Multiphase Flow*, Vol. 4, pp. 9-15, Kyoto, Japan.
- Mureithi, N.W., Nakamura, T., Hirota, K., Murata, M., Utsumi, S., Kusakabe, T. and Takamatsu, H., 2002. Dynamics of an in-line tube array subjected to steam-water cross-flow. Part II: unsteady fluid forces. *Journal of Fluids and Structures* 16, 137-152.

Nakamura, T., Hirota, K., Watanabe, Y., Mureithi, N.W., Kusakabe, T. and Takamatsu, H., 2002. Dynamics of an in-line tube array subjected to steam-water cross-flow. Part I: two-phase damping and added mass. *Journal of Fluids and Structures* 16, 123-136.

Pettigrew, M.J. and Taylor, C.E., 1994. Two-phase flow induced vibration: an overview. *ASME Journal of Pressure Vessel Technology* 116, 233-253.

Pettigrew, M.J., Taylor, C.E., and Kim, B.S., 2001. The effects of tube bundle geometry on vibration in two-phase cross flow. Special FSI Issue of *ASME Journal of Pressure Vessel Technology* 123, 414-420.

Pettigrew, M.J., Taylor, C.E., Janzen, V.P., and Whan, T., 2002. Vibration behavior of rotated triangular tube bundles in two-phase cross flows. *ASME Journal of Pressure Vessel Technology* 124, 144-153.

## CHAPTER 4

# VIBRATION EXCITATION FORCE MEASUREMENTS IN A ROTATED TRIANGULAR TUBE BUNDLE SUBJECTED TO TWO-PHASE CROSS FLOW

C. Zhang, M. J. Pettigrew\*, and N. W. Mureithi

BWC/AECL/NSERC Chair of Fluid-Structure Interaction, Department of Mechanical  
Engineering, École Polytechnique, Montréal, QC, Canada H3T 1J4

Published in *ASME Journal of Pressure Vessel Technology* 2007; 129 (1): 21-27

## 4.1 Abstract

Two-phase cross flow exists in many shell-and-tube heat exchangers. Flow-induced vibration excitation forces can cause tube motion that will result in long-term fretting-wear or fatigue. Detailed vibration excitation force measurements in tube bundles subjected to two-phase cross flow are required to understand the underlying vibration excitation mechanisms. An experimental program was undertaken with a rotated-triangular array of cylinders subjected to air/water flow to simulate two-phase mixtures over a broad range of void fraction and mass fluxes. Both the dynamic lift and drag forces were measured with strain gage instrumented cylinders. The experiments revealed somewhat unexpected but significant quasi-periodic forces in both the drag and lift directions. The periodic forces appeared well correlated along the cylinder with the drag force somewhat better correlated than the lift forces. The periodic forces are also dependent on the position of the cylinder within the bundle.

## 4.2 Introduction

Two-phase cross flow exists in many shell-and-tube heat exchangers. Flow-induced vibration excitation forces can cause tube motion that will result in long-term fretting-wear or fatigue. To prevent these tube failures in heat exchangers, designers and troubleshooters must have guidelines that incorporate flow-induced vibration excitation forces.

In single-phase flow, these forces have been extensively measured and analyzed. They have been related to periodic wake shedding and to the turbulence level created by the bundle itself. Experimental data obtained for different kinds of fluids and tube bundles have been satisfactorily compared through the use of adequate data-reduction procedures [1, 2].

In the case of two-phase flows, such an extensive study has not been undertaken, though it is known that there are significant differences between single- and two-phase situations. In particular, the relationship between the two phases must be considered in addition to another parameter that is void fraction. This results in different flow regime or patterns of two-phase flow. A few sets of experimental results have been obtained recently, as in Refs [2-12]. However many questions remain such as the effects of viscosity, surface tension, density ratio or flow regimes. Actually, the main problem is the understanding of the physical mechanism that induces these forces.

An experimental program was undertaken with a rotated-triangular array of cylinders subjected to air/water flow to simulate two-phase mixtures over a broad range of void fraction and mass fluxes. Vibration excitation forces were measured with a number of strain gage instrumented cylinders located in several positions within the bundle as explained in detail later.

Somewhat unexpected but significant quasi-periodic forces were measured in both the drag and lift directions. The results of the above measurements are presented in this paper. By correlating the force measurements with two-phase flow characteristic measurements [12, 13], an attempt is made to understand vibration excitation mechanisms in two-phase cross flow.

### **4.3 Experimental considerations**

#### **4.3.1 Test loop**

The experiments were done in an air-water loop to simulate two-phase flows. The loop comprised a 25 l/s variable speed pump, a magnetic flow meter, a 2500 l tank, a 250 l/s compressed air supply system and connecting piping as shown in Fig. 4.1. The compressed air was injected below a suitably designed mixer to homogenize and

distribute the two-phase mixture uniformly below the test-section. The air flow was measured with orifice plates connected to a differential pressure transducer and electronic readout system. The loop was operated at room temperature and the pressure in the test-section was slightly above atmospheric.

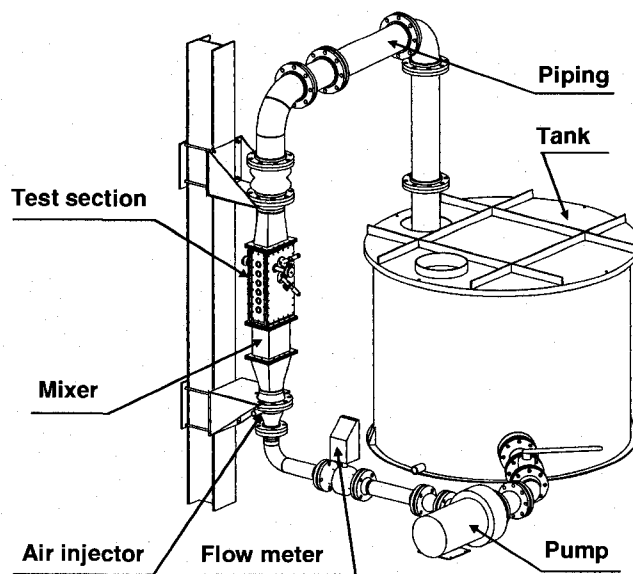


Fig.4.1 Test loop

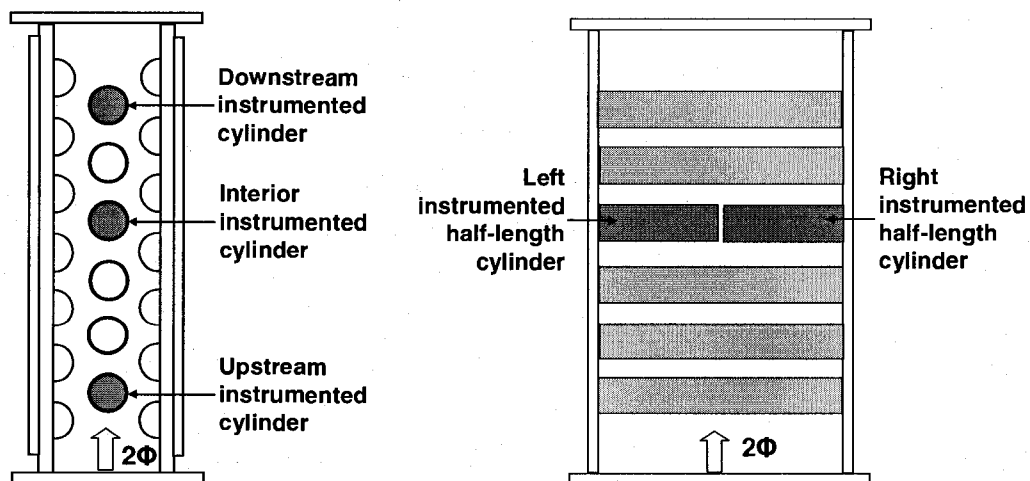


Fig. 4.2 Test section

#### 4.3.2 Test section

The test-section, which has an essentially rectangular cross section (99×191 mm), is shown in Fig. 4.2. It consists of a column of six 38 mm diameter cylinders flanked on either side by half cylinders to simulate essentially the flow path in a large array of cylinders in a rotated triangular configuration. The pitch-to-diameter ratio,  $P/D$ , was 1.5 resulting in an inter-cylinder gap of 19 mm. The test-section length-to-gap width ratio is ten, thus, adequate to maintain essentially uniform two-dimensional flow.

#### 4.3.3 Instrumentation

Tests were conducted with (1) a strain gage instrumented cylinder located in the interior position (the fourth position from the upstream end of the test-section as shown in Fig. 4.2); (2) two strain gage instrumented half-length cylinders end-to-end located in the same interior position in the test section (as shown in Fig. 4.2); (3) two strain gage instrumented cylinders located in the upstream and downstream positions (the first and last positions from the upstream end of the test-section), and (4) a single strain gage instrumented cylinder located in the interior position without any other cylinder, but with half cylinders flanked on the two sidewalls in the test section. In all cases, the instrumented cylinders were cantilevered and both the dynamic lift and drag forces were measured. Two pairs of diametrically opposite strain gages were installed in the cylinders at 90 deg from each other to measure the forces in the flow direction (drag) and in the direction normal to the flow (lift). The strain gages were connected to strain indicators. The natural frequency of the cantilever cylinders was much higher (i.e., >150Hz) than the excitation force frequencies such that the cantilever cylinder functioned essentially as a dynamic force transducer. The static strain-force relation was determined via a careful calibration. The signals were analyzed on an OR38 8-32 channel real time multi-analyzer/recorder coupled to a laptop computer.



The experiments were performed over a homogeneous void fraction range from 5 percent to 95 percent and a flow velocity range from 1m/s to 20 m/s.

## 4.4 Results

### 4.4.1 Vibration excitation forces in the interior position of the bundle

Typical lift and drag force spectra for the cylinder in the interior position of the bundle are shown in Fig. 4.3. The spectra reveal narrow band or quasi-periodic forces. This is somewhat unexpected and unlike typical random turbulence excitation. For 80% void fraction, the periodic force frequency in the lift direction increases from about 5.75 to 16.75 Hz for a corresponding increase in pitch flow velocity of 1 to 10 m/s (Fig. 4.3(a)). This yields Strouhal numbers ( $S_l=fD/U_p$ ) from 0.22 to 0.07. Although periodic wake shedding was not believed to have occurred at such high void fraction, the wake between cylinders was observed visually to be quite unsteady.

Periodicity was also observed in the drag direction as shown in Fig. 4.3(b). Surprisingly, the frequency of the periodic drag forces decreases slightly from 6.6 to 3.0 Hz at 6 m/s pitch flow velocity and then increases slightly from 3.0 to 5.0 Hz for an increase in pitch flow velocity from 6 to 10 m/s. The resulting drag forces increase with pitch flow velocity from 1 to 8 m/s and then decrease slightly above 8 m/s pitch flow velocity. They reach a maximum of roughly 6 N/m r.m.s. at 8 m/s pitch flow velocity which is not insignificant. Some very sharp peaks at low frequency (around 2 Hz) also appeared at high mass fluxes as shown in Fig. 4.3(b). The same results presented in terms of the relationship between frequency and pitch flow velocity, and the relationship between r.m.s. periodic force and pitch flow velocity may be found in Figs 4 and 5. These results were obtained at 80% void fraction. However similar trends were also observed at other void fractions except that the periodic forces in the drag direction were not so pronounced below 25% void fraction.

The very sharp peaks at low frequency (around 2 Hz) were also found with a pressure sensor in the test section and just after the pump for both water and two-phase flow. It was not found in the water tank. Detailed accelerometer measurements showed that it was not due to the loop vibration. Therefore, this sharp peak frequency is not related to the nature of two-phase flow. It is an unwanted signal component which should not be considered further.

The latest investigation showed that the quasi-periodic drag and lift forces are generated by different mechanisms that have not been observed so far. A brief summary of the test results is presented here. The reader is referred to [13] for a more comprehensive discussion. The dynamic characteristics of the two-phase flow in terms of local void fraction fluctuation, and the dynamic lift and drag forces were measured simultaneously. The tests revealed that the quasi-periodic drag forces appear related to the momentum flux fluctuations in the main flow path between the cylinders; the quasi-periodic lift forces, on the other hand, are mostly correlated to oscillations in the wake of the cylinders.

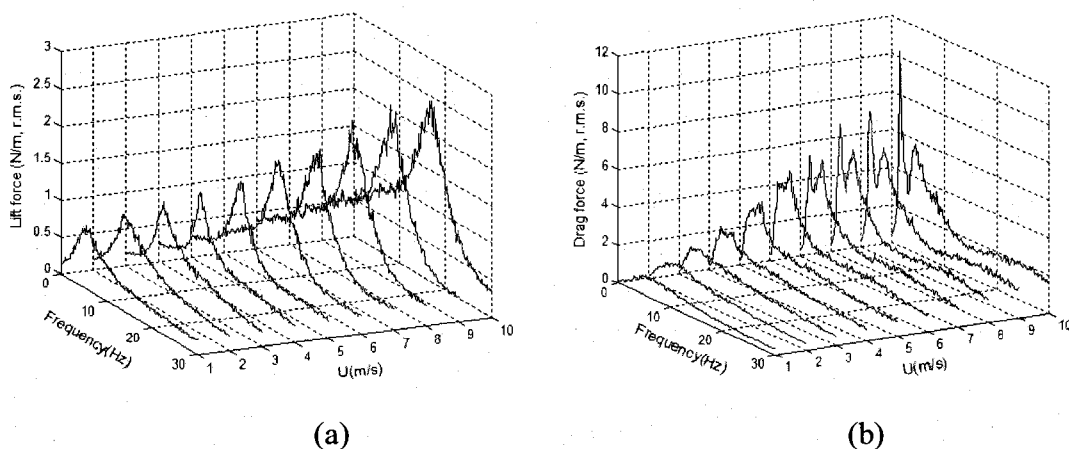


**Fig. 4.3** Typical dynamic force spectra for the interior cylinder at 80% void fraction:  
(a) Lift force spectra and (b) Drag force spectra

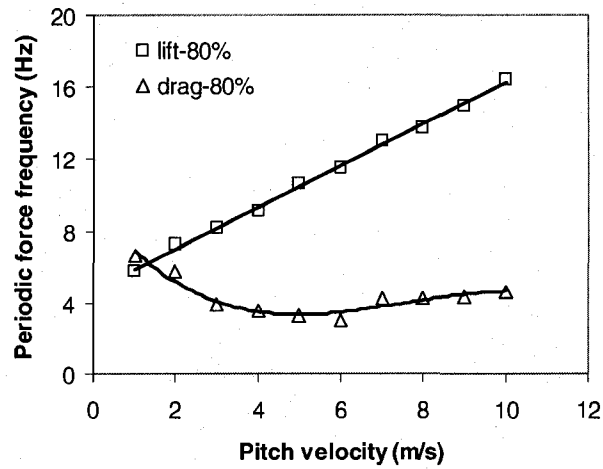


**Fig. 4.4** Relationship between periodic force frequency and pitch velocity

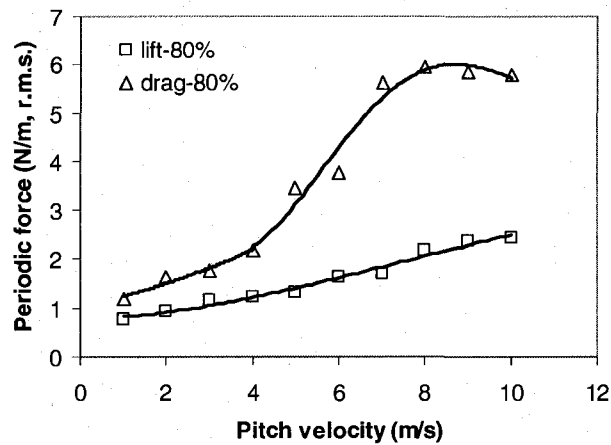


**Fig. 4.5** Relationship between r.m.s. periodic force and pitch velocity

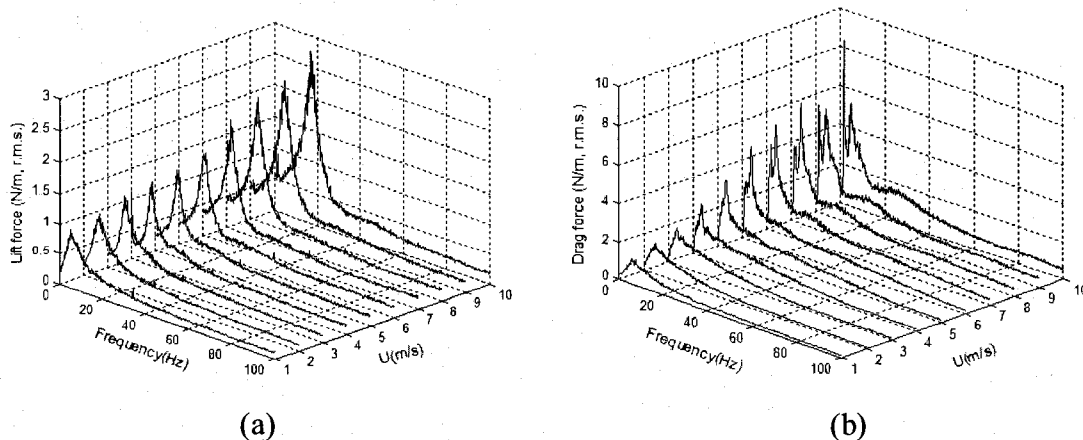


**Fig. 4.6** Typical dynamic force spectra for the left interior half-length cylinder at 80% void fraction: (a) Lift force spectra and (b) Drag force spectra

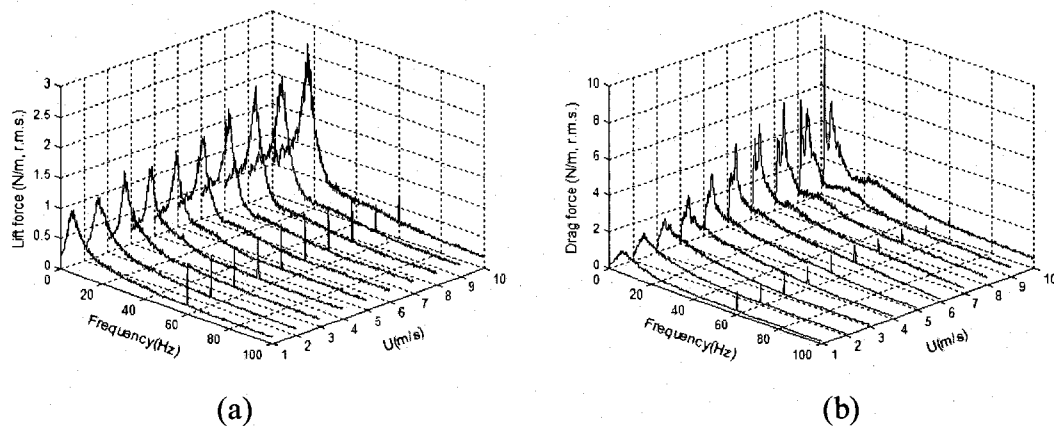


**Fig. 4.7** Typical dynamic force spectra for the right interior half-length cylinder at 80% void fraction: (a) Lift force spectra and (b) Drag force spectra

#### 4.4.2 Correlation of vibration excitation forces along the cylinder in the interior position of the bundle

Typical lift and drag force spectra for the two half-length cylinders located in the interior position in the test section are shown in Figs 4.6 and 4.7. As expected these spectra also reveal narrow band or quasi-periodic forces. For 80% void fraction, the periodic force frequency and r.m.s. periodic force for each half-length cylinder are very similar to one another for both the lift and drag directions (Figure 4.6(a) versus 4.7(a), and Fig. 4.6(b) versus Fig. 4.7(b)). These results are also consistent with those of the full-length cylinder located in the interior position (Figs 4.3(a) and 4.3(b)). The comparison of both lift and drag spectra for 80% void fraction at 5 m/s and 10 m/s pitch flow velocity may be seen in Figs 4.8 and 4.9 respectively. They show that the magnitude of the excitation force per unit length for the half-length cylinders is very similar to that of the full-length cylinder. This indicates that the periodic components of excitation forces are spatially correlated along the length of the cylinder. The same conclusion may be reached from Figs 4.10(a) and 4.10(b), which show the coherences of the two half-length cylinders for 80% void fraction at 5 m/s and 10 m/s pitch flow velocity respectively. This was somewhat unexpected because it is quite different than in single-phase flow [1, 2]. The correlation length for periodic vortex shedding for a

stationary cylinder in single phase flow is generally small. Here, in the lift direction, we appear to have a different phenomenon which is more like periodic fluctuation in the wake.

The results for other void fractions are similar except that the responses of the two half-length cylinders are not so well spatially correlated below 50 percent void fraction. Generally, the two-phase periodic drag forces are slightly better correlated than the two-phase periodic lift forces.

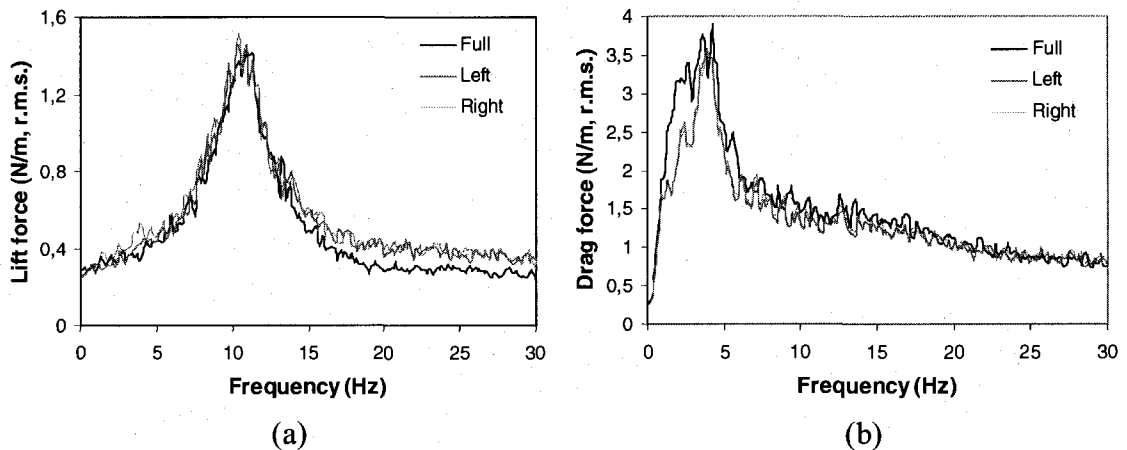


**Fig. 4.8** Comparison of force spectra for 80% void fraction at 5 m/s pitch flow velocity: (a) Lift force spectra and (b) Drag force spectra

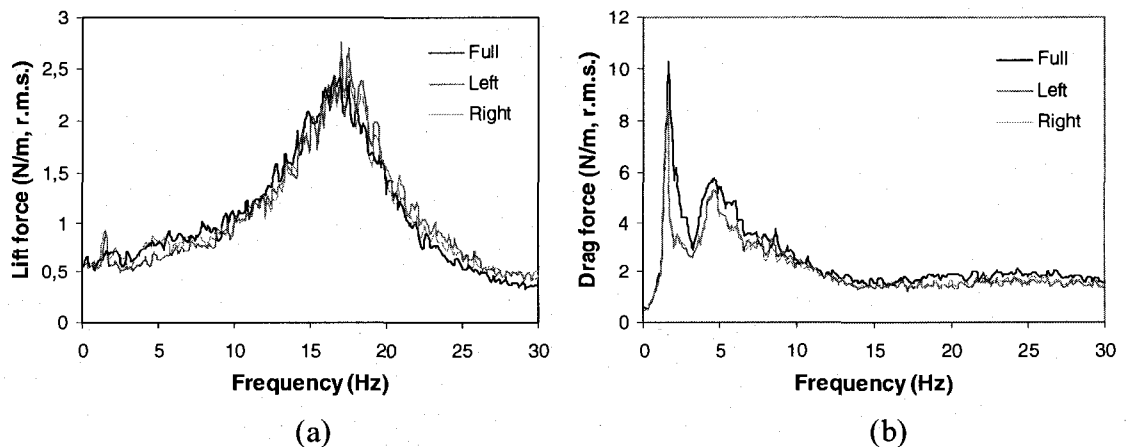


**Fig. 4.9** Comparison of force spectra for 80% void fraction at 10 m/s pitch flow velocity: (a) Lift force spectra and (b) Drag force spectra

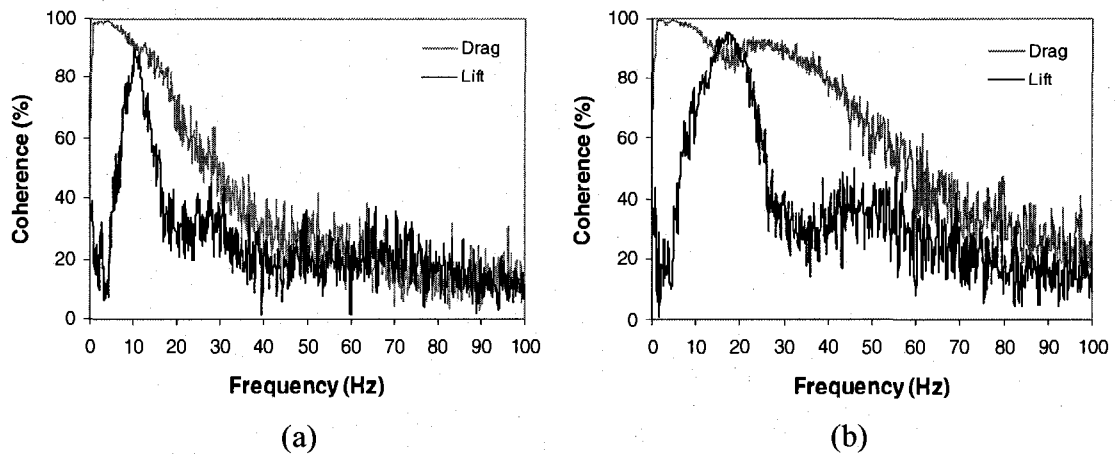


**Fig. 4.10** Coherences of the two half-length cylinders for 80% void fraction: (a) at 5 m/s pitch flow velocity and (b) at 10 m/s pitch flow velocity

#### 4.4.3 Effect of cylinder positions on excitation forces

Typical lift and drag force spectra at 80% void fraction for the cylinders located at the upstream and downstream positions are shown in Figs 4.11 and 4.12 respectively. In the drag direction the force spectra are quite similar for both the upstream and downstream cylinders. On the other hand the force spectra in the lift direction are relatively small in the upstream position but much larger in the downstream position. This indicates that the periodic forces in the lift direction are developing within the cylinder array. The behavior of the interior cylinder is quite similar to that of the downstream cylinder (Fig. 4.3 versus Fig. 4.12). In both cases the periodic force peaks in the spectra for the lift direction become more prominent with flow velocity. This is not the case for the upstream cylinder where the periodicity becomes less prominent and the broad band random turbulence forces become more dominant with flow velocity (see Fig. 4.11(a)).

Lift force spectra for upstream, interior, downstream and single cylinder positions are shown in Figs 4.13(a) and 4.13(b) for 5 and 10 m/s pitch flow velocity respectively. Similarly drag force spectra are shown in Figs 4.14(a) and 4.14(b). For the so called “single cylinder position” all cylinders except the interior cylinder and the half cylinders on the sidewalls are removed. Therefore it is not surprising that the force spectra for the

single cylinder and the upstream cylinder are similar. In the lift direction the spectra of the single cylinder are largely broad band random in appearance and somewhat smaller than the upstream excitation forces (see Fig. 4.13). In the drag direction the force spectra of the single cylinder and the upstream cylinder are quite similar.

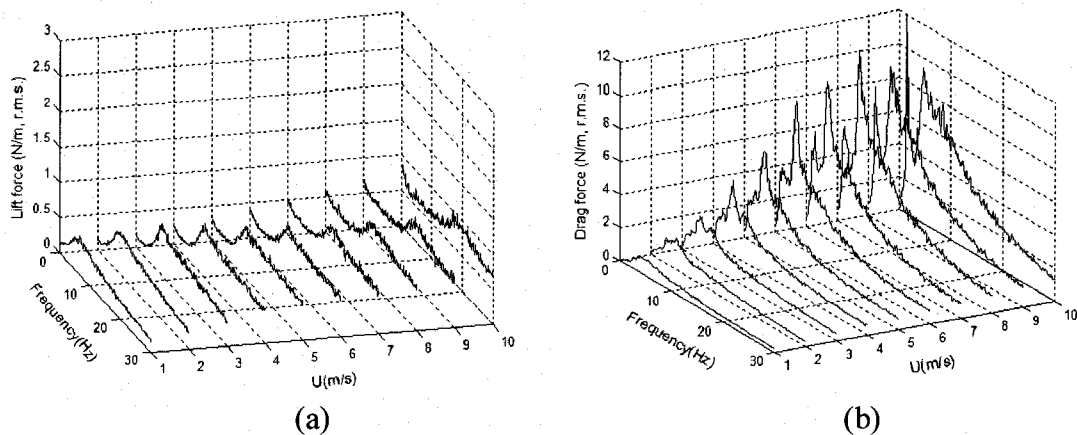


**Fig. 4.11** Typical dynamic force spectra for the upstream cylinder at 80% void fraction: (a) Lift force spectra and (b) Drag force spectra

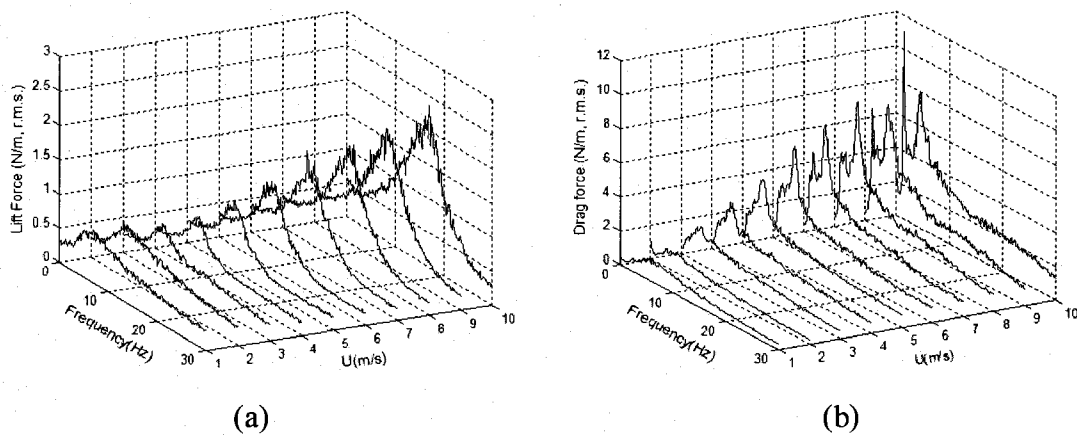


**Fig. 4.12** Typical dynamic force spectra for the downstream cylinder at 80% void fraction: (a) Lift force spectra and (b) Drag force spectra

Similarly, the force spectra for the interior and downstream cylinder are very similar in the drag direction but a little lower than for the upstream cylinder (see Figs 4.14(a) and 4.14(b)). In the lift direction, on the other hand, the force spectra are much larger for the

interior and downstream cylinders than for the upstream and single cylinder as observed earlier (see Figs 4.13(a) and 4.13(b)). At a flow velocity of 10 m/s the force spectra in the lift direction for the interior and downstream cylinders are nearly identical (see Fig.4.13(b)). At 5 m/s, the downstream spectrum is slightly lower.

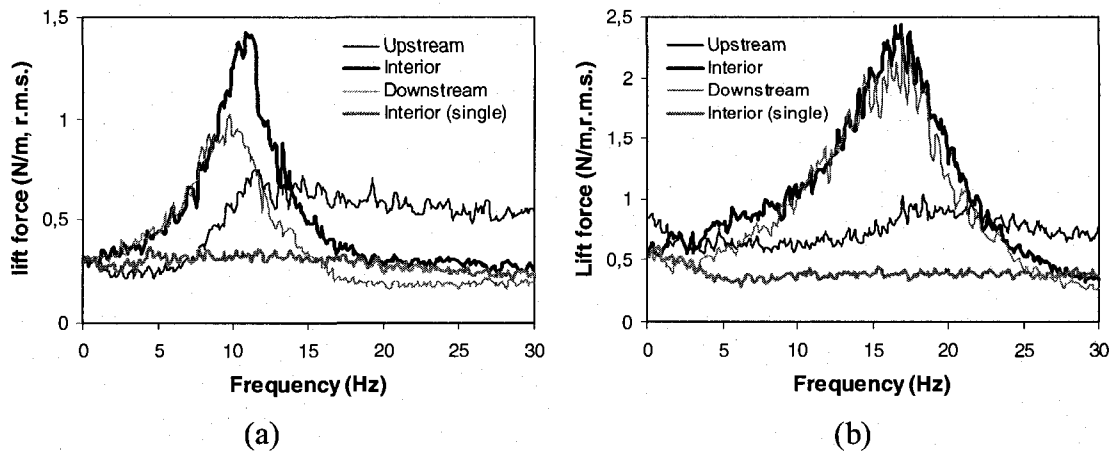


**Fig. 4.13** Comparison of lift spectra along the flow path for 80% void fraction: (a) at 5 m/s pitch velocity and (b) at 10 m/s pitch velocity

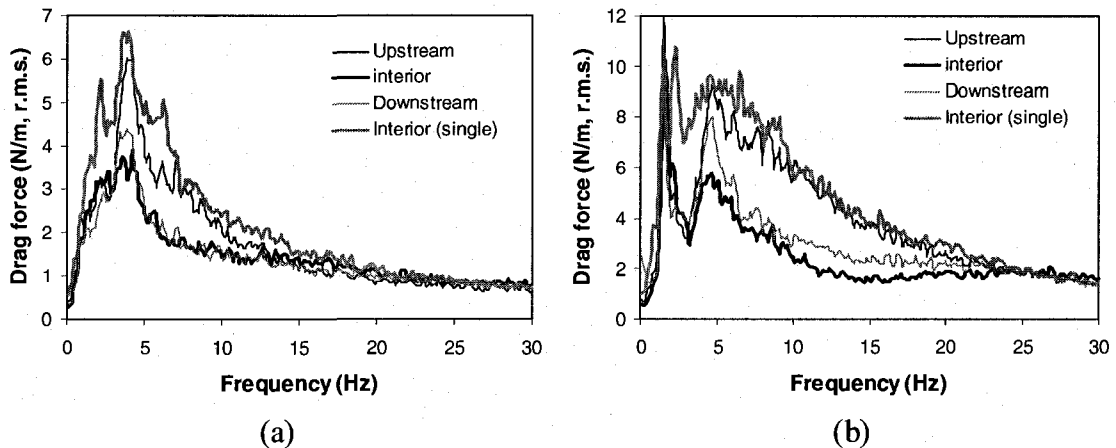


**Fig. 4.14** Comparison of drag spectra along the flow path for 80% void fraction: (a) at 5 m/s pitch velocity and (b) at 10 m/s pitch velocity

The effect of flow velocity in the force spectra for the single cylinder is shown in Figs 4.15(a) and 4.15(b) for the lift and drag direction respectively. Fig. 4.15(a) shows the near lack of periodicity in the lift direction and Fig. 4.15(b) the prominent periodicity in the drag direction.



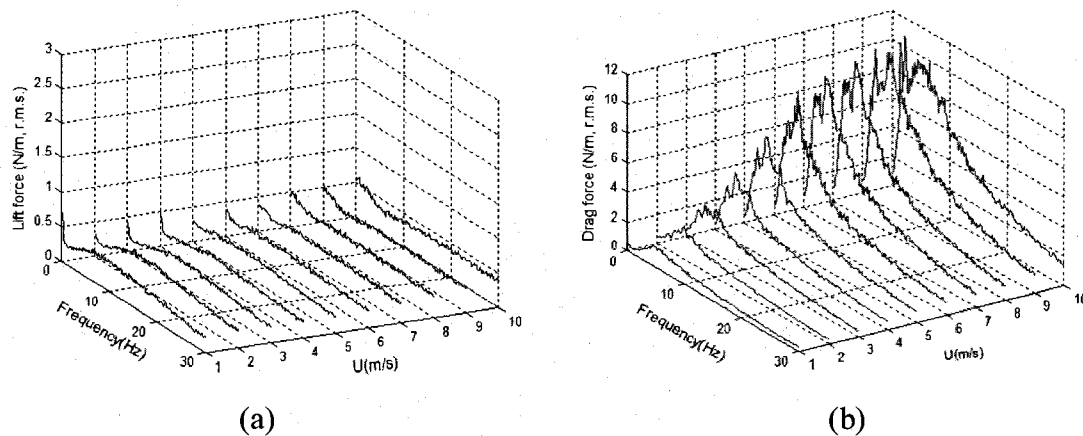


**Fig. 4.15** Typical dynamic force spectra for the single cylinder at 80% void fraction:  
 (a) Lift force spectra and (b) Drag force spectra

#### 4.5 Discussion

The results of force measurements indicate that unexpected but significant quasi-periodic forces were measured in both the drag and lift direction. These forces are significantly larger in the drag direction. However, the excitation force frequency is relatively low (i.e., 3-6 Hz) and not directly dependent on flow velocity in the drag direction. On the other hand much higher frequencies (up to 16 Hz) were observed in the lift direction at the higher flow velocities. The frequency appears directly related to flow velocity in the lift direction. This kind of quasi-periodic forces should not be surprising, because flow patterns in both vertical and horizontal pipes are characterized by periodic structures. Data from many sources comprising many flow patterns were correlated as Strouhal number against the Lockhart-Martinelli parameter with some degree of success by Azzopardi and Baker [14]. Fig. 4.16 shows that our data may be similarly correlated and found to be in reasonable agreement with that of Ref. [14]. For the purpose of comparison with the data in Ref. [14], the Strouhal number is defined as  $S_2 = f(P-D)/U_g$ , where  $U_g = 0.866U_p$ . Subsequent measurements showed that the quasi-periodic drag and lift forces are generated by different mechanisms that have not been observed so far. The quasi-periodic drag forces appear related to the momentum flux fluctuations in the main flow path between the cylinders. The quasi-periodic lift forces,

on the other hand, are mostly correlated to oscillations in the wake of the cylinders. Although further investigations are needed, these initial results are encouraging since some understanding of the phenomenon is emerging.

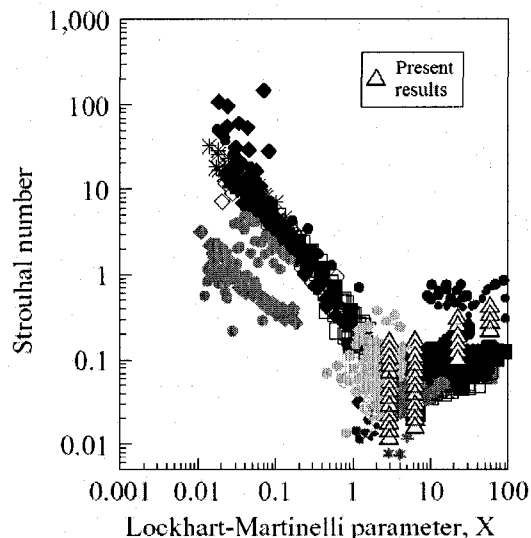


**Fig. 4.16** The relationship between Lockhart-Martinelli parameter and Strouhal number (from Ref [14])

## 4.6 Conclusion

Detailed force measurements were taken in a rotated triangular array of cylinders subjected to two-phase cross-flow. The experiments revealed somewhat unexpected but significant quasi-periodic forces in both the drag and lift directions. The periodic forces appeared well correlated along the cylinder with the drag force somewhat better correlated than the lift forces. The periodic forces are also dependent on the position of the cylinder within the bundle.

## 4.7 Acknowledgments

The authors are grateful to Dragos Pamfil for the two-phase flow test loop and test section design. Thanks also to Thierry Lafrance, Bénédict Besner and Nour Aimène for their help throughout the project.

## 4.8 Nomenclature

$f$ : Frequency (Hz)

$P, D$ : Pitch and tube diameter (m)

$S_1, S_2$ : Strouhal number

$U_p, U_g$ : Pitch, gap velocity (m/s)

$X$ : Martinelli parameter

## 4.9 References

- [1] Blevins, R. D., 1990, "Flow-induced vibration", New York: Van Nostrand Reinhold, 2nd edition.
- [2] Axisa, F., Antunes, J., and Villard, B., 1990, "Random excitation of heat exchanger tubes by cross-flows", *Journal of Fluid and Structures*, 4, pp. 321-341.
- [3] De Langre, E., and Villard, B., 1998, "An upper bound on random buffeting forces caused by two-phase flows across tubes", *Journal of Fluids Structures*, 12, pp. 1005–1023.
- [4] Feenstra, P.A., Weaver, D.S., and Nakamura, T., 2003, "Vortex shedding and Fluid-elastic instability in a normal square tube array excited by two-phase Cross-flow", *Journal of Fluids and Structures*, 17, pp. 793–811.
- [5] Nakamura, T., Fujita, K., Kowanishi, N., Yamaguchi, N., and Tsuge, A., 1995, "Study on the Vibration Characteristics of a Tube Array Caused by Two-Phase Flow, Part 1: Random Vibration", *Journal of Fluids and Structures*, 9, pp. 519–538.
- [6] Pettigrew, M.J., and Taylor, C.E., 1994, "Two-phase flow-induced vibration: an overview", *ASME Journal of Pressure Vessel Technology*, 116, pp. 233-253.
- [7] Pettigrew, M.J., Taylor, C.E. and Kim, B.S., 2001, "The effects of bundle geometry on heat exchanger tube vibration in two-phase cross-flow", *ASME Journal of Pressure Vessel Technology*, 123, pp. 414–420.

- [8] Pettigrew, M.J., Taylor, C.E., Janzen, V. P., and Whan, T., 2002, "Vibration behavior of rotated triangular tube bundles in two-phase cross-flow", *ASME Journal of Pressure Vessel Technology*, 124, pp. 144–153.
- [9] Taylor, C.E., Currie, I.G., Pettigrew, M.J. and Kim, B.S., 1989. "Vibration of tube bundles in two-phase cross-flow". Part 3: Turbulent induced excitation. *ASME Journal of Pressure Vessel Technology*, 111, pp. 488–500.
- [10] Taylor, C. E., Pettigrew, M. J., and Currie, I. G., 1996, "Random excitation forces in tube bundles subjected to two-phase cross-flow", *ASME Journal of Pressure Vessel Technology*, 118, pp. 265–277.
- [11] Taylor, C., and Pettigrew, M. J., 2000, "Random excitation forces in heat exchanger tube bundles", *ASME Journal of Pressure Vessel Technology*, 122, pp. 509–514.
- [12] Pettigrew, M.J., Zhang, C, Mureithi, N.W, and Pamfil, D., 2005, "Detailed flow and force measurements in a rotated triangular tube bundle subjected to two-phase cross-flow", *Journal of Fluids and Structures*, 20, pp. 567-575.
- [13] Zhang, C., Pettigrew, M.J., and Mureithi, N.W., 2006, "Correlation between vibration excitation forces and the dynamic characteristics of two-phase flow in a rotated triangular tube bundle", *Proceeding of ASME PVP2006-ICPVT-11, 6th FSI, AE & FIV and N Symposium*, (Paidoussis, M.P., editor), Vancouver, Canada, ASME (to appear).
- [14] Azzopardi, B.J., and Baker, G., 2003, "Characteristics of periodic structures in gas/liquid two-phase flow", *Proceedings of UK/Japan Two-Phase Flow Meeting*, Guildford, UK, pp. 14-15.

## CHAPTER 5

# CORRELATION BETWEEN VIBRATION EXCITATION FORCES AND THE DYNAMIC CHARACTERISTICS OF TWO-PHASE CROSS FLOW IN A ROTATED TRIANGULAR TUBE BUNDLE

C. Zhang, M. J. Pettigrew\*, and N. W. Mureithi

BWC/AECL/NSERC Chair of Fluid-Structure Interaction, Department of Mechanical  
Engineering, École Polytechnique, Montréal, QC, Canada H3T 1J4

To appear in *ASME Journal of Pressure Vessel Technology* 2008; 130 (1)

## 5.1 Abstract

Two-phase cross flow exists in many shell-and-tube heat exchangers. Flow-induced vibration excitation forces can cause tube motion that will result in long-term fretting-wear or fatigue. Detailed flow and vibration excitation force measurements in tube bundles subjected to two-phase cross flow are required to understand the underlying vibration excitation mechanisms. Some of this work has already been done. The distributions of both void fraction and bubble velocity in rotated-triangular tube bundles were obtained. Somewhat unexpected but significant quasi-periodic forces in both the drag and lift directions were measured.

The present work aims at understanding the nature of such unexpected drag and lift quasi-periodic forces. An experimental program was undertaken with a rotated-triangular array of cylinders subjected to air/water flow to simulate two-phase mixtures. Fiber-optic probes were developed to measure local void fraction. Both the dynamic lift and drag forces were measured with a strain gage instrumented cylinder.

The investigation showed that the quasi-periodic drag and lift forces are generated by different mechanisms that have not been previously observed. The quasi-periodic drag forces appear related to the momentum flux fluctuations in the main flow path between the cylinders. The quasi-periodic lift forces, on the other hand, are mostly correlated to oscillations in the wake of the cylinders. The quasi-periodic lift forces are related to local void fraction measurements in the unsteady wake area between upstream and downstream cylinders. The quasi-periodic drag forces correlate well with similar measurements in the main flow stream between cylinders.

## 5.2 Introduction

Two-phase cross flow exists in many shell-and-tube heat exchangers, for instance, in the U-tube region of nuclear steam generators. Flow-induced vibration excitation forces can

cause excessive vibration that may result in long-term fretting-wear or fatigue. To prevent such tube failures in heat exchangers, designers and troubleshooters must have guidelines that incorporate flow-induced vibration excitation forces.

In single-phase flow, these forces have been extensively measured and analyzed. They are related to periodic wake shedding and to turbulence generated within the bundle. Experimental data obtained for different kinds of fluids and tube bundles have been satisfactorily compared through the use of adequate data-reduction procedures [1, 2].

In the case of two-phase flows, such extensive studies have not been undertaken, though it is known that there are significant differences between single- and two-phase flows. In particular, the relationship between the two phases must be considered in addition to another parameter that is void fraction. This results in different flow regime or patterns of two-phase flow. A few sets of experimental results have been obtained recently, as in Refs [2-12]. However many questions remain such as the effects of viscosity, surface tension, density ratio and flow regimes. Actually, the main problem is the understanding of the physical mechanism that induces these forces. Detailed flow and vibration excitation force measurements in tube bundles subjected to two-phase cross flow are required to understand the underlying vibration excitation mechanisms. Some of this work has already been done by Pettigrew et al. [11] and Zhang et al. [12]. The distributions of both void fraction and bubble velocity in rotated-triangular tube bundles were obtained. Somewhat unexpected but significant quasi-periodic forces in both the drag and lift directions were measured.

The present work aims at understanding the nature of such unexpected drag and lift quasi-periodic forces. An experimental program was undertaken with a rotated-triangular array of cylinders subjected to air/water flow to simulate two-phase mixtures. Fiber-optic probes were used to measure local void fraction. Both the dynamic lift and drag forces were measured with a strain gage instrumented cylinder.

The investigation showed that the quasi-periodic drag and lift forces are generated by different mechanisms that have not been previously observed. The quasi-periodic drag forces appear related to the momentum flux fluctuations in the main flow path between the cylinders. These momentum flux fluctuations are caused by void fraction fluctuations in the main flow path between the cylinders. The quasi-periodic lift forces, on the other hand, are mostly related to oscillation in the wake of the cylinders. The quasi-periodic lift forces are correlated to local void fraction measurements in the unsteady wake area between upstream and downstream cylinders. The quasi-periodic drag forces correlate well with similar measurements in the main flow stream between cylinders.

### 5.3 Nomenclature

$f$ : Frequency (Hz)

$P, D$ : Pitch and tube diameter (m)

$U_p = U_\infty P / (P - D)$ : Pitch flow velocity (m/s)

$U_\infty$ : Upstream homogenous flow velocity (m/s)

$\alpha(t)$ : Instantaneous local void fraction

### 5.4 Experimental consideration

#### 5.4.1 Test section

The experiments were done in an air-water loop to simulate two-phase flows. The loop was described in details by Pettigrew et al. [11] and Zhang et al. [12]. Compressed air was injected below a suitably designed mixer to homogenize and distribute the two-phase mixture uniformly below the test-section. The air flow was measured with orifice plates connected to a differential pressure transducer and electronic readout system. The



loop was operated at room temperature and the pressure in the test section was slightly above atmospheric.

The test section, which has an essentially rectangular cross section ( $99 \times 191$  mm), is shown in Fig. 5.1. It consists of a column of six 38 mm diameter cylinders flanked on either side by half cylinders to simulate essentially the flow path in a large array of cylinders in a rotated triangular configuration. The pitch-to-diameter ratio,  $P/D$ , was 1.5 resulting in an inter-cylinder gap of 19 mm which allowed sufficient space for detailed flow measurements. The test-section length-to-gap width ratio is ten, thus, adequate to maintain essentially two-dimensional flow. The measurements were taken at several positions with fiber-optic probes assembled within a traversing mechanism. The tip of the probes could be positioned accurately with a micrometer head.

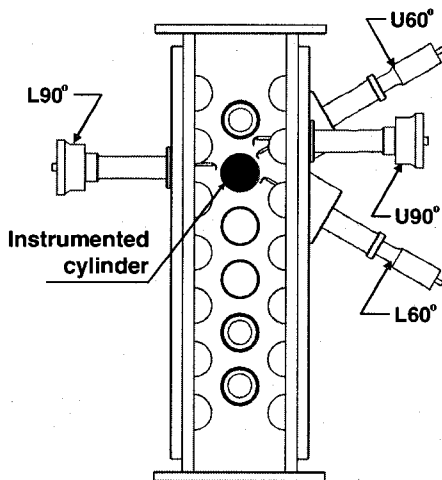


**Fig. 5.1** Test section

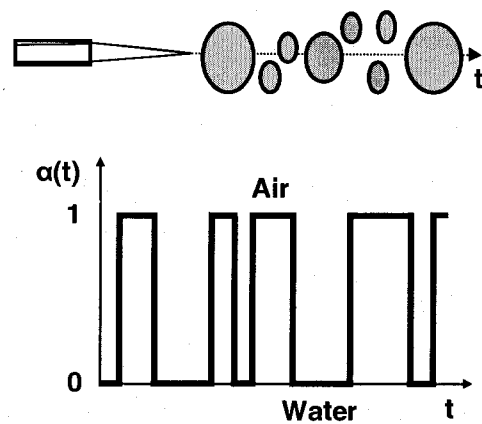


**Fig. 5.2** Idealized two-phase flow signal from fiber-optic probes

The probe assemblies were installed at four principal positions in the array as shown in Fig. 5.1. These positions are henceforth called lower and upper 60° ( $L60^\circ$  and  $U60^\circ$ ) for the narrow gaps between cylinders and lower and upper 90° ( $L90^\circ$  and  $U90^\circ$ ) for the larger flow areas between upstream and downstream cylinders. One cylinder was

instrumented with strain gauges to measure the dynamic drag and lift forces due to the two-phase flow.

#### 5.4.2 Fiber-optic probes for two-phase flow measurements

Each fiber-optic probe has a conical tip and is made of an optical fiber of 170  $\mu\text{m}$  diameter. It acts as a phase sensor based on the different level of light reflection between air and water (Fig. 5.2). Four probes were used to measure simultaneously the dynamic characteristics of two-phase flow surrounding the instrumented cylinder. Several different probe combinations as shown in Fig. 5.3 were selected for two-phase flow measurements, i.e., LLLL, CCCC, RRRR, etc. Here L, C and R represent the left, center and right positions of probe  $L60^\circ$ ,  $L90^\circ$ ,  $U60^\circ$  and  $U90^\circ$  in the main flow path, respectively. Additionally  $L_0$  is a point on the center line of the test section at the Probe  $U90^\circ$  position.  $L_1$  is about 5 mm from  $L_0$ .

#### 5.4.3 Instrumentation

Both the dynamic lift and drag forces were measured with a strain gage instrumented cylinder located in the fifth position from the upstream end of the test-section (Fig. 5.1). The instrumented cylinder was cantilevered and surrounded by rigid tubes. Two pairs of diametrically opposite strain gages were installed in the cylinder at 90 deg from each other to measure the forces in the flow direction (drag) and in the direction normal to the flow (lift). The strain gages were connected to strain indicators. The natural frequency of the cantilever cylinders was much higher (i.e.,  $>150\text{Hz}$ ) than the excitation force frequencies such that the cantilever cylinder functioned essentially as a dynamic force transducer. The static strain-force relation was determined via a careful calibration.

Two-phase flow, and dynamic lift and drag force measurements were performed simultaneously. Four flow conditions were investigated in detail, i.e., 80% and 90%

homogeneous void fractions at a nominal pitch flow velocity,  $U_p$ , of 5 m/s and 10 m/s. Both the void probe and the force signals were analyzed on an OR38 8-32 channel real time multi-analyzer/recorder coupled to a laptop computer.

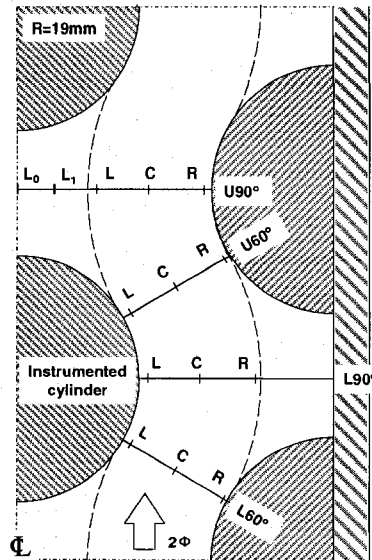


Fig. 5.3 Probe positions for flow measurements

## 5.5 Experimental results and discussion

### 5.5.1 Dynamic lift and drag force measurements

Detailed vibration excitation force measurements in a rotated triangular tube bundle subjected to two-phase cross flow have been taken by Zhang et al. [12]. Both the dynamic lift and drag forces were measured. The experiments revealed somewhat unexpected but significant quasi-periodic forces in both the drag and lift directions. These forces are significantly larger in the drag direction. However, the excitation force frequency is relatively low (i.e., 3-6 Hz) and not directly dependent on flow velocity in the drag direction. On the other hand much higher frequencies (up to 16 Hz) were observed in the lift direction for 80% void fraction at 10 m/s pitch flow velocity. The frequency appears directly related to flow velocity in the lift direction. The periodic forces appeared well correlated along the cylinder with the drag force somewhat better

correlated than the lift forces. The periodic forces are also dependent on the position of the cylinder within the bundle.

To understand the nature of these unexpected drag and lift quasi-periodic forces, measurements were taken with an instrumented cylinder located in the fifth cylinder position from the upstream end of the test-section (see Fig. 5.1). Typical lift and drag force spectra are shown in Figs 5.4 and 5.5. The spectra reveal narrow band or quasi-periodic forces. For the case of 80% void fraction, the periodic force frequency in the lift direction increases from about 11 to 16 Hz for a corresponding increase in pitch flow velocity of 5 to 10 m/s (Figs 5.4(a) and 5.5(a)). This yields Strouhal numbers ( $fD/U_p$ ) from 0.08 to 0.06. Although periodic vortex shedding was not believed to have occurred at such high void fraction, the wake between cylinders was observed visually to be quite unsteady.

Periodicity was also observed in the drag direction as shown in Figs 5.4(b) and 5.5(b). Surprisingly, for the case of 80% void fraction, the frequency of the periodic drag forces is relatively low and does not change so much (4 Hz for 5 m/s, 4.625 Hz for 10 m/s), and these forces are significantly larger. Some very sharp peaks at low frequency (around 2 Hz) also appeared at high mass fluxes as shown in Fig. 5.5(b).

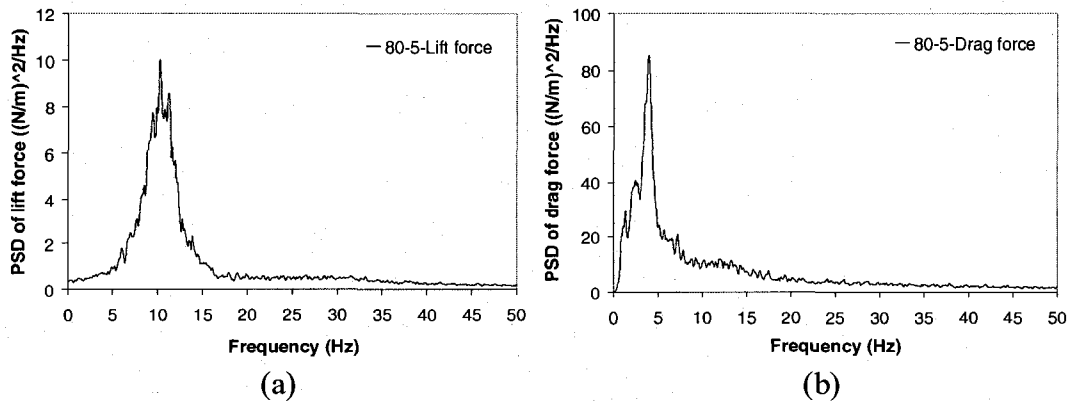


**Fig. 5.4** Typical dynamic force spectra for 80% void fraction at 5 m/s pitch flow velocity: (a) Lift force spectra and (b) Drag force spectra

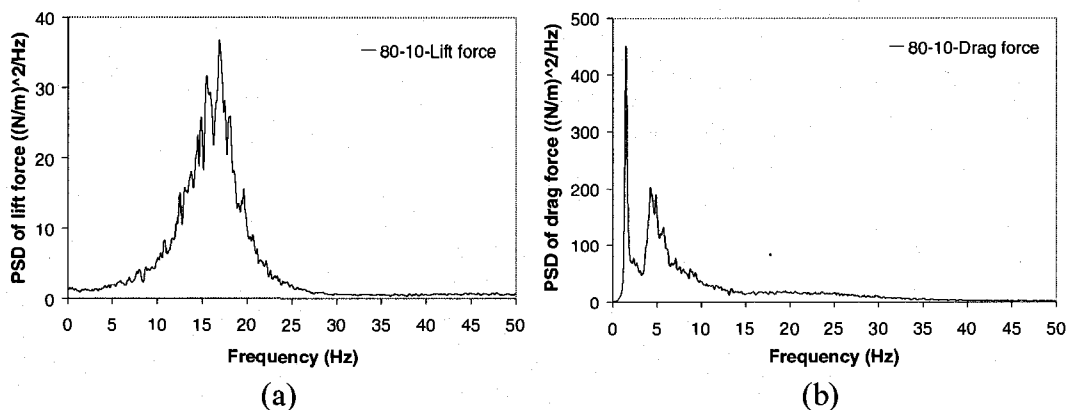


**Fig. 5.5** Typical dynamic force spectra for 80% void fraction at 10 m/s pitch flow velocity: (a) Lift force spectra and (b) Drag force spectra

### 5.5.2 Dynamic characteristics of two-phase flow

The detailed flow measurements previously taken by Pettigrew et al. [11] show that the flow tends to stream between the cylinders and that within that stream the flow velocity is fairly uniform but the void fraction distribution is not uniform. In fact, the flow path resembles a series of two-dimensional  $60^\circ$  elbows as shown in Fig. 5.3.

In this paper only the dynamic characteristics of the two-phase flow in terms of local void fraction fluctuations are considered. The original void fraction fluctuation signals were processed into 0-1 ideal signals, where 0 means liquid phase and 1 means gas phase. The power spectra of the local void fraction fluctuation detected by the fiber-optic probes were analyzed. Typical power spectra of the local void fraction fluctuation on the right side of the main flow path are shown in Figs 5.6 and 5.7. The power spectra show the non-random and somewhat narrow band characters of the void fraction fluctuation. For the case of 80% void fraction, at 5 m/s pitch flow velocity (Fig. 5.6), the spectra have a dominant frequency of about 4 Hz; at 10 m/s pitch flow velocity (Fig. 5.7), the spectra have a dominant frequency of about 4.6 Hz. These dominant frequencies are consistent with those of the dynamic drag forces (Figs 5.4(b) and 5.5(b)). This clearly indicates a possible dynamic link between the void fraction fluctuation on the right side of the main flow path and the dynamic drag forces.

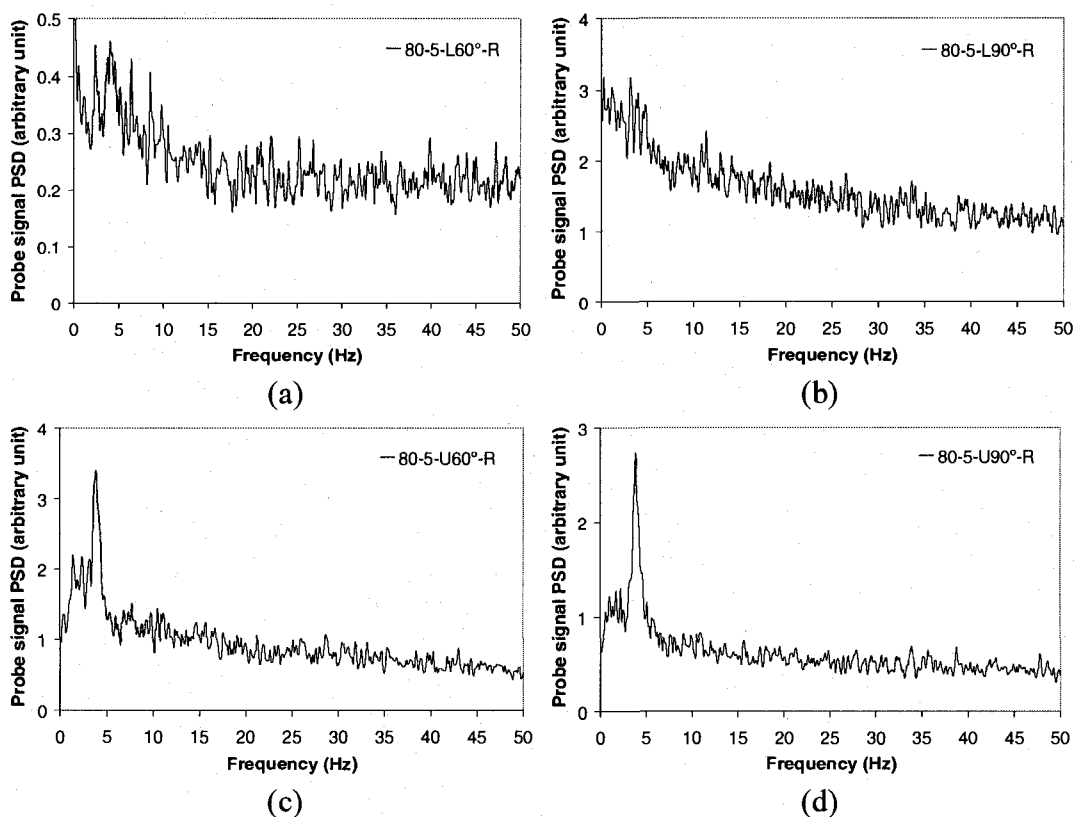


**Fig. 5.6** Power spectra of the local void fraction fluctuation at four different positions on the right side of the main flow path for 80% void fraction at 5 m/s pitch flow velocity: (a) L60° position, (b) L90° position, (c) U60° position, and (d) U90° position

The very sharp peak at low frequency (about 2 Hz) was also found with a pressure sensor in the test section and just after the pump for both water and two-phase flow. It was not found in the water tank. Detailed accelerometer measurements showed that it was not due to vibration of the loop. Therefore, this sharp frequency peak is not related to the nature of two-phase flow. It is an unwanted signal component which should not be considered further.

Typical power spectra of the local void fraction fluctuation on the left side of the main flow path are shown in Figs 5.8 and 5.9. They also show the non-random and somewhat narrow band character of the void fraction fluctuations. For 80% void fraction, at 5 m/s pitch flow velocity (Fig. 5.8), the spectra have a dominant frequency of about 11 Hz; at

10 m/s pitch flow velocity (Fig. 5.9), the spectra have a dominant frequency of about 16 Hz. These dominant frequencies are consistent with those of the dynamic lift forces (Figs 5.4(a) and 5.5(a)). This clearly indicates a possible dynamic link between the void fraction fluctuations on the left side of the main flow path and the dynamic lift forces. Furthermore, the void fraction fluctuations at that location are probably caused by the flow oscillation in the wake between the upstream and downstream cylinders. These flow oscillations were observed visually during the tests. Some less prominent low frequency peaks are also shown in Figures 5.8 and 5.9: at 5 m/s pitch flow velocity (Fig. 5.8), a low frequency peak is at about 4 Hz; at 10 m/s pitch flow velocity (Fig. 5.9), a low frequency peak exists around 4.6 Hz. These frequencies are also present in the dynamic drag force spectra (Figs 5.4(b) and 5.5(b)).

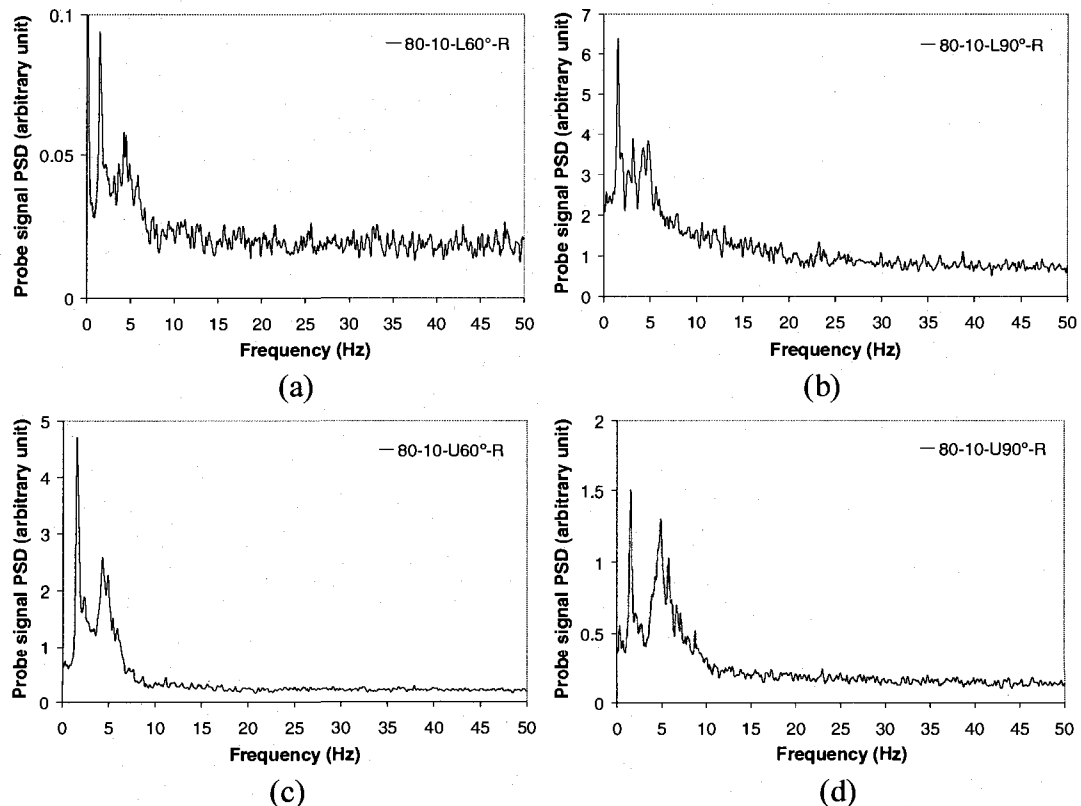


**Fig. 5.7** Power spectra of the local void fraction fluctuation at four different positions on the right side of the main flow path for 80% void fraction at 10 m/s pitch flow velocity: (a) L60° position, (b) L90° position, (c) U60° position, and (d) U90° position

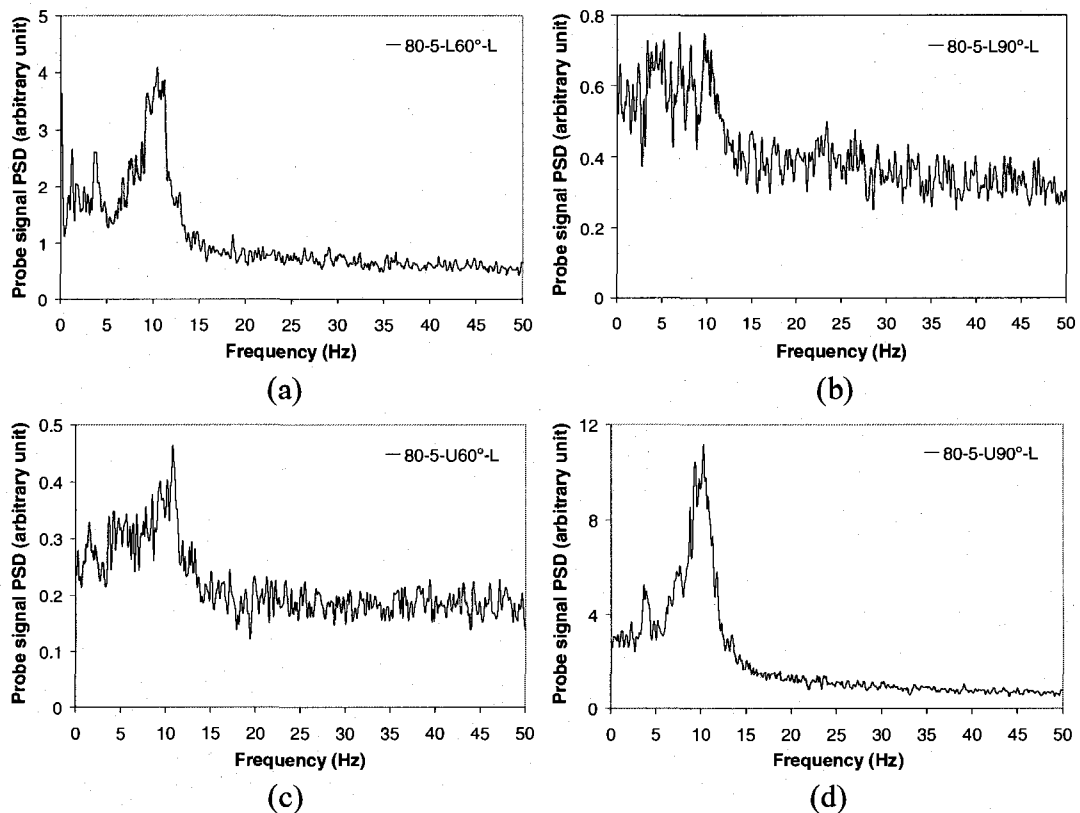


**Fig. 5.8** Power spectra of the local void fraction fluctuation at four different positions on the left side of the main flow path for 80% void fraction at 5 m/s pitch flow velocity: (a) L60° position, (b) L90° position, (c) U60° position, and (d) U90° position

Typical power spectra of the local void fraction fluctuation along the center line of the main flow path are shown in Figs 5.10 and 5.11. The spectra appear to be a combination of those on the right and left sides of the main flow path (Figs 5.6 & 5.8, and Figs 5.7 & 5.9). For 80% void fraction, at both 5 m/s and 10 m/s pitch flow velocity, the spectra are very similar to those of the left side of the main flow path (Figs 5.8 and 5.9), except that the magnitudes of power spectral density of the higher frequency peak (11 Hz for 5 m/s pitch flow velocity, and 16 Hz for 10 m/s pitch flow velocity) are getting smaller, which means that the effect of the flow oscillation in the wake between the upstream and downstream cylinders becomes gradually weaker from the left to the center.



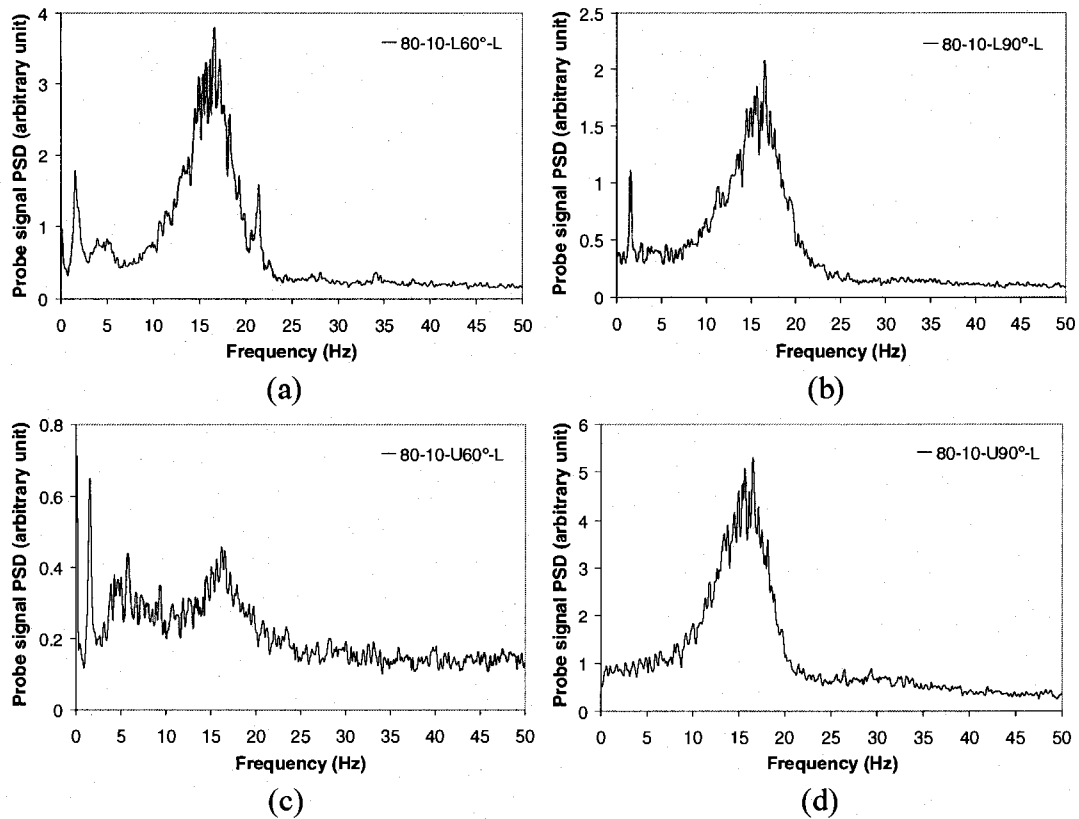


**Fig. 5.9** Power spectra of the local void fraction fluctuation at four different positions on the left side of the main flow path for 80% void fraction at 10 m/s pitch flow velocity: (a) L60° position, (b) L90° position, (c) U60° position, and (d) U90° position

Further tests revealed the same trend, which is that the magnitudes of power spectral density of the higher frequency peak are getting smaller, and that the lower frequency peaks are getting more prominent when the probes are traversed from the left to the right direction.

Some interesting trends may be observed by comparing the spectra of Probes L60° and U60°. For Probe L60°, the power spectral density is getting smaller (Figs 5.6(a), 5.8(a) and 5.10(a) or Figs 5.7(a), 5.9(a) and 5.11(a)), when the probe is moved from left to right. On the other hand, for Probe U-60°, the power spectral density is getting larger (Figs 5.6(c), 5.8(c) and 5.10(c) or Figs 5.7(c), 5.9(c) and 5.11(c)), when the probe is moved from left to right. Except for the near 11 and 16 Hz peaks (corresponding to a

pitch flow velocity of 5 and 10 m/s respectively), the power spectral density of the void fraction fluctuations at positions L60°-L and U60°-R are somewhat similar as expected because of symmetry in the flow path. As shown in Figure 5.3 the main flow path is essentially a series of 60° elbows. Positions L60°-L and U60°-R are similarly located on the elbows. More precisely, L60°-L and U60°-R are the extrados, L60°-R and U60°-L are the intrados at the exits of the two successive 60° elbows [11].

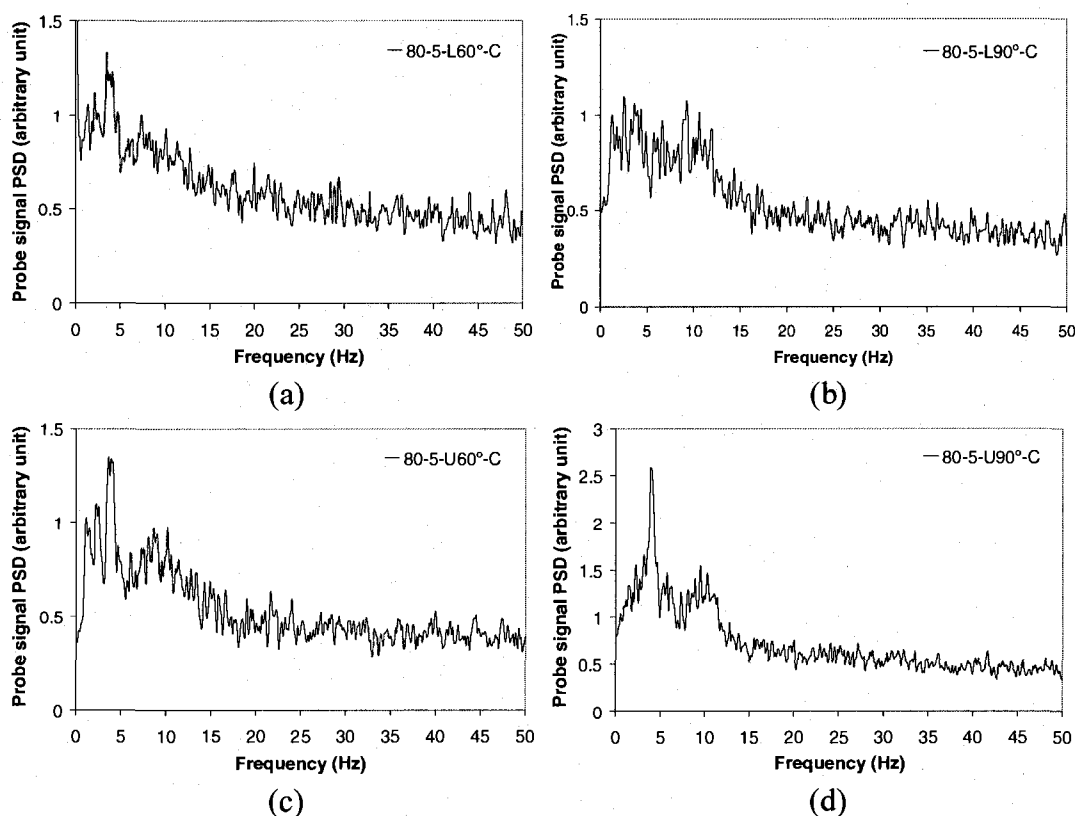


**Fig. 5.10** Power spectra of the local void fraction fluctuation at four different positions along the center line of the main flow path for 80% void fraction at 5 m/s pitch flow velocity: (a) L60° position, (b) L90° position, (c) U60° position, and (d) U90° position

The 11 and 16 Hz peaks, on the other hand are due to the oscillating nature of the flow at the center of the test section between upstream and downstream cylinders. These oscillations are largely prevented by the presence of the wall between half-cylinders at the side of the test section.

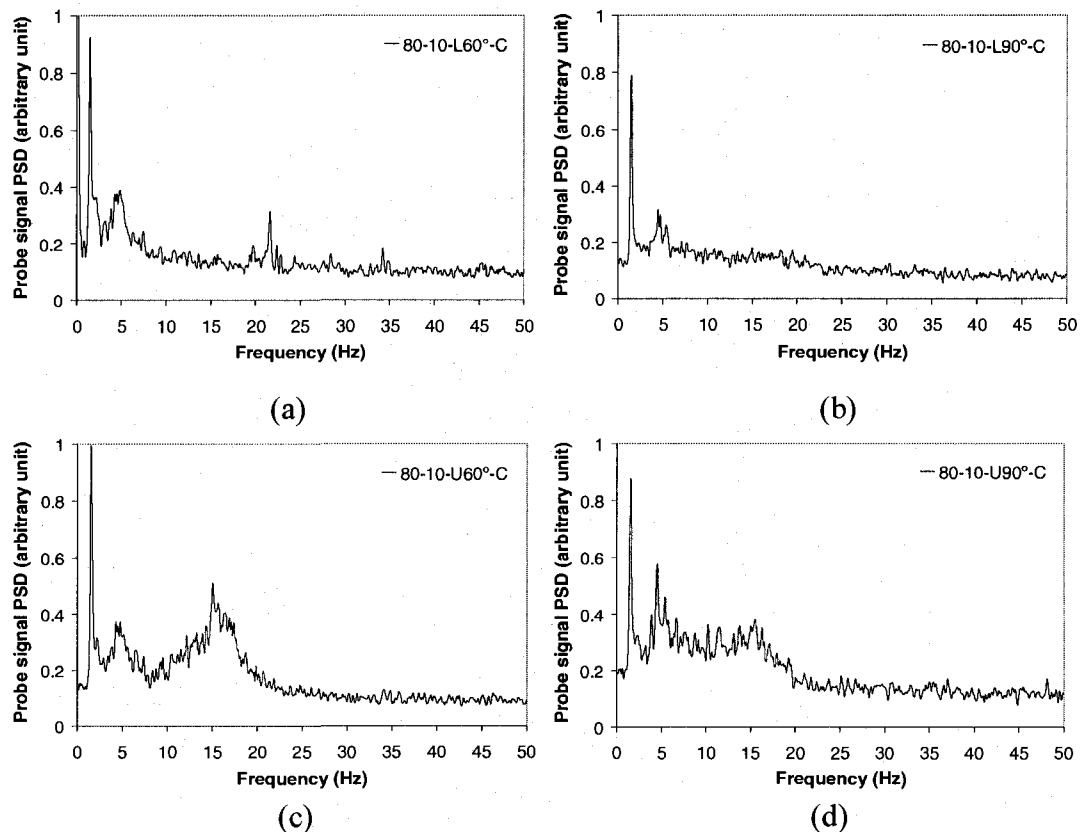
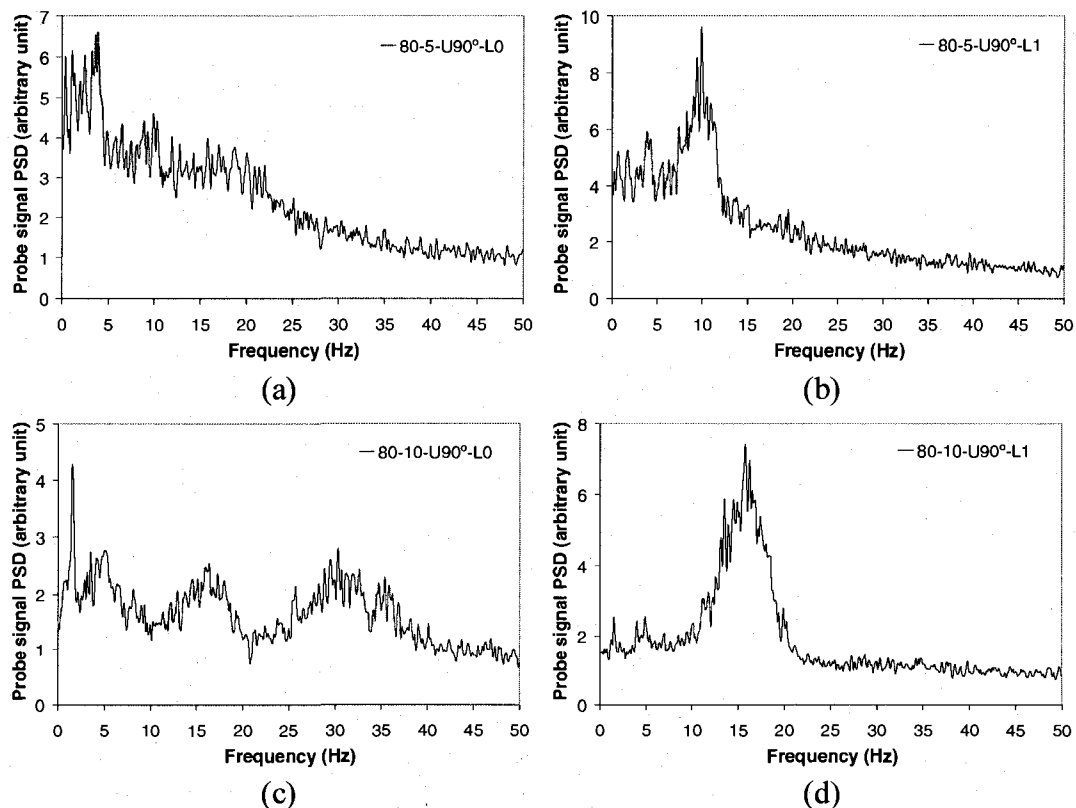


**Fig. 5.11** Power spectra of the local void fraction fluctuation at four different positions along the center line of the main flow path for 80% void fraction at 10 m/s pitch flow velocity: (a) L60° position, (b) L90° position, (c) U60° position, and (d) U90° position

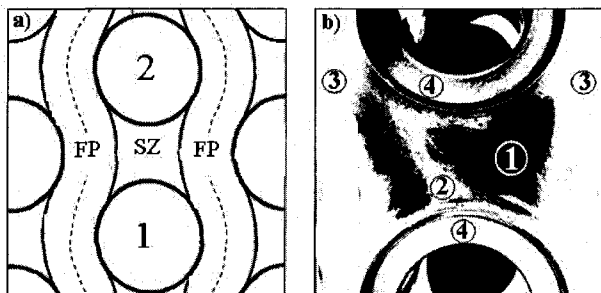
Typical power spectra of local void fraction fluctuations at positions U90°-L<sub>0</sub> and U90°-L<sub>1</sub> are shown in Fig. 5.12. For 80% void fraction, at both 5 m/s and 10 m/s pitch flow velocity, the spectra at position L<sub>0</sub> are very similar to those of the center line of the main flow path (Figs 5.10d and 5.11d), except that the magnitudes of power spectral density are higher at L<sub>0</sub>. The spectra at position L<sub>1</sub> are very similar to those of the left side of the main flow path (Figs 5.8d and 5.9d) in both magnitude and frequency. This may be explained by the following observation.

Fig. 5.13a gives a simplified schematic representation of the flow structure inside a rotated triangular tube bundle. The flow is mostly inside the flow path (FP). In between adjacent tubes of the same column (Tubes 1 and 2), the flow velocity is much less than

in the flow paths and is taken to be near zero. This zone is called the stagnation zone or recirculation zone (SZ). In two-phase continuous flow, the mixture inside the flow paths appears to be very fine and homogenous. On the other hand, in the stagnation zone (SZ), the two-phase mixture is coarse and non-homogeneous, and transverse oscillations in the wake of the cylinders exist. Fig. 5.13b shows a black and white picture of the structure of the two-phase flow inside a rotated triangular array for high void fraction (95%) and flow velocity (12 m/s). Except for the tubes themselves, light tones indicate high void fraction mixtures and dark tones indicate very low void fraction two-phase mixtures. From Fig. 5.13b, it can be seen that there is a large volume of very low void fraction mixture inside the stagnation zone and that a small portion of the space is occupied by a high void fraction mixtures. Similar phenomena were observed visually for 80% void fraction at 5 and 10 m/s pitch flow velocity.



**Fig.5.12** Power spectra of the local void fraction fluctuation at points  $L_0$  and  $L_1$  of  $U_{90^\circ}$  position: (a), (b) for 80% void fraction at 5 m/s pitch flow velocity, and (c), (d) for 80% void fraction at 10 m/s pitch flow velocity, respectively



**Fig. 5.13** Two-phase flow structure in a rotated triangular tube bundle: (a) simplified figure (FP: flow path, SZ: “stagnation” zone), (b) flow picture (1: low void fraction mixture belonging to the stagnation zone, 2: oscillating high void fraction mixture in stagnation zone, 3: flow path, 4: rigid tubes)

The above investigation showed that the quasi-periodic drag and lift forces are generated by different mechanisms. The quasi-periodic drag forces appear related to the momentum flux fluctuations in the main flow path between the cylinders. The quasi-periodic lift forces, on the other hand, are mostly correlated to the oscillation in the wake of the cylinders.

### 5.5.3 Correlation between void fraction fluctuations and dynamic lift and drag forces

Further evidence of the correlation between void fraction fluctuations and the dynamic lift and drag forces is given in Fig. 5.14, which show the coherence between the void fraction fluctuations at L60°-C and U90°-L and the dynamic lift and drag forces for 80% void fraction at 5 m/s and 10 m/s pitch flow velocity. Figs 5.14(a) and 5.14(b) show that the coherence between void fraction fluctuations at L60°-C and drag forces is relatively high in the frequency range 0-20 Hz. Figs 5.14(c) and 5.14(d) reveal that the coherence between void fraction fluctuation at U90°-L and lift forces is relatively high up to 20 Hz (for 5 m/s pitch flow velocity) and up to 25 Hz (for 10 m/s pitch flow velocity). It seems that the coherence between void fraction fluctuations at U90°-L and lift forces is somewhat better than the coherence between void fraction fluctuations at L60°-C and drag forces. More results on the coherence between void fraction fluctuations and the dynamic lift and drag forces at the quasi-periodic frequency for 80% void fraction at 5 m/s and 10 m/s pitch flow velocity may be found in Tables 5.1 and 5.2. On the whole,

the coherence is higher at 10 m/s than at 5 m/s pitch flow velocity. For the coherence between void fraction fluctuations and the dynamic lift forces, this is probably because the wake oscillation phenomenon is steady and better defined at the higher pitch flow velocity as observed visually. For the same reason, the spectra of the void fraction fluctuation are narrower at the higher pitch flow velocity (Figs 5.8 and 5.9).

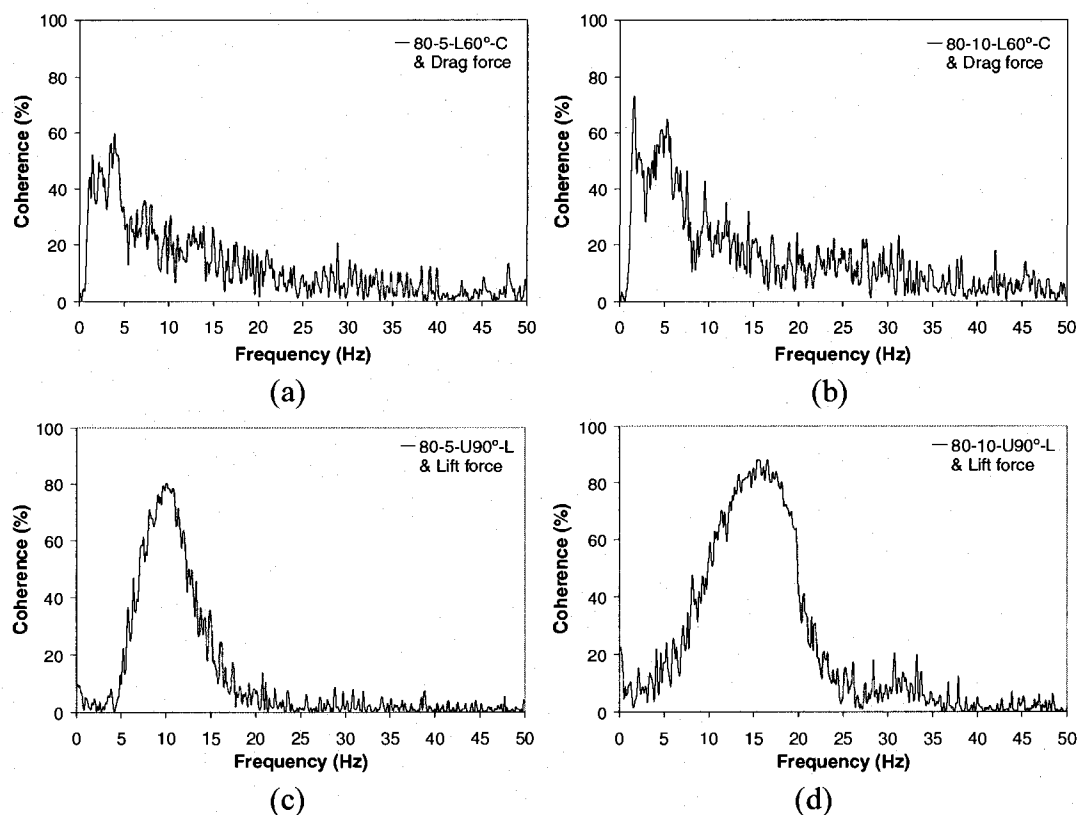


**Fig. 5.14** Coherences between the local void fraction fluctuation and the dynamic lift and drag forces for 80% void fraction: (a), (b) void fraction fluctuation at L60°-C and drag force, and (c), (d) void fraction fluctuation at U90°-L and lift force, at 5 m/s and 10 m/s pitch flow velocity, respectively

## 5.6 Future work

One may have the opinion that the present observations are possibly an artifact of this particular experimental set-up and would not be observed in another configuration of the same array geometry and flow conditions. This particular tube array may be too narrow to permit diffusion of the flow laterally across the wake area between upstream and

downstream cylinders, a phenomenon perhaps even more important in two-phase flows because of void differences between the main flow path and the wake area between upstream and downstream cylinders. To answer these questions we have recently done some tests with a wider test section including three columns of cylinders instead of the one column used in this study. We found very similar results. These results will be presented in a subsequent paper.

After understanding the nature of the observed drag and lift quasi-periodic forces, the logical next step is to develop models to predict these forces starting from the observed dynamic characteristics of two-phase flow. A model is being developed to correlate the void fraction fluctuation in the main flow path and the dynamic drag forces. Another model for correlating the oscillation in the wake of the cylinders and the dynamic lift forces is also being developed. Both models can predict the forces reasonably well. The development of these models will be presented in a future paper.

**Table 5.1** Coherence between void fraction fluctuations and the dynamic lift and drag forces at the quasi-periodic frequency for 80% void fraction at 5 m/s pitch flow velocity

Probe positions Coherence (%)	In the bundle Within the main flow path	L60°	L90°	U60°	U90°
		With drag force	Center line	59.7	47.4
	Right side	37.2	11.1	65.6	76.2
	Left side	57.4	33.8	88.9	50.8
With lift force	Left side	71.6	21	54.6	80

**Table 5.2** Coherence between void fraction fluctuations and the dynamic lift and drag forces at the quasi-periodic frequency for 80% void fraction at 10 m/s pitch flow velocity

Probe positions Coherence (%)	In the bundle Within the main flow path	L60°	L90°	U60°	U90°
		With drag force	Center line	64.5	57.4
	Right side	41.3	43.4	80.7	75.1
	Left side	52.6	25.9	49.6	26
With lift force	Left side	91.1	92.6	59.3	87.5

## 5.7 Conclusion

The results of two-phase flow dynamic characteristics and force measurements indicate that quasi-periodic drag and lift forces are generated by different mechanisms that have not been previously observed. The quasi-periodic drag forces appear related to the momentum flux fluctuations in the main flow path between the cylinders. These momentum flux fluctuations are caused by the void fraction fluctuations in the main flow path between the cylinders. The quasi-periodic lift forces, on the other hand, are mostly correlated to the oscillation in the wake of the cylinders. The quasi-periodic lift forces are related to local void fraction measurements in the unsteady wake area between upstream and downstream cylinders. The quasi-periodic drag forces correlate well with similar measurements in the main flow stream between cylinders.

## 5.8 Acknowledgments

The authors are grateful to Dragos Pamfil for the test section design and the development of the fiber-optic probes. Thanks are also due to Thierry Lafrance, Bénédicte Besner and Nour Aimène for their help throughout the project.

## 5.9 References

- [1] Blevins, R. D., 1990, "Flow-induced vibration", New York: Van Nostrand Reinhold, 2nd edition.
- [2] Axisa, F., Antunes, J., and Villard, B., 1990, "Random excitation of heat exchanger tubes by cross-flows", *Journal of Fluid and Structures*, 4, pp. 321-341.
- [3] De Langre, E., and Villard, B., 1998, "An upper bound on random buffeting forces caused by two-phase flows across tubes", *Journal of Fluids Structures*, 12, pp. 1005-1023.



- [4] Feenstra, P.A., Weaver, D.S., and Nakamura, T., 2003, "Vortex shedding and Fluid-elastic instability in a normal square tube array excited by two-phase Cross-flow", *Journal of Fluids and Structures*, 17, pp. 793–811.
- [5] Nakamura, T., Fujita, K., Kowanishi, N., Yamaguchi, N., and Tsuge, A., 1995, "Study on the Vibration Characteristics of a Tube Array Caused by Two-Phase Flow, Part 1: Random Vibration", *Journal of Fluids and Structures*, 9, pp. 519–538.
- [6] Pettigrew, M.J., and Taylor, C.E., 1994, "Two-phase flow-induced vibration: an overview", *ASME Journal of Pressure Vessel Technology*, 116, pp. 233-253.
- [7] Pettigrew, M.J., Taylor, C.E. and Kim, B.S., 2001, "The effects of bundle geometry on heat exchanger tube vibration in two-phase cross-flow", *ASME Journal of Pressure Vessel Technology*, 123, pp. 414–420.
- [8] Pettigrew, M.J., Taylor, C.E., Janzen, V. P., and Whan, T., 2002, "Vibration behavior of rotated triangular tube bundles in two-phase cross-flow", *ASME Journal of Pressure Vessel Technology*, 124, pp. 144–153.
- [9] Taylor, C.E., Currie, I.G., Pettigrew, M.J. and Kim, B.S., 1989. "Vibration of tube bundles in two-phase cross-flow". Part 3: Turbulent induced excitation. *ASME Journal of Pressure Vessel Technology*, 111, pp. 488–500.
- [10] Taylor, C. E., Pettigrew, M. J., and Currie, I. G., 1996, "Random excitation forces in tube bundles subjected to two-phase cross-flow", *ASME Journal of Pressure Vessel Technology*, 118, pp. 265–277.
- [11] Pettigrew, M.J., Zhang, C, Mureithi, N.W, and Pamfil, D., 2005, "Detailed flow and force measurements in a rotated triangular tube bundle subjected to two-phase cross-flow", *Journal of Fluids and Structures*, 20, pp. 567-575.
- [12] Zhang, C., Pettigrew, M.J., and Mureithi, N.W., 2007, "Vibration excitation force measurements in a rotated triangular tube bundle subjected to two-phase cross-flow", *ASME Journal of Pressure Vessel Technology*, 129, pp. 21-27.

## CHAPTER 6

# FURTHER STUDY OF QUASI-PERIODIC VIBRATION EXCITATION FORCES IN ROTATED TRIANGULAR TUBE BUNDLES SUBJECTED TO TWO-PHASE CROSS FLOW

C. Zhang, M. J. Pettigrew\*, and N. W. Mureithi

BWC/AECL/NSERC Chair of Fluid-Structure Interaction, Department of Mechanical  
Engineering, École Polytechnique, Montréal, QC, Canada H3T 1J4

Accepted for publication in *ASME Journal of Pressure Vessel Technology*,

September 2007 (PVT-07-1097)

## 6.1 Abstract

Two-phase cross flow exists in many shell-and-tube heat exchangers. Flow-induced vibration excitation forces can cause tube motion that will result in long-term fretting-wear or fatigue. Detailed vibration excitation force measurements in tube bundles subjected to two-phase cross flow are required to understand the underlying vibration excitation mechanisms. Some of this work has already been done. Somewhat unexpected but significant quasi-periodic forces in both the drag and lift directions were measured. These forces are generally larger in the drag direction. However, the excitation force frequency is relatively low (i.e., 3-6 Hz) and not directly dependent on flow velocity in the drag direction. On the other hand much higher frequencies (up to 16 Hz) were observed in the lift direction at the higher flow velocities. The frequency appears directly related to flow velocity in the lift direction.

The present work aims at 1) providing further evidence of the quasi-periodic lift force mechanism, 2) determining the effect of cylinder position on such quasi-periodic drag and lift forces, 3) verifying the existence of quasi-periodic drag and lift forces in a more realistic larger tube array. The program was carried out with two rotated-triangular tube arrays of different width subjected to air/water flow to simulate two-phase mixtures from liquid to 95% homogeneous void fraction. Both the dynamic lift and drag forces were measured with strain gage instrumented cylinders.

## 6.2 Introduction

Two-phase cross flow exists in many shell-and-tube heat exchangers, for instance, in the U-tube region of nuclear steam generators. Flow-induced vibration excitation forces can cause tube motion that will result in long-term fretting-wear or fatigue. To prevent these tube failures in heat exchangers, designers and troubleshooters must have guidelines that incorporate flow-induced vibration excitation forces.

In single-phase flow, these forces have been extensively measured and analyzed. They are related to periodic wake shedding and to the turbulence level created by the tube bundle itself. Experimental data obtained for different kinds of fluids and tube bundles have been satisfactorily compared through the use of adequate data-reduction procedures [1-3].

In the case of two-phase flows, such an extensive study has not been undertaken, though it is known that there are significant differences between single- and two-phase situations. In particular, the relationship between the two phases must be considered in addition to another parameter that is void fraction. This results in different flow regime or patterns of two-phase flow. A few sets of experimental results have been obtained recently, as in Refs [3-16]. However the understanding of the physical mechanism that induces these forces is not yet reached. Detailed flow and vibration excitation force measurements in tube bundles subjected to two-phase cross flow are required to understand the underlying vibration excitation mechanisms. Some of this work has already been done by Pettigrew et al. [12] and Zhang et al. [13-16]. The distributions of both void fraction and bubble velocity in rotated-triangular tube bundles were measured and somewhat unexpected but significant quasi-periodic forces in both the drag and lift directions were observed [12]. These quasi-periodic forces appeared well correlated along the cylinder with the drag force being somewhat better correlated than the lift forces. These quasi-periodic forces are also dependent on the position of the cylinder within the bundle [13]. The results of two-phase flow dynamic characteristics and force measurements indicate that quasi-periodic drag and lift forces may be generated by different mechanisms that have not been observed before. The quasi-periodic drag forces appear related to the momentum flux fluctuations in the main flow path between the cylinders. These momentum flux fluctuations are caused by the void fraction fluctuations in the main flow path between the cylinders. The quasi-periodic lift forces, on the other hand, are mostly correlated to oscillation in the wake of the cylinders. The quasi-periodic lift forces are related to local void fraction measurements in the unsteady

wake area between upstream and downstream cylinders. The quasi-periodic drag forces correlate well with similar measurements in the main flow stream between cylinders [14, 15]. The relationships between the lift or drag forces and the dynamic characteristics of two-phase flow are established through fluid mechanics momentum equations. A model was developed to correlate the void fraction fluctuation in the main flow path and the dynamic drag forces. A second model was developed for correlating the oscillation in the wake of the cylinders and the dynamic lift forces. Although still preliminary, each model can predict the corresponding forces relatively well [16].

The present work aims at 1) providing further evidence of the quasi-periodic lift force mechanism, 2) determining the effect of cylinder position on such quasi-periodic drag and lift forces, 3) verifying the existence of quasi-periodic drag and lift forces in a more realistic larger tube array. An experimental program was carried out with two rotated-triangular tube arrays of different width subjected to air/water flow to simulate two-phase mixtures from liquid to 95% homogeneous void fraction. Both the dynamic lift and drag forces were measured with strain gage instrumented cylinders.

The investigation provided further evidence that the quasi-periodic lift forces are really due to oscillations of the wake between upstream and downstream cylinders. It showed that the quasi-periodic drag and lift forces should not increase with the cylinder position within a rotated triangular tube array. It also showed that quasi-periodic drag and lift forces essentially similar to those observed in the narrow test section also exist in the wider test section.

This kind of quasi-periodic forces should not be completely surprising. Two-phase flow patterns in both vertical and horizontal pipes are also characterized by periodic structures. Data from many sources comprising many flow patterns were compiled and correlated as Strouhal number against the Lockhart-Martinelli parameter with some degree of success by Azzopardi and Baker [17]. Although the mechanism for the

oscillation in the wake of the cylinders is not as yet completely understood, it may be similar to oscillations associated with low frequency mechanisms for some structures in single phase flow. This has been hypothesized to be due to an imbalance between flow entrained by the separated shear layer and that returned to the separation zone at reattachment [18]. The quasi-periodic lift forces may be generated in a manner similar to the first periodicity caused by instability of the shear layers formed in the gap between the cylinders as discussed in [19].

### **6.3 Experimental considerations**

#### 6.3.1 Test sections

The experiments were done in an air-water loop to simulate two-phase flows. The loop was described in details by Pettigrew et al. [12] or Zhang et al. [13]. Compressed air was injected below a suitably designed mixer to homogenize and distribute the two-phase mixture uniformly below the test-section. The air flow was measured with orifice plates connected to a differential pressure transducer and electronic readout system. The loop was operated at room temperature and the pressure in the test section was slightly above atmospheric.

The narrow test section, which has an essentially rectangular cross section (99×191 mm), is shown in Fig. 6.1(a). It consists of a column of six 38 mm diameter cylinders flanked on either side by half cylinders to simulate essentially the flow path in a large array of cylinders in a rotated triangular configuration. The pitch-to-diameter ratio,  $P/D$ , was 1.5 resulting in an inter-cylinder gap of 19 mm which allowed sufficient space for detailed flow measurements. The test section length-to-gap width ratio is ten, thus, adequate to maintain essentially two-dimensional flow. The wider test section is similar but includes three columns of cylinders instead of one (Fig. 6.1(b)). It was used to verify the existence of quasi-periodic drag and lift forces in a more realistic configuration.

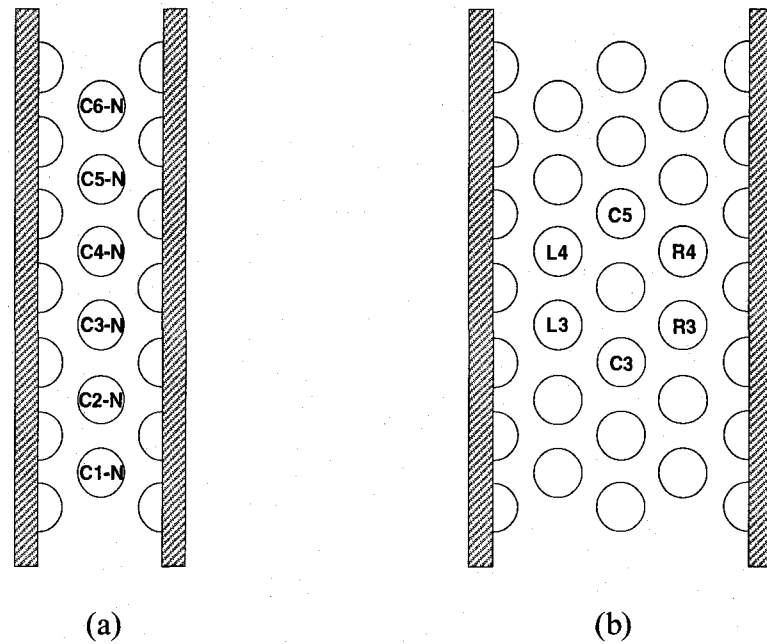


**Fig. 6.1** Test sections: (a) Narrow test section and (b) Wider test section

### 6.3.2 Instrumentation

Three cylinders in the narrow test section were instrumented with strain gauges to measure the dynamic drag and lift forces due to the two-phase flow. For one test condition, the measurements were done in two steps because of the limited numbers of instrumented cylinders: 1) positions C1-N, C2-N and C3-N, and 2) positions C4-N, C5-N and C6-N. Positions C1-N to C6-N as shown in Fig. 6.1(a) represent the first to sixth positions from the upstream end of the narrow test section, respectively. Six cylinders located at the positions (L3, L4, R3, R4, C3, C5) in the wider test section were instrumented. Tests were also done for a single cylinder (at position C3-N), and for two in-line cylinders with three different pitches along the flow (1.5D, 3D and 4.5D corresponding to cylinder positions C3-N & C4-N, C3-N & C5-N and C3-N & C6-N, respectively). These tests were conducted in the narrow test section for both single-phase water and two-phase air/water flow. In these cases, the test section was empty except for the test cylinders and the sidewalls were flat. The instrumented cylinders were cantilevered while the others were held at both ends. Two pairs of diametrically

opposite strain gages were installed in each instrumented cylinder at 90 deg from each other to measure the forces in the flow direction (drag) and in the direction normal to the flow (lift). The strain gages were connected to strain indicators. The natural frequency of the instrumented cylinders was much higher (i.e., >150Hz) than the excitation force frequencies such that the cantilever cylinder functioned essentially as a dynamic force transducer. The static strain-force relation was determined via a careful calibration. The signals were analyzed with an OR38 8-32 channel real time multi-analyzer/recorder coupled to a laptop computer.

The experiments were performed over a pitch flow velocity range from 1 m/s to 10 m/s at 80% homogeneous void fraction for two-phase flow and 0.25 m/s to 2 m/s in 0.25 m/s increment for water flow, respectively.

## **6.4 Results and discussion**

### 6.4.1 Comparison between periodic vortex shedding forces in water and quasi-periodic lift forces in air/water flow

#### **Periodic vortex shedding forces in water**

Lift force spectra for a single cylinder (C3-N) and for two cylinders with different pitches along the flow (1.5D, 3D and 4.5D, corresponding to cylinder positions C3-N & C4-N, C3-N & C5-N and C3-N & C6-N, respectively) in the narrow test section (without half-tubes at the side walls) are shown in Fig. 6.2 for 1 m/s pitch flow velocity in water flow. All the force spectra show very well defined vortex shedding peaks. For the case of two cylinders at 1.5D pitch, the magnitude of the peak for the upstream cylinder (at C3-N) is relatively less than that for the single cylinder (Fig. 6.2(d) vs. Fig. 6.2(a)). It indicates that the vortex shedding from the upstream cylinder was affected by the downstream cylinder due their proximity. For the cases at 3D and 4.5D pitches (Fig. 6.2(c) vs. Fig. 6.2(a) and Fig. 6.2(b) vs. Fig. 6.2(a)), the space between cylinders is



sufficient so that not much effect on the upstream cylinder occurs. Interestingly, the periodic lift force for the downstream cylinder is larger than that for the upstream cylinder. It is also larger than that for the single cylinder except for the smallest pitch case.

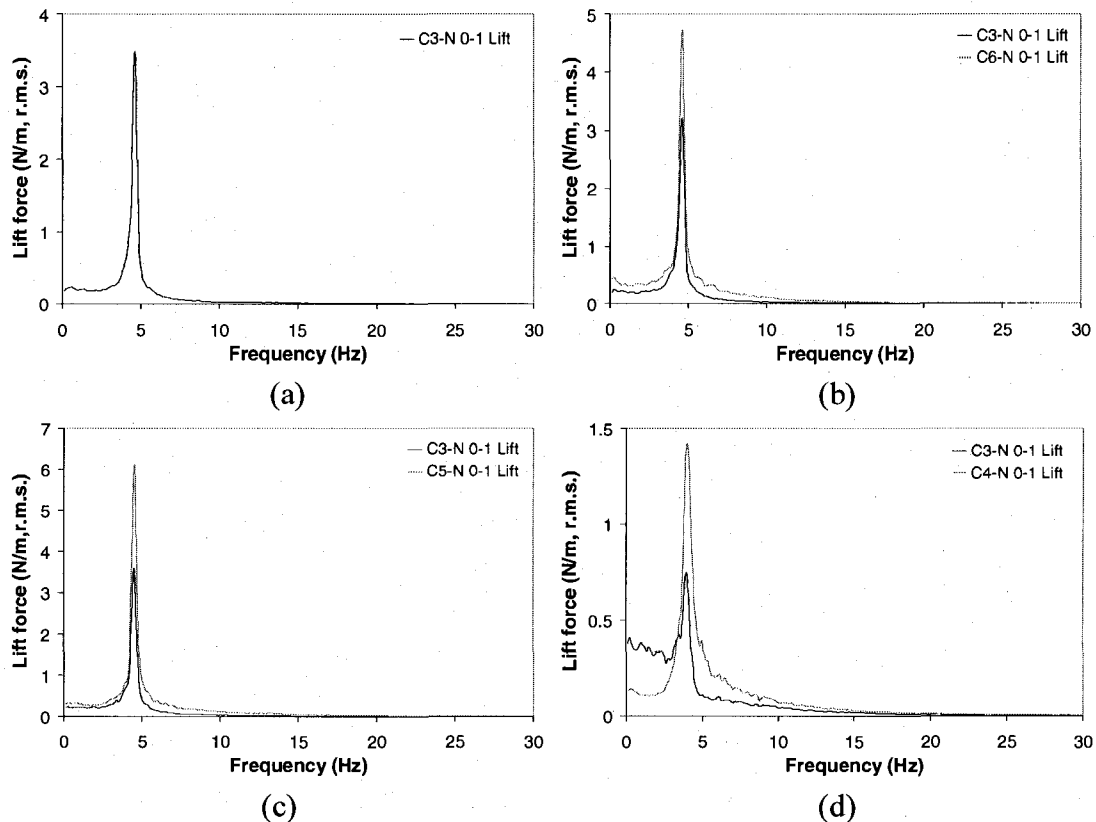


**Fig. 6.2** Typical dynamic lift force spectra for water flow at 1 m/s pitch flow velocity: (a) single cylinder, (b), (c) and (d) two cylinders at different pitches (4.5D, 3D and 1.5D, respectively)

### Quasi-periodic lift forces in air/water flow

Lift force spectra for a single cylinder (C3-N) and for two cylinders with different pitches along the flow (1.5D, 3D and 4.5D, corresponding to cylinder positions C3-N & C4-N, C3-N & C5-N and C3-N & C6-N, respectively) in the narrow test section (without half-tubes at the side walls) are shown in Fig. 6.3 for 80% void fraction at 5 m/s pitch flow velocity. The spectrum of the single cylinder is largely broad band random in appearance (Fig. 6.3(a)). For the case of two cylinders at 4.5D pitch, some

periodicity appears for the downstream cylinder (C6-N), while the spectrum of the upstream cylinder (C3-N) shows random and broad band characteristics typical of turbulence forces (Fig. 6.3(b)). For the case of two cylinders at 3D pitch, more prominent periodicity appears for the downstream cylinder (C5-N), while the spectrum of the upstream cylinder (C3-N) is still broad band random in appearance (Fig. 6.3(c)). For the case of two cylinders at 1.5D pitch, periodicity in the downstream cylinder (C4-N) is more dominant and the peak is sharper than other cases, while the magnitude of the spectrum for the upstream cylinder is significantly increased. It indicates that the periodicity in the lift forces is much affected by the space between upstream and downstream cylinders. The wake oscillation in the relatively narrow space is the source of this periodicity. It can be concluded that the mechanism of the quasi-periodic lift force in air/water flow is different than that of vortex lift force in water flow.

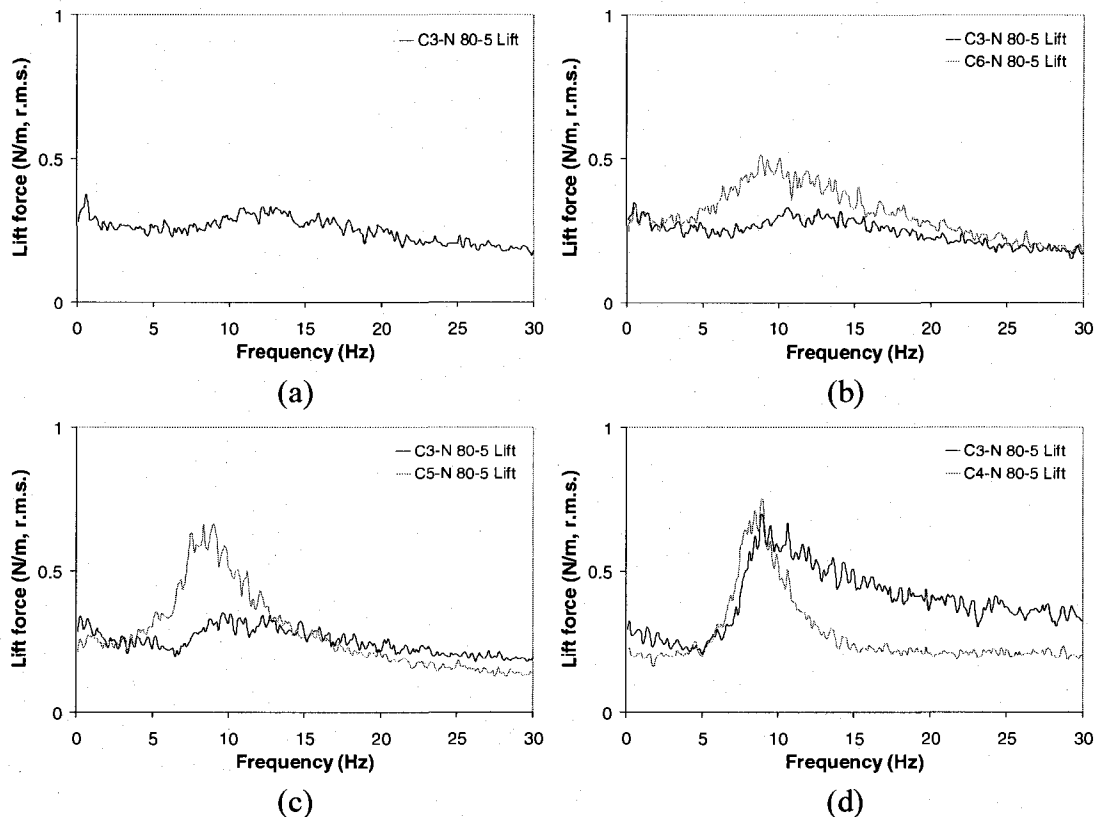


**Fig. 6.3** Typical dynamic lift force spectra for 80% void fraction at 5 m/s pitch flow velocity: (a) single cylinder, (b), (c) and (d) two cylinders at different pitches (4.5D, 3D and 1.5D, respectively)

### 6.4.2 Effect of cylinder position on the quasi-periodic drag and lift forces

#### Typical lift forces

Lift force spectra for all the six positions in the narrow test section are shown in Figs 6.4(a) and 6.5(a) for respectively, 5 and 10 m/s pitch flow velocity at 80% void fraction. The force spectrum magnitudes in the lift direction are relatively small in the upstream positions (C1-N & C2-N) but much larger in the interior (C3-N & C4-N) and in the downstream positions (C5-N & C6-N). The periodicity for the most upstream position (C1-N) is less prominent, but the force spectrum shows random and broad band characteristics of turbulence forces. This is because these quasi-periodic lift forces are mostly correlated to oscillations in the wake of the upstream cylinder and there is no cylinder upstream of C1-N [13-14]. The behavior of the interior cylinders is quite similar to that of the downstream cylinders (Figs 6.4(a) & 6.5(a)). It implies that the periodic lift force peak amplitude would not increase further with increasing tube bundle depth.

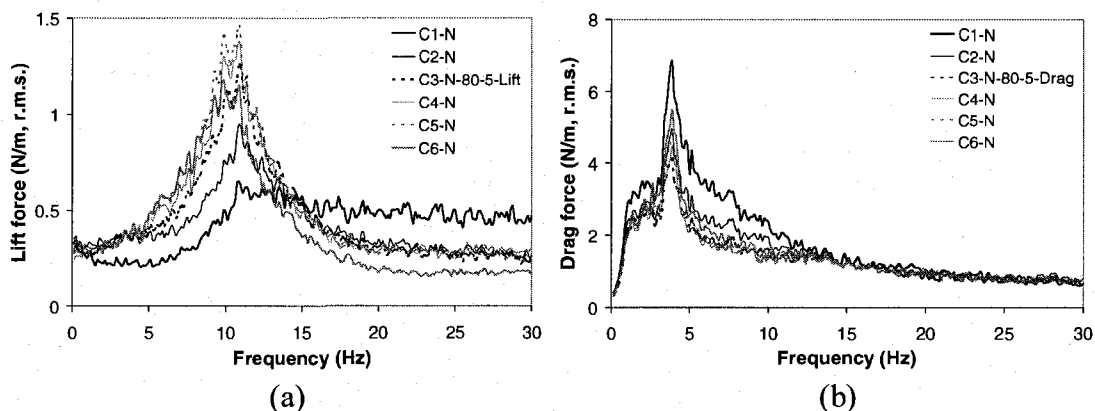
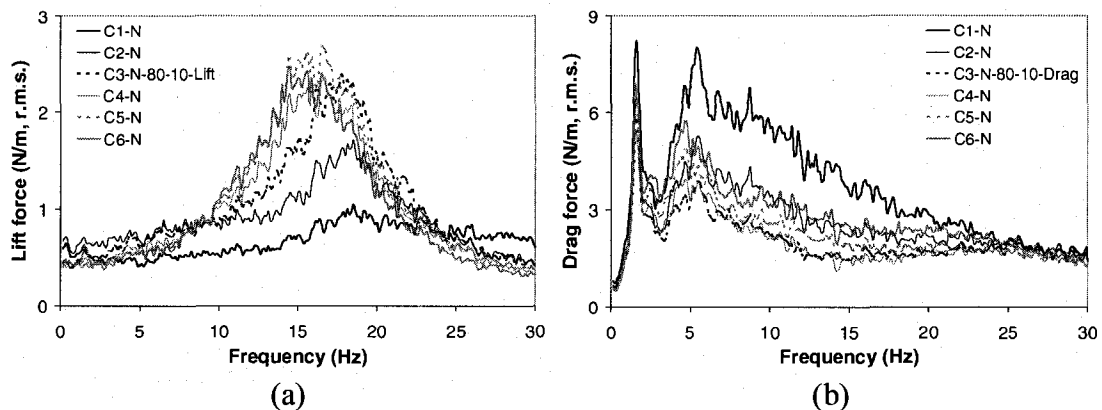


Fig. 6.4 Typical dynamic lift and drag force spectra for 80% void fraction at 5 m/s pitch flow velocity: (a) Lift force spectra and (b) Drag force spectra

#### Typical drag forces

Drag force spectra for all the six positions in the narrow test section are shown in Figs. 6.4(b) and 6.5(b) for respectively, 5 and 10 m/s pitch flow velocity at 80% void fraction. The force spectra are quite similar for all cylinders, except that the peak amplitude for

the most upstream position (C1-N) is a little larger than those of other positions. This is probably due to the fact that the cylinder at C1-N is directly exposed to the upstream two-phase flow fluctuations. The drag periodic forces do not appear to increase with tube bundle depth beyond the first upstream tube. The very sharp peak at low frequency (around 2 Hz) in Fig. 6.5(b) was found to be an unwanted signal component that should not be considered further [13].



**Fig. 6.5** Typical dynamic lift and drag force spectra for 80% void fraction at 10 m/s pitch flow velocity: (a) Lift force spectra and (b) Drag force spectra

### Correlation of the lift and drag forces between different cylinder positions

The coherences of the lift and drag forces between different cylinder positions are shown in Figs 6.6 and 6.7 for respectively, 5 and 10 m/s pitch flow velocity at 80% void fraction. For the lift forces, the coherences between every two positions are relatively high at periodic frequencies (11 Hz and 17 Hz for respectively, 5 and 10 m/s pitch flow velocity). The coherences between the most upstream position (C1-N) and the downstream positions (C2-N and C3-N) are generally low due probably to the fact that the periodicity for the most upstream position (C1-N) is less prominent. For the drag forces, the coherences between every two positions are higher than those of the lift forces.

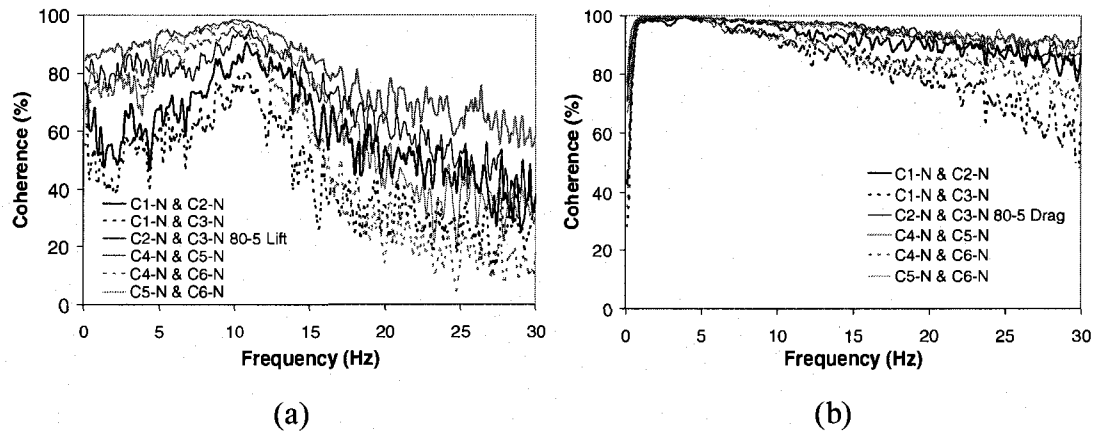


**Fig. 6.6** Correlation of the lift and drag forces between different cylinder positions for 80% void fraction at 5 m/s pitch flow velocity: (a) Lift and (b) Drag

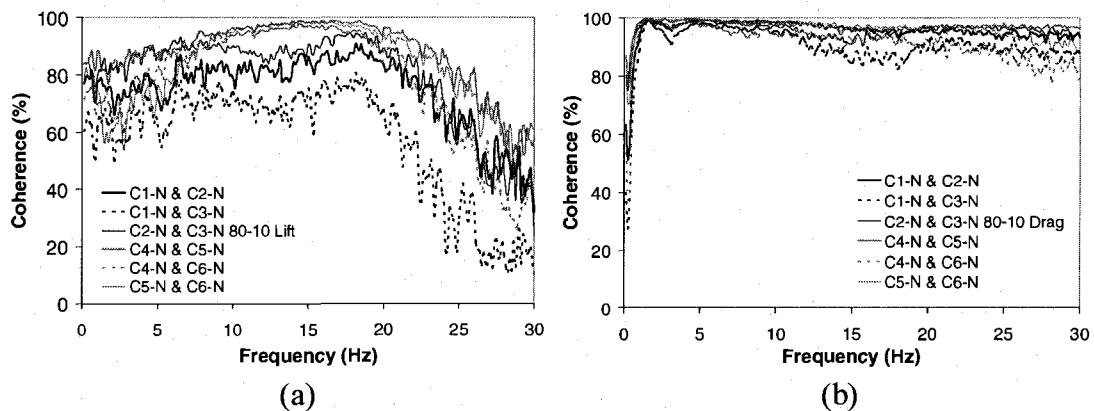


**Fig. 6.7** Correlation of the lift and drag forces between different cylinder positions for 80% void fraction at 10 m/s pitch flow velocity: (a) Lift and (b) Drag

#### 6.4.3 Quasi-periodic drag and lift forces in the wider test section

One may have the opinion that our recent observations [13-15] with the narrow test section are possibly an artifact of this particular experimental set-up and would not be observed in a wider array of the same geometry under similar flow conditions. This particular tube array may be too narrow to permit diffusion of the flow laterally across the wake area between upstream and downstream cylinders, a phenomenon perhaps even more important in two-phase flows because of void differences between the main flow path and the wake area between upstream and downstream cylinders. To answer these questions we have recently done some tests with a similar but wider test section

including three columns of cylinders instead of one (Fig. 6.1(b)). Six cylinders located in the positions (L3, L4, R3, R4, C3, C5) were instrumented with strain gages. Similar results were found as in Refs [13-15].

### **Typical lift forces**

Typical lift force spectra in the wider test section are shown in Figs 6.8(a), (b), (c) and 6.9(a), (b), (c). The lift force spectra reveal narrow band or quasi-periodic forces similar to those in the narrow test section. For the case of 80% void fraction, at both 5 and 10 m/s pitch flow velocity, the lift periodic frequency in the center column is a little higher than that in the narrow test section, although the amplitudes are quite similar. On the other hand, the lift periodic frequencies in adjacent columns (left and right columns) are similar to those in the narrow test section, although the amplitudes are a little less (Figs 6.8(a), (b), (c) and 6.9(a), (b), (c)). The difference in frequency may be related to the fact that the flow paths on each side of the columns are not identical. The two adjacent columns have a solid flow boundary on one side and an open flow boundary on the other side. On the other hand the center column has two open flow boundaries. Interestingly, some components of the drag force frequency may be found in the lift force spectra. Further tests revealed that the presence of drag force components in the lift force spectra is much less pronounced when the pitch flow velocity is less than 5 m/s.

### **Typical drag forces**

Periodicity was also observed in the drag direction as shown in Figs 6.8(d), (e), (f) and Figs 6.9(e), (f), (g). For the case of 80% void fraction, at 5 m/s pitch flow velocity, the drag periodic frequency in both adjacent columns (L3, L4 and R3, R4) and for the centre column (C3, C5) is coincident with that in the narrow test section, although the amplitude seems smaller than that in the narrow test section (Figs 6.8(d), (e), and (f)). For the case of 80% void fraction, at 10 m/s pitch flow velocity, the drag force spectra show that two nearly similar peaks exist (Figs 6.9(e), (f), (g)). Both frequency and amplitude of the first peak are quite different than those of the drag force peak in the

narrow test section (Fig. 6.9(h)). The second peak may be expected from periodic lift components. It also reveals that the interaction between the two periodic force mechanisms are more pronounced in the wider test section when the pitch flow velocity is greater than 5 m/s.

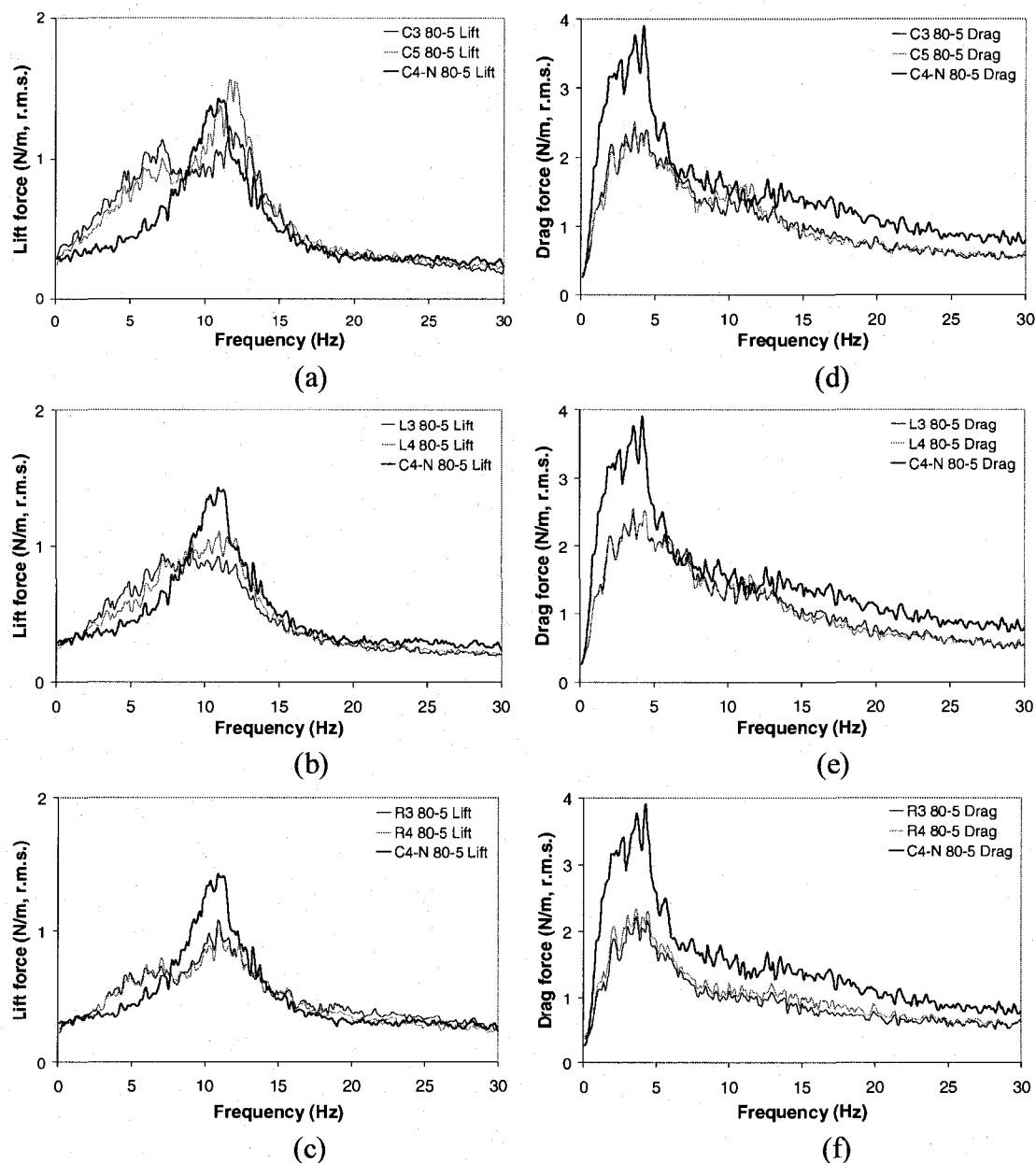


**Fig. 6.8** Comparison of the dynamic lift and drag forces between the wider test section and the narrow test section for 80% void fraction at 5 m/s pitch flow velocity: (a), (b) and (c) for lift forces, and (d), (e) and (f) for drag forces

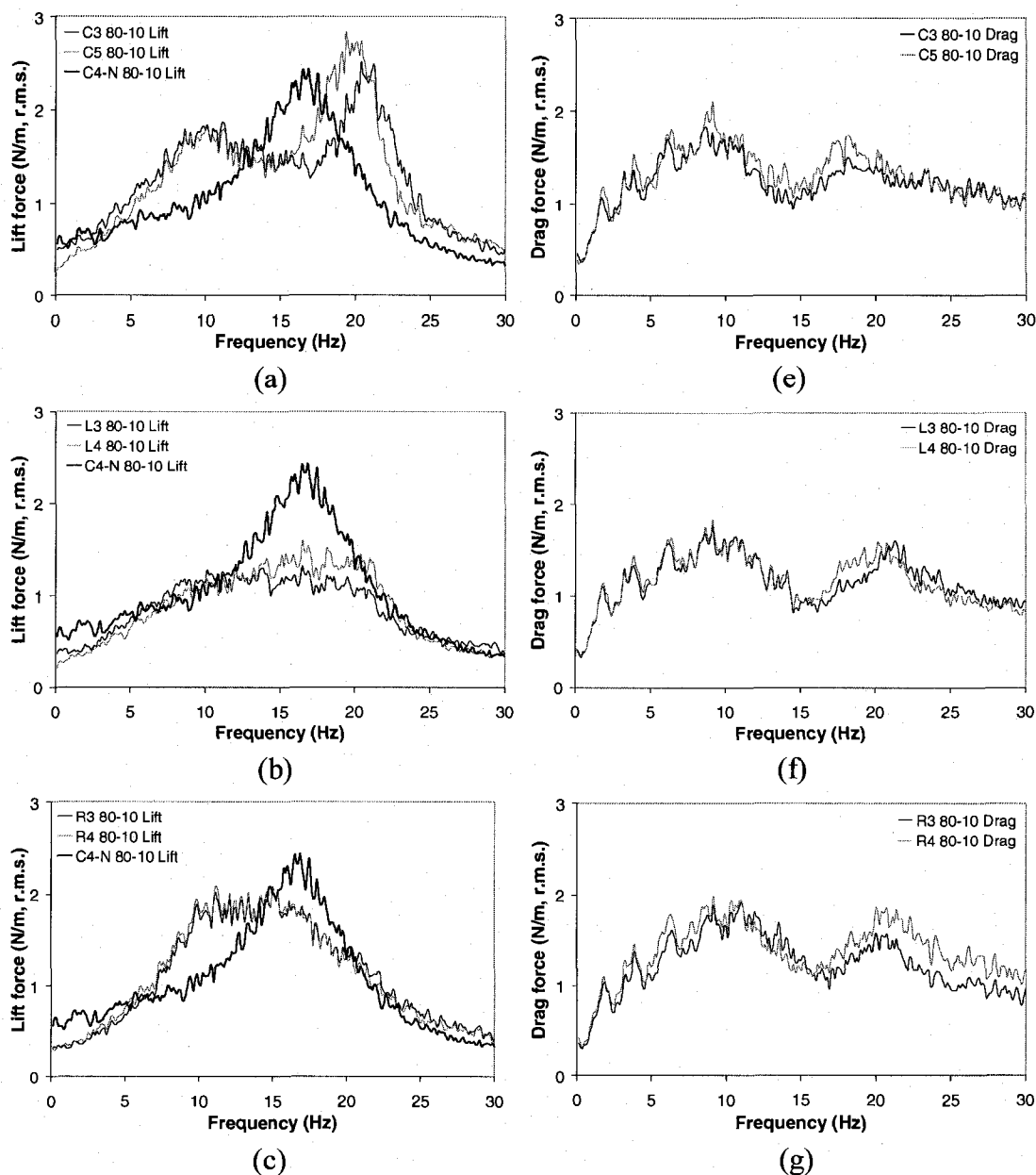


**Fig. 6.9** Comparison of the dynamic lift and drag forces between the wider test section and the narrow test section for 80% void fraction at 10 m/s pitch flow velocity: (a), (b), and (c) for lift forces, and (e), (f), and (g) for drag forces

### Correlation of the lift and drag forces between different cylinder positions

The coherences of the lift and drag forces between different cylinder positions are shown in Figs 6.10 and 6.11 for respectively, 5 and 10 m/s pitch flow velocity at 80% void fraction. For the lift forces, the coherences between two positions in the same



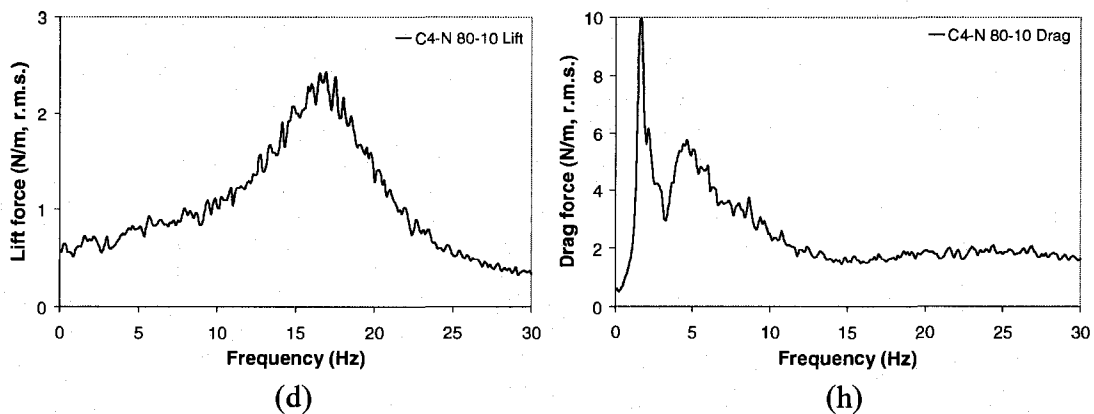


Fig. 6.9 continued (d) for the lift force and (h) for the drag force

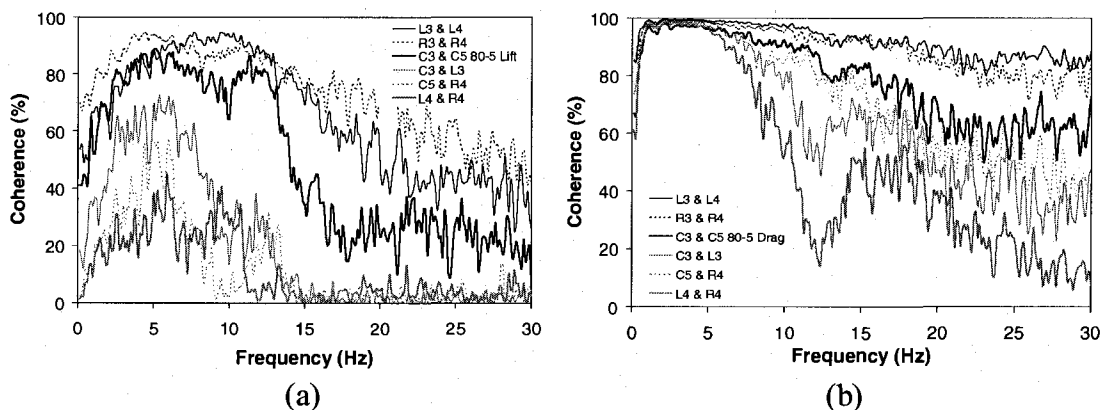


Fig. 6.10 Correlation of the lift and drag forces between different cylinder positions for 80% void fraction at 5 m/s pitch flow velocity: (a) Lift and (b) Drag

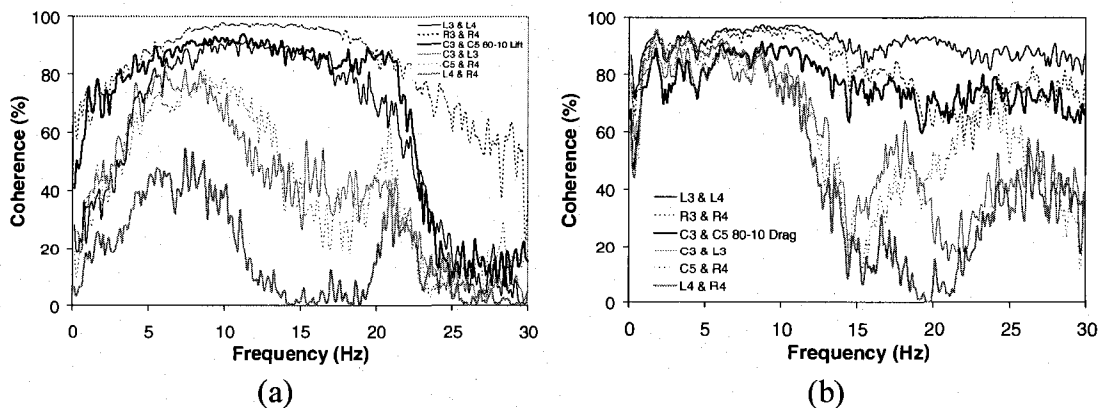


Fig. 6.11 Correlation of the lift and drag forces between different cylinder positions for 80% void fraction at 10 m/s pitch flow velocity: (a) Lift and (b) Drag

columns (L3&L4, R3&R4, and C3&C5 in Figs 6.10(a) and 6.11(a)) are relatively high at periodic frequencies (11 Hz and 17 Hz for respectively, 5 and 10 m/s pitch flow velocity). This is quite similar to the results obtained in the narrow test section. However, the coherences between two positions in adjacent columns (C3&L3, C5&R4, and L4&R4 in Figs 6.10(a) and 6.11(a)) are very low at the same lift periodic frequencies. This may indicate that the wakes between adjacent columns are not correlated. Relatively high coherence peaks at low frequencies for C3&L3, C5&R4, and L4&R4 in Figs 6.10(a) and 6.11(a) may be expected from periodic drag components. For the drag forces, the coherences between every two positions are generally high at the drag periodic frequencies. It seems that the coherence for 5 m/s pitch flow velocity is a little bit higher than that for 10 m/s pitch flow velocity. It may be due to different two-phase flow regime. Beyond these drag periodic frequencies, the coherences between two neighboring positions in the same column (L3&L4, R3&R4 in Figs 6.10(b) and 6.11(b)) are highest, while the coherences between every two other positions in the same column (C3&C5 in Figs 6.10(b) and 6.11(b)) is higher than those between two positions in adjacent columns (C3&L3, C5&R4, and L4&R4 in Figs 6.10(b) and 6.11(b)). Relatively high coherences peaks at high frequencies for C3&L3, C5&R4, and L4&R4 in Figs 6.10(b) and 6.11(b) may be expected from periodic lift components and pump noise.

In summary, quasi-periodic lift and drag forces essentially similar to those in the narrow test section also exist in the wider test section.

## 6.5 Conclusion

This investigation provided further evidence that the quasi-periodic lift forces are really due to oscillations of the wake between upstream and downstream cylinders. It showed that the observed quasi-periodic drag and lift forces should not increase with cylinder depth within a rotated triangular tube array. It also showed that quasi-periodic drag and

lift forces essentially similar to those observed in the narrow test section also exist in the wider test section.

## 6.6 Acknowledgments

The authors are grateful to Dragos Pamfil and Christine Monnette for the test section design and the development of the fiber-optic probes. Thanks are also due to Thierry Lafrance, Bénédicte Besner and Nour Aimène for their help throughout the project.

## 6.7 References

- [1] Blevins, R. D., 1990, "Flow-induced vibration", New York: Van Nostrand Reinhold, 2nd edition.
- [2] Taylor, C.E., and Pettigrew, M.J., 2000, "Random excitation forces in heat exchanger tube bundles", *ASME Journal of Pressure Vessel Technology*, 122, pp. 509–514.
- [3] Axisa, F., Antunes, J., and Villard, B., 1990, "Random excitation of heat exchanger tubes by cross-flows", *Journal of Fluid and Structures*, 4, pp. 321-341.
- [4] De Langre, E., and Villard, B., 1998, "An upper bound on random buffeting forces caused by two-phase flows across tubes", *Journal of Fluids Structures*, 12, pp. 1005–1023.
- [5] Feenstra, P.A., Weaver, D.S., and Nakamura, T., 2003, "Vortex shedding and Fluid-elastic instability in a normal square tube array excited by two-phase Cross-flow", *Journal of Fluids and Structures*, 17, pp. 793–811.
- [6] Nakamura, T., Fujita, K., Kowanishi, N., Yamaguchi, N., and Tsuge, A., 1995, "Study on the Vibration Characteristics of a Tube Array Caused by Two-Phase Flow, Part 1: Random Vibration", *Journal of Fluids and Structures*, 9, pp. 519–538.
- [7] Pettigrew, M.J., and Taylor, C.E., 1994, "Two-phase flow-induced vibration: an overview", *ASME Journal of Pressure Vessel Technology*, 116, pp. 233-253.

- [8] Pettigrew, M.J., Taylor, C.E. and Kim, B.S., 2001, "The effects of bundle geometry on heat exchanger tube vibration in two-phase cross-flow", *ASME Journal of Pressure Vessel Technology*, 123, pp. 414–420.
- [9] Pettigrew, M.J., Taylor, C.E., Janzen, V. P., and Whan, T., 2002, "Vibration behavior of rotated triangular tube bundles in two-phase cross-flow", *ASME Journal of Pressure Vessel Technology*, 124, pp. 144–153.
- [10] Taylor, C.E., Currie, I.G., Pettigrew, M.J. and Kim, B.S., 1989. "Vibration of tube bundles in two-phase cross-flow". Part 3: Turbulent induced excitation. *ASME Journal of Pressure Vessel Technology*, 111, pp. 488–500.
- [11] Taylor, C. E., Pettigrew, M. J., and Currie, I. G., 1996, "Random excitation forces in tube bundles subjected to two-phase cross-flow", *ASME Journal of Pressure Vessel Technology*, 118, pp. 265–277.
- [12] Pettigrew, M.J., Zhang, C, Mureithi, N.W, and Pamfil, D., 2005, "Detailed flow and force measurements in a rotated triangular tube bundle subjected to two-phase cross-flow", *Journal of Fluids and Structures*, 20, pp. 567-575.
- [13] Zhang, C., Pettigrew, M.J., and Mureithi, N.W., 2007, "Vibration excitation force measurements in a rotated triangular tube bundle subjected to two-phase cross-flow", *ASME Journal of Pressure Vessel Technology*, 129, pp. 21-27
- [14] Zhang, C., Pettigrew, M.J., and Mureithi, N.W., 2008, "Correlation between vibration excitation forces and the dynamic characteristics of two-phase cross flow in a rotated triangular tube bundle", *ASME Journal of Pressure Vessel Technology*, 130(1).
- [15] Zhang, C., Pettigrew, M. J., and Mureithi, N. W., 2006, "Correlation Between Vibration Excitation Forces and the Dynamic Characteristics of Two-Phase Flow in a Rotated Triangular Tube Bundle," Paper No. 93797, Proceedings, ASME PVP2006-ICPVT-11, 6th FSI, AE & FIV and N Symposium, M. P. Paidoussis, ed., Vancouver, Canada, July 23-27.
- [16] Zhang, C., Pettigrew, M. J., and Mureithi, N. W., 2007, "Development of Models Correlating Vibration Excitation Forces to Dynamic Characteristics of Two-Phase Flow in a Tube Bundle," Paper No. 26077, Proceedings, ASME PVP2007/CREEP8,

Symposium on Flow-Induced Vibration, N. W. Mureithi, ed., San Antonio, Texas, USA, July 22-26.

[17] Azzopardi, B.J. and Baker, G., 2003, "Characteristics of periodic structures in gas/liquid two-phase flow", Proceeding of UK/Japan Two-Phase Flow Meeting, Guildford, UK, April 14-15.

[18] Rockwell, D., 1983, "Oscillation of impinging shear layers", AIAA Journal, 21, pp. 645-664.

[19] Mohany, A. and Ziada, S., 2005, "Flow-excited acoustic resonance of two tandem cylinders in cross-flow", Journal of Fluids and Structures 21, pp. 103-119.

**CHAPTER 7****DEVELOPMENT OF MODELS CORRELATING VIBRATION  
EXCITATION FORCES TO  
DYNAMIC CHARACTERISTICS OF  
TWO-PHASE FLOW IN A TUBE BUNDLE**

**C. Zhang, N. W. Mureithi\*, and M. J. Pettigrew**

BWC/AECL/NSERC Chair of Fluid-Structure Interaction, Department of Mechanical  
Engineering, École Polytechnique, Montréal, QC, Canada H3T 1J4

Submitted to *International Journal of Multiphase Flow*,

October 2007 (IJMF-D-07-00167)

## 7.1 Abstract

Recent experiments revealed significant quasi-periodic forces in both the drag and lift directions in a rotated triangular tube bundle subjected to two-phase cross flow. The quasi-periodic drag forces were found to be related to the momentum flux fluctuations in the main flow path between the cylinders. The quasi-periodic lift forces, on the other hand, are mostly correlated to the oscillation in the wake of the cylinders. In this work we develop semi-analytical models for correlating vibration excitation forces to dynamic characteristics of two-phase flow in a rotated triangular tube bundle and for better understanding of the nature of vibration excitation forces. The relationships between the lift or drag forces and the dynamic characteristics of two-phase flow are established through fluid mechanics momentum equations. A model has been developed to correlate the void fraction fluctuation in the main flow path and the dynamic drag forces. A second model has been developed for correlating the oscillation in the wake of the cylinders and the dynamic lift forces. Although still preliminary, each model can predict the corresponding forces relatively well.

*Keywords:* Two-phase flow; Tube bundle; Quasi-periodic forces; Momentum flux fluctuations; Wake oscillations

## 7.2 Introduction

Two-phase cross flow exists in many shell-and-tube heat exchangers, for instance, in the U-tube region of nuclear steam generators. Flow-induced vibration excitation forces can cause excessive vibration that may result in long-term fretting-wear or fatigue. To prevent such tube failures in heat exchangers, designers and troubleshooters must have guidelines that incorporate flow-induced vibration excitation forces.

In single-phase flow, these forces have been extensively measured and analyzed. They are related to periodic wake shedding and to turbulence generated within the bundle. Experimental data obtained for different kinds of fluids and tube bundles have been satisfactorily compared through the use of adequate data-reduction procedures (Axisa et al., 1990; Blevins, 1990).

In the case of two-phase flows, such extensive studies have not been undertaken, though it is known that there are significant differences between single- and two-phase flows. In particular, the relationship between the two phases must be considered in addition to another parameter which is the void fraction. This results in different flow regimes or patterns of two-phase flow. A few sets of experimental results have been obtained recently, e.g., Axisa et al. (1990), Pettigrew and Taylor (1994, 2005), Nakamura et al. (1995), and Zhang et al. (2006a, b, 2007, 2008). However many questions remain such as the effects of viscosity, surface tension, density ratio and flow regimes. Indeed the main problem is the understanding of the physical mechanism that induces these forces. Detailed flow and vibration excitation force measurements in tube bundles subjected to two-phase cross flow are required to understand the underlying vibration excitation mechanisms. Some of this work has already been done by Pettigrew et al. (2005) and Zhang et al. (2006a, b, 2007, 2008). The distributions of both void fraction and bubble velocity in rotated-triangular tube bundles were obtained (Pettigrew et al., 2005). Significant quasi-periodic forces in both the drag and lift directions were measured (Zhang et al., 2007). The quasi-periodic drag forces appear to be related to the momentum flux fluctuations in the main flow path between the cylinders. The quasi-periodic lift forces, on the other hand, are mostly correlated to the oscillation in the cylinder wakes (Zhang et al., 2006a, 2008).

The objective of this work is to develop semi-analytical models for correlating these vibration excitation forces to dynamic characteristics of two-phase flow in a rotated triangular tube bundle and understanding the nature of vibration excitation forces. The



relationships between the lift or drag forces and the dynamic characteristics of two-phase flow are established through fluid mechanics momentum equations. A model has been developed to correlate the void fraction fluctuation in the main flow path and the dynamic drag forces. A second model has been developed for correlating the oscillation in the wake of the cylinders and the dynamic lift forces.

## 7.3 Experiment

### 7.3.1 Experimental set-up

The experiments were done in an air-water loop to simulate two-phase flows. The loop was described in details by Pettigrew et al. (2005) and Zhang et al. (2007). Compressed air was injected below a suitably designed mixer to homogenize and distribute the two-phase mixture uniformly below the test-section. The air flow was measured with orifice plates connected to a differential pressure transducer and electronic readout system. The loop was operated at room temperature and the pressure in the test section was slightly above atmospheric.

The test section, which has essentially a rectangular cross section (99 × 191 mm), is shown in Fig. 7.1. It consists of a column of six 38 mm diameter cylinders flanked on either side by half cylinders to simulate essentially the flow path in a large array of cylinders in a rotated triangular configuration. The pitch-to-diameter ratio,  $P/D$ , was 1.5 resulting in an inter-cylinder gap of 19 mm which allowed sufficient space for detailed flow measurements. The test-section length-to-gap width ratio is ten, thus, adequate to maintain essentially two-dimensional flow. The measurements were taken at several positions with fiber-optic probes assembled within a traversing mechanism. The tip of the probes could be positioned accurately with a micrometer head.

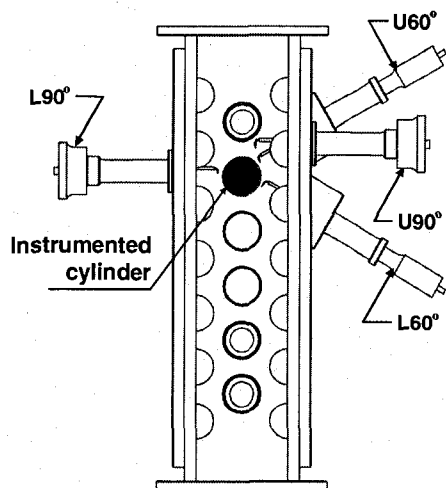


Fig. 7.1 Test section

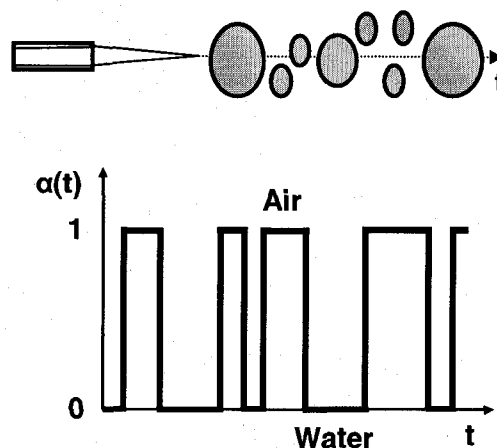
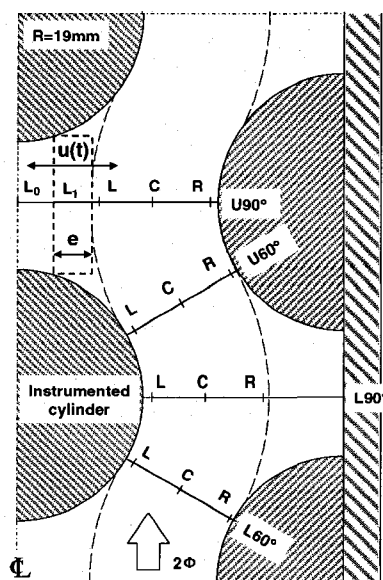


Fig. 7.2 Idealized two-phase flow signal from fiber-optic probes

The probe assemblies were installed at four principal positions in the array as shown in Fig. 7.1. These positions are henceforth called lower and upper 60° (L60° and U60°) for the narrow gaps between cylinders and lower and upper 90° (L90° and U90°) for the larger flow areas between upstream and downstream cylinders. One cylinder was instrumented with strain gauges to measure the dynamic drag and lift forces due to the two-phase flow.

Each fiber-optic probe has a conical tip and is made of an optical fiber of 170  $\mu\text{m}$  diameter. It acts as a fluid phase sensor based on the different level of light reflection between air and water (Fig. 7.2). Four probes were used to measure simultaneously the dynamic characteristics of two-phase flow surrounding the instrumented cylinder. Several different probe locations as shown in Fig. 7.3 were selected for two-phase flow measurements, i.e., LLLL, CCCC, RRRR, etc. Here L, C and R represent the left, center and right positions of probe L60°, L90°, U60° and U90° in the main flow path, respectively. Additionally  $L_0$  is a point on the center line of the test section at the Probe U90° position.  $L_1$  is about 5 mm from  $L_0$ .



**Fig. 7.3** The main flow path and probe positions for flow measurements

Both the dynamic lift and drag forces were measured with a strain gage instrumented cylinder located in the fifth position from the upstream end of the test-section (Fig. 7.1). The instrumented cylinder was cantilevered and surrounded by rigid tubes. Two pairs of diametrically opposite strain gages were installed in the cylinder at 90 deg from each other to measure the forces in the flow direction (drag) and in the direction normal to the flow (lift). The strain gages were connected to strain indicators. The natural frequency of the cantilever cylinders was much higher (i.e., >150Hz) than the excitation force frequencies such that the cantilever cylinder functioned essentially as a dynamic force transducer. The static strain-force relation was determined via a careful calibration.

The analysis of two-phase flow-induced vibration requires suitable parameters to express the experimental data. Three flow parameters such as homogeneous void fraction,  $\alpha$ , freestream velocity,  $U_\infty$ , and pitch flow velocity,  $U_p$ , are defined as follows:

$$\alpha = \frac{Q_a}{Q_a + Q_w} \quad (7-1)$$

$$U_{\infty} = \frac{Q_a + Q_w}{A_{\infty}} \quad (7-2)$$

$$U_p = U_{\infty} \left( \frac{P}{P - D} \right) \quad (7-3)$$

where  $Q_a$  is the volume flow rate of air,  $Q_w$  is the volume flow rate of water,  $P$  is the pitch or distance between tube centres and  $D$  is the tube diameter, respectively.

Two-phase flow, and dynamic lift and drag force measurements were performed simultaneously. Four flow conditions were investigated in detail, i.e., 80% and 90% homogeneous void fractions at a nominal pitch flow velocity,  $U_p$  of 5 m/s and 10 m/s. Both the void probe and the force signals were analyzed on an OR38 8-32 channel real time multi-analyzer/recorder coupled to a laptop computer.

### 7.3.2 Experimental results

Typical lift and drag force spectra are shown in Fig. 7.4. Typical power spectra of the local void fraction fluctuation on the right side, the left side, and along the center line of the main flow path, as well as at positions U90°-L0 and U90°-L1 are shown in Figs 7.5, 7.6, 7.7 and 7.8, respectively. Detailed analyses of these results are discussed in Zhang et al. (2006a, 2008). They are only briefly reviewed here. These results show that:

(1) Both the dynamic drag and lift forces and the local void fraction fluctuation spectra show non-random narrow band characteristics;

(2) For the case of 80% void fraction, at 5 m/s pitch flow velocity, the spectra of the local void fraction fluctuation on the right side of the main flow path have a dominant frequency of about 4 Hz (Fig. 7.5). This dominant frequency is consistent with that of the dynamic drag force (Fig. 7.4(a)). This clearly indicates a possible dynamic

link between the void fraction fluctuation on the right side of the main flow path and the dynamic drag forces;

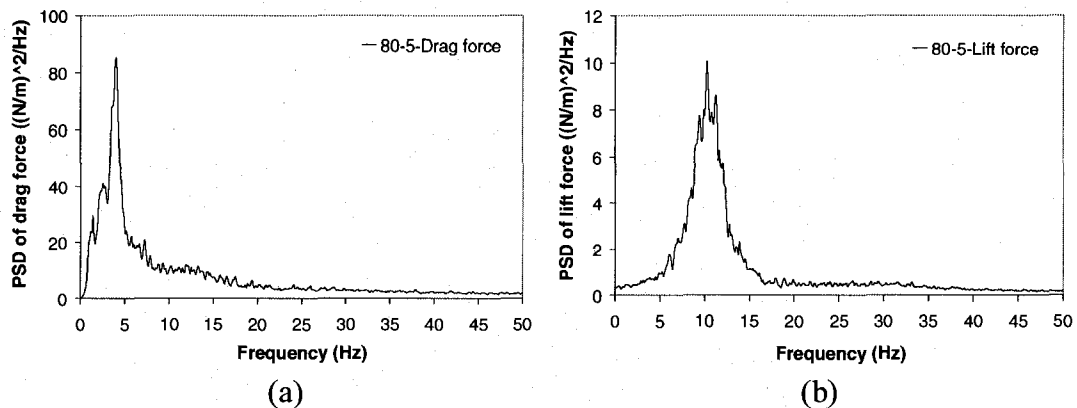


**Fig. 7.4** Typical dynamic force spectra for 80% void fraction at 5 m/s pitch flow velocity: (a) Drag force spectra and (b) Lift force spectra

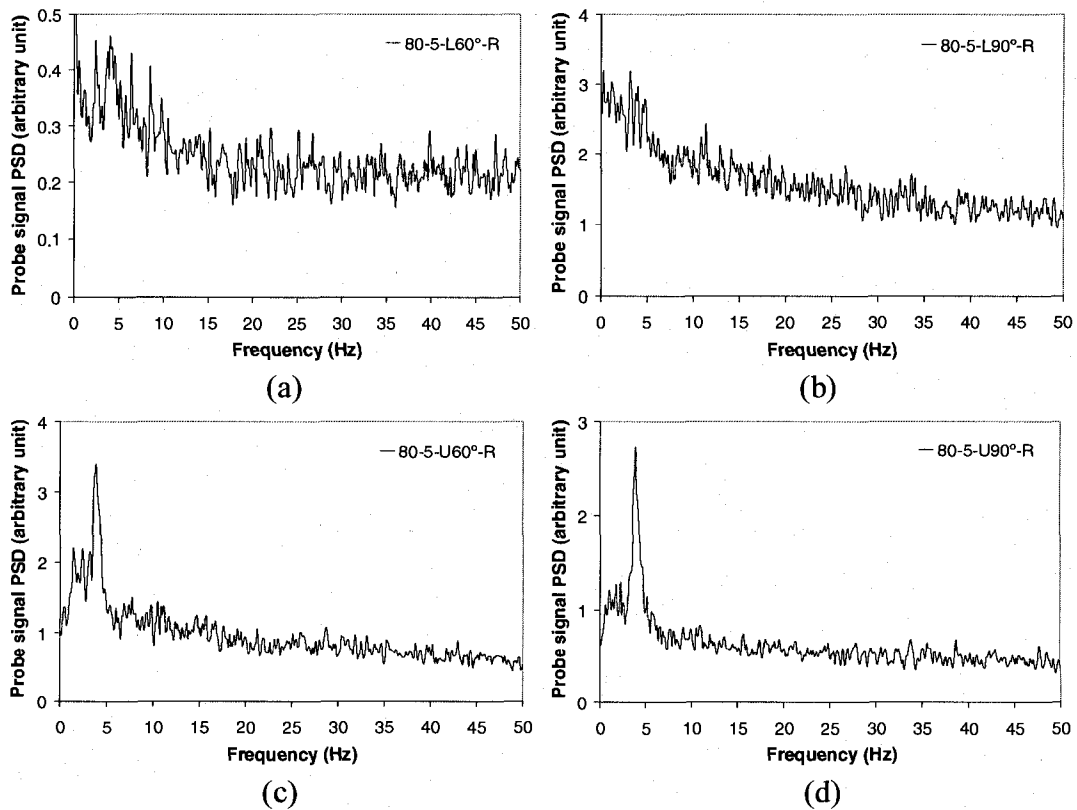


**Fig. 7.5** Power spectra of the local void fraction fluctuation at four different positions on the right side of the main flow path for 80% void fraction at 5 m/s pitch flow velocity: (a) L60°-R position, (b) L90°-R position, (c) U60°-R position, and (d) U90°-R position

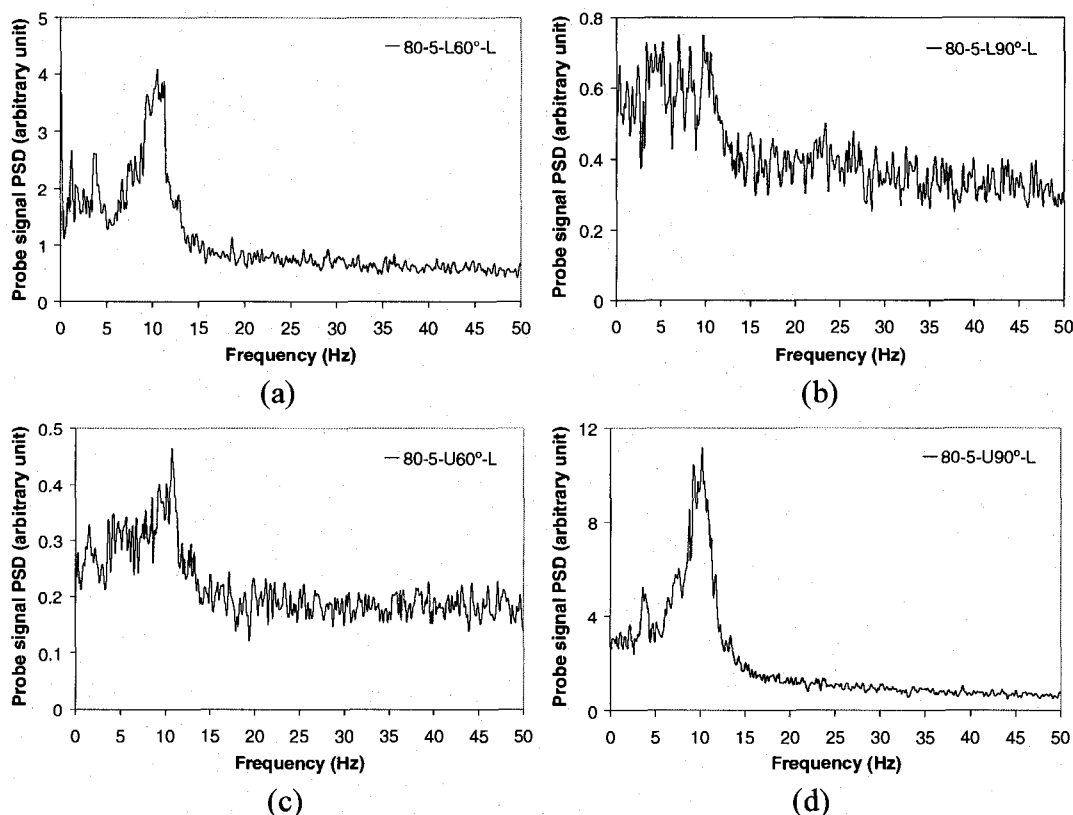


**Fig. 7.6** Power spectra of the local void fraction fluctuation at four different positions on the left side of the main flow path for 80% void fraction at 5 m/s pitch flow velocity: (a) L60°-L position, (b) L90°-L position, (c) U60°-L position, and (d) U90°-L position

(3) For the same flow conditions, the spectra of the local void fraction fluctuation on the left side of the main flow path have a dominant frequency of about 11 Hz (Fig. 7.6). This dominant frequency is consistent with that of the dynamic lift force (Fig. 7.4(b)). This suggests a possible dynamic relation between the void fraction fluctuation on the left side of the main flow path and the dynamic lift forces;

(4) The spectra of the local void fraction fluctuation along the center line of the main flow path as shown in Fig. 7.7, appear to be a combination of those on the right and left sides of the main flow path (Figs 7.5 and 7.6);

(5) The spectrum at position U90°-L0 is very similar to that of the center line of the main flow path (Figs 7.8(a) and 7.7(d)), except that the magnitudes of the power spectral density are higher at L0. The spectrum at position U90°-L1 is very similar to

that of the left side of the main flow path (Figs 7.8(b) and 7.6(d)) in both magnitude and frequency. This may be explained by the following observation.

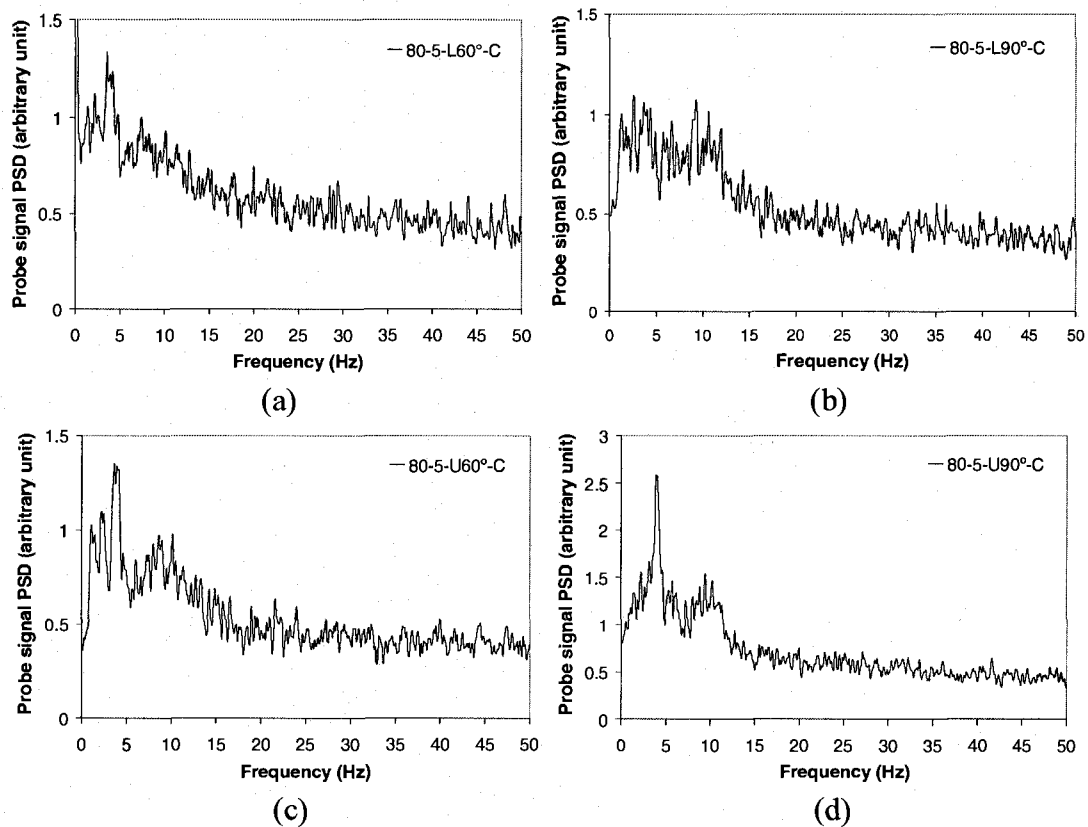


**Fig. 7.7** Power spectra of the local void fraction fluctuation at four different positions along the center line of the main flow path for 80% void fraction at 5 m/s pitch flow velocity: (a) L60°-C position, (b) L90°-C position, (c) U60°-C position, and (d) U90°-C position

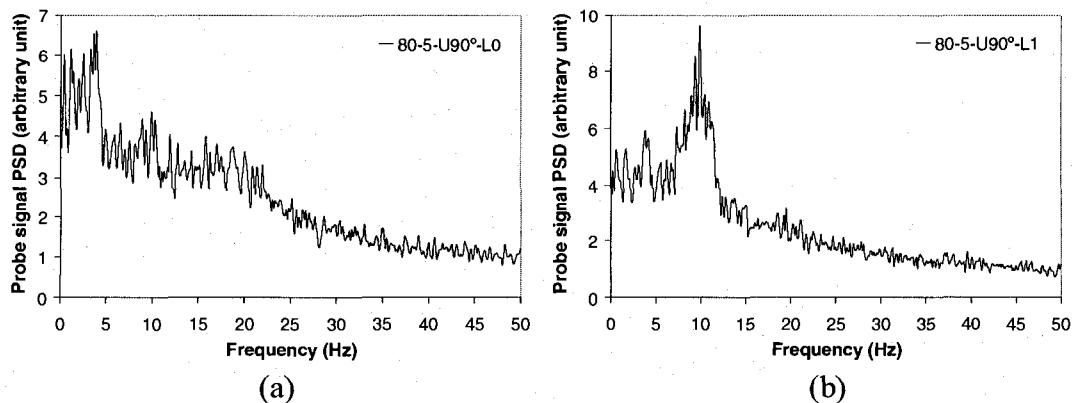


**Fig. 7.8** Power spectra of the local void fraction fluctuation at points L<sub>0</sub> and L<sub>1</sub> of U90° position for 80% void fraction at 5 m/s pitch flow velocity

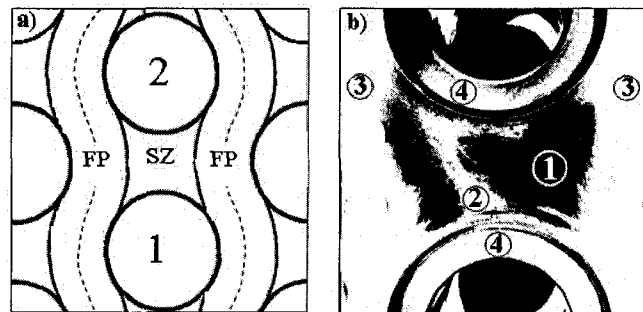


**Fig. 7.9** Two-phase flow structure in a rotated triangular tube bundle: (a) simplified figure (FP: flow path, SZ: “stagnation” zone), (b) flow picture (1: low void fraction mixture belonging to the stagnation zone, 2: oscillating high void fraction mixture in stagnation zone, 3: flow path, 4: rigid tubes)

Fig. 7.9(a) is a simplified schematic representation of the flow structure inside a rotated triangular tube bundle. The flow is mostly along the flow path (FP). In between adjacent tubes in the same column (e.g., Tubes 1 and 2), the flow velocity is much less than in the flow paths and is taken to be near zero. This zone is called the stagnation zone or recirculation zone (SZ). In two-phase continuous flow, the mixture inside the flow paths appears to be very fine and homogenous. On the other hand, in the stagnation zone (SZ), the two-phase mixture is coarse and non-homogeneous, and transverse oscillations in the wake of the cylinders exist. It is these oscillations that will lead to an oscillatory lift force on the tube. Fig. 7.9(b) shows a black and white picture of the structure of the two-phase flow inside a rotated triangular array for a high void fraction (95%) and flow velocity of 12 m/s. Except for the tubes themselves, light tones indicate high void fraction mixtures and dark tones indicate very low void fraction two-phase mixtures. From Fig. 7.9(b), it can be seen that there is a large volume of very low void fraction mixture inside the stagnation zone and that a small portion of the space is occupied by a high void fraction mixture. Fig. 7.9(b) therefore shows an instantaneous configuration of the non-homogenous wake during periodic oscillations. A similar phenomenon was observed visually for 80% void fraction at 5 and 10 m/s pitch flow velocities.

The above investigation showed that the quasi-periodic drag and lift forces are generated by different mechanisms. The quasi-periodic drag forces appear related to the



momentum flux fluctuations in the main flow path between the cylinder columns. The quasi-periodic lift forces, on the other hand, are mostly correlated to the oscillation in the wake of the cylinders.

One may have the opinion that these observations with the narrow test section are possibly an artifact of this particular experimental set-up and would not be observed in a wider array of the same geometry under similar flow conditions. This particular tube array may be too narrow to permit diffusion of the flow laterally across the wake area between upstream and downstream cylinders, a phenomenon perhaps even more important in two-phase flows because of void differences between the main flow path and the wake region between upstream and downstream cylinders. To answer these questions we have recently done some tests with a similar but wider test section including three columns of cylinders instead of one. Similar results were found (Zhang et al., 2006b). Quasi-periodic lift and drag forces essentially similar to those in the narrow test section were found to exist also in the wider test section.

## **7.4 Development of models correlating vibration excitation forces to the dynamic characteristics of two-phase flow**

### **7.4.1 Model correlating void fraction fluctuations in the main flow path and the dynamic drag forces**

The results of the detailed flow measurements indicate that the flow tends to stream between the cylinders and that within that stream the flow velocity is fairly uniform (Pettigrew et al., 2005). In fact, the flow path resembles a series of two-dimensional 60° elbows as shown in Fig. 7.3. This observation serves as the starting point for the development of a model correlating the void fraction fluctuation in the main flow path and the dynamic drag forces.

The vertical forces exerted on the elbows due to two-phase flow may be assumed to be equal to the excitation drag forces on the tubes. There are two  $60^\circ$  elbows surrounding a given tube. The resultant vertical drag force on the tube can be expressed as

$$F_Y(t) = F_{Elbow1,Y}(t) + F_{Elbow2,Y}(t) \quad (7-4)$$

where  $F_Y(t)$ ,  $F_{Elbow,Y}(t)$  are the excitation drag force along the cylinder length (N/m) and the vertical force exerted on the elbow (N/m), respectively, and the subscripts 1, 2 refer to each elbow. The power spectral density,  $S_Y(f)$  and the r.m.s value of the measured force are related to the elbow forces. If it is assumed that the elbow forces  $F_{Elbow1,Y}(t)$  and  $F_{Elbow2,Y}(t)$  are of equal magnitude and fully correlated, then the PSD and the r.m.s. force become

$$S_Y(f) = 4S_{F_{Elbow,Y}}(f); \quad F_Y^{rms}(t) = 2F_{Elbow,Y}^{rms}(t) \quad (7-5)$$

The forces exerted on a  $60^\circ$  elbow are determined by considering the control volume shown in Fig. 7.10. The total force on the control volume is the sum of surface and body forces:

$$\vec{F}_{Surface} + \vec{F}_{Body} = \int_{CS} \vec{U} \cdot \rho \vec{U} d\vec{A} + \frac{\partial}{\partial t} \left( \int_{CV} \rho \vec{U} dV \right) \quad (7-6)$$

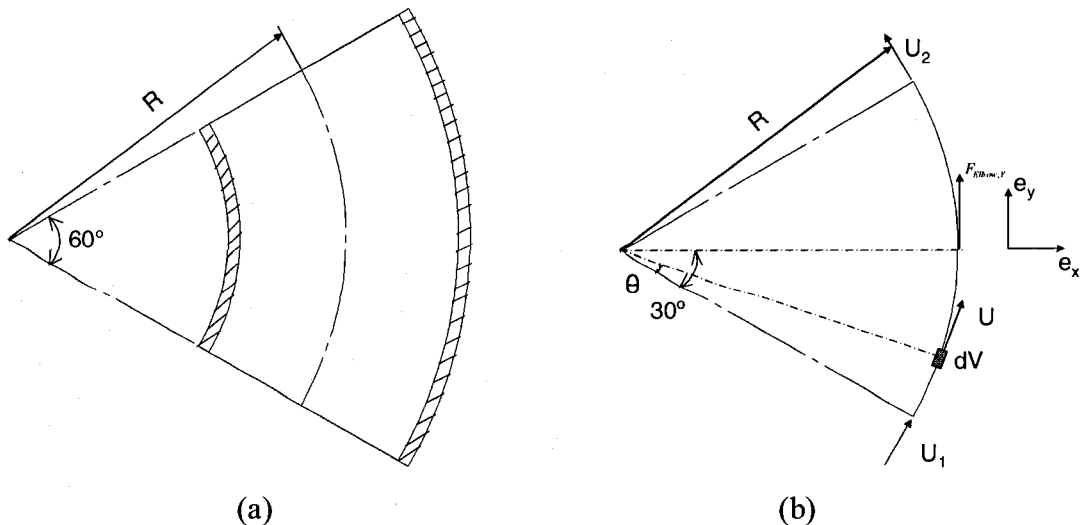


Fig. 7.10 Sketch of  $60^\circ$  elbow for modeling drag forces

where  $\bar{U}$ ,  $\rho$  and  $V$  are the gap flow velocity (m/s), two-phase flow mixture density ( $\text{kg/m}^3$ ) and control volume of a  $60^\circ$  elbow ( $\text{m}^3$ ). Following Yih and Griffith (1970) the fluctuating force may be related to the variation with time of the fluid momentum. The elbow force in the Y direction  $F_{Elbow,Y}(t)$  is given by Eq. (7-6) projected in the  $\bar{e}_y$  (the vertical unit vector) direction:

$$F_{Elbow,Y}(t) = -\frac{\sqrt{3}}{2} \int_{inlet} \rho U^2 dA + \frac{\sqrt{3}}{2} \int_{outlet} \rho U^2 dA + \frac{\partial}{\partial t} \left( \int_{Elbow-V} \rho \bar{U} \bar{e}_y dV \right) \quad (7-7)$$

where the first two surface integrals relate to the flow characteristics at the entrance and exit of the elbow. The third one is a volume integral over the whole fluid domain in the elbow. This is identical to the formulation used by Yih and Griffith (1970) to relate the force exerted by the flow on a tee to variation in void fraction, except that gravity effects are neglected here. It is also equivalent to the formulation developed by Tay and Thorpe (2002, 2004), named Piston Flow Model, except that the pressure gradients due to friction are neglected here. For simplicity, the two-phase flow mixture density is assumed to be homogenous across a section of the elbow and is equal to

$$\rho(t) = \rho_L [1 - \alpha(t)] \quad (7-8)$$

where  $\rho_L$ ,  $\alpha(t)$  are the liquid density and the instantaneous local void fraction, respectively and the gas density is neglected. Let us develop term 3 in Eq. (7-7). In Fig.

7-10, the angular position  $\theta = \frac{\pi/3}{\pi R/3U} \tau$ , so,  $d\theta = \frac{U}{R} d\tau$

$$dV = AR d\theta = AR \frac{U}{R} d\tau = AU d\tau \quad (7-9)$$

$$\bar{U} \cdot \bar{e}_y = U \sin\left(\frac{\pi}{3} + \theta\right) \quad (7-10)$$

where  $R$ ,  $A$ , and  $\tau$  are the radius of the center line of the main flow path (m), gap area ( $\text{m}^2$ ), and the time lag between the inlet and the position ( $\theta$ ) along the elbow (s), respectively.

Introducing Eqs (7-9) and (7-10) into term 3 of Eq. (7-7), we have

$$\begin{aligned}
\frac{\partial}{\partial t} \left( \int_{Elbow-V} \rho \vec{U} \cdot \vec{e}_y dV \right) &= \frac{\partial}{\partial t} \left\{ \int_0^\delta \rho_L [1 - \alpha(t)] U \sin\left(\frac{\pi}{3} + \theta\right) A U d\tau \right\} \\
&= \rho_L U^2 A \frac{\partial}{\partial t} \left\{ \int_0^\delta [1 - \alpha(t)] \sin\left(\frac{\pi}{3} + \theta\right) d\tau \right\} \\
&= -\rho_L U^2 A \frac{\partial}{\partial t} \left[ \int_0^\delta \alpha(t) \sin\left(\frac{\pi}{3} + \theta\right) d\tau \right] \\
&= -\rho_L U^2 A \left[ \int_0^\delta \left( \frac{\partial \alpha}{\partial t} \right)_{t-\tau} \sin\left(\frac{\pi}{3} + \theta\right) d\tau \right] \\
&= -\rho_L U^2 A \left[ \int_0^\delta \left( \frac{\partial \alpha}{\partial t} \right)_{t-\tau} \sin\left(\frac{\pi}{3} + \frac{U}{R} \tau\right) d\tau \right]
\end{aligned} \tag{7-11}$$

In the above derivation, it is assumed that the void fraction pattern across the channel is convected by the gap flow velocity  $U$  ( $U = \frac{\sqrt{3}}{2} U_p$ , for rotated triangular tube bundles), thus the density at the inlet, outlet and inside of the elbow are related by time lags only. This means that we could estimate parameters such as  $\rho(t)$  and  $\alpha(t)$  at any position within the elbow according to the inlet value of  $\alpha(t)$ . In other words, at any moment  $t$ , the void fraction at the inlet is  $\alpha(t)$ , while at the position ( $\theta$ ) within the elbow it will be  $\alpha(t - \tau)$ , where  $\tau$  is the time lag between the inlet and the position ( $\theta$ ) along the elbow. The time lag between the inlet and outlet is  $\delta = \pi R / (3U)$ . So the void fraction at the outlet will be  $\alpha(t - \delta)$ . Finally Eq. (7-7) becomes

$$F_{Elbow,Y}(t) = \frac{\sqrt{3}}{2} \rho_L U^2 A [\alpha(t) - \alpha(t - \delta)] - \rho_L U^2 A \left[ \int_0^\delta \left( \frac{\partial \alpha}{\partial t} \right)_{t-\tau} \sin\left(\frac{\pi}{3} + \frac{U}{R} \tau\right) d\tau \right] \tag{7-12}$$

Similar equations were also developed by Riverin et al. (2006). Note that the derivative of the instantaneous void fraction  $\alpha(t)$  at L60°-C appears in Eq. (7-12).

The r.m.s. value of the elbow force  $F_{Elbow,Y}^{rms}$  could be easily deduced by doing a Fourier transform of Eq. (7-12). Let us separate the right side of Eq. (7-12) into two equations. The first one,  $F_{Elbow,YS}(t)$  is due to momentum change at the surface (inlet and outlet), and the second one,  $F_{Elbow,YV}(t)$  is due to momentum change within the volume of the elbow.

$$F_{Elbow,YS}(t) = \frac{\sqrt{3}}{2} \rho_L U^2 A [\alpha(t) - \alpha(t - \delta)] \quad (7-13)$$

$$F_{Elbow,YV}(t) = -\rho_L U^2 A \left[ \int_0^\delta \left( \frac{\partial \alpha}{\partial t} \right)_{t-\tau} \sin\left(\frac{\pi}{3} + \frac{U}{R} \tau\right) d\tau \right] \quad (7-14)$$

We now define the Fourier Transform of  $F_{Elbow,YS}(t)$  as  $F_{Elbow,YS}(\omega)$ , where

$$F_{Elbow,YS}(\omega) = \int_{-\infty}^{+\infty} F_{Elbow,YS}(t) e^{-j\omega t} dt = \frac{\sqrt{3}}{2} \rho_L U^2 A \alpha(\omega) (1 - e^{-j\omega\delta}) \quad (7-15)$$

and  $F_{Elbow,YS}^*(\omega)$  is the complex conjugate of  $F_{Elbow,YS}(\omega)$ , thus

$$F_{Elbow,YS}^*(\omega) = \frac{\sqrt{3}}{2} \rho_L U^2 A \alpha^*(\omega) (1 - e^{j\omega\delta}) \quad (7-16)$$

The PSD of  $F_{Elbow,YS}(t)$ ,  $S_{F_{Elbow,YS}}(f_\pm)$  can be expressed as:

$$\begin{aligned} S_{F_{Elbow,YS}}(f_\pm) &= \lim_{T \rightarrow \infty} \left[ \frac{1}{T} F_{Elbow,YS}(f) F_{Elbow,YS}^*(f) \right] \\ &= \frac{3}{4} \rho_L^2 U^4 A^2 \lim_{T \rightarrow \infty} \left[ \frac{1}{T} \alpha(\omega) \alpha^*(\omega) (1 - e^{-j\omega\delta}) (1 - e^{j\omega\delta}) \right] \\ &= \frac{3}{2} \rho_L^2 U^4 A^2 \left[ 1 - \cos\left(\frac{\pi R}{3U} 2\pi f\right) \right] S_\alpha(f_\pm) \end{aligned} \quad (7-17)$$

Similarly, the Fourier Transforms of  $F_{Elbow,YV}(t)$  is  $F_{Elbow,YV}(\omega)$ .

$$\begin{aligned} F_{Elbow,YV}(\omega) &= \int_{-\infty}^{+\infty} F_{Elbow,YV}(t) e^{-j\omega t} dt \\ &= -\rho_L U^2 A j \omega \alpha(\omega) \int_0^\delta \left[ \sin\left(\frac{\pi}{3} + \frac{U}{R} \tau\right) e^{-j\omega\tau} \right] d\tau \end{aligned} \quad (7-18)$$

$F_{Elbow,YV}^*(\omega)$  is the conjugate of  $F_{Elbow,YV}(\omega)$ .

$$F_{Elbow,YV}^*(\omega) = \rho_L U^2 A j \omega \alpha^*(\omega) \int_0^\delta \left[ \sin\left(\frac{\pi}{3} + \frac{U}{R} \tau\right) e^{j\omega\tau} \right] d\tau \quad (7-19)$$

The PSD of  $F_{Elbow,YV}(t)$ ,  $S_{F_{Elbow,YV}}(f_{\pm})$  can be expressed as:

$$\begin{aligned}
 S_{F_{Elbow,YV}}(f_{\pm}) &= \lim_{T \rightarrow \infty} \frac{1}{T} F_{Elbow,YV}(f) F_{Elbow,YV}^*(f) \\
 &= \frac{1}{2} \rho_L^2 U^4 A^2 (2\pi f)^2 S_{\alpha}(f_{\pm}) \left[ \frac{1 - \cos\left(\frac{\pi}{3} + \frac{\pi R}{3U} 2\pi f\right)}{\left(\frac{U}{R} + 2\pi f\right)^2} + \frac{1 - \cos\left(\frac{\pi}{3} - \frac{\pi R}{3U} 2\pi f\right)}{\left(\frac{U}{R} - 2\pi f\right)^2} + 2 \frac{\cos\left(\frac{\pi R}{3U} 2\pi f\right) + \cos\frac{2\pi}{3}}{\left(\frac{U}{R}\right)^2 - (2\pi f)^2} \right] \quad (7-20)
 \end{aligned}$$

Recalling Eqs (7-12)-(7-14), we have

$$F_{Elbow,Y}(t) = F_{Elbow,YS}(t) + F_{Elbow,YV}(t) \quad (7-21)$$

The power spectral density of  $F_{Elbow,Y}(t)$ ,  $S_{F_{Elbow,Y}}(f_{\pm})$  can be expressed as follows.

$$S_{F_{Elbow,Y}}(f_{\pm}) = S_{F_{Elbow,YS}}(f_{\pm}) + S_{F_{Elbow,YV}}(f_{\pm}) + S_{F_{Elbow,YSV}}(f_{\pm}) + S_{F_{Elbow,YSY}}(f_{\pm}) \quad (7-22)$$

The last two terms of Eq. (7-22) are cross power spectral densities between the volume force  $F_{Elbow,YS}(t)$  and the surface force  $F_{Elbow,YV}(t)$ . They are neglected being secondary terms.

$$S_{F_{Elbow,Y}}(f_{\pm}) = S_{F_{Elbow,YS}}(f_{\pm}) + S_{F_{Elbow,YV}}(f_{\pm}) \quad (7-23)$$

The mean square (MS) value of  $F_{Elbow,Y}(t)$ ,  $\bar{F}_{Elbow,Y}^2(t)$  will be

$$\begin{aligned}
 \bar{F}_{Elbow,Y}^2(t) &= \int_0^{\infty} S_{F_{Elbow,Y}}(f) df \\
 &= \frac{1}{2} \rho_L^2 U^4 A^2 \int_0^{\infty} S_{\alpha}(f) \left[ 3 \left( 1 - \cos \frac{\pi R}{3U} 2\pi f \right) \right] df + \frac{1}{2} \rho_L^2 U^4 A^2 \int_0^{\infty} S_{\alpha}(f) (2\pi f)^2 \left[ \frac{1 - \cos\left(\frac{\pi}{3} + \frac{\pi R}{3U} 2\pi f\right)}{\left(\frac{U}{R} + 2\pi f\right)^2} \right] df + \\
 &\quad \frac{1}{2} \rho_L^2 U^4 A^2 \int_0^{\infty} S_{\alpha}(f) (2\pi f)^2 \left[ \frac{1 - \cos\left(\frac{\pi}{3} - \frac{\pi R}{3U} 2\pi f\right)}{\left(\frac{U}{R} - 2\pi f\right)^2} \right] df + \frac{1}{2} \rho_L^2 U^4 A^2 \int_0^{\infty} S_{\alpha}(f) (2\pi f)^2 \left[ 2 \frac{\cos\left(\frac{\pi R}{3U} 2\pi f\right) + \cos\frac{2\pi}{3}}{\left(\frac{U}{R}\right)^2 - (2\pi f)^2} \right] df \quad (7-24)
 \end{aligned}$$

$S_{\alpha}(f)$  in Eq. (7-24) could be obtained directly from probe signal at L60° (Position C).

Introducing Eq. (7-24) into Eq. (7-5), the r.m.s. value of the resultant vertical drag force on the tube will be

$$F_Y^{rms}(t) = 2\sqrt{\overline{F_{Elbow,Y}^2}}(t) \quad (7-25)$$

A computer code was programmed by using of Eqs (7-24) and (7-25) for estimating the drag force according to void signal (probe signal of L60°-C).

The resulting r.m.s. values are presented in Table 7.1, where comparison with the direct measurements of the forces is made. Although the measured values are lower than the calculations, they are both within the same order of magnitude. An important reason for the difference is that the coherence between void fraction fluctuation at L60°-C and drag forces is relatively high only in the range 0-10 Hz (Zhang et al., 2006a, 2008). One of figures showing that coherence (Zhang et al., 2006a, 2008) is represented in Fig. 7.11. Beyond 10 Hz, the coherence is extremely low. If only the frequency range 0-10 Hz is considered for the measured and estimated forces, much better agreement is found as shown in Table 7.2. This and other possible explanations are currently being considered which should lead to a more refined model.

**Table 7.1** Comparison between measured and estimated r.m.s. drag forces (N/m) within 0 to 20 Hz

Pitch flow velocity $U_p$ (m/s)	$\alpha=80\%$		$\alpha=90\%$	
	Measured	Estimated	Measured	Estimated
5	18.1	51.5	13.7	54.7
10	31.9	49	20.3	50.9

**Table 7.2** Comparison between measured and estimated r.m.s. drag forces (N/m) within 0 to 10 Hz

Pitch flow velocity $U_p$ (m/s)	$\alpha=80\%$		$\alpha=90\%$	
	Measured	Estimated	Measured	Estimated
5	15.9	21.1	12.4	23.9
10	28.8	20.7	18.5	20.3

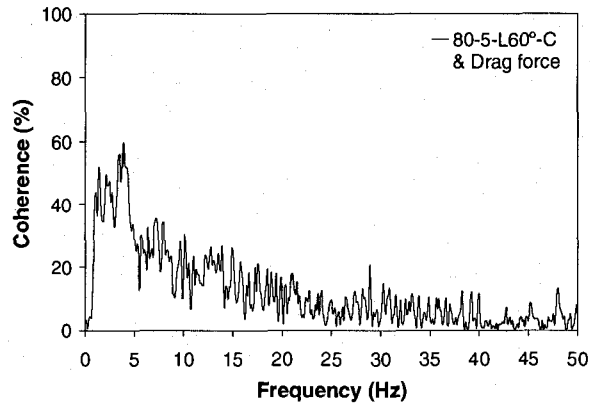


**Fig. 7.11** Coherences between the local void fraction fluctuation at L60°-C and the dynamic drag force for 80% void fraction at 5 m/s pitch flow velocity

#### 7.4.2 Model correlating oscillations in the wake of the cylinders and the dynamic lift forces

A model for correlating oscillations in the wake of the cylinders and the dynamic lift forces is also developed. Although the mechanism for the oscillation in the wake of the cylinders is not as yet completely understood, it may be similar to oscillations associated with low frequency mechanisms for some structures in single phase flow. It has been hypothesized to be due to an imbalance between flow entrained by the separated shear layer and that returned to the separation zone at reattachment (Rockwell, 1983). For the purpose of model development, based on our visualizations, video-photography and fiber-optic probe measurements, this wake oscillation could be thought as two low void shear layers self-excited transversely between the upstream and downstream cylinders. This characteristic of wake oscillation is assumed to be sustained when this wake flow passes through the main flow path.

Only the oscillation at the dominant frequency is taken into account on here, so the motion and velocity equations of the oscillating wake will be

$$x(t) = \frac{1}{2} e \sin(2\pi ft); \quad u(t) = \pi e f \cos(2\pi ft) \quad (7-26)$$



where  $e, f$  are the width of the wake (Fig. 7.1) and dominant frequency, the oscillating amplitude of the wake was assumed to be half of  $e$  as deduced from the experiments.

The horizontal forces exerted on the elbows due to the wake oscillation may be assumed to be equal to the excitation lift forces on the tubes. There are two  $60^\circ$  elbows surrounding the tube. The resultant horizontal lift force on the tube can be expressed as

$$F_x(t) = F_{Elbow1,x}(t) + F_{Elbow2,x}(t) \quad (7-27)$$

where  $F_x(t), F_{Elbow,x}(t)$  are the excitation lift force along the cylinder length (N/m) and the horizontal force exerted on the elbow (N/m), respectively, and the subscripts 1, 2 refer to each elbow. The r.m.s value of the measured force is related to that of the elbow forces. If it is assumed that the elbow forces  $F_{Elbow1,x}(t)$  and  $F_{Elbow2,x}(t)$  are of equal magnitude and not correlated, then the r.m.s. force becomes

$$F_x^{rms}(t) = \sqrt{2} F_{Elbow,x}^{rms}(t) \quad (7-28)$$

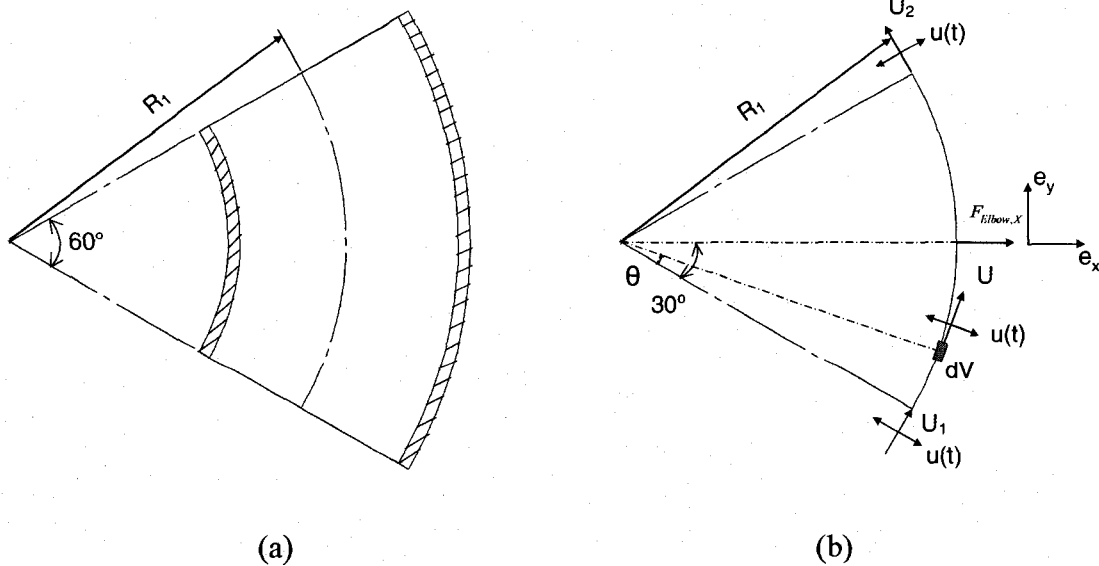


Fig. 7.12 Sketch of  $60^\circ$  elbow for modeling lift forces

The control volume for the evaluating of the forces exerted on a 60° elbow are considered as shown in Fig. 7.12. The fluctuating lift force may be related to the variation with time of the wake momentum in a 60° elbow. The elbow force in the X direction  $F_{Elbow,X}(t)$  is given by Eq. (7-6) projected in the  $\bar{e}_x$  (the horizontal unit vector) direction.

$$F_{Elbow,X}(t) = \frac{\partial}{\partial t} \left[ \int_{Elbow-V} \rho_L \bar{u}(t) \bar{e}_x dV \right] \quad (7-29)$$

The term on the right hand is a volume integral over the whole fluid domain in the elbow. Based on experiments, the mean radius of the wake in the main flow path,  $R_1$  was taken as the radius of the tube plus wake width. In the 60° elbow, the wake oscillation velocity  $\bar{u}(t)$  is just in the normal or transverse direction and is assumed to keep the same oscillation amplitude as that in between upstream and downstream cylinders. The term related to the surface integral is zero due to  $\bar{u}(t)$  being perpendicular to  $d\bar{A}$ . Further derivation is given as follows.

$$\begin{aligned} F_{Elbow,X}(t) &= \frac{\partial}{\partial t} \left[ \int_{Elbow-V} \rho_L \bar{u}(t) \bar{e}_x dV \right] \\ &= \frac{\partial}{\partial t} \left[ \int_0^{\frac{\pi}{3}} \rho_L \pi e f \cos(2\pi ft) \cos\left(\frac{\pi}{6} - \theta\right) e R_1 d\theta \right] \\ &= \frac{\partial}{\partial t} \left\{ \rho_L \pi e^2 R_1 f \cos(2\pi ft) \left[ -\sin\left(\frac{\pi}{6} - \theta\right) \right]_0^{\frac{\pi}{3}} \right\} \\ &= -2\pi^2 \rho_L R_1 e^2 f^2 \sin(2\pi ft) \end{aligned} \quad (7-30)$$

Introducing final result of Eq. (7-30) into Eq. (7-28), the r.m.s. value of the resultant horizontal lift force on the tube will be

$$F_X^{rms}(t) = -2\sqrt{2}\pi^2 \rho_L R_1 e^2 f^2 \sin(2\pi ft) \quad (7-31)$$

If the periodic frequency is introduced in Eq. (7-31), the r.m.s. value of the resultant horizontal lift force can be estimated.

The corresponding r.m.s. values are presented in Table 7.3, and compared to the direct measurement of the force. Although the measured values are generally lower than the calculations, they are both reasonably close for a first attempt at estimating these forces deriving from a complex two-phase flow phenomenon.

**Table 7.3** Comparison between measured and estimated r.m.s. lift forces (N/m) at the dominant frequency

Pitch flow velocity $U_p$ (m/s)	$\alpha=80\%$		$\alpha=90\%$	
	Measured	Estimated	Measured	Estimated
5	1.3	1.65	1.13	1.04
10	2.42	4.34	1.69	2.31

## 7.5 Conclusion

Quasi-periodic drag and lift forces were measured on an array of cylinders subjected to two-phase flow. Measurements of the dynamic characteristics of the two-phase flow indicate that quasi-periodic drag and lift forces are generated by different mechanisms that have not been observed previously. The quasi-periodic drag forces appear related to the momentum flux fluctuations in the main flow path between the cylinders. These momentum flux fluctuations are caused by the void fraction fluctuations in the main flow path between the cylinders. The quasi-periodic lift forces, on the other hand, are mostly correlated to oscillations in the wake of the cylinders. The relationships between the lift or drag forces and the dynamic characteristics of two-phase flow are established through fluid mechanics momentum equations. A model has been developed to correlate the void fraction fluctuation in the main flow path and the dynamic drag forces. A second model has been developed for correlating the oscillation in the wake of the cylinders and the dynamic lift forces. Although further development is needed, these preliminary models are encouraging since plausible prediction is reached.

## 7.6 Acknowledgments

The authors are grateful to Dragos Pamfil for the test section design and the development of the fiber-optic probes. Thanks are also due to Thierry Lafrance, Bénédict Besner and Nour Aimène for their help throughout the project.

## 7.7 References

Axisa, F., Antunes, J., Villard, B., 1990. Random excitation of heat exchanger tubes by cross-flows. *Journal of Fluid and Structures* 4, 321-341.

Blevins, R. D., 1990. *Flow-induced vibration* (2nd edition), Van Nostrand Reinhold, New York.

Nakamura, T., Fujita, K., Kowanishi, N., Yamaguchi, N., Tsuge, A., 1995. Study on the Vibration Characteristics of a Tube Array Caused by Two-Phase Flow, Part 1: Random Vibration. *Journal of Fluids Structures* 9, 519–538.

Pettigrew, M.J., Taylor, C.E., 1994. Two-phase flow-induced vibration: an overview. *ASME Journal of Pressure Vessel Technology* 116, 233-253.

Pettigrew, M.J., Zhang, C., Mureithi, N.W, Pamfil, D., 2005. Detailed flow and force measurements in a rotated triangular tube bundle subjected to two-phase cross-flow. *Journal of Fluids and Structures* 20, 567–575.

Riverin, J.L., de Langre, E., Pettigrew, M.J., 2006. Fluctuating forces caused by internal two-phase flow on bends and tees. *Journal of Sound and Vibration* 298, 1088-1098.

Rockwell, D., 1983. Oscillation of impinging shear layers. *AIAA Journal* 21, 645-664.

Tay, B.L., Thorpe, R.B., 2004. Effect of liquid physical properties on the forces acting on a pipe bend in gas-liquid slug flow. *Chemical Engineering Research and Design* 82, 344-356.

Tay, B.L., Thorpe, R.B., 2002. Forces on a pipe bend due to slug flow. *Proceeding of the 3rd North American Multiphase Technology Conference, Banff*, 281-300

Yih, T.S., Griffith, P., 1970. Unsteady momentum fluxes in two-phase flow and the vibration of nuclear system components. *Proceeding of the International Conference on Flow-Induced Vibration in Reactor System Components, Argonne Ill., Report ANL-7685*, 91-111.

Zhang, C., Pettigrew, M.J., Mureithi, N.W., 2006a. Correlation between vibration excitation forces and the dynamic characteristics of two-phase cross flow in a rotated triangular tube bundle. *Proceedings of ASME PVP2006-ICPVT-11, 6th FSI, AE & FIV and N Symposium (M. P. Paidoussis, ed.), Vancouver, Canada, CD-ROM, #93797*

Zhang, C., Pettigrew, M.J., Mureithi, N.W., 2006b. Quasi-periodic vibration excitation mechanism due to two-phase cross flow in steam generator tube bundles. *Proceedings of 5th CNS International Steam Generator Conference, Toronto, Canada, CD-ROM, #26*

Zhang, C., Pettigrew, M.J., Mureithi, N.W., 2007. Vibration excitation force measurements in a rotated triangular tube bundle subjected to two-phase cross-flow. *ASME Journal of Pressure Vessel Technology* 129, 21-27.

Zhang, C., Pettigrew, M.J., Mureithi, N.W., 2008. Correlation between vibration excitation forces and the dynamic characteristics of two-phase cross flow in a rotated triangular tube bundle. Scheduled for publication in *ASME Journal of Pressure Vessel Technology* 130, No.1.

## CHAPTER 8

### DISCUSSIONS AND CONCLUSIONS

In this chapter, a review of progress achieved with relation to the objectives outlined in Chapter 1 is given first. Then, discussions on quasi-periodic vibration excitation forces in rotated triangular tube bundles due to two-phase cross flow are presented. Thirdly, the main contributions are summarized. Finally, recommendations for further work are given. These correspond to Sections 8.1, 8.2, 8.3 and 8.4, respectively.

#### 8.1 Review of objectives

Reviewing the objectives outlined in Chapter 1 is a convenient way to outline the progress in the understanding of quasi-periodic vibration excitation forces in rotated triangular tube bundles due to two-phase cross flow. A good understanding of the nature of these excitation forces was reached by achieving each objective.

The first objective was to measure the characteristics of two-phase flow such as void fraction, bubble velocity and bubble size within a heat exchanger tube bundle. Fiber-optic probes were used to determine the detailed profiles of void fraction, bubble velocity and bubble size. The results are presented in Chapter 3. To our knowledge such measurements were not done before for two-phase flow in tube bundles.

The second objective was to determine experimentally the excitation forces associated with heat exchanger tubes subjected to two-phase cross flow. The forces were measured directly using strain gauge instrumented cylinders. The experiments included some tests with one single tube and several tests with two in-line tubes with different pitches along the flow. However, most of the testing was done with a rotated-triangular array of

cylinders. The test matrix included a wide range of flow conditions. The test results were analyzed and are presented in Chapters 4, 6 and in the Appendix. The experimental program provided a large amount of data used in completing the remaining objectives. In total, the results of over 600 different tests were analyzed.

The third objective was to correlate quasi-periodic and random turbulence excitation forces with the dynamic characteristics of two-phase flow. Two-phase flow characteristic and dynamic lift and drag force measurements were performed simultaneously. Correlation between vibration excitation forces and the dynamic characteristics of two-phase flow were analyzed and are presented in Chapter 5.

The fourth objective was to understand the nature of the periodic and random turbulence excitation forces. Based on the outcome of Objective 3, two semi-analytical models were developed for correlating vibration excitation forces to the dynamic characteristics of two-phase flow and understanding the nature of such vibration excitation forces. These models are presented in Chapter 7.

## **8.2 Further discussion**

Detailed discussion on the results obtained in this study is given within Chapters 3 to 7. It may be noticed that little comparison between our results and those of other researchers was presented. This is mainly due to scarcity of information on the fundamental mechanisms of random turbulence excitation in tube bundles subjected to two-phase cross flow. As mentioned in Chapter 4, significant quasi-periodic forces exist in both the drag and lift direction within tube bundles. The frequency of these excitation forces is relatively low (i.e., 3-6 Hz) and not directly dependent on flow velocity in the drag direction. On the other hand, much higher frequencies (up to 16 Hz) were observed in the lift direction at the higher flow velocities. The frequency appears directly related to flow velocity in the lift direction. It seems that the peak frequencies in the lift

direction are more dominant. Some further studies related to periodic forces in either two-phase flow or single-phase flow on a single cylinder, two in-line cylinders and cylinder arrays are briefly discussed below. The results are briefly compared.

### 8.2.1 Periodic vortex shedding

#### **A single cylinder**

In single-phase flow, the vortices shed from a single cylinder produce a fluctuating lift force at the frequency of the shedding of vortex pairs and a fluctuating drag force at twice this frequency (Weaver et al., 2000). The shedding frequency,  $f_s$ , is defined by the Strouhal number,  $f_s D/U$  which is approximately 0.2 for a cylinder in a Reynolds number range between  $10^2$  and  $10^5$ . If the vortex-shedding frequency is equal to the resonant frequency of the cylinder, vortex-induced vibration can produce large amplitude vibrations.

In two-phase flow, vortices are only found at very low void fractions (<15 percent). The explanation is that the existence of bubble structure in two-phase flow destroys the vortex street.

#### **Two in-line cylinders and cylinder arrays**

When more than one cylinder is placed in a fluid flow, vortex shedding pattern may be completely different from those found in a single cylinder at the same Reynolds number (Zdravkovich, 1987). They may produce other phenomena such as wake-induced instability of downstream cylinder in the case of two tandem cylinders, and bistable jets behind the cylinders in the case of side-by-side arrangements (Blevins, 1990). Vortex shedding phenomena are more complicated in heat exchanger tube bundles and strongly dependent on tube array geometry and pitch ratio. In two-phase flow, vortex shedding is similar to that in liquid flow at very low void fractions and becomes insignificant at void fractions above 15 percent (Taylor et al., 1989).



### 8.2.2 Periodicity excited by shear layers

The phenomena of flow-excited acoustic resonance of two tandem cylinders in air cross flow was studied by Mohany and Ziada (2005). It was found that the aeroacoustic response of tandem cylinders is significantly different than that of a single cylinder. For a single cylinder, the acoustic resonance of a given mode occurs over a single range of flow velocities and is excited by the natural vortex shedding process observed in the absence of acoustic resonance. In the case of tandem cylinders with a spacing ratio (ratio of center-to-center distance between cylinders over cylinder diameter, i.e.,  $L/D$ ) inside the proximity region,  $L/D < 3.5$ , a dual resonance phenomenon occurs over two different ranges of flow velocity, as shown in Fig. 8.1. The first one occurs at much lower flow velocities than reported before. The second one is similar to that observed for single cylinders and is due to the natural vortex shedding phenomena. The first resonance is believed to be excited by the instability of the shear layers in the gap between the cylinders. In the absence of sound waves, this proximity interference range is characterized by a quasi-steady reattachment of the shear layers separated from the upstream cylinder onto the downstream cylinder. The interaction of these shear layers with sound waves is expected to affect the mechanisms of acoustic resonance (Mohany and Ziada, 2005). Outside the proximity region, the aeroacoustic response of the two tandem cylinders is similar to that of single cylinder.

As mentioned in Chapter 6, the periodicity of the lift forces is much affected by the space between upstream and downstream cylinders. The wake oscillation in this relatively narrow space is the source of the periodicity. It can be concluded that the mechanism of quasi-periodic lift forces in air/water flow is different than that of vortex lift forces in water flow. From this, it may also be suggested that the quasi-periodic lift forces are generated in a manner similar to the first periodicity caused by instability of the shear layers formed in the gap between the cylinders as discussed above. Comparison of the Strouhal numbers in this study and those of Mohany and Ziada

(2005) are given in Fig. 8.2. Strouhal numbers in this study are considerably lower than those of shear layer instability (Mohany and Ziada, 2005). However, this is not completely surprising since this study was done in two-phase flow. Further study is obviously needed.

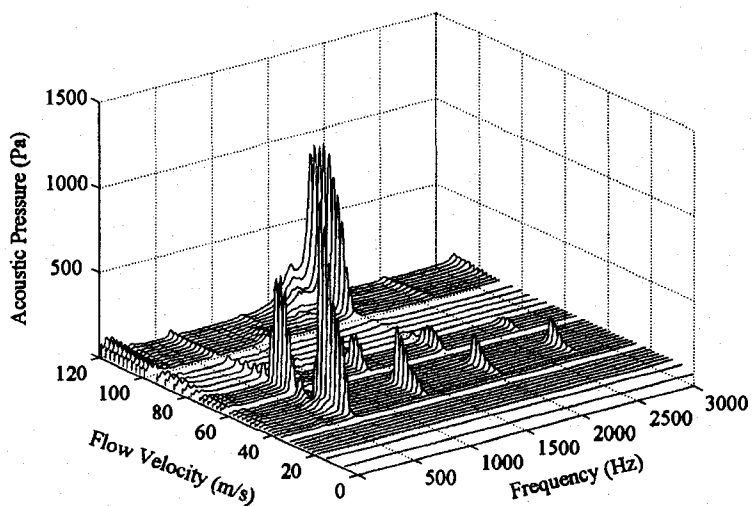


**Fig. 8.1** Pressure spectra for a range of flow velocities for two tandem cylinders ( $D=12.7$  mm,  $L/D=3$ , Mohany and Ziada, 2005)

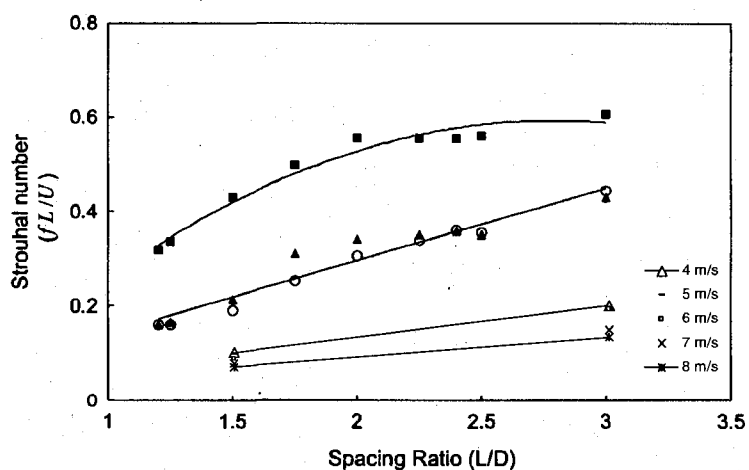


**Fig. 8.2** Comparison of the Strouhal numbers of vortex shedding and at the onset of resonance for both the pre-coincidence range and the post coincidence range,  $\blacksquare$ , for pre-coincidence;  $\blacktriangle$ , for post-coincidence;  $\circ$ , for vortex shedding (Mohany and Ziada, 2005), and Strouhal number for 80% homogeneous void fraction two-phase flow in this study. All values of Strouhal number are based on center-to-center distance  $L$

### 8.3 Main contributions

From this study, several contributions to the development of appropriate design guidelines and to the understanding of the underlying vibration excitation mechanisms can be noted. The first contribution is the large body of empirical data generated in the laboratory. These data cover a wide range of void fractions and flow rates. These data should be useful to other researchers and to heat exchanger designers.

A second major contribution is the finding that quasi-periodic excitation mechanism governs two-phase flow induced vibration in tube bundles. Two different quasi-periodic excitation mechanisms not reported before, were found. These mechanisms were discovered by detailed two-phase flow and vibration excitation force measurements. The quasi-periodic drag forces appear related to the momentum flux fluctuations in the main flow path between the cylinders. These momentum flux fluctuations are caused by void fraction fluctuations in the main flow path between the cylinders. The quasi-periodic lift forces, on the other hand, are mostly correlated to oscillations in the wake of the cylinders. The quasi-periodic lift forces are very different from vortex shedding forces in single-phase flow. Little available data for vibration excitation forces could be found in the literatures. This is mainly because most researchers up to now have focused on fluidelastic instability. One source of data that was found is Taylor (1994). She actually found similar quasi-periodic force peaks in both drag and lift force spectra. Unfortunately not much attention was paid to the latter because she was primarily interested in random excitation.

A third significant contribution is the development of two semi-analytical models. The relationships between the lift or drag forces and the dynamic characteristics of two-phase flow are established through basic fluid mechanics momentum equations. A model has been developed to correlate the void fraction fluctuation in the main flow path and the dynamic drag forces. It can also be used to predict the periodic forces due

to two-phase flow in bends of piping systems. A second model was developed for correlating the oscillation in the wake of the cylinders and the dynamic lift forces. Although further development is needed, these preliminary models are encouraging since plausible predictions are reached.

A fourth contribution is the development of a simple and innovative method for measuring correlation. Two instrumented half-length cylinders were designed to measure the correlation along the cylinder length. The correlations along the tube length for both vortex shedding forces for water flow and quasi-periodic drag and/or lift forces for air/water were measured. It was proved to be an effective way of assessing correlation in this study.

A fifth contribution is the measurement of void fraction, bubble velocity and bubble size profiles in the tube bundle for several typical flow conditions. The results of the flow measurements indicate that the flow tends to stream between the cylinders and that within that stream the flow velocity is fairly uniform. In fact, the flow path resembles a series of two-dimensional  $60^\circ$  elbows. Thus, it is not surprising that the void fraction distribution is not uniform. The lowest void fraction corresponds to the extrados and the highest void fraction to the intrados at the exit of the elbows (Figures 3.8(a), (b) and (c)) as would be expected of two-phase flow in elbows. The void fraction distribution is completely reversed from one side to the other within half a cylinder pitch. It implies that two-phase flow is very well mixed in rotated triangular tube bundles. It also implies that two-phase flow regimes in rotated tube bundles may be quite different than those for upward flow in vertical pipe.

This study has probably resulted in more questions being raised than answered. The knowledge required to ask appropriate questions can be a significant contribution to future work.

## 8.4 Recommendations for future work

Recommendations for future work in this area include the following:

- 1) Flow regime maps for two-phase cross flow in tube bundles are required. This will require the development of sophisticated flow visualization techniques to determine local flow pattern. For example, new methods like PIV for measuring flow, should be considered.
- 2) Tests for the same bundle configuration but for smaller tube diameters are required to determine if these quasi-periodic vibration excitation mechanisms are significant in also more realistic tube geometries.
- 3) Tests in other two-phase fluids are required to determine if these quasi-periodic vibration excitation mechanisms in air/water also exists in steam-water flow.
- 4) Both semi-analytical models need to be refined.

## REFERENCES

- Au-Yang, M. K., 2001. Flow-induced vibration of power and process plant components, New York: ASME Press, Professional Engineering Publishing Limited.
- Axisa, F., Villard, B., Gibert, R. J., Hetsroni, G., and Sundheimer, P., 1984. Vibration of tube bundles subjected to air-water and steam-water cross flow: Preliminary results on fluidelastic instability. Proceedings of ASME Symposium on Flow-Induced Vibrations, Vol. 2, New Orleans, LA, pp. 269-284.
- Axisa, F., Antunes, J. and Villard, B., 1990. Random excitation of heat exchanger tubes by cross-flows. *J. Fluid Struct.* 4, pp. 321-341.
- Azzopardi, B.J. and Baker, G., 2003. Characteristics of periodic structures in gas/liquid two-phase flow. UK/Japan Two-Phase Flow Meeting, Guildford, UK, April 14-15.
- Barrau, E., and Cartellier, A., 1998. Monofiber optical probes for gas detection and gas velocity measurement: Conical probes. *Int. J. Multiphase Flow* 24, pp.1265-1294
- Barrau, E., Riviere, N., Poupot, Ch., and Cartellier, A., 1999. Single and double optical probes in air-water two-phase flows: Real time signal processing and sensor performance. *Int. J. Multiphase Flow* 25, pp. 229-256.
- Bergles, A.E., and Ishigai, S., 1979. Two-phase flow dynamics (Japan-U.S. Seminar on Two-Phase Flow Dynamics, Kobe-shi, Japan), New York: McGraw-Hill Book Company.
- Blevins, R.D., 1990. Flow-induced vibration, New York: Van Nostrand Reinhold, 2<sup>nd</sup> edition.
- Carlucci, L.N., 1980. Damping and hydrodynamic mass of a cylinder in simulated two-phase flow. *ASME J. Mech. Des.* 102, pp. 597-602.
- Carlucci, L.N. and Brown, J.D., 1983. Experimental studies of damping and hydrodynamic mass of a cylinder in confined two-phase flow. *ASME J. Vibrat. Acoust. Stress Reliability Des.* 105, pp. 83-89.

- Cartellier, A., and Barrau, E., 1998. Monofiber optical probes for gas detection and gas velocity measurements: Optimized sensing tips. *Int. J. Multiphase Flow* 24, pp. 1295-1315.
- Chan, A.M.C. and Bannerjee, S., 1981. Design aspects of gamma densitometers for void fraction measurements in small scale two-phase flow. *Nuclear Instrum. Methods* 190, pp. 135-148.
- Chen, S.S. and Jendrzeczyk, J. A., 1987. Fluid excitation forces acting on a square tube array. *ASME J. Fluids Eng* 109, pp.415-423.
- Chen, S.S., 1987. A general theory for dynamic instability of tube arrays in cross-flow. *J. Fluids Struct.* 1, pp. 35-53.
- Collier, J.G. and Thome, J.R., 1996. Convective Boiling and Condensation, Oxford Science Publication, Oxford: Clarendon Press, 3<sup>rd</sup> edition.
- Connors, H.J., 1978. Fluid-elastic vibration of heat exchanger tube arrays. *ASME J. Mech. Des.* 100, pp. 347-353.
- De Langre, E., and Villard, B., 1998. An upper bound on random buffeting forces caused by two-phase flows across tubes. *J. Fluids Struct.* 12, pp. 1005-1023.
- Delhaye, J.M., Giot, M., and Riethmuller, M.L., 1980. Thermohydraulics of two-phase flow systems for industrial design and nuclear engineering. McGraw-Hill Book Company, New York, NY.
- Dowlati, R., Chan, A.M.C. and Kawaji, M., 1992. Hydrodynamics of two-phase flow across a horizontal in-line and staggered rod bundle. *ASME J. Fluids Engng* 114, pp. 450-456.
- Feenstra, P.A., Judd, R.L. and Weaver, D.S., 1995. Fluid-elastic instability in a tube array subjected to two-phase R-11 Cross-flow. *J. Fluids Struct.* 9, pp. 747-771.
- Feenstra, P.A., Weaver, D.S., and Judd, R.L., 2000. Improved void fraction model for two-phase cross-flow in horizontal tube bundles. *Int. J. Multiphase Flow* 26, pp. 1851-1873.

- Feenstra, P.A., Weaver, D.S. and Judd, R.L., 2002. Modelling two-phase flow-excited damping and fluidelastic instability in tube arrays. *J. Fluids Struct.* 16, pp. 811-840.
- Feenstra, P.A., Weaver, D.S., and Nakamura, T., 2003. Vortex shedding and Fluid-elastic instability in a normal square tube array excited by two-phase Cross-flow, *J. Fluids Struct.* 17, pp. 793-811.
- Fordham, E.J., Holmes, A., Ramos, R.T., Simonian, S., Huang, S-M. and Lenn, C. P., 1999a. Multi-phase-fluid discrimination with local fibre-optical probes: I. Liquid/liquid flows. *Meas. Sci. Technol.* 10, pp. 1329-1337.
- Fordham, E.J., Simonian, S., Ramos, R.T., Holmes, A., Huang, S-M. and Lenn, C.P. 1999b. Multi-phase-fluid discrimination with local fibre-optical probes: II. Gas/liquid flows. *Meas. Sci. Technol.* 10, pp.1338-1346.
- Fordham, E.J., Ramos, R.T., Holmes, A., Simonian, S., Huang, S-M. and Lenn, C.P. 1999c. Multi-phase-fluid discrimination with local fibre-optical probes: III. Three-phase flows. *Meas. Sci. Technol.* 10, pp.1347-1352.
- Grant, I.D.R. and Murray, I., 1972. Pressure drop on the shell side of a segmentally baffled shell-and tube heat exchanger with vertical two-phase flow. Report NEL-500, National Engineering Laboratory.
- Grant, I.D.R. and Chisholm, D., 1979. Two-phase flow on the shell-side of a segmentally baffled shell-and-tube heat exchanger. *ASME J. Heat Transfer* 101, pp. 38-42.
- Heilker, W.J. and Vincent, R.Q., 1981. Vibration in nuclear heat exchangers due to liquid and two-phase flow. *ASME J. Eng. Power* 103, pp. 358-366.
- Hirota, K., Nakamura, T., Mureithi, N. W., Kasahara, J., Kusakabe, T. and Takamatsu, H., 2002. Dynamics of an in-line tube array subjected to steam-water cross-flow. Part III: fluidelastic instability tests and comparison with theory. *J. Fluids Struct.* 16, pp. 153-173.
- Inada, F., Kawamura, K., Yasuo, A., Yoneda, K., 2000. An experimental study on the fluid-elastic forces acting on a square tube bundle in two-phase cross-flow: the



- effect of vibration amplitude. Proceedings of FIV-2000, Lucerne, Switzerland, June 19-21, pp. 555-568.
- Lever, J.H., and Weaver D.S., 1982. A theoretical model for fluidelastic instability in heat exchanger tube bundles. *ASME J. Pres. Ves. Technol.* 104, pp. 147-158.
- Lever, J.H., and Weaver D.S., 1986. On the stability behaviour of heat exchanger tube bundles. Part I-Modified theoretical model. *Journal of Sound and Vibration* 107, pp. 375-410.
- Lian, H.Y., Noghrehker, G., Chan, A.M.C. and Kawaji, M., 1997. Effect of void fraction on vibrational behaviour of tubes in tube bundle under two-phase cross-flow. *J. Vibrat. Acoust.* 119, pp. 457-463.
- Mann, W. and Mayinger, F., 1995. Flow-induced vibration of tube bundles subjected to single- and two-phase cross-flow. Proceedings of the 2nd International Conference on Multiphase Flow, Vol. 4, pp. 9-15, Kyoto, Japan.
- Marn, J. and Catton, I., 1996. On analysis of fluid-elastic instability in air-water mixture. *ASME J. Pres. Ves. Technol.* 118, pp. 188-193.
- McQuillan, K. W. and Whalley, P. B., 1985. Flow patterns in vertical two-phase flow. *Int. J. Multiphase Flow* 11, pp. 161-175.
- Mohany, A. and Ziada, S., 2005. Flow-excited acoustic resonance of two tandem cylinders in cross-flow. *J. Fluids Struct.* 21, pp. 103-119.
- Morris, D., Teyssedou, A., Lapierre, J., and Tapucu, A., 1987. Optical fiber probe to measure local void fraction profiles. *Appl. Optics* 26, pp.4660-4664.
- Mureithi, N. W., Nakamura, T., Hirota, K., Murata, M., Utsumi, S., Kusakabe, T., Kusakabe, T. and Takamatsu, H., 2002. Dynamics of an in-line tube array subjected to steam-water cross-flow; Part II: Unsteady fluid forces. *J. Fluids Struct.* 16, pp. 137-152.
- Mureithi, N.W., Zhang, C., Ruel, M., and Pettigrew, M.J., 2005. Fluidelastic instability tests on an array of tubes preferentially flexible in the flow direction. *J. Fluids Struct.* 21, pp. 75-87.

- Nakamura, T., Fujita, K., Kowanishi, N., Yamaguchi, N., and Tsuge, A., 1995. Study on the Vibration Characteristics of a Tube Array Caused by Two-Phase Flow, Part 1: Random Vibration. *J. Fluids Struct.* 9, pp. 519-538.
- Nakamura, T., Murerithi, N.W., Chen, S.S., 2001. Correlation based fluidelastic analysis of tube arrays in two-phase flow. *JSME International Journal, Series B* 44, pp. 213-220.
- Nakamura, T., Hirota, K., Watanabe, Y., Mureithi, N. W., Kusakabe, T. and Takamatsu, H., 2002. Dynamics of an in-line tube array subjected to steam-water cross-flow. Part I: two-phase damping and added mass. *J. Fluids Struct.* 16, pp. 123-136.
- Noghrehkar, G.R., Kawaji, M., Chan, A.M.C., 1999. Investigation of two-phase flow regimes in tube bundles under cross-flow conditions. *Int. J. Multiphase Flow* 25, pp. 857-874.
- Paidoussis, M.P., 1982. A review of flow induced vibrations in reactors and reactor components. *Nuclear Eng. Des.* 74, pp. 36-40.
- Paidoussis, M. P., 1998. Fluid-structure interactions, slender structures and axial flow, London (U.K): Academic Press.
- Papp, L. and Chen, S.S., 1994. Turbulence-induced vibration of tube arrays in two-phase flow. *ASME J. Pres. Ves. Technol.* 116, pp. 312-316.
- Pettigrew, M.J., Gorman, D.J., 1973. Experimental studies on flow-induced vibration to support steam generator design. Part III. Proceedings of the International Symposium on Vib. Prob. in Industry, AECL-5804.
- Pettigrew, M.J., Tromp, J.H. and Mastorakos, J., 1985. Vibration of tube bundles subjected to two-phase cross-flow. *ASME J. Pres. Ves. Technol.* 107, pp. 335-343.
- Pettigrew, M.J., Taylor, C.E. and Kim, B.S., 1989a. Vibration of tube bundles in two-phase cross-flow. Part 1. Hydrodynamic mass and damping. *ASME J. Pres. Ves. Technol.* 111, pp. 466-477.
- Pettigrew, M.J., Tromp, J.H., Taylor, C.E. and Kim, B.S., 1989b. Vibration of tube bundles in two-phase cross-flow. Part 2. Fluid-elastic instability. *ASME J. Pres. Ves. Technol.* 111, pp. 478-487.

- Pettigrew, M.J., Carlucci, L.N., Taylor, C.E. and Fisher, N.J., 1991. Flow induced vibration and related technologies in nuclear components. *Nuclear Eng. Des.* 131, pp. 81-100.
- Pettigrew, M.J. and Taylor, C.E., 1994. Two-phase flow induced vibrations: an overview (survey paper). *ASME J. Pres. Ves. Technol.* 116, pp. 233-253.
- Pettigrew, M.J., Taylor, C.E., Jong, J.H. and Currie, I.G., 1995. Vibration of tube bundles in two-phase Freon cross-flow. *ASME J. Pres. Ves. Technol.* 117, pp. 321-329.
- Pettigrew, M.J., Taylor, C.E., Fisher, N.J., Yetisir, M., and Smith, B.A.W., 1998. Flow-induced vibration: Recent findings and open questions. *Nuclear Eng. Des.* 185, pp. 249-276.
- Pettigrew, M.J., Taylor, C.E. and Kim, B.S., 2001. The effects of bundle geometry on heat exchanger tube vibration in two-phase cross-flow. *ASME J. Pres. Ves. Technol.* 123, pp. 414-420.
- Pettigrew, M.J., Taylor, C.E., Janzen, V. P., and Whan, T., 2002. Vibration behavior of rotated triangular tube bundles in two-phase cross-flow. *ASME J. Pres. Ves. Technol.* 124, pp. 144-153.
- Pettigrew, M.J. and Taylor, C.E., 2003a. Vibrations analysis of shell-and-tube heat exchangers: an overview-Part1: flow, damping, fluidelastic instability. *J. Fluids Struct.* 18, pp. 469-483.
- Pettigrew, M.J. and Taylor, C.E., 2003b. Vibrations analysis of shell-and-tube heat exchangers: an overview-Part2: vibration response, fretting-wear, guidelines. *J. Fluids Struct.* 18, pp. 485-500.
- Pettigrew, M. J., Zhang, C., Mureithi, M. W., and Pamfil, D., 2005. Detailed flow and force measurements in a rotated triangular tube bundle subjected to two-phase cross-flow. *J. Fluids Struct.* 20, pp. 567-575.
- Remy, R.M., 1982. Flow induced vibration of tube bundles in two-phase cross-flow. Paper 1.9, Proceedings of the 3rd International Conference on Vibration in Nuclear Plant, Keswick, U.K., pp. 135-160.

- Riverin, J.L., de Langre, E., and Pettigrew, M.J., 2006. Fluctuating forces caused by internal two-phase flow on bends and tees. *Journal of Sound and Vibration*, 298, pp. 1088-1098.
- Riverin, J.L. and Pettigrew, M.J., 2007. Vibration excitation forces due to two-phase flow in piping elements. *ASME J. Pres. Ves. Technol.* 129, pp. 7-13.
- Rockwell, D., 1983. Oscillation of impinging shear layers. *AIAA Journal*, 21, pp. 645-664.
- Schrage, D., 1988. Two-phase pressure drop in vertical cross-flow across horizontal tube bundle. *AIChE J.* 341, pp. 107-115.
- Serizawa, A., Kataoka, I., and Michiyoshi, I., 1975. Turbulence structure of air-water bubbly flow: 1. Measuring techniques. *Int. J. Multiphase Flow* 2, pp. 221-233.
- Smith, S., 1968. Void fractions in two-phase flow: a correlation based upon an equal velocity head model. Proc. Inst. Mech. Eng. Standards of Tubular Exchanger Manufacturers Association Inc. (TEMA) Sec. 6 8th ed. Flow Induced Vibration Program (FIV).
- Taitel, Y., Barnea, D. and Dukler, A., 1980. Modeling flow pattern transition for steady upward gas-liquid flow in vertical tubes. *AIChE J.* 26, pp. 345-354.
- Tay, B.L., Thorpe, R.B., 2004. Effect of liquid physical properties on the forces acting on a pipe bend in gas-liquid slug flow. *Chemical Engineering Research and Design*, 82, pp. 344-356.
- Tay, B.L., Thorpe, R.B., 2002. Forces on a pipe bend due to slug flow. Proceeding of the Third North American Multiphase Technology Conference, Banff, pp. 281-300.
- Taylor, C.E., Currie, I.G., Pettigrew, M.J. and Kim, B.S., 1989. Vibration of tube bundles in two-phase cross-flow. Part 3. Turbulent induced excitation. *ASME J. Pres. Ves. Technol.* 111, pp. 488-500.
- Taylor, C.E., 1994. Random excitation forces in tube arrays subjected to water and air-water cross-flow. Thesis of doctor of philosophy, Mechanical Engineering, University of Toronto.

- Taylor, C. E., Pettigrew, M. J., and Currie, I. G., 1996. Random excitation forces in tube bundles subjected to two-phase cross-flow. *ASME J. Pressure Vessel Technol.* 118, pp. 265-277.
- Taylor, C., and Pettigrew, M. J., 2000. Random excitation forces in heat exchanger tube bundles. *ASME J. Pres. Ves. Technol.* 122, pp. 509-514.
- Taylor, C.E., and Pettigrew, M.J., 2001. Effect of flow-regime and void fraction on tube bundles vibration. *ASME J. Pressure Vessel Technol.* 123, pp. 407-413
- Teysseidou, A., Lortie, M., and Tapucu, A., 1988. Impedance probe to measure local void fractions profiles. *Rev. Sci. Instrum.* 59, pp. 631-638.
- Teysseidou, A., Aube, F., and Champagne, P., 1992. Void fraction measurement system for high temperature flows. *Meas. Sci. Technol.* 3, pp.485-494.
- Ulbrich, R. and Mewes, D., 1994. Vertical, upward gas liquid two-phase flow across a tube bundle. *Int. J. Multiphase Flow* 20, pp. 249-272.
- Ulbrich, R., Reinecke, N., Mewes, D., 1997. Recognition of flow pattern for two-phase flow across tube bundle. Proceedings of the Fourth World Conference on Experimental Heat Transfer, Fluid Mechanics and Thermodynamics, Brussels, June 2-6.
- Violette, R., Pettigrew, M.J., and Mureithi, N.W., Fluidelastic instability of an array of tubes preferentially flexible in the flow direction subjected to two-phase cross flow. *ASME J. Pres. Ves. Technol.* 128, pp. 148-159.
- Weaver, D. S. and Fitzpatrick, J.A., 1988. A review of cross-flow induced vibrations in heat exchanger tube arrays. *J. Fluids Struct.* 2, pp. 73-93.
- Weaver, D.S., Ziada, S., Au-Yang, M.K., Chen, S.S., Paidoussis, M.P., and Pettigrew, M.J., 2002. Flow-induced vibrations in power and process plant components—progress and prospects. *ASME J. Pres. Ves. Technol.* 122, pp. 339-348.
- Yih, T.S., Griffith, P., 1970. Unsteady momentum fluxes in two-phase flow and the vibration of nuclear system components. Proceeding of the International Conference on Flow-Induced Vibration in Reactor System Components, Argonne Ill., Report ANL-7685, pp. 91-111.

- Zhang, C., Pettigrew, M.J., and Mureithi, N.W., 2006. Correlation between vibration excitation forces and the dynamic characteristics of two-phase flow in a rotated triangular tube bundle. Proceeding, ASME PVP2006-ICPVT-11, 6th FSI, AE & FIV and N Symposium, Paidoussis, M.P., ed., Vancouver, Canada, July 23-27.
- Zhang, C., Pettigrew, M.J., and Mureithi, N.W., 2007. Vibration excitation force measurements in a rotated triangular tube bundle subjected to two-phase cross-flow. *ASME J. Pres. Ves. Technol.* 129, pp. 21-27
- Zhang, C., Pettigrew, M.J., and Mureithi, N.W., 2007. Development of Models Correlating Vibration Excitation Forces to Dynamic Characteristics of Two-Phase Flow in a Tube Bundle. Proceedings, ASME PVP2007/CREEP8, Symposium on Flow-Induced Vibration, N. W. Mureithi, ed., San Antonio, Texas, USA, July 22-26.
- Zhang, C., Pettigrew, M.J., and Mureithi, N.W., 2008. Correlation between vibration excitation forces and the dynamic characteristics of two-phase cross flow in a rotated triangular tube bundle. *ASME J. Pres. Ves. Technol.* 130 (1), (to appear).
- Zuber, N. and Findlay, J., 1965. Average volumetric concentration in two-phase flow systems. *ASME J. Heat Transfer* 87, pp. 453-468.

## APPENDIX

### EXPERIMENTAL CONDITIONS AND DATA

#### A1 Experimental conditions

About 200 flow conditions were tested in the course of this study. One sample flow condition corresponding to homogeneous void fraction  $\alpha=80\%$ , is given here as an example.

**Table A.1** Sample of experimental flow conditions ( $\alpha=80\%$ ) in the narrow test section

$U_p$ (m/s)	1	2	3	4	5	6	7	8	9	10
$Q$ (l/s)	1.25	2.5	3.75	5.0	6.25	7.5	8.75	10	11.25	12.5
$Q_w$	5	10	15	20	25	30	35	40	45	50
$Q_a$ @STP										

The flow meters that were used to measure the volume flow rate of air into the test section were a system with orifice plates connected to a differential pressure transducer and electronic readout system. The readout can directly show the volume air flow at standard conditions. The following calculation was made to correct for the pressure in the test section because the test section was not at standard pressure.

$$Q_m = Q_a \frac{P_t + 14.7}{14.7} \quad (\text{A.1})$$

where,  $Q_a$  is the desired test section flow rate,  $Q_m$  is the flow meter reading, and  $P_t$  is the gauge pressure within the test section.

The test section pressure  $P_t$  was measured with a pressure gauge. It was necessary to perform an iteration process because neither the pressure in the test section nor the flow-

meter reading was known parameters. The pressure in the test section could be estimated from a reasonable approximation of the flow rate. Generally, the initial flow rate was  $Q_a$  @STP.

## A2 Calibration of instrumented cylinders

The lengths of the full-length and half-length tubes,  $L$ , are respectively 190 and 95 mm. Both lengths were measured from the center positions of the gauges to the free ends of tubes.

The equivalent bending moment for distributed loading along the tube,  $q$ , and concentrated loading,  $P$ , at the free end of the tube were analyzed (Fig. A1). The following relationship holds,

$$\frac{1}{2}qL^2 = PL \quad \text{or} \quad q = \frac{P}{2L} \quad (\text{A2})$$

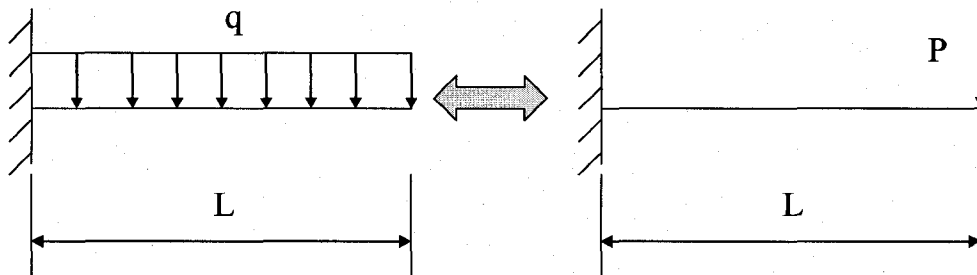


Fig. A.1 Sketch of equivalent loading analysis

During the calibration, a  $1000 \mu\epsilon$  strain input, corresponding to 400 mV voltmeter output for the strain gauge indicator, was applied. Weights of 250, 500, 750 and 1000 grams hanging at the free end of the tube were used as concentrated loads to produce the reference calibration strains. Finally the relationship between the distributed loads and the voltage reading was determined. The ratio of the voltage reading over the



corresponding distributed loads is the sensitivity. The sensitivity was used to set the OROS analysis system. Tables A2 and A3 show the sensitivities for all the instrumented cylinders within the narrow and wider test sections used in this study, respectively.

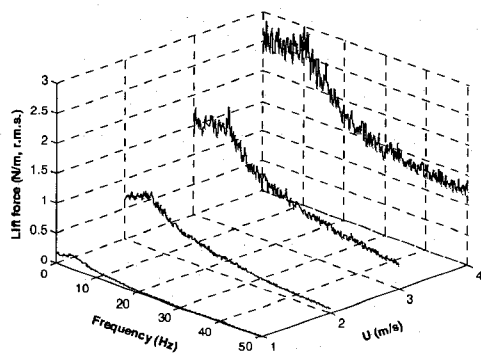
**Table A.2** Sensitivities (mV/(N/m)) for instrumented cylinders within the narrow test section

Tube Position	Tube 1	Tube 2	Tube 3	Tube 4(Half-L)	Tube 5(Half-R)
Left and Right (Lift)	3.359	3.320	3.417	0.864	0.820
Up and Down (Drag)	3.34	3.447	3.456	0.806	0.825

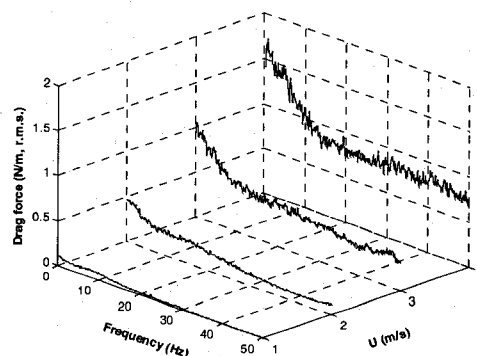
**Table A.3** Sensitivities (mV/(N/m)) for instrumented cylinders within the wider test section

Tube Position	Tube 1	Tube 2	Tube 3	Tube 4	Tube 5	Tube 6
Left and Right (Lift)	3.605	3.677	3.737	3.794	3.831	3.635
Up and Down (Drag)	3.667	3.784	3.837	3.898	3.897	3.716

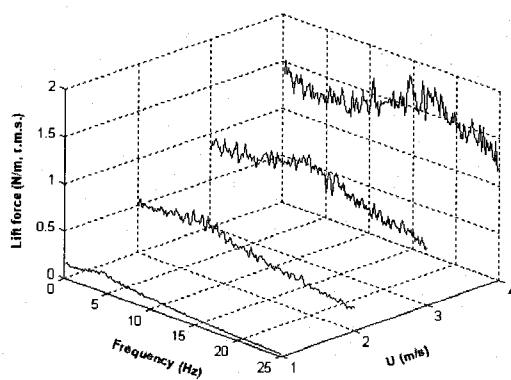
### A3 Summary of results related to Chapter 3



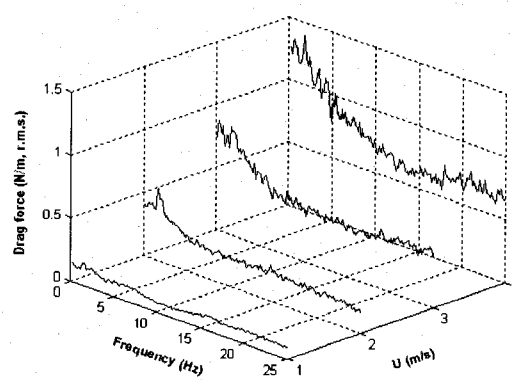
(a) Lift



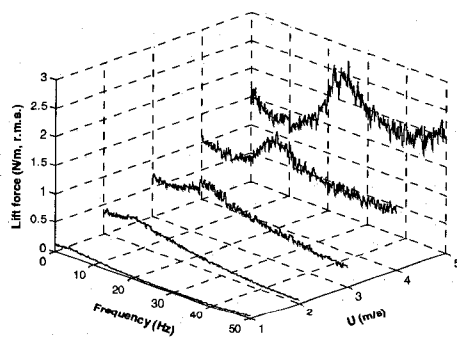
(b) Drag



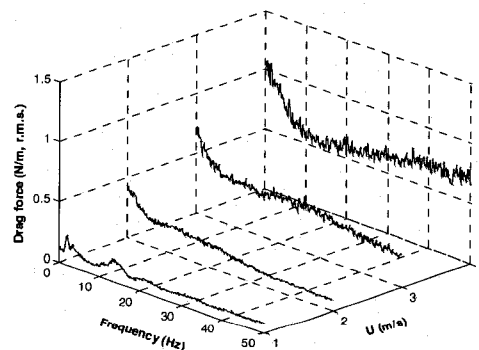
(c) Lift



(d) Drag

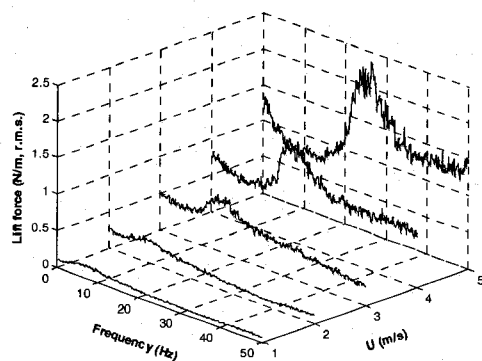


(e) Lift

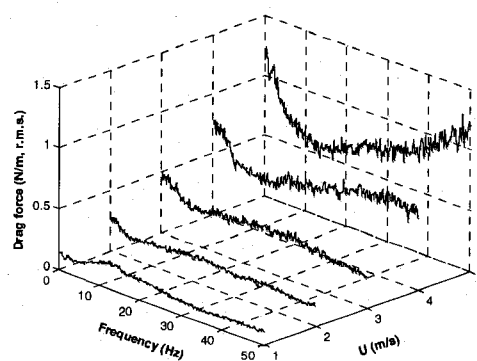


(f) Drag

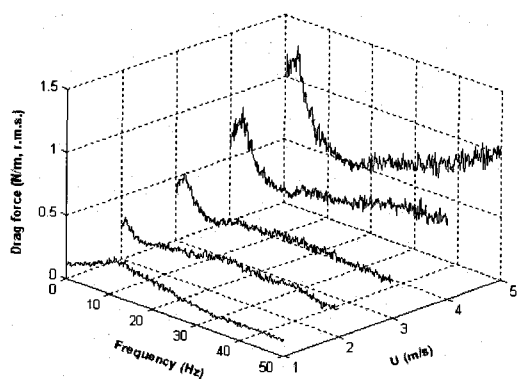
Fig. A.2 Dynamic force spectra: (a), (b) for  $\alpha=0\%$ , (c), (d) for  $\alpha=5\%$ , and (e), (f) for  $\alpha=10\%$



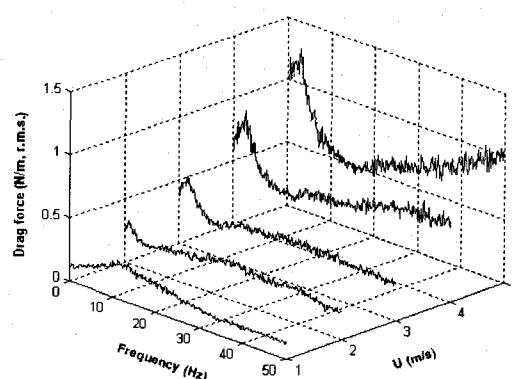
(g) Lift



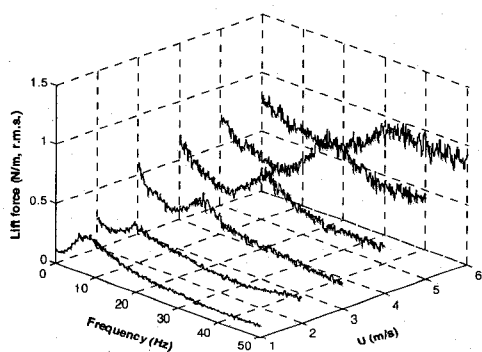
(h) Drag



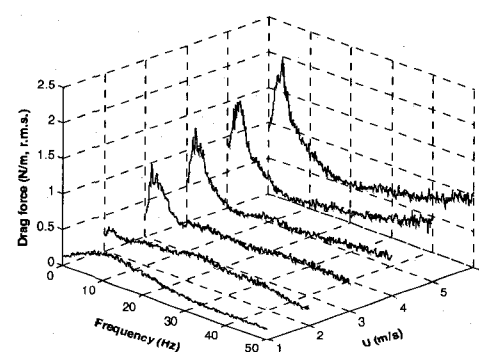
(i) Lift



(j) Drag

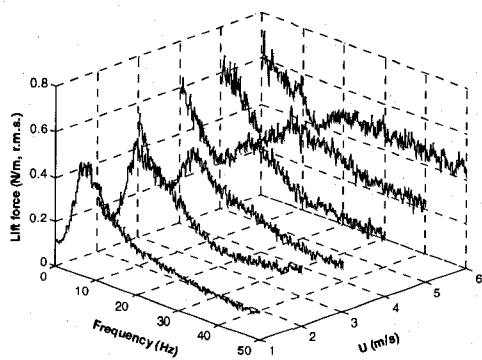


(k) Lift

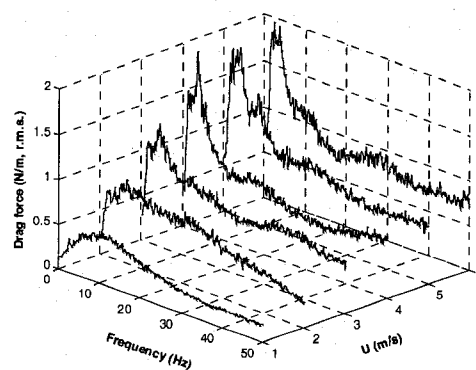


(l) Drag

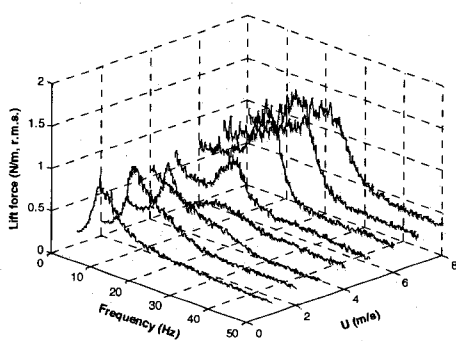
Fig. A.2 continued (g), (h) for  $\alpha=20\%$ , (i), (j) for  $\alpha=25\%$ , and (k), (l) for  $\alpha=30\%$



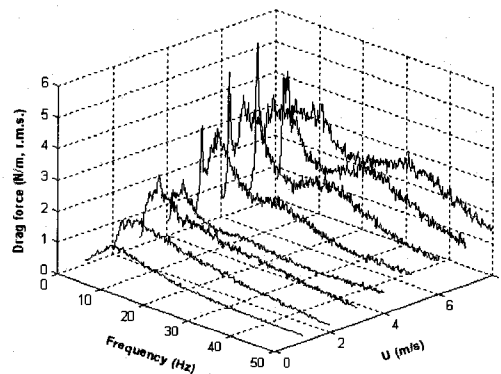
(m) Lift



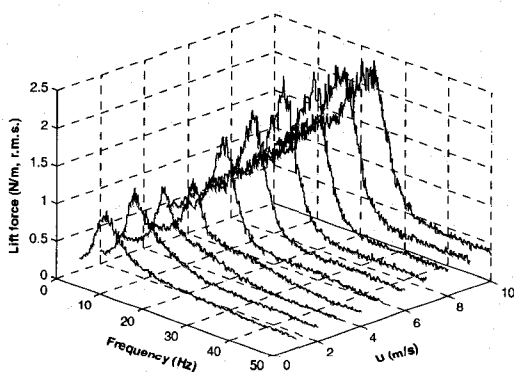
(n) Drag



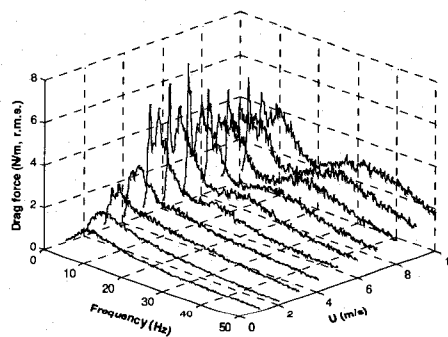
(o) Lift



(p) Drag

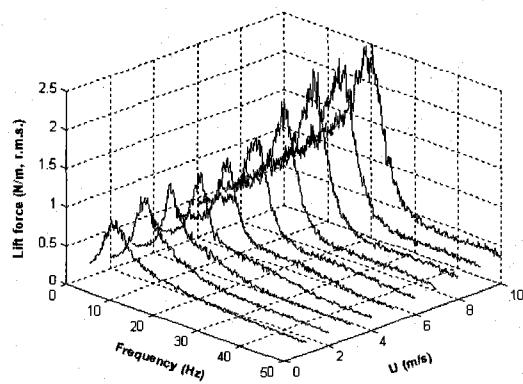


(q) Lift

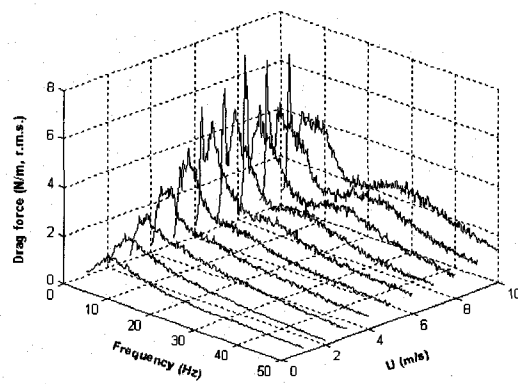


(r) Drag

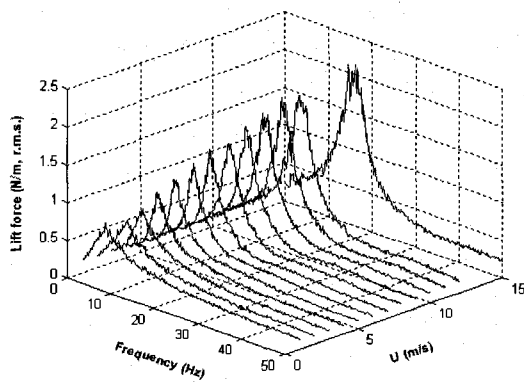
Fig. A.2 continued (m), (n) for  $\alpha=40\%$ , (o), (p) for  $\alpha=60\%$ , and (q), (r) for  $\alpha=70\%$



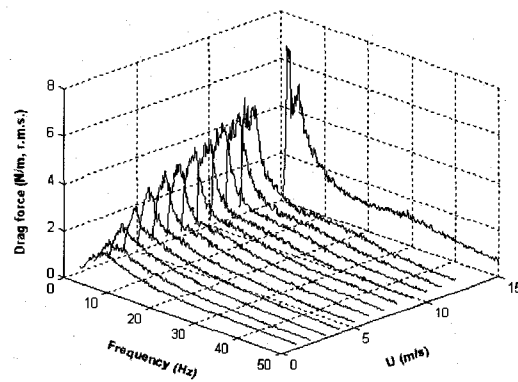
(s) Lift



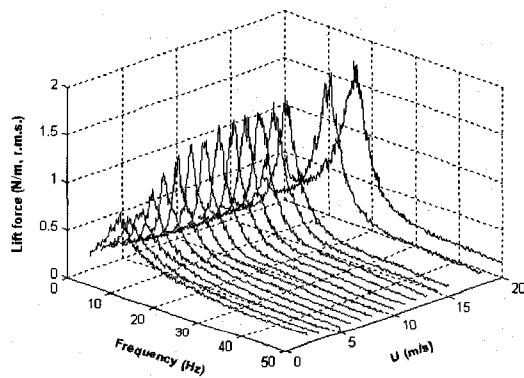
(t) Drag



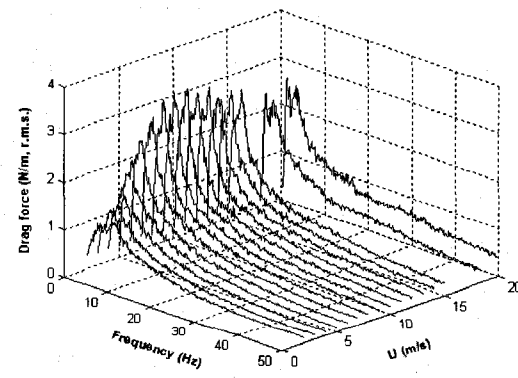
(u) Lift



(v) Drag



(w) Lift



(x) Drag

**Fig. A.2 continued** (s), (t) for  $\alpha=75\%$ , (u), (v) for  $\alpha=90\%$ , and (w), (x) for  $\alpha=95\%$

Table A.4 Summary of results related to Chapter 3

 $\alpha=0\%$ 

$U_p$ (m/s)	Drag direction			Lift direction		
	Periodic force (N/m) & frequency (Hz)	Static force (N/m)	Resonance fre. (Hz)	Periodic force (N/m) & frequency (Hz)	Static force (N/m)	Resonance fre. (Hz)
1	no	16.36	71.3	0.243	5.03	72.3
2	no	43.27	71.1	0.94	5.15	72.3
3	no	86.2	70.9	2.014	6.41	71.6
4	no	150.1	71.9	2.985	7.83	70.4

 $\alpha=5\%$ 

$U_p$ (m/s)	Drag direction			Lift direction		
	Periodic force (N/m) & frequency (Hz)	Static force (N/m)	Resonance fre. (Hz)	Periodic force (N/m) & frequency (Hz)	Static force (N/m)	Resonance fre. (Hz)
1	no	19.12	76.1	0.208	5.24	76.8
2	no	44.43	73.1	0.665	5.36	72.9
3	no	65.3	71.3	1.147	5.1	71.9
4	no	146.5	69.5	1.835	8.39	70

Table A.4 (continued)

 $\alpha=10\%$ 

$U_p$ (m/s)	Drag direction			Lift direction		
	Periodic force (N/m) & frequency (Hz)	Static force (N/m)	Resonance fre. (Hz)	Periodic force (N/m) & frequency (Hz)	Static force (N/m)	Resonance fre. (Hz)
1		9.96	78	0.165	6.34	77
2	no	35.9	70.8	0.507	6.25	72.5
3	no	79.1	69.4	0.971	6.47	73.6
4	no	142.3	65	1.665	7.78	71.3
5	no	236.8	65.4	0.947	11.94	68

 $\alpha=20\%$ 

$U_p$ (m/s)	Drag direction			Lift direction		
	Periodic force (N/m) & frequency (Hz)	Static force (N/m)	Resonance fre. (Hz)	Periodic force (N/m) & frequency (Hz)	Static force (N/m)	Resonance fre. (Hz)
1	no	9.16	83.3	0.172	4.671	79.5
2	no	32.61	88.8	0.354	4.879	80.1
3	no	76	74.4	0.781	7.4	72.6
4	no	134.8	----	1.349	9.99	71.3
5	no	219.6	----	2.362	11.4	70.3

Table A.4 (continued)

 $\alpha=25\%$ 

U <sub>p</sub> (m/s)	Drag direction			Lift direction		
	Periodic force (N/m) & frequency (Hz)	Static force (N/m)	Resonance fre. (Hz)	Periodic force (N/m) & frequency (Hz)	Static force (N/m)	Resonance fre. (Hz)
1	0.284 12.5	10.44	84.1	0.222 9.4	5.01	83.9
2	0.341 0.9	35.86	82.9	0.328 9.1	5.25	84.8
	0.325 26.3					
3	0.555 2	77.2	77.9	0.746 15.8	8.35	84.8
	0.362 30					
4	0.931 2.6	135.3	-----	1.159 20	12.32	77.8
	0.726 43.9					
5	1.275 2.9	213.4	60	1.671 25.9	13.41	71.4

 $\alpha=30\%$ 

U <sub>p</sub> (m/s)	Drag direction			Lift direction		
	Periodic force (N/m) & frequency (Hz)	Static force (N/m)	Resonance fre. (Hz)	Periodic force (N/m) & frequency (Hz)	Static force (N/m)	Resonance fre. (Hz)
1	0.404 11.8	10.78	82.3	0.318 7.4	2.181	85.5
2	0.307 1.6	32.67	93.4	0.338 9.1	2.433	86
3	1.057 1.6	74.3	100	0.544 16	0.639	79.9
	0.942 2.8					
4	1.364 2.3	129.3	61.4	0.696 21	3.393	92.5
5	1.573 2.9	199.1	62.3	0.961 26	4.854	71.5
6	2.003 3.3	290.3	69.5	1.004 34.4	4.545	76.3



Table A.4 (continued)

 $\alpha=40\%$ 

$U_p$ (m/s)	Drag direction				Lift direction				
	Periodic force (N/m) & frequency (Hz)	Static force (N/m)	Resonance fre. (Hz)	Periodic force (N/m) & frequency (Hz)	Static force (N/m)	Resonance fre. (Hz)	Periodic force (N/m) & frequency (Hz)	Static force (N/m)	Resonance fre. (Hz)
1	0.554 11.6	9.4	93.8	0.518 7.9	1.996	100	0.518 7.9	1.996	100
2	0.573 9.6	33.19	100	0.955 6.7	4.207	98.5	0.955 6.7	4.207	98.5
3	1.386 4.6	66.9	107	0.479 14.4	1.467	100	0.479 14.4	1.467	100
4	1.986 3.8	112.2	96	0.514 16.9	1.215	95.6	0.514 16.9	1.215	95.6
5	1.84 1.449 8.5	168.9	----	0.533 17.1	3.193	111.4	0.533 17.1	3.193	111.4
6	1.726 0.928 27	234.4	87.8	no no	3.922	85.9	no no	3.922	85.9

Table A.4 (continued)

 $\alpha=50\%$ 

$U_p$ (m/s)	Drag direction				Lift direction			
	Periodic force (N/m) & frequency (Hz)	Static force (N/m)	Resonance fre. (Hz)	Resonance fre. (Hz)	Periodic force (N/m) & frequency (Hz)	Static force (N/m)	Resonance fre. (Hz)	Resonance fre. (Hz)
1	0.743 10.3	13.63	99	99	0.651 7.1	0.574	100	100
2	1.044 0.868 17.1	28.47	106	106	0.705 9.3	0.303	97	97
3	1.444 5.1	56.1	110	110	0.592 12.3	0.836	105	105
4	2.019 2.406 4.5	94.5	120	120	0.561 15.3	3.431	92	92
5	2.214 2.537 5	139.1	----	----	0.593 16.2	5.64	105	105
6	2.273 2.394 4.3 2.098 10	189.8	85	85	0.624 0.627 2.3 18.8	5.75	122	122
7	2.611 2.489 4.8 2.207 11.4	269.2	100	100	0.714 0.689 2.3 20	8.26	100	100
8	2.666 2.439 5 1.802 12.8 1.541 30.4	325.7	110	110	0.651 0.545 2.4 21.1	6.11	104	104

Table A.4 (continued)

 $\alpha=60\%$ 

$U_p$ (m/s)	Drag direction			Lift direction		
	Periodic force (N/m) & frequency (Hz)	Static force (N/m)	Resonance fre. (Hz)	Periodic force (N/m) & frequency (Hz)	Static force (N/m)	Resonance fre. (Hz)
1	0.97 8.5	6.36	107.9	0.931 6	2.257	102
2	1.482 6.8	23.84	121.9	0.969 8.6	3.706	108.4
3	2.462 4.5	43.54	124.6	0.952 10.9	3.262	113.9
4	3.111 4.3	73.5	129.3	0.842 13.3	2.098	119.4
5	3.287 1.8	110	126.8	0.855 14.9	1.063	110.9
	3.373 5.4					
	1.938 19.4					
6	4.696 1.8	172.1	108.3	1.502 17.1	1.576	128.9
	3.87 5					
	2.602 23.9					
7	5.33 1.9	226.9	117.1	1.533 18.4	4.953	140.9
	3.861 5.6					
	2.745 26.6					
8	3.93 1.8	288.9	120	1.328 21.1	9.55	126
	4.177 2.8					
	2.928 30.6					

Table A.4 (continued)

$\alpha = 70\%$

$U_p$ (m/s)	Drag direction				Lift direction				
	Periodic force (N/m) & frequency (Hz)	Static force (N/m)	Resonance fre. (Hz)	Periodic force (N/m) & frequency (Hz)	Static force (N/m)	Resonance fre. (Hz)	Periodic force (N/m) & frequency (Hz)	Static force (N/m)	Resonance fre. (Hz)
1	1.008 7.6	5.17	112.5	0.933 6.4	2.555	103.9			
2	1.483 6.4	14.34	114.8	1.334 7.8	3.936	121			
3	2.399 4	30.13	122	1.124 9.8	3.441	129.6			
4	2.968 4	51.5	130.4	1.152 11.1	2.807	131.6			
5	5.39 5.37 1.8 4.1	94.7	143.4	1.667 13.9	1.462	132.1			
6	6.07 5.16 1.9 4.7	129.2	136.9	1.947 14.8	0.389	133.5			
7	6.64 5.03 1.6 4.9	170.2	137.4	2.336 17	1.475	140			
8	5.12 1.6	214	131.7	2.334 18.9	3.312	139.2			
9	4.821 1.9	267.9	132.4	2.327 19	5.36	138.8			
10	5.04 2	333.4	125.6	2.374 22.8	8.55	139.3			

Table A.4 (continued)

$\alpha=75\%$

U <sub>p</sub> (m/s)	Drag direction				Lift direction				
	Periodic force (N/m) & frequency (Hz)	Static force (N/m)	Resonance fre. (Hz)	Periodic force (N/m) & frequency (Hz)	Static force (N/m)	Resonance fre. (Hz)	Periodic force (N/m) & frequency (Hz)	Static force (N/m)	Resonance fre. (Hz)
1	1.185 6.4	3.636	116.4	0.854 6.3	2.715	104.3			
2	1.496 5.7	14.48	123	1.254 7.4	3.222	117.4			
3	1.803 4.8	25.92	129.6	1.084 9	2.616	124.5			
4	2.948 3.6	42.88	136.3	1.25 10.5	2.244	133.8			
5	4.177 3.6	63.1	140.3	1.363 11.9	1.952	134.5			
6	5.48 4.125 4.1	92.2	138.9	1.532 13.5	0.849	142			
7	5.91 5.2 4.4	122.7	130.4	1.966 15	0.373	140.4			
8	5.58 5.09 5.1	163.4	-----	2.317 16.7	1.607	139.1			
9	5.56 4.891 4.8	199.8	133	2.372 17.5	2.992	141.6			
10	6.34 3.853 7.5	243.9	136.3	2.454 18.9	4.633	142.8			



Table A.4 (continued)

$\alpha=90\%$

$U_p$ (m/s)	Drag direction				Lift direction				
	Periodic force (N/m) & frequency (Hz)	Static force (N/m)	Resonance fre. (Hz)	Periodic force (N/m) & frequency (Hz)	Static force (N/m)	Resonance fre. (Hz)	Periodic force (N/m) & frequency (Hz)	Static force (N/m)	Resonance fre. (Hz)
1	1.309	6.5	10.03	118	0.78	5.3	0.182	113	
2	1.293	5.4	10.35	130	0.768	7.1	0.183	130	
3	1.603	3.8	12.98	136	0.849	7.1	0.174	136	
4	2.226	3	17.77	139	0.941	7.4	0.152	139	
5	2.507	2.9	24.83	145	1.13	8.3	0.134	145	
6	3.174	3.1	30.38	147	1.293	9	3.349	147	
7	3.442	3.1	40.13	148	1.417	9.4	3.162	148	
8	3.64	3	53.5	147	1.424	10.5	2.842	149	
9	3.785	2.9	63.9	150	1.564	11.1	2.57	150	
10	4.56	3	79.9	150	1.694	11.9	2.096	150	
11	4.375	3.1	100.1	150	1.898	12.5	1.33	150	
12	4.194	2.9	113.2	150	1.872	13.3	1.073	150	
15	6.1	1.6	200.9	150	2.032	15.4	2.584	150	
18	12.51	1.6	291	150	2.268	17.3	5.02	150	
20	13.76	1.8	337.3	150	1.125	1.8	6.85	150	
	4.122	4.3			2.459	18.6			

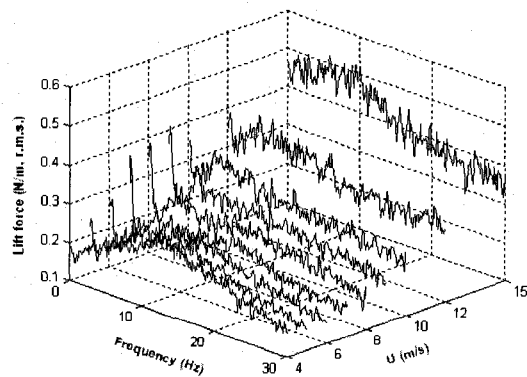
Table A.4 (continued)

 $\alpha=95\%$ 

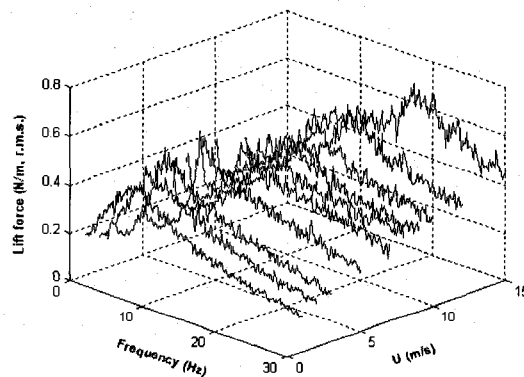
$U_p$ (m/s)	Drag direction			Lift direction		
	Periodic force (N/m) & frequency (Hz)	Static force (N/m)	Resonance fre. (Hz)	Periodic force (N/m) & frequency (Hz)	Static force (N/m)	Resonance fre. (Hz)
2	1.19 5.5	11.36	132	0.678 6.9	1.001	132
3	1.143 5.1	11.12	137.5	0.594 7	0.949	140
4	1.664 3.3	6.24	140	1.144 6.6	3.47	142
5	2.024 2.8	9.05	144	0.839 7	3.378	146
6	2.441 2.6	11.54	146	0.962 7	3.283	148
7	2.772 2.5	16.5	149	1.003 7.6	3.226	150
8	3.009 2.6	20.89	150	1.207 8.4	3.147	150
9	3.228 2.8	26.18	151	1.195 9	3.079	151
10	3.152 2.8	32.88	151	1.349 9.8	2.974	152
11	2.86 2.9	40.19	151	1.383 10.6	2.818	152.3
12	2.851 2.9	46.84	151	1.223 11	2.725	153
13	2.79 2.9	56.8	152	1.353 11.6	2.637	153.8
14	2.327 2.9	65.3	152	1.466 12.3	2.573	153
15	2.553 3	72.8	151	1.451 12.8	2.736	152
18	2.425 3.1	126.8	151	1.479 14.8	0.397	154
20	2.602 2.9	154.6	151	1.728 15.9	0.452	154



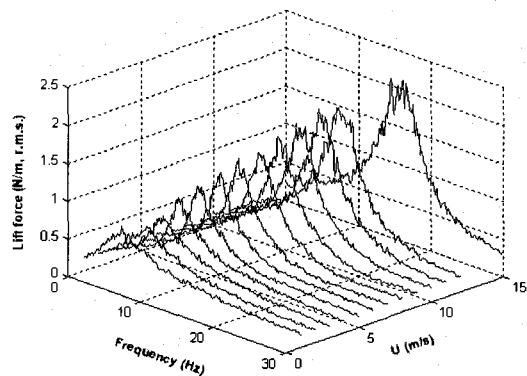
### A4 Additional results related to Chapter 4



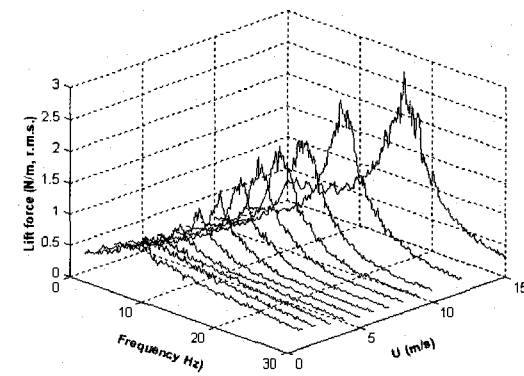
(a) Single cylinder



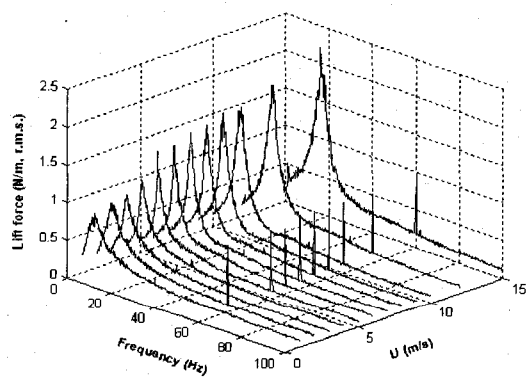
(b) Upstream cylinder



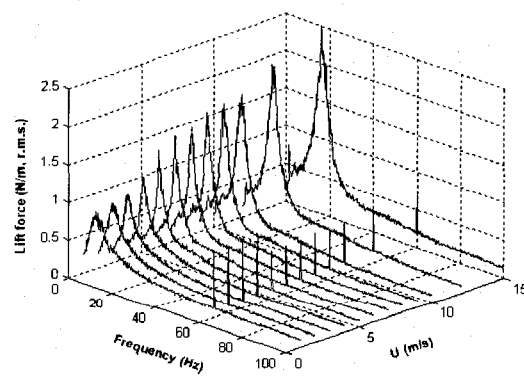
(c) Interior cylinder



(d) Downstream cylinder

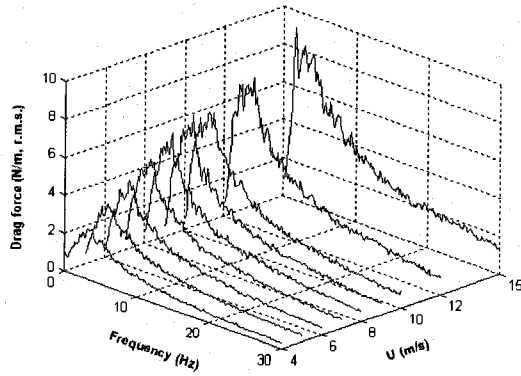


(e) Left interior half-length cylinder

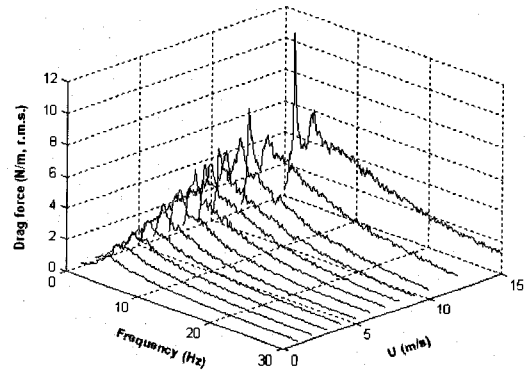


(f) Right interior half-length cylinder

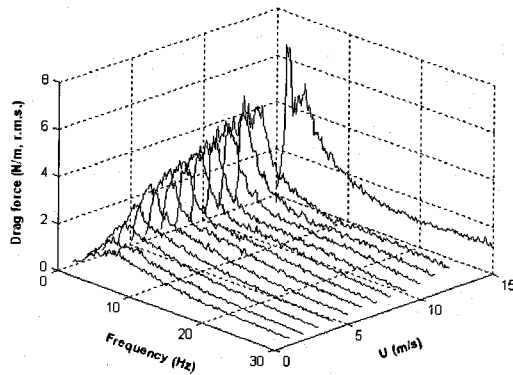
**Fig. A.3** Dynamic lift force spectra at 90% void fraction



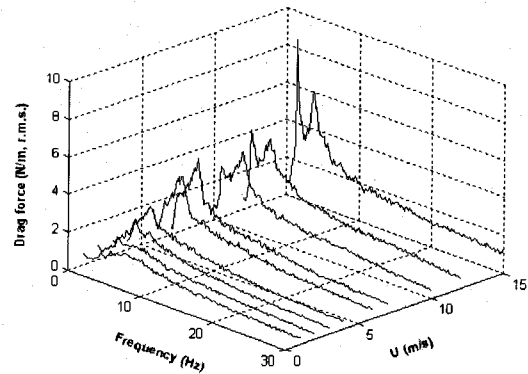
(a) Single cylinder



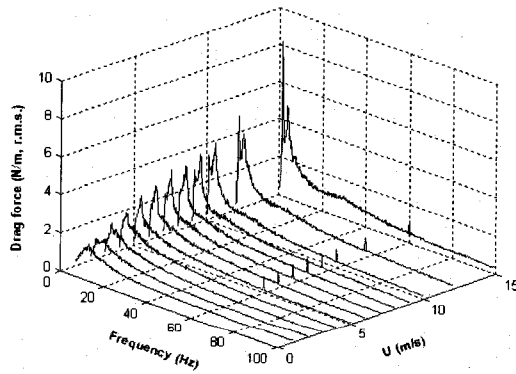
(b) Upstream cylinder



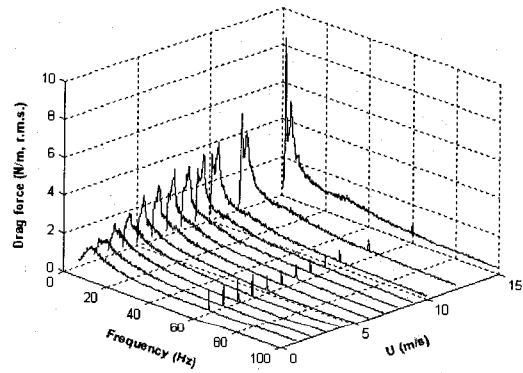
(c) Interior cylinder



(d) Downstream cylinder



(e) Left interior half-length cylinder



(f) Right interior half-length cylinder

**Fig. A.4** Dynamic drag force spectra at 90% void fraction

### A5 Additional results related to Chapter 5

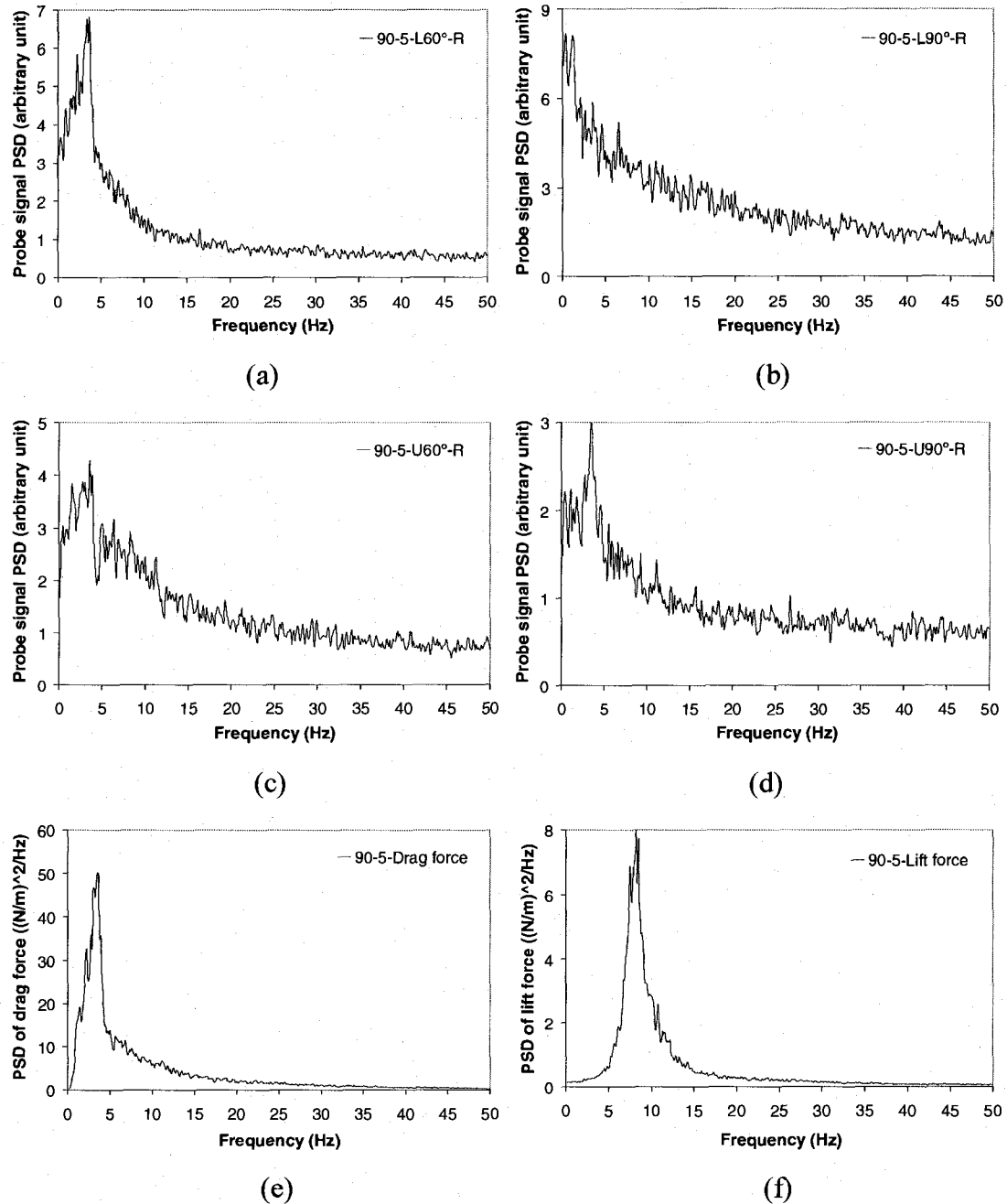


**Fig. A.5** Power spectra of the local void fraction fluctuation at four different positions on the right side of the main flow path for 90% void fraction at 5 m/s pitch flow velocity: (a) L60° position, (b) L90° position, (c) U60° position, and (d) U90° position; and dynamic force spectra: (e) Drag and (f) Lift

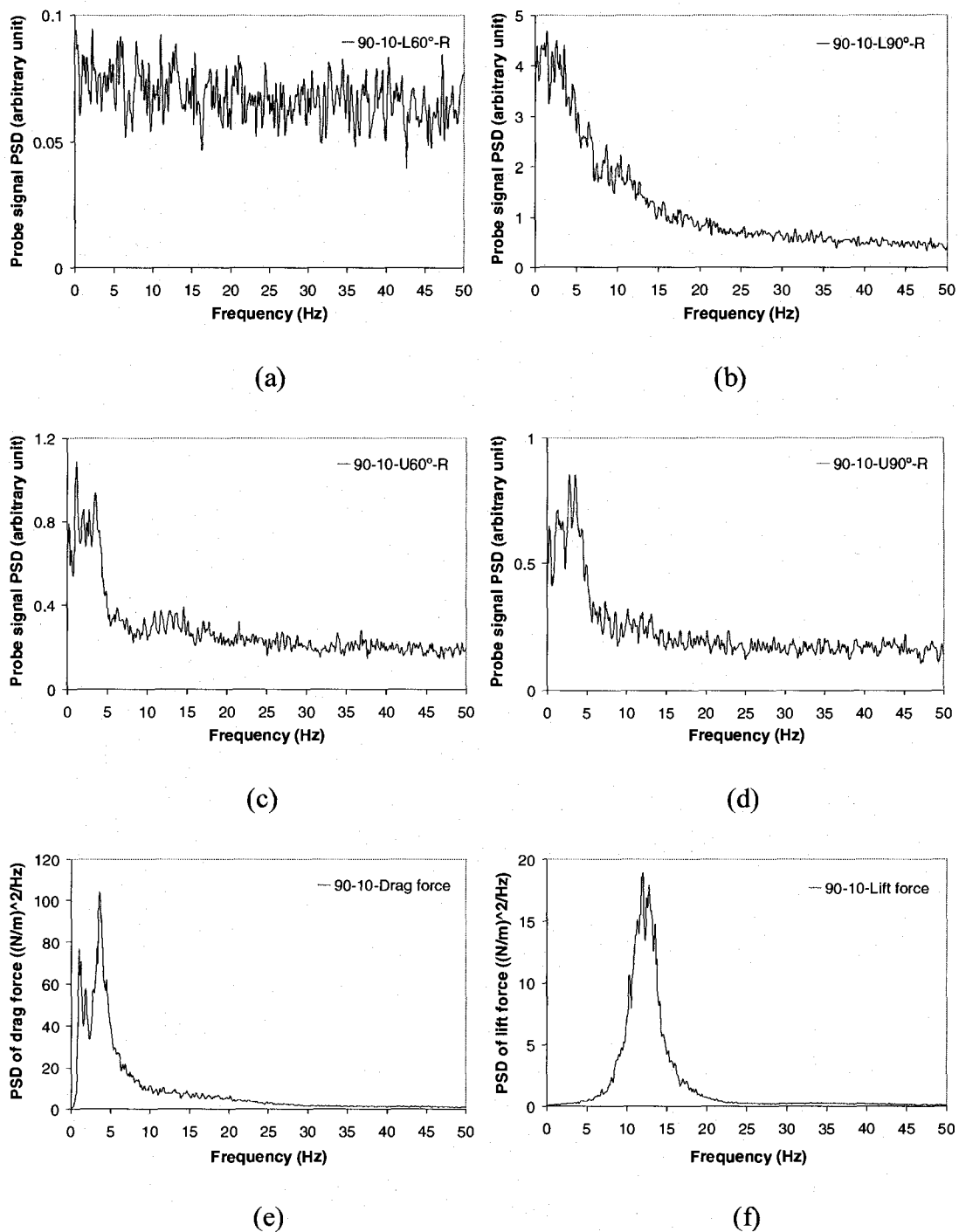


**Fig. A.6** Power spectra of the local void fraction fluctuation at four different positions on the right side of the main flow path for 90% void fraction at 10 m/s pitch flow velocity: (a) L60° position, (b) L90° position, (c) U60° position, and (d) U90° position; and dynamic force spectra: (e) Drag and (f) Lift

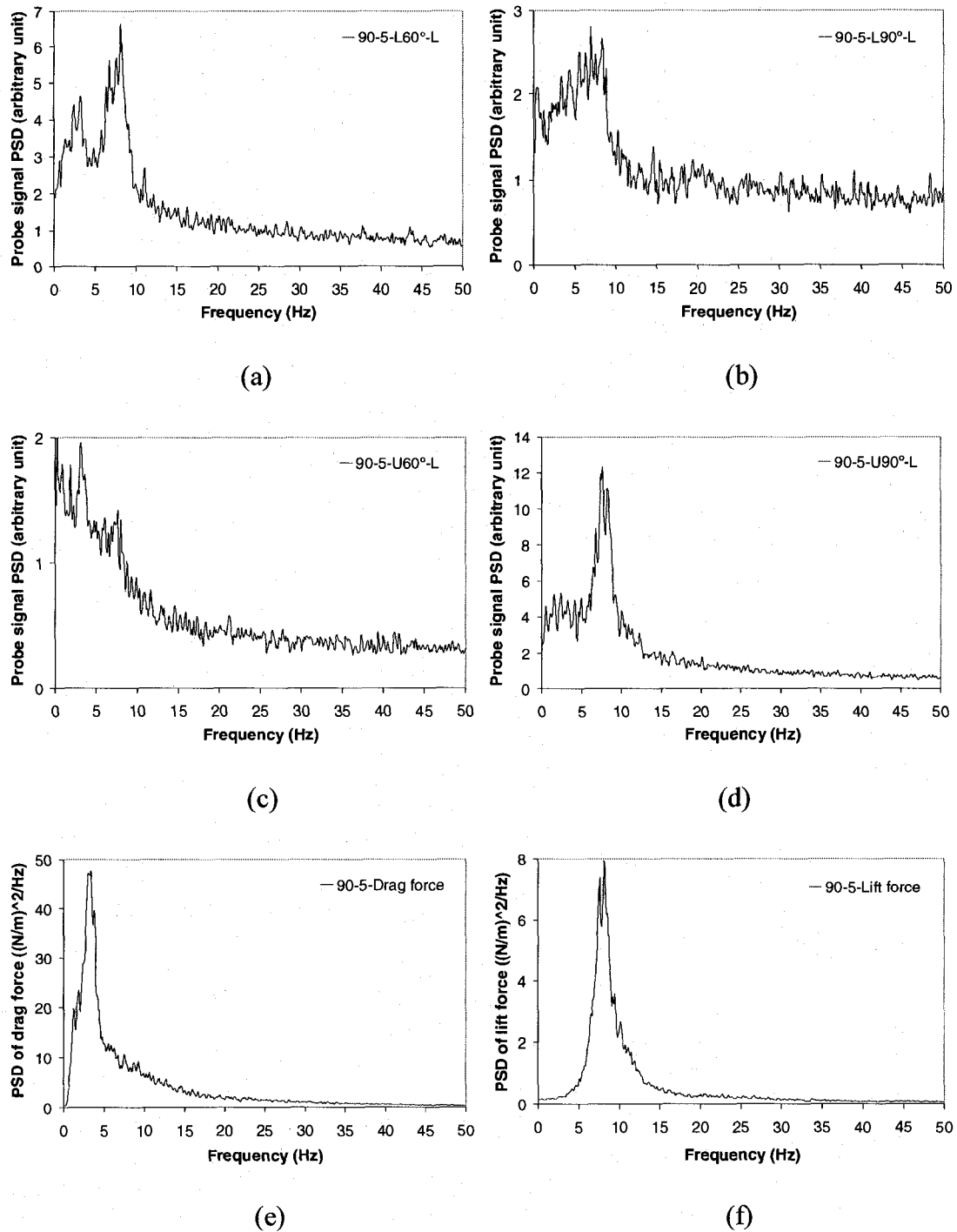


**Fig. A.7** Power spectra of the local void fraction fluctuation at four different positions on the left side of the main flow path for 90% void fraction at 5 m/s pitch flow velocity: (a) L60° position, (b) L90° position, (c) U60° position, and (d) U90° position; and dynamic force spectra: (e) Drag and (f) Lift

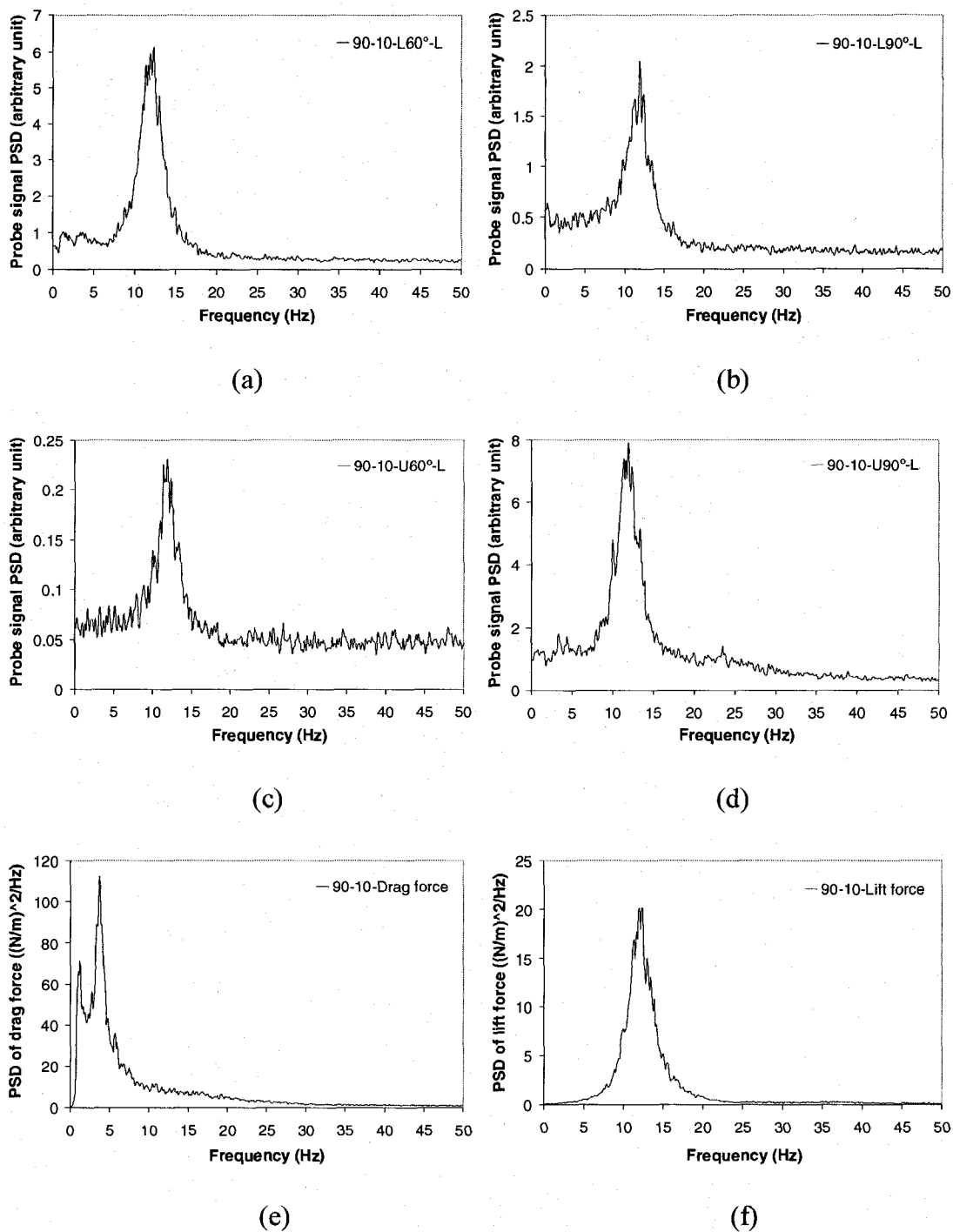


**Fig. A.8** Power spectra of the local void fraction fluctuation at four different positions on the left side of the main flow path for 90% void fraction at 10 m/s pitch flow velocity: (a) L60° position, (b) L90° position, (c) U60° position, and (d) U90° position; and dynamic force spectra: (e) Drag and (f) Lift

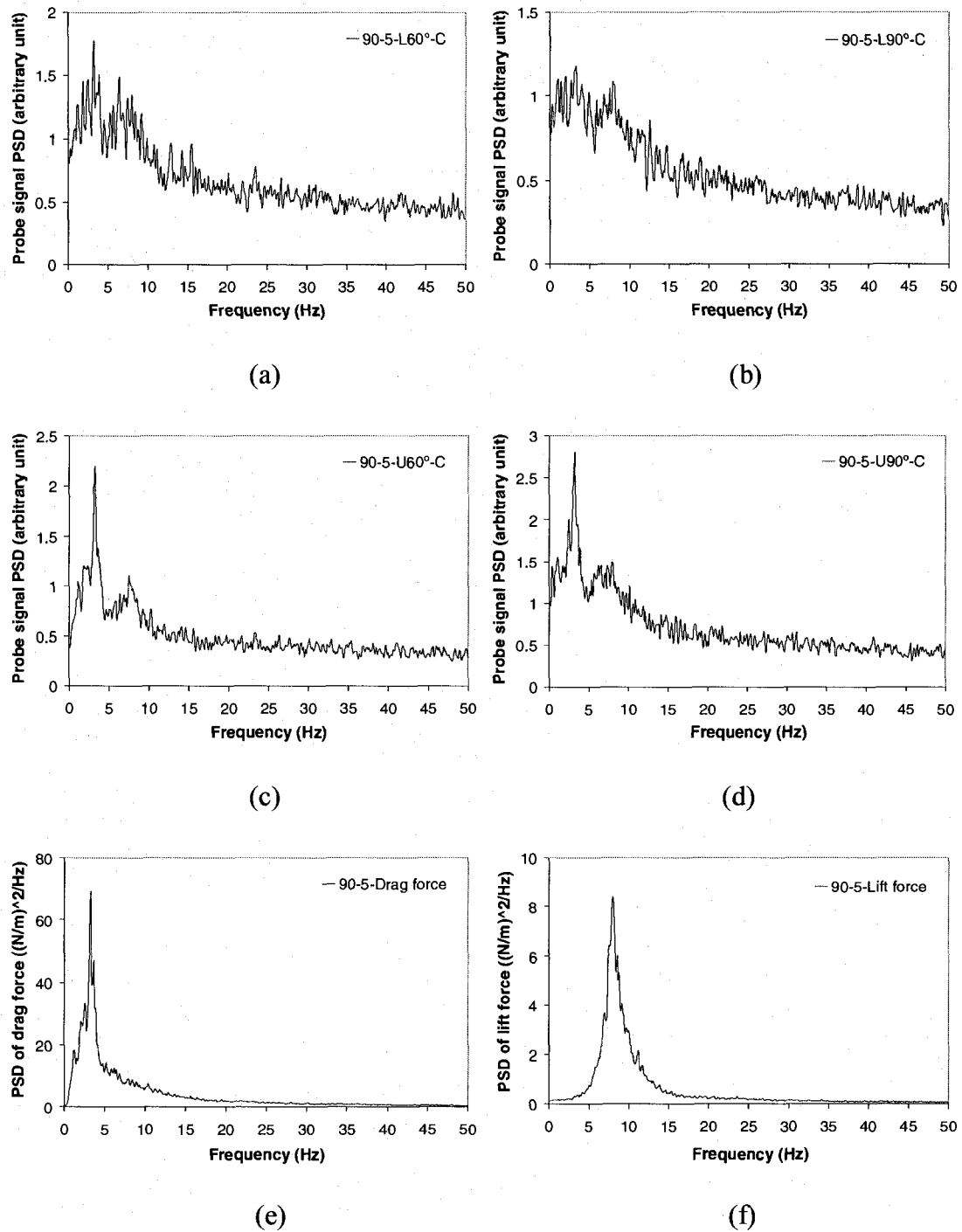


**Fig. A.9** Power spectra of the local void fraction fluctuation at four different positions along the center line of the main flow path for 90% void fraction at 5 m/s pitch flow velocity: (a) L60° position, (b) L90° position, (c) U60° position, and (d) U90° position; and dynamic force spectra: (e) Drag and (f) Lift

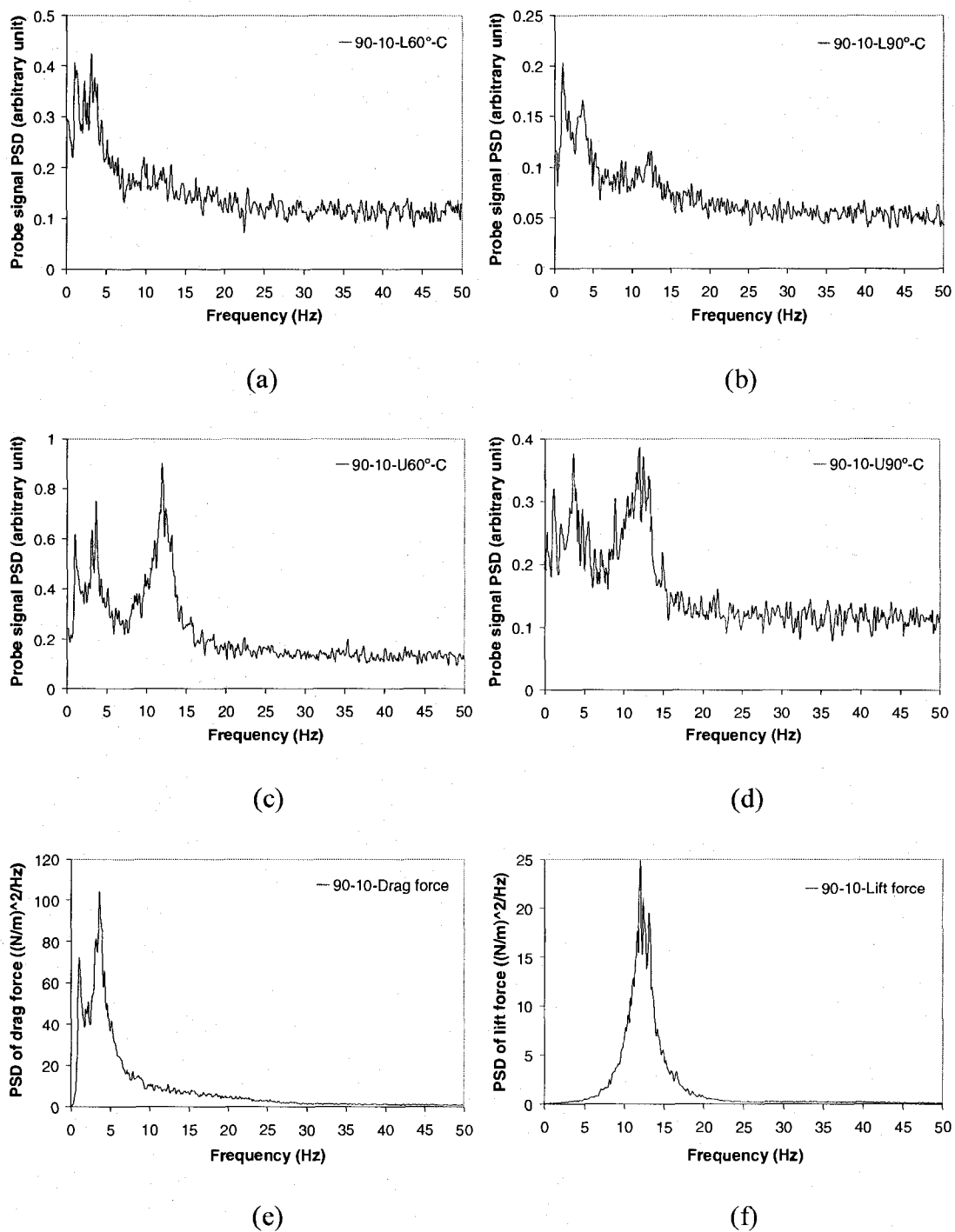


**Fig. A.10** Power spectra of the local void fraction fluctuation at four different positions along the center line of the main flow path for 90% void fraction at 10 m/s pitch flow velocity: (a) L60° position, (b) L90° position, (c) U60° position, and (d) U90° position; and dynamic force spectra: (e) Drag and (f) Lift



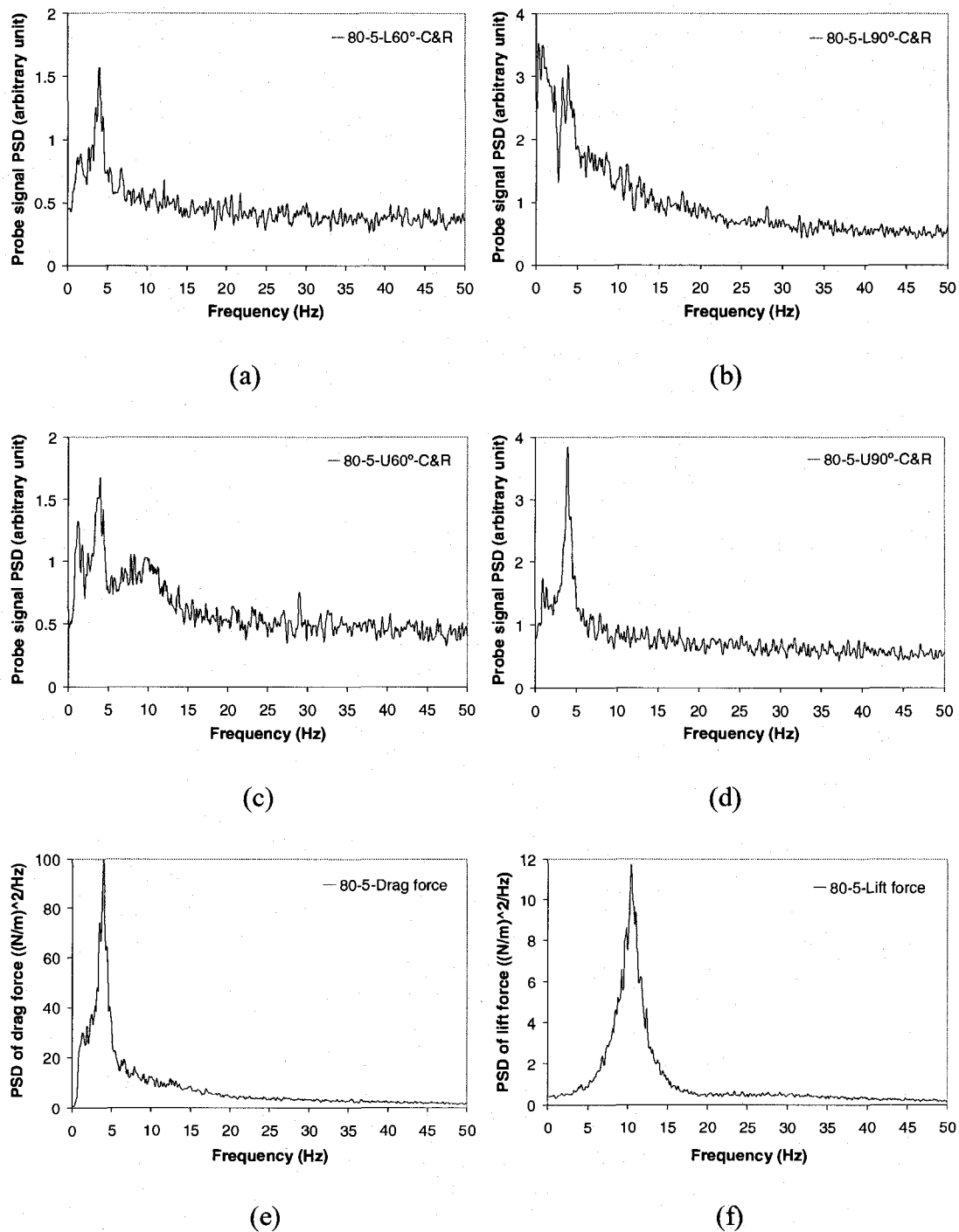


**Fig. A.11** Power spectra of the local void fraction fluctuation at four different positions along a line between the center line and right side of the main flow path for 80% void fraction at 5 m/s pitch flow velocity: (a) L60° position, (b) L90° position, (c) U60° position, and (d) U90° position; and dynamic force spectra: (e) Drag and (f) Lift

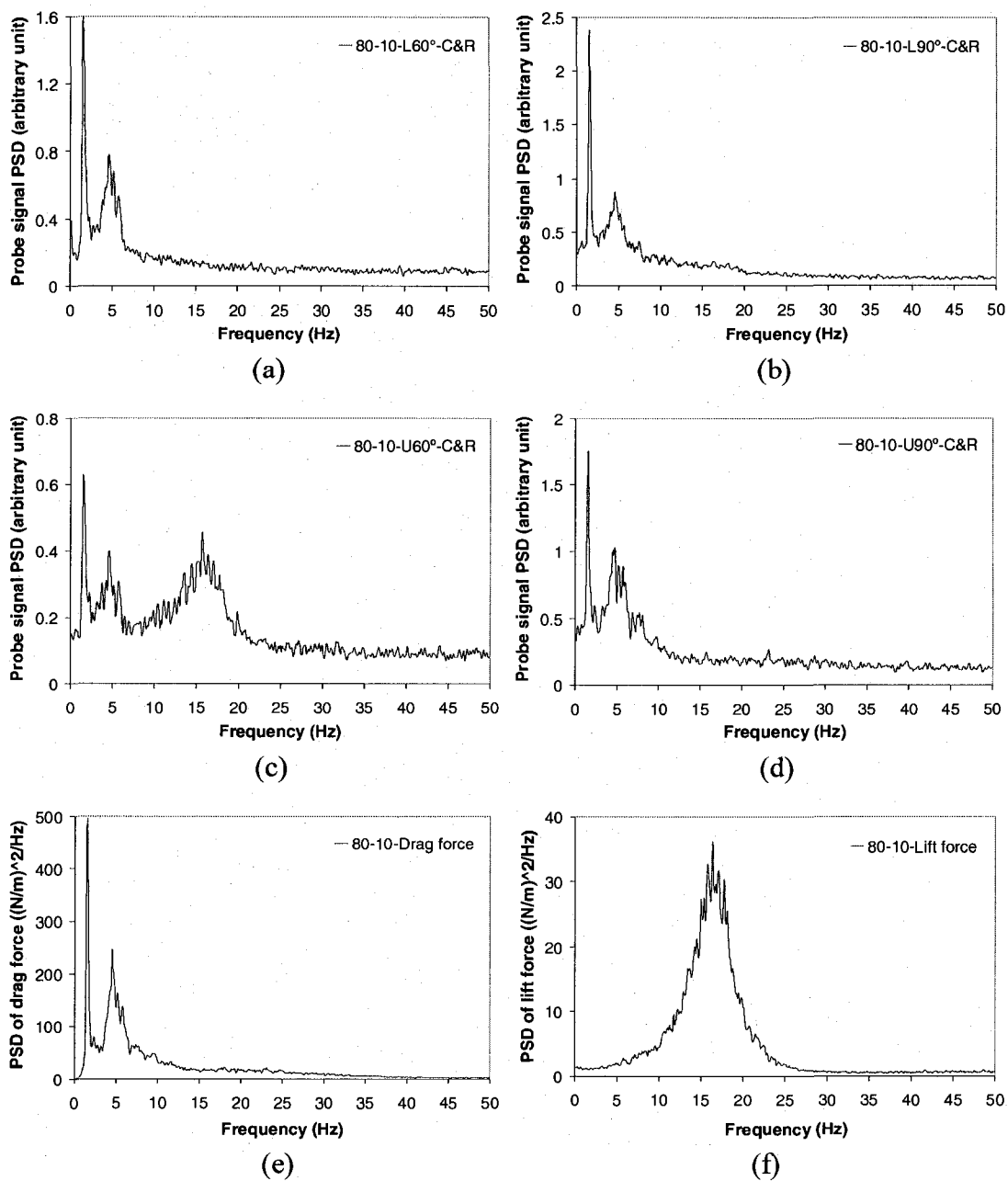


**Fig. A.12** Power spectra of the local void fraction fluctuation at four different positions along a line between the center line and right side of the main flow path for 80% void fraction at 10 m/s pitch flow velocity: (a) L60° position, (b) L90° position, (c) U60° position, and (d) U90° position; and dynamic force spectra: (e) Drag and (f) Lift

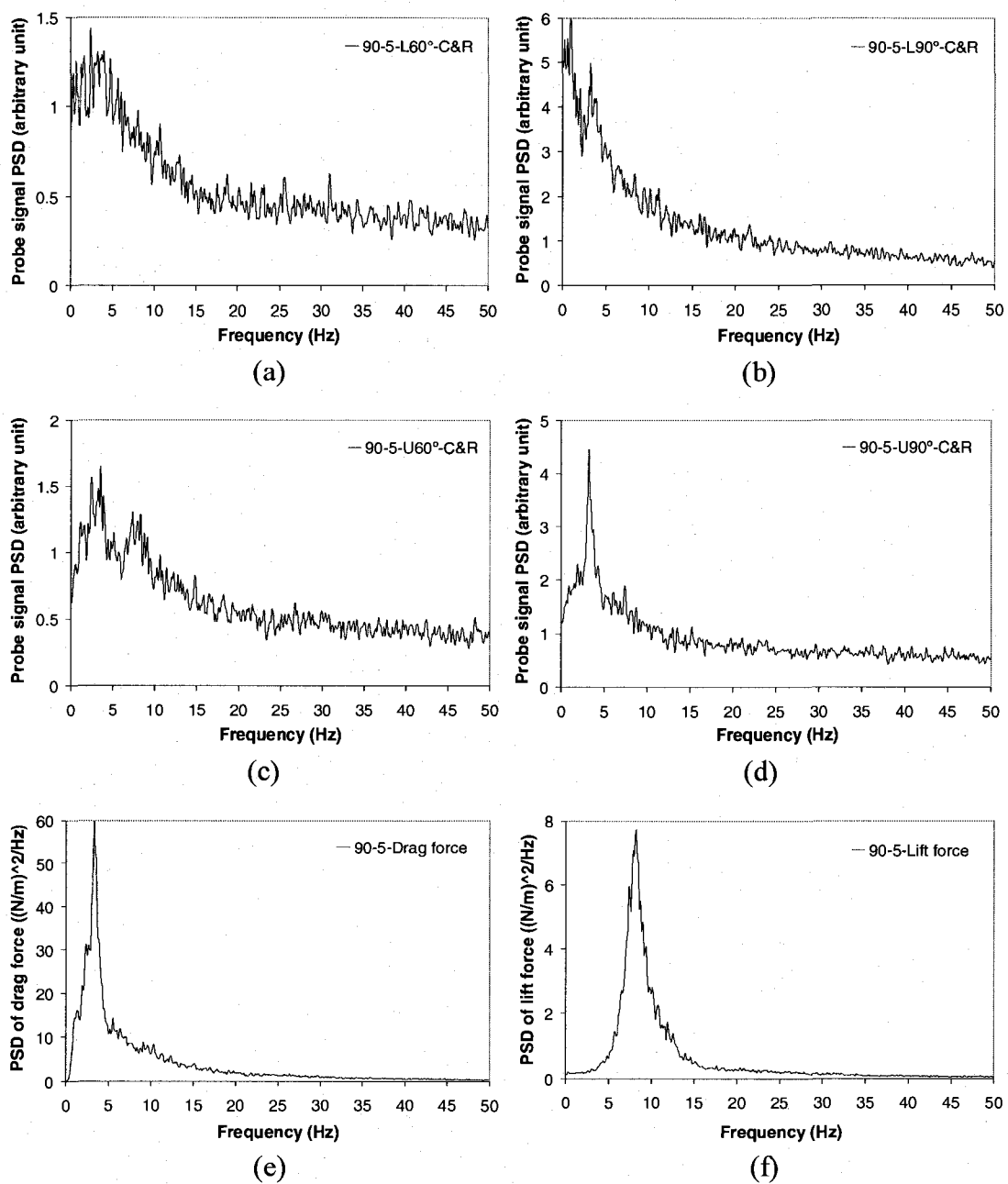


**Fig. A.13** Power spectra of the local void fraction fluctuation at four different positions along a line between the center line and right side of the main flow path for 90% void fraction at 5 m/s pitch flow velocity: (a) L60° position, (b) L90° position, (c) U60° position, and (d) U90° position; and dynamic force spectra: (e) Drag and (f) Lift

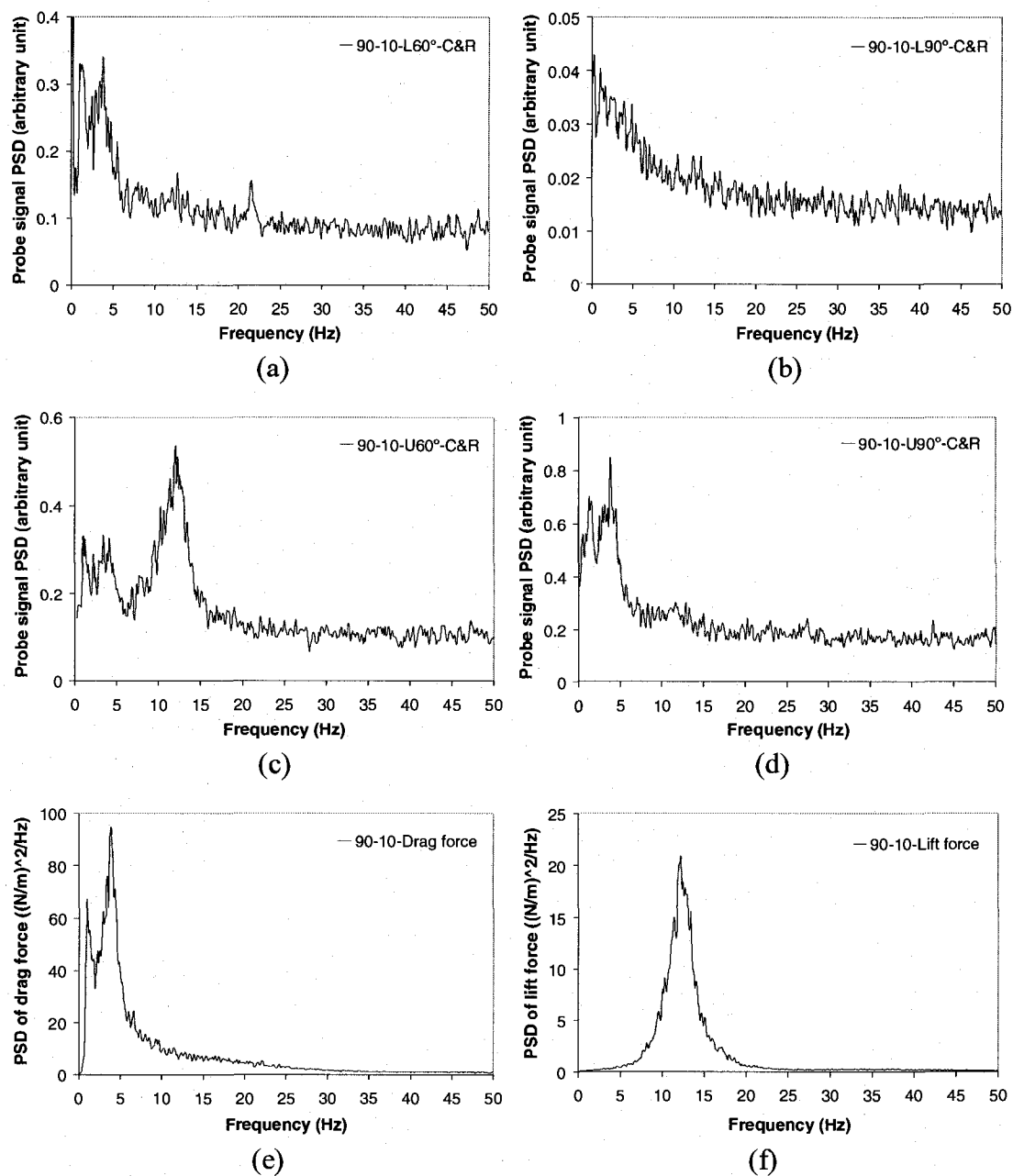


**Fig. A.14** Power spectra of the local void fraction fluctuation at four different positions along the line between the center line and right side of the main flow path for 90% void fraction at 10 m/s pitch flow velocity: (a) L60° position, (b) L90° position, (c) U60° position, and (d) U90° position; and dynamic force spectra: (e) Drag and (f) Lift

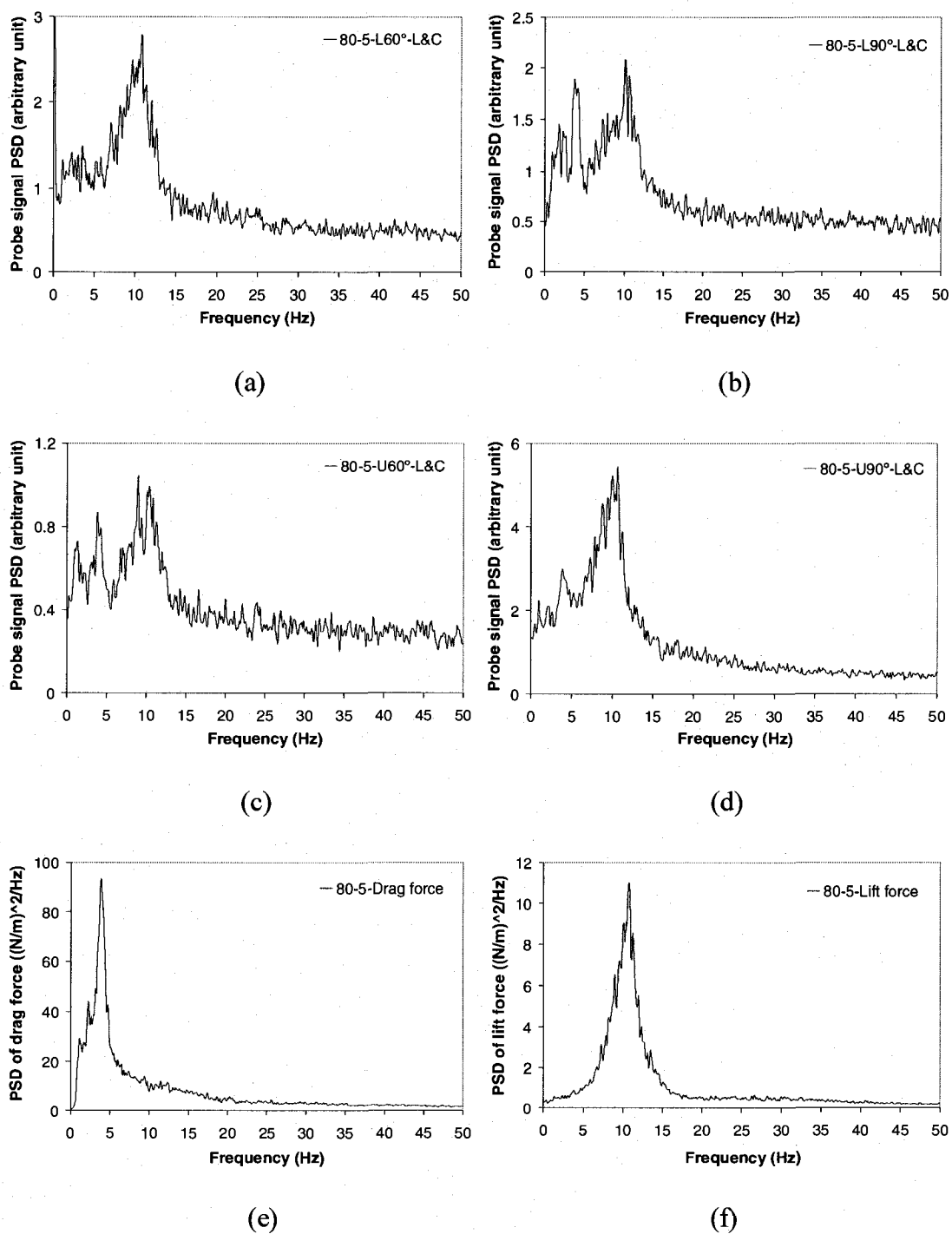


**Fig. A.15** Power spectra of the local void fraction fluctuation at four different positions along a line between the center line and left side of the main flow path for 80% void fraction at 5 m/s pitch flow velocity: (a) L60° position, (b) L90° position, (c) U60° position, and (d) U90° position; and dynamic force spectra: (e) Drag and (f) Lift

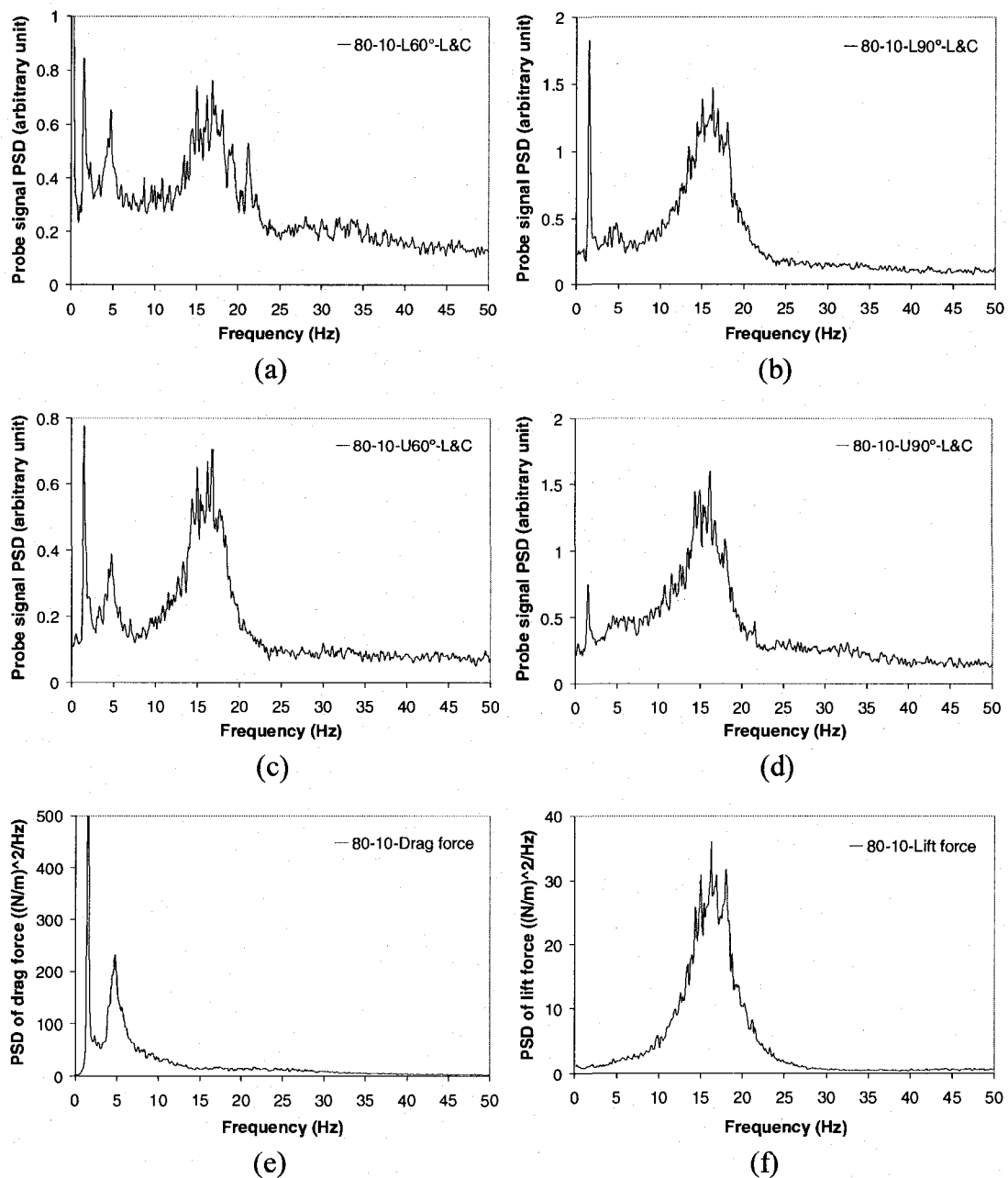


**Fig. A.16** Power spectra of the local void fraction fluctuation at four different positions along a line between the center line and left side of the main flow path for 80% void fraction at 10 m/s pitch flow velocity: (a) L60° position, (b) L90° position, (c) U60° position, and (d) U90° position; and dynamic force spectra: (e) Drag and (f) Lift

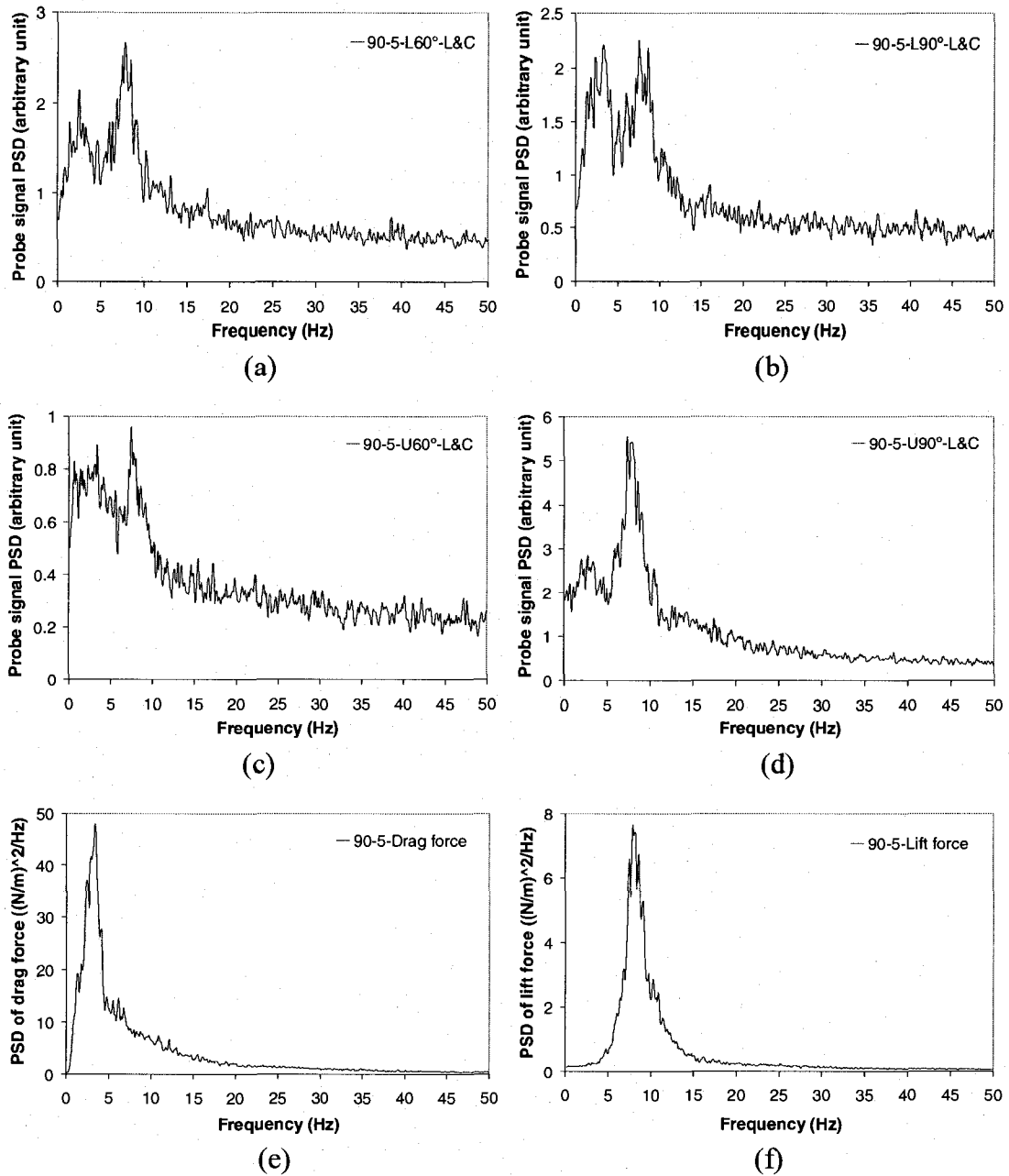


**Fig. A. 17** Power spectra of the local void fraction fluctuation at four different positions along a line between the center line and left side of the main flow path for 90% void fraction at 5 m/s pitch flow velocity: (a) L60° position, (b) L90° position, (c) U60° position, and (d) U90° position; and dynamic force spectra: (e) Drag and (f) Lift

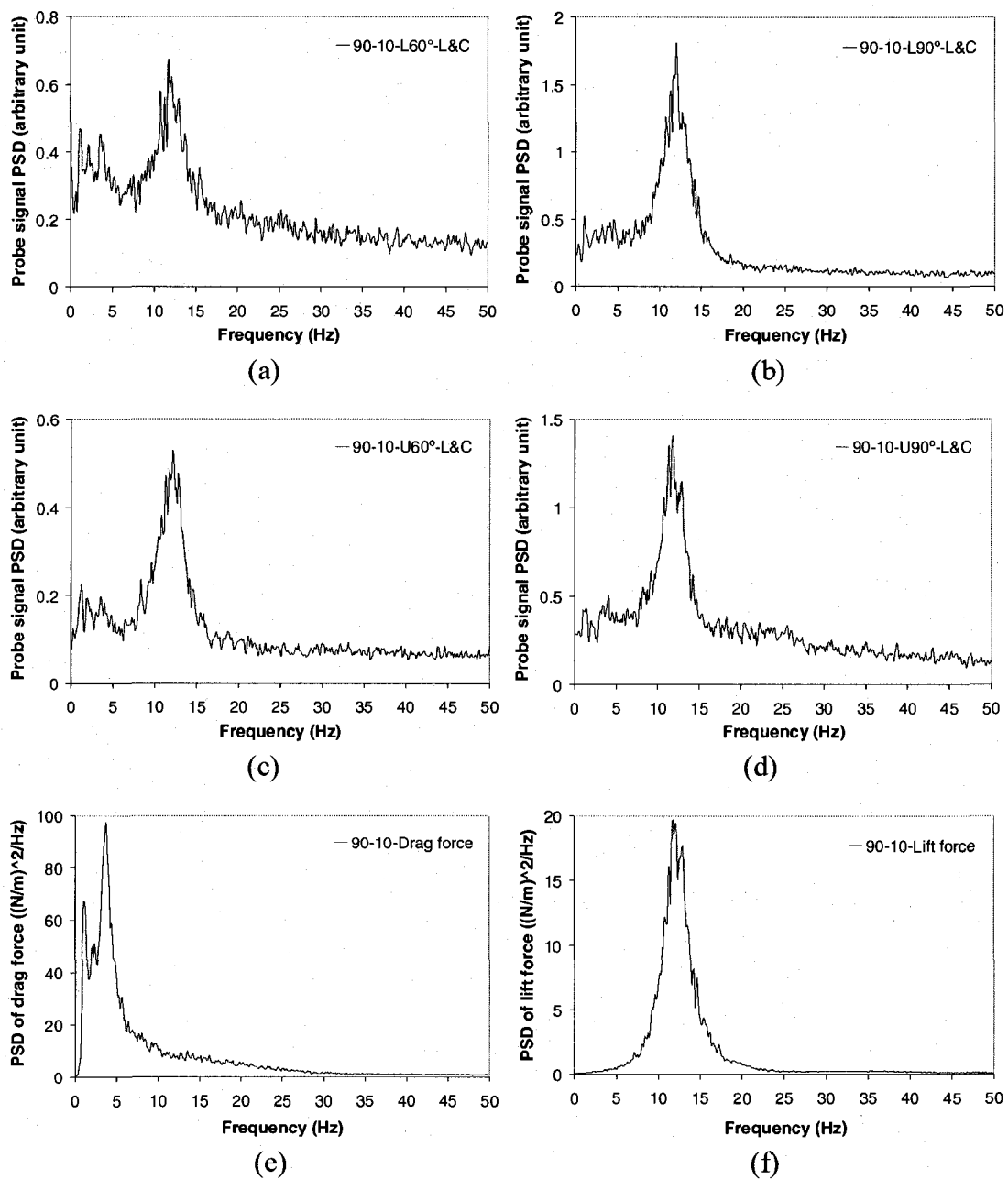


**Fig. A.18** Power spectra of the local void fraction fluctuation at four different positions along a line between the center line and left side of the main flow path for 90% void fraction at 10 m/s pitch flow velocity: (a) L60° position, (b) L90° position, (c) U60° position, and (d) U90° position; and dynamic force spectra: (e) Drag and (f) Lift



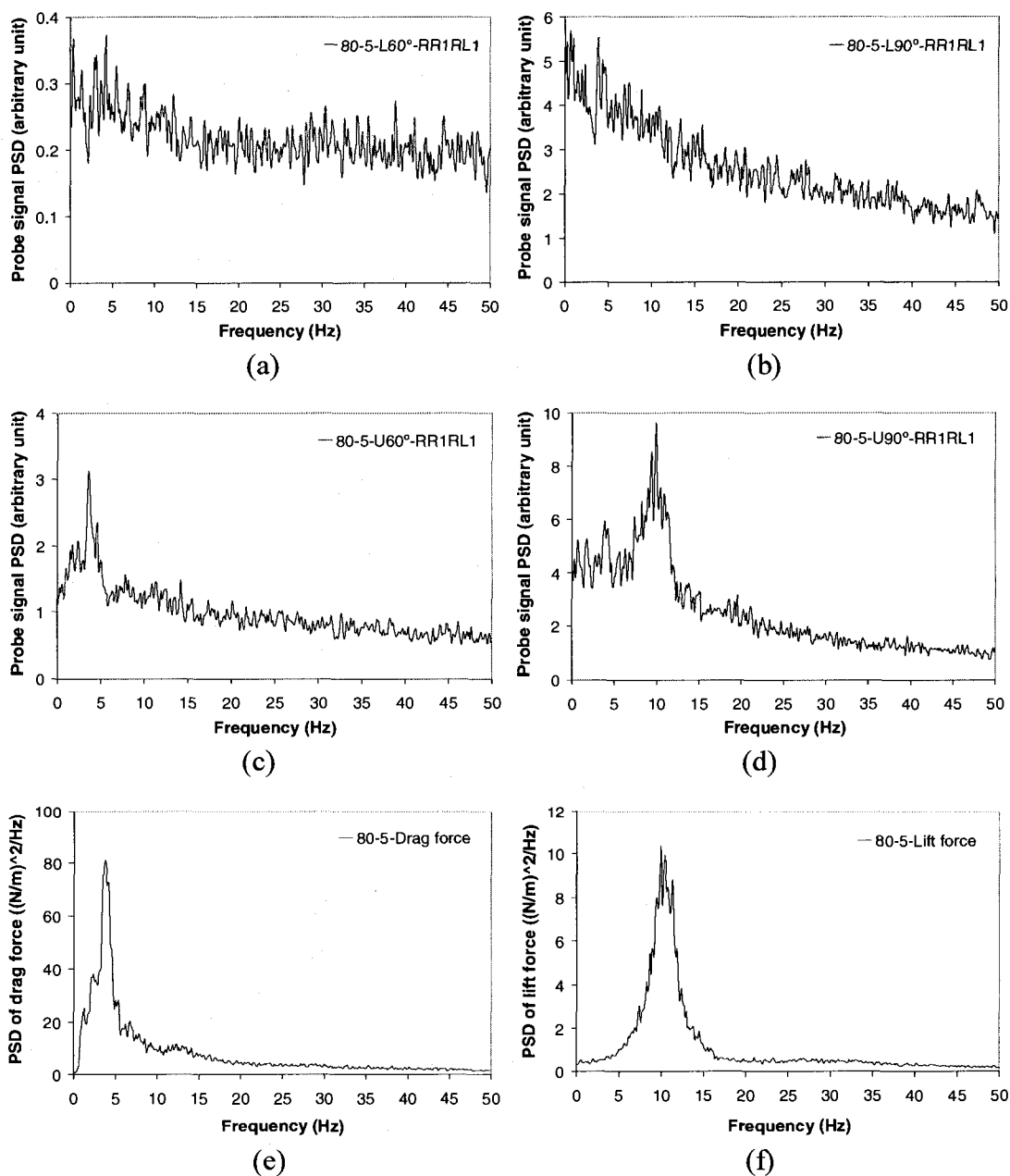


**Fig. A.19** Power spectra of the local void fraction fluctuation at four different positions RR1RL1 of the main flow path for 80% void fraction at 5 m/s pitch flow velocity: (a) L60° position, (b) L90° position, (c) U60° position, and (d) U90° position; and dynamic force spectra: (e) Drag and (f) Lift

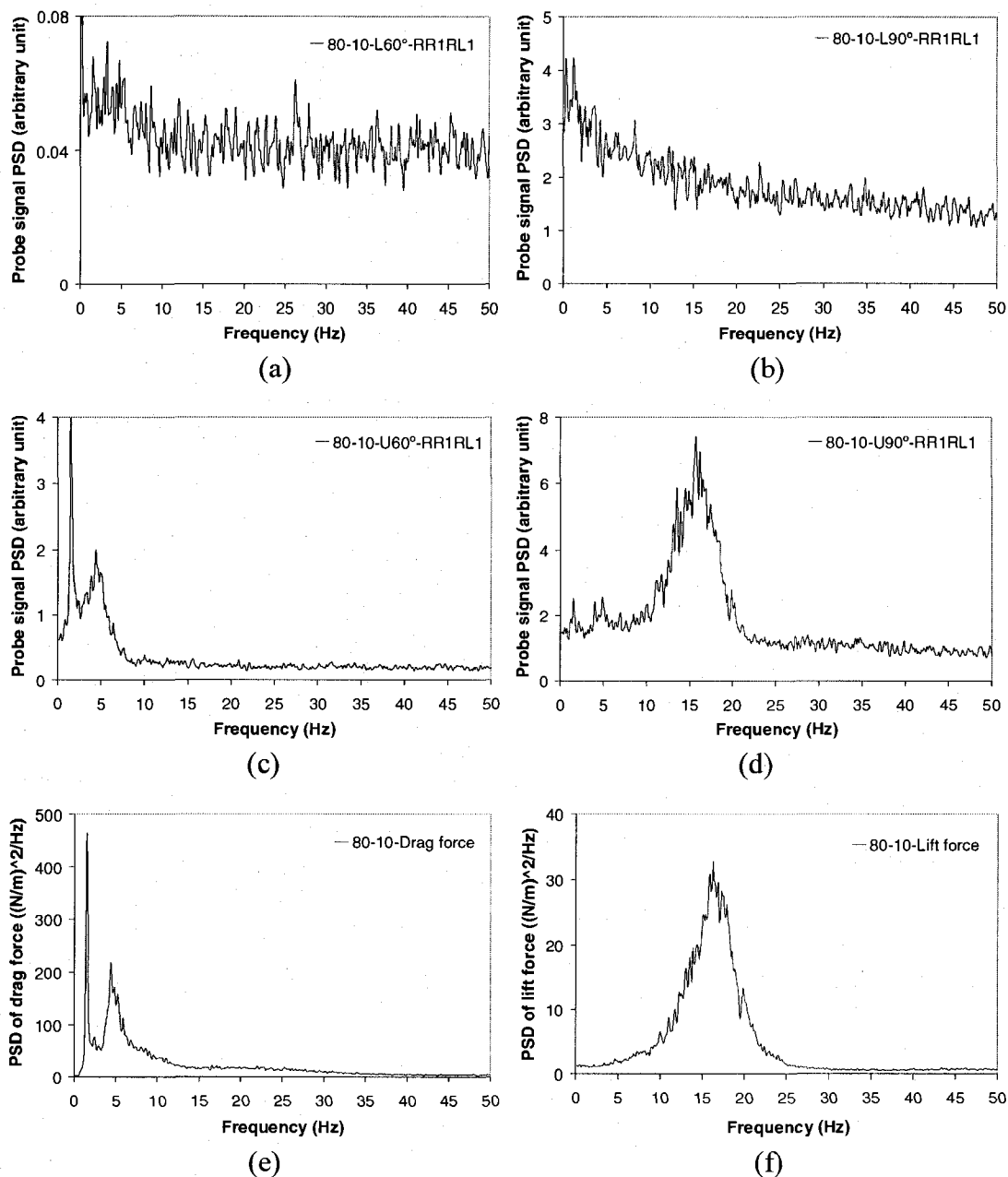


**Fig. A.20** Power spectra of the local void fraction fluctuation at four different positions RR1RL1 of the main flow path for 80% void fraction at 10 m/s pitch flow velocity: (a) L60° position, (b) L90° position, (c) U60° position, and (d) U90° position; and dynamic force spectra: (e) Drag and (f) Lift

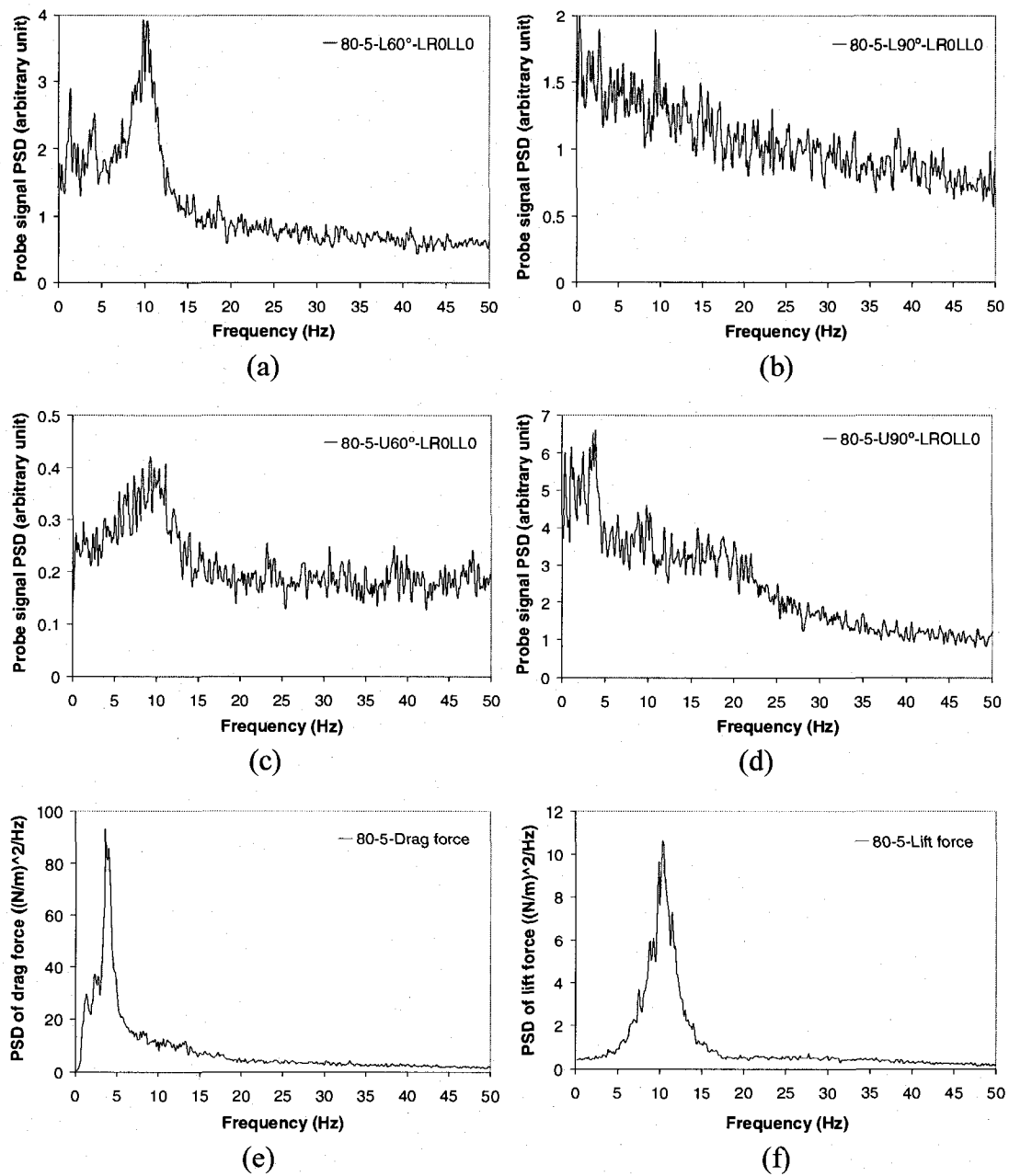


**Fig. A.21** Power spectra of the local void fraction fluctuation at four different positions LLR0L0 of the main flow path for 80% void fraction at 5 m/s pitch flow velocity: (a) L60° position, (b) L90° position, (c) U60° position, and (d) U90° position; and dynamic force spectra: (e) Drag and (f) Lift.

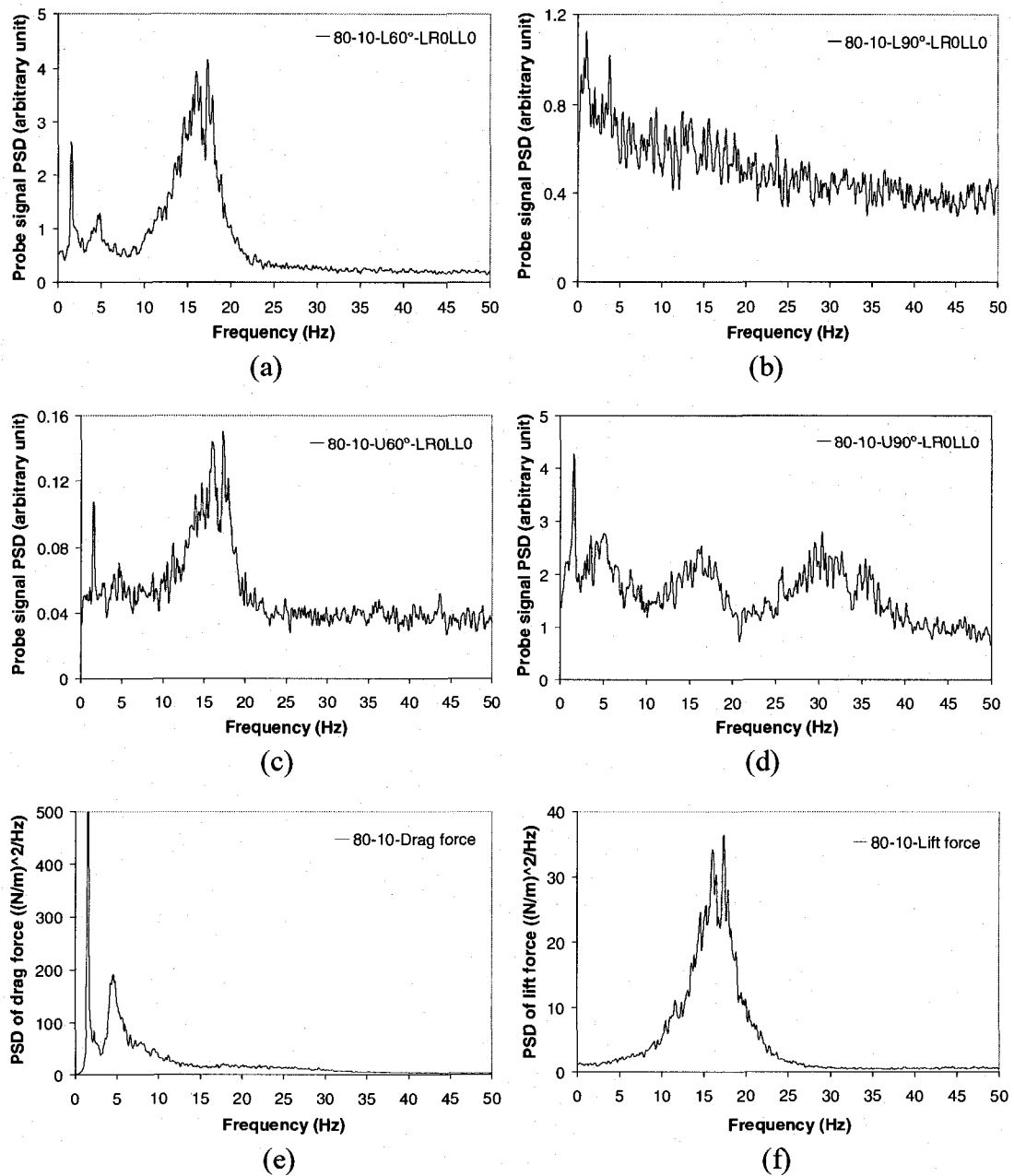


**Fig. A.22** Power spectra of the local void fraction fluctuation at four different positions LR0LL0 of the main flow path for 80% void fraction at 10 m/s pitch flow velocity: (a) L60° position, (b) L90° position, (c) U60° position, and (d) U90° position; and dynamic force spectra: (e) Drag and (f) Lift

## A6 Additional results related to Chapter 6

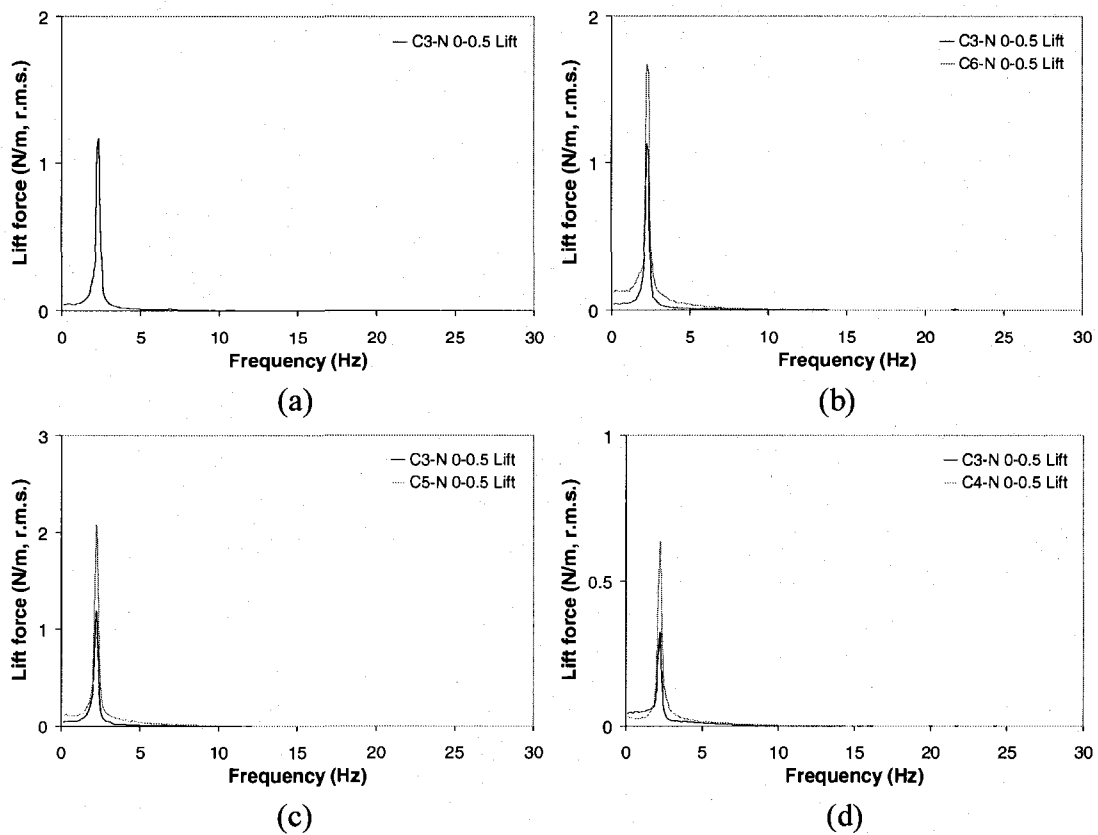


**Fig. A23** Typical dynamic lift force spectra for water flow at 1 m/s pitch flow velocity: (a) single cylinder, (b), (c) and (d) two cylinders at different pitches (4.5D, 3D and 1.5D, respectively)

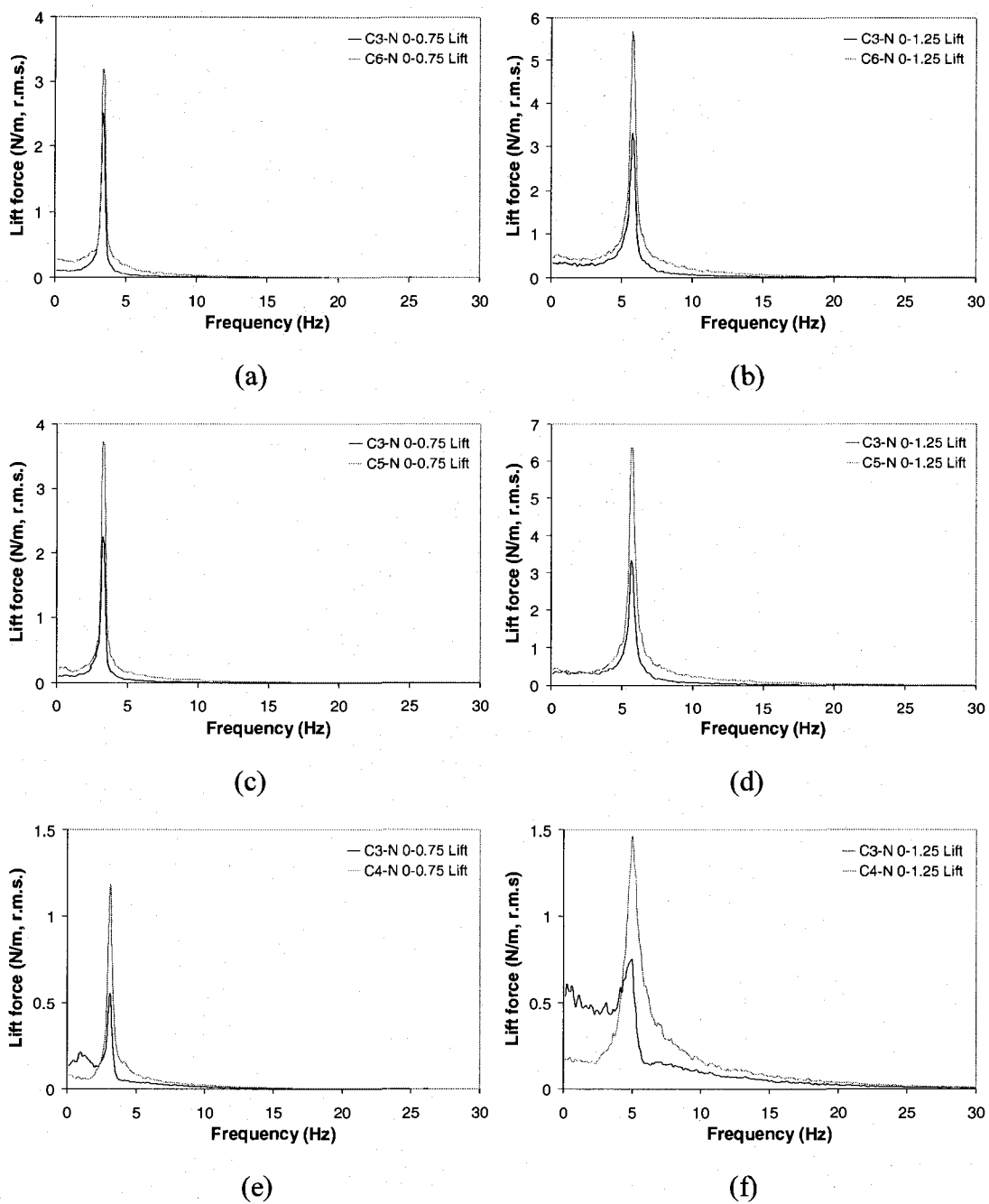


**Fig. A24** Typical dynamic lift force spectra for water flow: at 0.75 m/s pitch flow velocity, (a), (c) and (e) two tandem cylinders at different pitches (4.5D, 3D and 1.5D, respectively); at 1.25 m/s pitch flow velocity, (b), (d) and (f) two tandem cylinders at different pitches (4.5D, 3D and 1.5D, respectively)

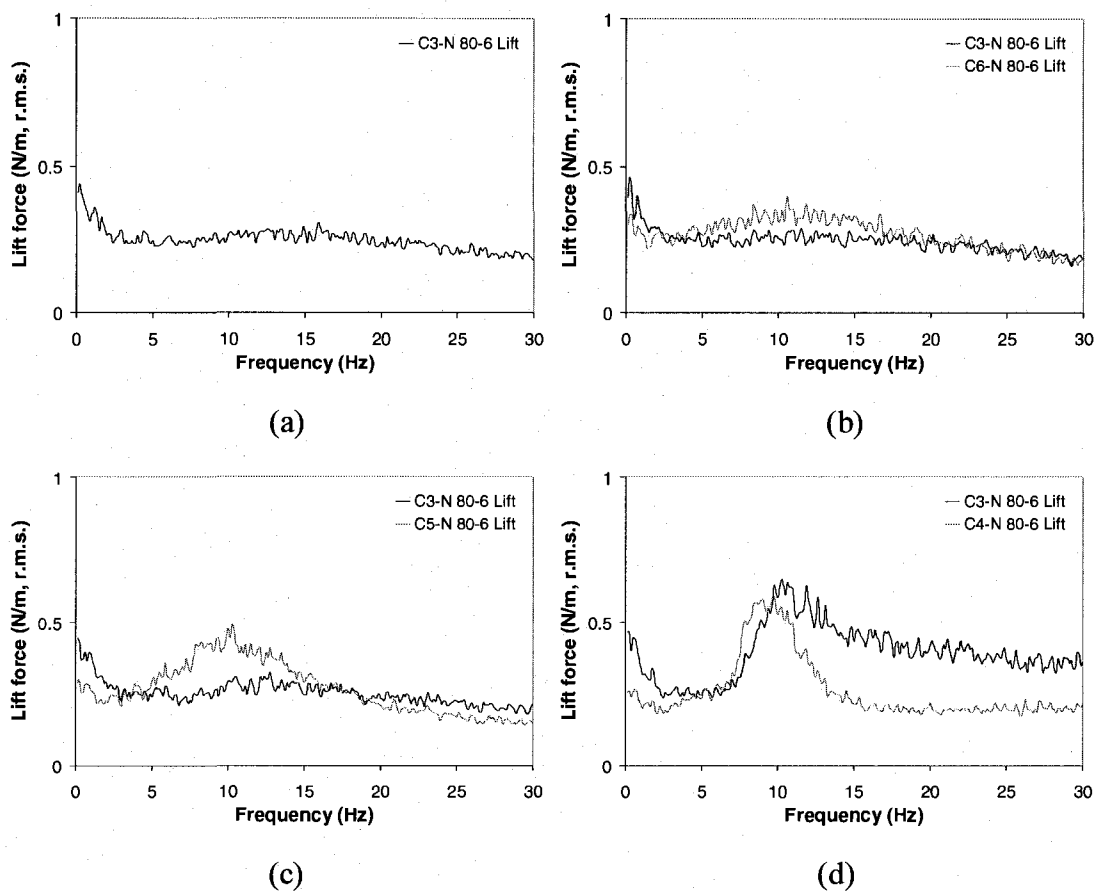


**Fig. A25** Typical dynamic lift force spectra for 80% void fraction at 6 m/s pitch flow velocity: (a) single cylinder, (b), (c) and (d) two cylinders at different pitches (4.5D, 3D and 1.5D, respectively)

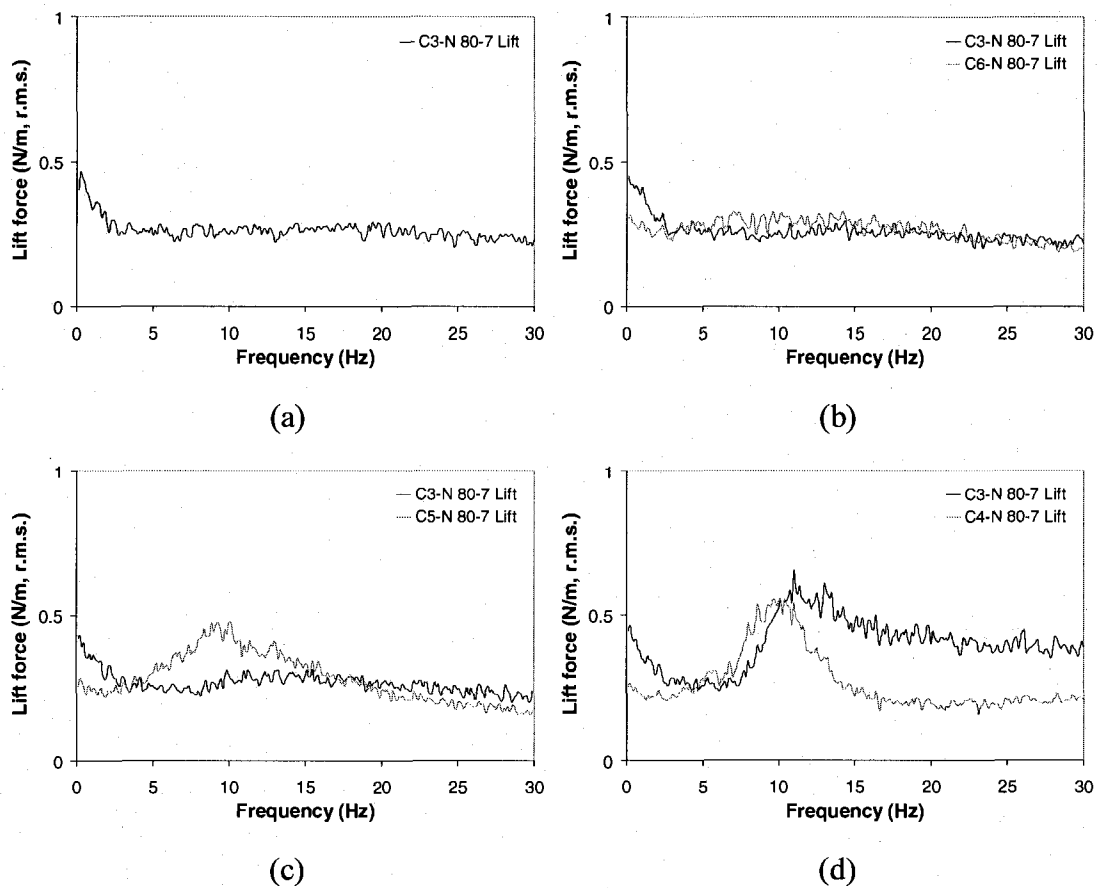


**Fig. A26** Typical dynamic lift force spectra for 80% void fraction at 7 m/s pitch flow velocity: (a) single cylinder, (b), (c) and (d) two cylinders at different pitches (4.5D, 3D and 1.5D, respectively)



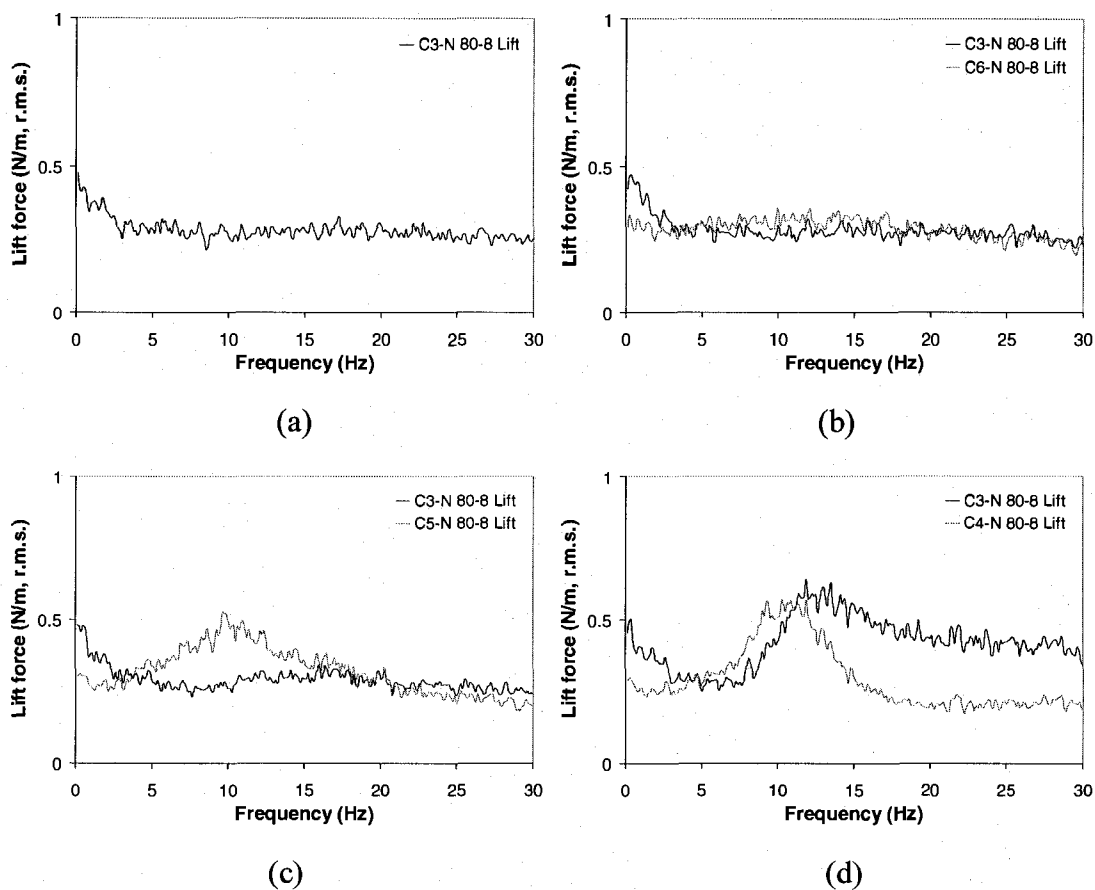


**Fig. A27** Typical dynamic lift force spectra for 80% void fraction at 8 m/s pitch flow velocity: (a) single cylinder, (b), (c) and (d) two cylinders at different pitches (4.5D, 3D and 1.5D, respectively)

**Table A.5** Strouhal number for water flow (vortex shedding)

L/D \ U <sub>p</sub> (m/s)		0.5	0.75	1.0	1.25	1.5	1.75	2.0
$S_1=fL/U_p$	1.5	0.257	0.238	0.228	0.228	0.228	0.236	0.249
	3.0	0.513	0.495	0.513	0.525	0.531	0.5378	0.612
	4.5	0.770	0.770	0.797	0.788	0.797	0.832	0.931
$S_2=fD/U_p$	1.5	0.171	0.158	0.152	0.152	0.152	0.157	0.166
	3.0	0.171	0.165	0.171	0.175	0.177	0.179	0.204
	4.5	0.171	0.171	0.177	0.175	0.177	0.185	0.207
	S-C	0.181	---	0.176	---	0.177	---	0.204

**Table A.6** Strouhal number for air-water flow at 80% void fraction (wake oscillations or instability of boundary layers)

L/D \ U <sub>p</sub> (m/s)		4	5	6	7	8
$S_1=fL/U_p$	1.5	0.105	0.103	0.093	0.082	0.075
	3.0	0.203	0.191	0.195	0.153	0.137
	4.5	0.352	0.320	N/A	N/A	N/A
$S_2=fD/U_p$	1.5	0.070	0.069	0.062	0.054	0.050
	3.0	0.067	0.064	0.065	0.051	0.046
	4.5	0.078	0.071	N/A	N/A	N/A

Note:

- 1)  $S_1=fL/U_p$ , based on the pitch of two tandem cylinders  $L$ ;  $S_2=fD/U_p$  based on cylinder diameter  $D$  (38 mm);
- 2) The values in Tables A.5 and A.6 are for the downstream tandem cylinder;
- 3) N/A means not applicable;
- 4) --- means not available.

## A7 Validation of correlation measuring method

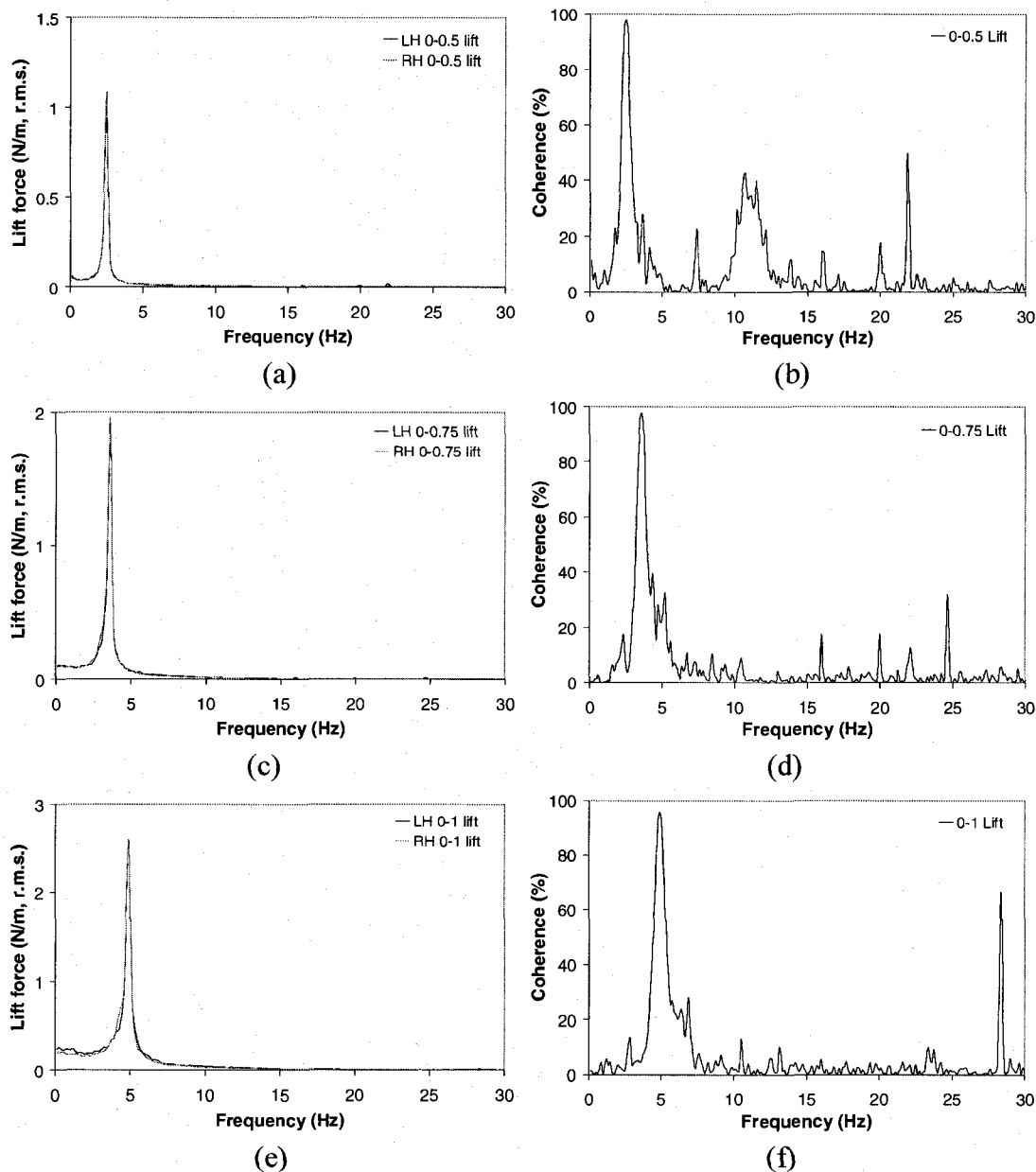


**Fig. A28** Dynamic lift force spectra for the left and right interior half-length cylinders in water flow: (a), (c) and (e) for pitch flow velocity 0.5, 0.75 and 1 m/s, respectively; and coherence of the two half-length cylinders, (b), (d) and (f) for pitch flow velocity 0.5, 0.75 and 1 m/s, respectively